Technical Report Documentation Page

1. Report No.	2. Government Accession No.	3. Recipient's Catalog No.
Preliminary Review Copy		

4. Title and Subtitle	5. Report Date
Use of Carbon Fiber Reinforced Polymer Composites to Increase the Flexural Capacity of Reinforced Concrete Beams	*April 2001*
	6. Performing Organization Code
7. Author(s)	8. Performing Organization Report No.
Sergio F. Breña, Regan M. Bramblett, Michaël A. Benouaich, Sharon L. Wood, and Michael E. Kreger	Research Report 1776-1
9. Performing Organization Name and Address	10. Work Unit No. (TRAIS)
Center for Transportation Research The University of Texas at Austin 3208 Red River, Suite 200 Austin, TX 78705-2650	11. Contract or Grant No. Research Study 0-1776
12. Sponsoring Agency Name and Address	13. Type of Report and Period Covered
Texas Department of Transportation Research and Technology Transfer Office P.O. Box 5080 Austin, TX 78763-5080	Research Report (9/97-10/00)
	14. Sponsoring Agency Code

15. Supplementary Notes

16. Abstract

A large portion of the off-system bridges and some on-system bridges in Texas were constructed in the 1950s using vehicle loads that are less than the current design standards. As a result, the legal load that is permitted to cross these bridges is often limited and many are scheduled for replacement. The use of carbon fiber reinforced polymer (CFRP) composites to increase the flexural capacity of reinforced concrete bridges was investigated in this research project. The overall goal was to develop design procedures for strengthening existing bridges using CFRP to avoid replacement of bridges that have been functioning satisfactorily for many years.

The first two phases of the research project are described in this report. A total of twenty-two, rectangular reinforced concrete beams were tested during the first phase of the project. The beams were strengthened using four CFRP systems and were subjected to monotonically increasing load. The primary test parameter was the layout of the CFRP system. Two layouts were identified that prevented premature debonding of the CRFP composites from the surface of the concrete.

Eight rectangular beams were strengthened using two of the previously tested CFRP systems and were subjected to fatigue loads in the second phase of the project. The composite/concrete interface did not degrade under the fatigue loads. Strengthened beams sustained one million cycles at service levels with only a negligible influence on the measured behavior.

An analytical model was developed to calculate the behavior of the strengthened beams. The model provided reasonable estimates of the measured mid-span deflections. However, the model was not capable of reproducing the measured strains in the materials due to local debonding of the CFRP from the surface of the concrete.

17. Key Words	18. Distribution Statement
woven CFRP fabric, pultruded CFRP plate, unidirectional CFRP fabric, epoxy, debonding, cracking, UV Exposure, fatigue tests	No restrictions. This document is available to the public through the National Technical Information Service, Springfield, Virginia 22161.

19. Security Classif. (of report)	20. Security Classif. (of this page)	21. No. of pages	22. Price
Unclassified	Unclassified	238	

Form DOT F 1700.7 (8-72) Reproduction of completed page authorized

USE OF CARBON FIBER REINFORCED POLYMER COMPOSITES TO INCREASE THE FLEXURAL CAPACITY OF REINFORCED CONCRETE BEAMS

by

Sergio F. Breña, Regan M. Bramblett, Michaël A. Benouaich, Sharon L. Wood, and Michael E. Kreger

Research Report 1776-1

Research Project 0-1776

DEVELOPMENT OF METHODS TO STRENGTHEN EXISTING STRUCTURES WITH COMPOSITES

conducted for the

Texas Department of Transportation

in cooperation with the

U.S. Department of Transportation
Federal Highway Administration

by the

CENTER FOR TRANSPORTATION RESEARCH
BUREAU OF ENGINEERING RESEARCH
THE UNIVERSITY OF TEXAS AT AUSTIN

April 2001

Research performed in cooperation with the Texas Department of Transportation and the U.S. Department of Transportation, Federal Highway Administration.

ACKNOWLEDGEMENTS

This research project was sponsored by the Texas Department of Transportation (TxDOT) under Project No. 0-1776. The involvement of Mark Steves and Richard Wilkison from TxDOT were extremely important for the successful completion of the research project. Their fruitful suggestions were incorporated into the research project to guarantee the applicability of the results from the experimental program to actual field situations.

The manufacturers of the composite systems graciously donated the composites that were used to strengthen the laboratory specimens. The assistance of Bill Light, Sika Corporation; Howard Kliger and Bob Snider, Master Builders Technology; Paul Gugenheim, Delta Structural Technology, Inc. (Fyfe Co.); and Ali Ganjehlou, Mitsubishi/Sumitomo Corp. is very much appreciated.

This research project was conducted at the Ferguson Structural Engineering Laboratory (FSEL). The assistance of laboratory technicians and administrative staff was fundamental for the completion of this project. Nicole García, Sarah Orton, and Janna Renfro participated during the fabrication and testing of specimens during different phases of the project.

DISCLAIMERS

The contents of this report reflect the views of the authors, who are responsible for the facts and the accuracy of the data presented herein. The contents do not necessarily reflect the view of the Federal Highway Administration or the Texas Department of Transportation. This report does not constitute a standard, specification, or regulation.

NOTICE

The United States Government and the state of Texas do no endorse products or manufacturers. Trade or manufacturer's names appear herein solely because they are considered essential to the object of this report.

NOT INTENDED FOR CONSTRUCTION,

PERMIT, OR BIDDING PURPOSES

S. L. Wood, Texas P.E. #83804

M. E. Kreger, Texas P.E. #65541

Research Supervisors

TABLE OF CONTENTS

LIST OF FIGURES

LIST OF TABLES

SUMMARY

A large portion of the off-system bridges and some on-system bridges in Texas were constructed in the 1950s using vehicle loads that are less than the current design standards. As a result, the legal load that is permitted to cross these bridges is often limited and many are scheduled for replacement. The use of carbon fiber reinforced polymer (CFRP) composites to increase the flexural capacity of reinforced concrete bridges was investigated in this research project. The overall goal was to develop design procedures for strengthening existing bridges using CFRP to avoid replacement of bridges that have been functioning satisfactorily for many years.

The first two phases of the research project are described in this report. A total of twenty-two, rectangular reinforced concrete beams were tested during the first phase of the project. The beams were strengthened using four CFRP systems and were subjected to monotonically increasing load. The primary test parameter was the layout of the CFRP system. Two layouts were identified that prevented premature debonding of the CRFP composites from the surface of the concrete.

Eight rectangular beams were strengthened using two of the previously tested CFRP systems and were subjected to fatigue loads in the second phase of the project. The composite/concrete interface did not degrade under the fatigue loads. Strengthened beams sustained one million cycles at service levels with only a negligible influence on the measured behavior.

An analytical model was developed to calculate the behavior of the strengthened beams. The model provided reasonable estimates of the measured mid-span deflections. However, the model was not capable of reproducing the measured strains in the materials due to local debonding of the CFRP from the surface of the concrete.

Chapter 1: Introduction

1.1 BACKGROUND

The need to develop economic and efficient methods to upgrade, repair, or strengthen existing reinforced concrete bridges has received considerable attention recently. The motivation to strengthen an existing reinforced concrete bridge typically comes from two sources: a desire to increase the strength of the bridge to keep pace with increases in the weight of design vehicles, and a desire to repair deterioration that has taken place over the years of operation.

According to the National Bridge Inventory (NBI) there are approximately 47,000 bridges in Texas. Of these, only 15,300 form part of the National Highway System (NHS). Therefore, approximately 70% of the total number of bridges are part of the off-system roadways [FHWA, 1999].

Many of the reinforced concrete bridges on off-system roads, as well as some on-system roads, were constructed over 50 years ago. The trucks currently crossing these bridges often correspond to overload conditions because legal truck loads have increased considerably during this time. The Texas Department of Transportation (TxDOT) has an ongoing bridge rating and inspection program to ensure that these bridges can remain in operation and to mitigate the potential risk of structural failure. Bridges need to be inspected every year or every other year, depending on the load rating of the bridge. Current practice is to inspect bridges that do not meet an HS-20 inventory rating on a yearly basis. Therefore, the Department of Transportation can incur significant savings if the numbers of bridges that currently have a low load rating are upgraded.

Additionally, off-system roadways often require widening to accommodate larger traffic volume due to an increase in the market activity of an area. Internal TxDOT policies require that bridges that do not meet the current design-truck standard (HS-20) can not qualify for widening and therefore need to be replaced when the road is widened. The economic impact of bridge replacement is represented by not only the direct costs associated with demolition and construction of a new bridge, but also by the indirect costs associated with the loss of roadway use and traffic disruption. The latter are often difficult to quantify and foresee.

An alternative to bridge replacement is strengthening using well-established methods. Casting additional elements, increasing cross-section size, and bonding steel plates are techniques that have been used in the past when widening an existing bridge. These solutions can be expensive and difficult to implement, especially for low-river crossings. Therefore, TxDOT was interested in developing economic and efficient methods to strengthen existing reinforced concrete bridges and increase their live-load capacity as an alternative to bridge replacement.

The use of carbon fiber reinforced polymer (CFRP) composites to increase the flexural capacity of elements in the bridge superstructure was identified as a possible alternative to other strengthening methods. This alternative was considered particularly attractive to increase the live-load capacity of the bridges because the increase in dead loads is insignificant with these materials. Therefore, the increase in capacity after strengthening is used entirely to resist the increase in live loads.

1.2 OBJECTIVES AND SCOPE OF RESEARCH

The objectives of this research project were to investigate the effectiveness of composite materials to strengthen reinforced concrete bridges, and to develop design guidelines for the safe implementation of these materials in existing bridges. To meet the goals of this project, a comprehensive research program was developed in coordination with TxDOT engineers. The overall research project was divided into three phases.

This report presents the results from the first and second phases of the research project. The third phase of the project is described in detail in a separate research report. [Breña, et al., 2001] Phase 3 involved the design and testing of four full-scale bridge components strengthened using CFRP composites. The results from the first two phases of the project were used for the design of the strengthening schemes for these specimens.

The first phase of the research project included testing 22 reinforced concrete beams under monotonically applied loads. The main goal of this phase of the research project was to develop methods for reliably attaching carbon fiber composites to reinforced concrete beams for the purpose of increasing flexural strength. Twenty beams were strengthened using CFRP composites to increase their flexural capacity and two were unstrengthened. These two specimens were used as a baseline for comparison of strengthening efficiency (control specimens). A number of strengthening schemes were designed and tested to identify any differences in behavior of the strengthened specimens. Composites from four different manufacturers were used to strengthen the beams. Also, two strengthened specimens were subjected to continuous environmental exposure including wetting and drying cycles for approximately 8 months prior to testing.

The goal of the second phase of the experimental study was to identify the influence of repeated loads on the serviceability and ultimate behavior of strengthened beams using two different CFRP systems. The composite systems and strengthening schemes were selected based on the results from phase 1. These two composite systems were considered representative of the global behavior of the different composite systems used in phase 1. Bond between the composites and the surface of the concrete was identified as a potential source of fatigue failure of the strengthened specimens. This type of failure could be caused by the accumulation of damage in the strengthened beams.

Eight specimens strengthened using CFRP composites were subjected to different numbers of cycles and amplitudes of loading. The loading amplitudes were representative of either service-load conditions or overload conditions on a bridge. Five beams were subjected to load amplitudes representative of service-load conditions. These beams were tested monotonically to failure after being subjected to a predetermined number of loading cycles. The response of these beams was compared with the response of companion specimens tested in phase 1 to evaluate the effects of cycling. Finally, three beams were tested under repeated application of loads representative of overload conditions on a bridge. The purpose of these tests was to cause failure by fatigue of the strengthened specimens, and identify the source of failure. These tests were not considered representative of loading conditions commonly encountered on a bridge.

1.3 ORGANIZATION OF REPORT

This research report is divided into nine chapters. The use of CFRP composites to strengthen existing reinforced concrete elements has been investigated in the past by other researchers. The conclusions and observations from these programs, as they relate to this research project, are summarized in Chapter 2. Areas where additional information is required or conclusions need verification are also identified.

To meet the objectives of this investigation, it was considered essential to be able to calculate the capacity and reproduce the behavior of the laboratory specimens representing the strengthened bridge elements that were selected for this project. The analytical model presented in Chapter 3 was able to reproduce the behavior of the strengthened elements. A discussion of the assumptions used in the development of the analytical model is also presented.

The procedure used for the design of the laboratory specimens in phases 1 and 2 is presented in Chapter 4. The details of the reinforced concrete beams and the composite systems are also presented. Chapter 5 gives a description of the laboratory tests conducted in the first two phases of the research project. The test setup, instrumentation, and loading sequence are presented and discussed.

The measured response of the beams tested in phase 1 is presented in Chapter 6. A discussion of the failure sequence of different groups of beams is presented first. Afterwards the measured strain and deflection response of the different groups of beams is presented and discussed. The general characteristics of the response of the specimens are described and discussed.

The measured response is compared with the calculated response of the specimens in Chapter 7. Some of the assumptions used in the analytical model were also evaluated using the measured strain response. The limitations of the analytical model are also identified.

Chapter 8 presents the measured response of the specimens subjected to fatigue loading. The accumulation of damage and the failure sequence of the specimens are first discussed. The measured strain response and displacement response are presented. The measured response of the beams tested monotonically to failure after cyclic loading are compared with the response of the companion specimens in phase 1. Finally Chapter 9 presents a summary and conclusions from the results of the first two phases of this research project.

Chapter 2: Literature Review

2.1 INTRODUCTION

A review of previous investigations on the strengthening of reinforced concrete elements using CFRP composites is presented in this chapter. A brief overview of the evolution of the use of composites in civil engineering is presented in Section 2.2. The main failure modes observed during previous testing and the conclusions drawn from these programs are presented in Section 2.3. Static-load testing of beams strengthened using CFRP composites has been studied extensively as indicated in this chapter. However, the number of studies on the fatigue performance of strengthened beams is limited. The available results of previous testing on the fatigue performance of beams strengthened using CFRP composites are presented in Section 2.4. A review of the literature indicated that although CFRP composites are already being used to repair and strengthen existing structural concrete bridges, the technology is still in its developmental stage.

2.2 HISTORICAL BACKGROUND

Fiber reinforced composites have been consistently used in other fields of engineering since the late 1960s. Their use had been restricted mainly to the aerospace and automotive industries, where the use of high strength, lightweight materials results in significant fuel savings and the possibility of increasing the payload. Airplane and automobile parts that were traditionally fabricated using aluminum are being replaced with composites [Mallick, 1993]. Other fields such as the boating industry and sporting goods industry have also benefitted from the used of fiber reinforced composites. For pressure vessels and piping applications where corrosion protection is a primary concern, fiber reinforced plastics have also been used extensively [ASME, 1992 and 1998].

In civil engineering, the use of composites is only beginning to gain acceptance because composite materials have not been economically competitive with traditional building materials such as steel or concrete, and comprehensive design guidelines [ASCE, 1984] are not available. The use of these materials for the repair and strengthening of the aging infrastructure provides an interesting alternative to traditional methods, because of their high strength-to-weight ratio, corrosion resistance, and excellent fatigue performance. Although the technology of the use of composites in the aerospace industry has advanced significantly over the last 30 years, many methods for their application to strengthen existing structures are still under investigation.

To assess the applicability of composite materials for the bridge infrastructure in the United States, the Federal Highway Administration conducted a scanning tour of Europe (UK, Switzerland, Germany) and Japan, where composites had already been used to strengthen existing bridges [FHWA, 1997]. During this survey, applications that did not require modification for use in the United States were identified. In addition, areas where further research was needed before the technology could be implemented in field applications were highlighted. In the case of strengthening of existing bridges using CFRP composites, areas that need further research include the development of design guidelines consistent with U.S. practice and the development of adequate details to ensure the full participation of the concrete substrate.

2.3 BEAMS TESTED UNDER STATIC LOAD

Research on strengthening existing structures using fiber reinforced composites (FRP) was motivated by the need to eliminate some of the problems associated with the traditional method of strengthening by

bonding steel plates to the surface of the concrete. By using FRP composite plates, the corrosion potential of the plates was eliminated and the use of heavy equipment to handle the plates during construction was minimized.

Investigations on the use of fiber reinforced composites to strengthen bridge structures began in the late 1980s. These investigations examined the behavior of strengthening reinforced concrete beams using glass fiber reinforced polymers (GFRP). Relatively thick GFRP plates (more than ¼ in.) had to be used to achieve from 40% to 100% increase in strength, if anchorage was provided at the ends of the plates [Saadatmanesh and Ehsani, 1991]. The predominant failure mode that was observed in these tests was similar to that observed during tests on beams strengthened using steel plates. The composite material debonded from the surface of the concrete at failure, and debonding of the plates initiated at the ends due to the presence of large normal and shear stresses. Therefore, measures were taken to prevent this type of failure by anchoring the ends of the GFRP plates to the concrete.

One of the earliest research programs that investigated the use of CFRP composites to strengthen reinforced concrete elements was conducted at the Swiss Federal Institute of Technology [Meier et al., 1992] in the late 1980s. Bridges that had been strengthened using steel plates were showing signs of corrosion after only a few years in service and carbon fiber composites were selected as an alternative. A qualitative comparison of the performance of carbon, glass, and aramid composites is presented in Table 2.1 [Meier and Winistörfer, 1995].

Table 2.1 Qualitative Comparison of Different Fibers used in Composites [Meier and Winistörfer, 1995]

Criterion	Type of Fiber used in Composite		
	Carbon Fibers	**Glass Fibers**	**Aramid Fibers**
Tensile strength	Very good	Very good	Very good
Compressive strength	Very good	Inadequate	Good
Young's modulus	Very good	Good	Adequate
Long-term behavior	Very good	Good	Adequate
Fatigue behavior	Excellent	Good	Adequate
Bulk density	Good	Excellent	Adequate
Alkaline resistance	Very good	Good	Inadequate
Price	Adequate	Adequate	Very good

2.3.1 Flexural Tests on Small-Scale Specimen

During the early and mid 1990s, a large number of studies were conducted in several parts of the world to investigate the use of CFRP composites to increase the flexural strength of existing beams. The majority of the laboratory tests were conducted on small-scale rectangular beams tested under four-point bending. The main modes of failure for these specimens are identified in Figure 2.1, where the critical crack is indicated using a thick line:

- Tensile rupture of the CFRP composites (sheets).
- Failure by crushing of the concrete in compression.

- Diagonal tension failure at end of CFRP composites (plates).
- Debonding (peeling) of the CFRP composites.

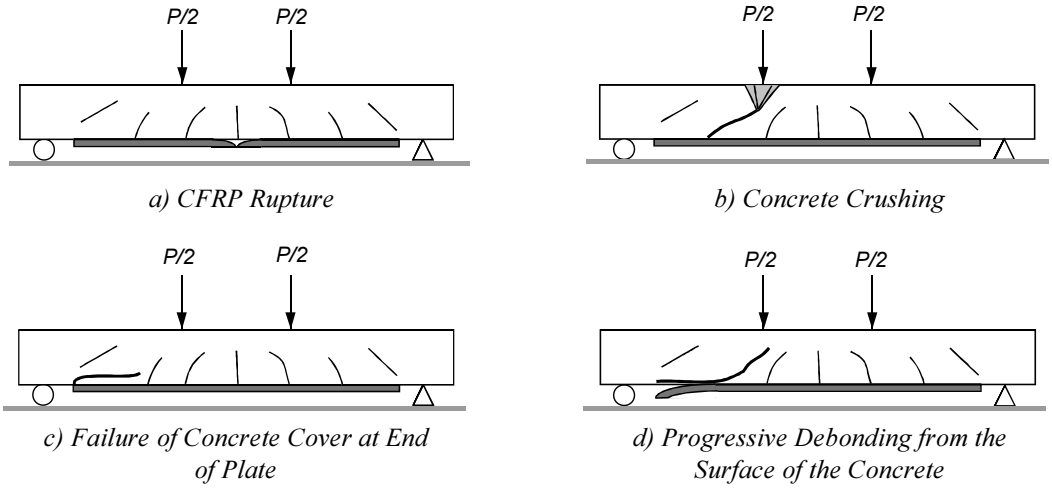

Figure 2.1 Observed Failure Modes of Strengthened Members Using CFRP Composites

A list of the research programs that were included in this investigation and the experimental parameters are summarized in Table 2.2. These studies were selected to give an overview of the most important parameters that influence the performance of strengthened beams. The specimen characteristics tested in these research programs are summarized in Tables 2.3 and 2.4. The predominant modes of failure and main conclusions are summarized in Table 2.5.

A common observation in these research programs was that failure of the beams was often controlled by CFRP debonding from the surface of the concrete (Table 2.5). Therefore, several researchers investigated the use of different techniques to delay or eliminate debonding as a failure mode. Some of the techniques that were investigated are illustrated in Figure 2.2.

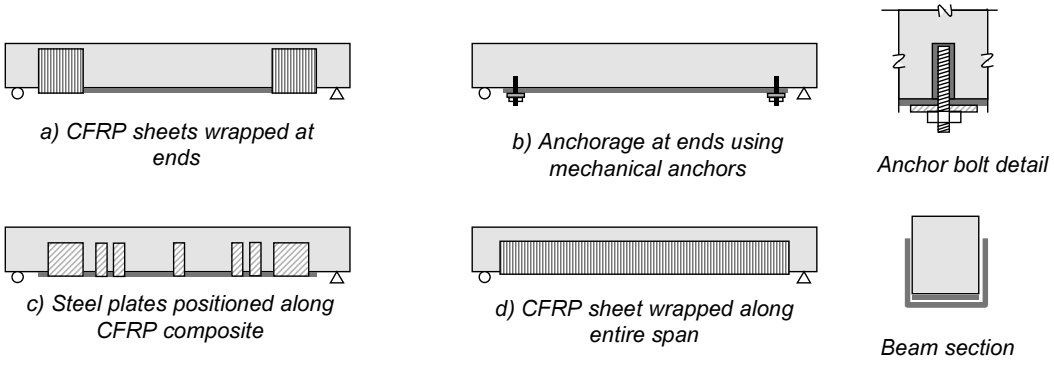

Figure 2.2 Techniques used by Previous Researchers to Anchor Longitudinal CFRP Composites

Table 2.2 Summary of Previous Investigations on Flexural Tests

Test Series	Research Group	Experimental Parameters
1	Ritchie, Thomas, Lu, and Connelly (1991)	• Composite type • Anchorage at end of plate
2	Arduini and Nanni (1997)	• Composite type • Shear span/depth ratio • Effect of precracking • Surface preparation
3	Norris, Saadatmanesh, and Ehsani (1997)	• Configuration of CFRP system • Fiber orientation
4	Arduini, DiTommaso, and Nanni (1997)	• Number of composite plates • Anchorage at end of plates
5	He, Pilakoutas, and Waldron (1997)	• Anchorage technique at ends of plates
6	David, Djelal, and Buyle-Bodin (1997)	• Composite type • Thickness and/or number of plies
7	GangaRao and Vijay (1998)	• Number of plies • Effect of precracking • Anchorage by wrapping with CFRP sheets
8	Spadea, Bencardino, and Swamy (1998)	• External anchorage for CFRP plates (to control slip)
9	Garden and Hollaway (1998)	• Shear span to depth ratio • Plate end anchorage
10	Ross, Jerome, Tedesco, and Hughes (1999)	• Existing reinforcement ratio • Effect of composite area to steel ratio
11	Grace, Sayed, Soliman, and Saleh (1999)	• Placement of CFRP system • Anchorage with vertical sheets

The ends of the composites received particular attention due to the normal stresses that are generated at the ends of the plates. To anchor the composite ends, the use of steel bolts or composite wraps were investigated (Figure 2.2a and b). However, these methods were only partially effective in delaying debonding of the composites. Anchoring the composites to the surface of the concrete at other locations along the span was required (Figure 2.2c). To develop the maximum strength of the composite in tension, composites wrapped along the entire beam length were used to anchor the longitudinal laminates [GangaRao and Vijay, 1998]. However, this technique can be extremely expensive because a large amount of material is required to strengthen a full-scale structure (Figure 2.2d).

Numerous anchoring techniques have been investigated without achieving uniform results. The locations where the CFRP composites require anchorage have been determined based on the characteristics of the particular specimens used in each research program. Additionally, the effectiveness of these anchoring techniques has not been evaluated in large-scale elements. Therefore, a uniform criterion is required for the design of the strengthening schemes using composites for its application to actual bridges.

Table 2.3 Summary of Flexural Tests by Previous Investigators

Group No.	No. of Beams	Strengthening Method				
		Control	CFRP	GFRP	AFRP	Steel
1	16	2	2	9	1	2
2	18	2	16	-	-	-
3	13	1	12	-	-	-
4	6	2	4	-	-	-
5	10	5	3	-	-	2
6	10	1	4	5	-	-
7	24	4	17	-	-	3
8	4	1	3	-	-	-
9	18	2	16	-	-	-
10	24	6	18	-	-	-
11	14	1	6	7	-	-

CFRP – Carbon FRP composite.

GFRP – Glass FRP composite.

AFRP – Aramid FRP composite.

Steel – Steel plates bonded to bottom.

Table 2.4 Geometry and Reinforcement of Flexural Specimens from Previous Investigators

Research No.	Section Properties						Span Geometry		
	b, in. (mm)	h, in. (mm)	d, in. (mm)	d', in. (mm)	A_s, in.^{2} (mm^2)	A'_s, in.^{2} (mm^2)	L, in. (mm)	a, in. (mm)	x, in. (mm)
1	6 (152)	12 (305)	-	-	0.4 (258)	-	96 (2,440)	36 (915)	24 (610)
2a*	12.5 (320)	6.3 (160)	4.3 (110)	2 (50)	0.4 (258)	0.4 (258)	43.3 (1,100)	16.5 (420)	10.2 (260)
2b*	6.3 (160)	12.6 (320)	10.6 (270)	2 (50)	0.62 (400)	0.62 (400)	82.7 (2,100)	37.4 (950)	7.9 (200)
3	5 (127)	8 (203)	-	-	0.22 (142)	0.22 (142)	90 (2,286)	22.5 (572)	45 (1,145)
4	8 (200)	8 (200)	6.4 (163)	1.5 (37)	0.48 (308)	0.48 (308)	78.7 (2,000)	27.6 (700)	23.6 (600)
5	6 (150)	10 (250)	8.5 (215)	1.4 (35)	0.97 (628)	0.1 (56)	90 (2,300)	30 (767)	30 (766)
6	6 (150)	12 (300)	-	-	0.48 (308)	-	110 (2,800)	35 (900)	40 (1,000)
7	6 (150)	12 (300)	10.6 (270)	1.2 (30)	0.88 (568)	0.22 (142)	107 (2,730)	35.8 (910)	35.8 (910)

Span Geometry

Note: Values not indicated in table were not reported in the literature.

* Beams from same investigation with different cross section and span.

Table 2.4 (Continued) Geometry and Reinforcement of Flexural Specimens from Previous Investigators

Research No.	Section Properties						Span Geometry		
	b, in. (mm)	h, in. (mm)	d, in. (mm)	d', in. (mm)	A_s, in.^{2} (mm^2)	A'_s, in.^{2} (mm^2)	L, in. (mm)	a, in. (mm)	x, in. (mm)
8	5.5 (140)	12 (300)	10.8 (275)	1 (25)	0.62 (400)	0.62 (400)	189 (4,800)	71 (1,800)	47 (1,200)
9a	4 (100)	4 (100)	3.3 (84)	3.3 (16)	0.13 (85)	0.09 (57)	40 (1,000)	Variable	32 (400)
9b$^+$	4 (100)	4 (100)	3.3 (84)	0.6 (16)	0.13 (85)	0.09 (57)	40 (1,000)	Variable	-
10	8 (200)	8 (200)	6 (152)	2 (48)	Variable	0.22 (142)	108 (2,742)	36 (914)	36 (914)
11^{++}	6 (152)	11.5 (292)	-	-	0.62 (400)	0.62 (400)	108 (2,742)	54 (1,371)	0

$^+$ Cantilever beam.

$^{++}$ Beams tested with single concentrated load at midspan.

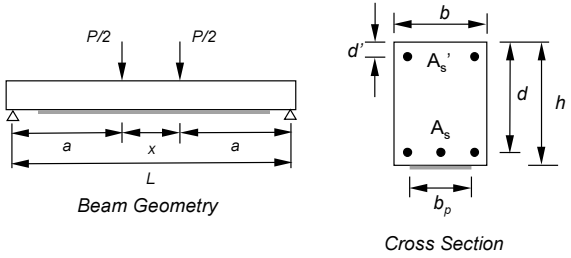

Table 2.5 Observed Failure Modes and Main Conclusions from Previous Flexural Tests

Test Series	Observed Modes of Failure	Main Conclusions
1	• Debonding after yielding of reinforcing steel	• Stress concentration at end of plates needs more study • Selection of bonding agent is critical
2	• Debonding at adhesive-concrete interface • Shear-peeling at ends of plates	• Improve concrete-FRP adhesion • Wrapping entire length effective as anchorage
3	• Debonding of FRP composite	• Fiber orientation has large effect on maximum strength • Pre-cracking has negligible effect
4	• Concrete crushing • FRP composite debonding • Shear at ends of plates	• Brittle failure modes need to be considered in design • Need to improve knowledge on adhesion performance
5	• Peeling-off at end of plates • Shear/peeling-off	• Peeling-off related to thickness and stiffness of plates • Unless anchored, plates peel off
6	• Peeling-off along concrete cover	• Use anchoring system to avoid brittle mode of failure
7	• Debonding • Crushing (fully wrapped beams) • Debonding along concrete cover	• Full wrap required to achieve maximum strength without debonding
8	• Debonding if not anchored • Gradual slip if anchored	• Anchorage required for adequate performance
9	• Shear/Peeling along concrete cover • Debonding	• Failure mode depends on shear span/depth ratio • Anchorage required at ends especially for low a/d ratios
10	• Concrete crushing (high ρ) • FRP debonding (low ρ)	• Unable to develop full FRP strength without anchorage
11	• FRP rupture if transverse sheets are used along entire length • Debonding when plates are placed on bottom of beams	• Wrapping along full length of CFRP increases maximum load • Bonding plates on bottom and sides improves performance

2.3.2 Flexural Tests of Large-Scale Specimens

Very few tests have been conducted on large-scale strengthened specimens that do not have a rectangular cross section. A testing program was conducted on strengthened half-scale beams by the Florida DOT [Shahawy and Beitelman, 1996]. A total of eight tee-beams representative of a type of bridge

construction in Florida were tested, both under static and fatigue loads. They were strengthened using three different types of CFRP laminates wrapping the entire length of the specimens (Figure 2.3). The results reported indicate that strengthening existing elements using CFRP composites is a viable option. However, it is evident that the configuration that was used would demand a significant amount of material.

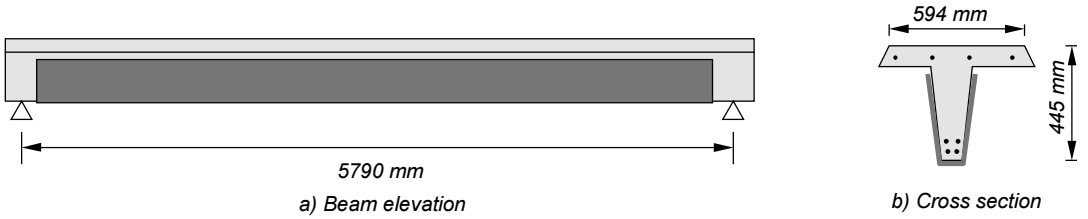

Figure 2.3 Strengthening of Tee-Beams Using CFRP Composite Sheets [Shahawy and Beitelman, 1996]

2.3.3 Tests to Characterize the Concrete-Composite Interface

A common observation in the research projects reported in Section 2.3.1 was that the behavior of the interface between the concrete and the composite needed further study to be able to calculate the capacity of the strengthened members reliably. Therefore, several investigators designed laboratory specimens to obtain more information about the behavior of the composites. However, the mechanisms that are involved in the debonding phenomenon are difficult to replicate with a simple testing apparatus.

Chajes et al. [1996] studied the effects of surface preparation, concrete strength, and adhesive type on the bond strength of single lap joints between composite plates and a concrete block (Figure 2.4). In these tests, the length of the joint was kept constant to identify the set of parameters that gave the highest strength. The ideal parameters were then used to investigate the force transfer between the composites and the surface of the concrete by attaching strain gages to the composites along the length of the connection. The test results indicated that the maximum measured load did not increase when the bonded length was more than 4 in.

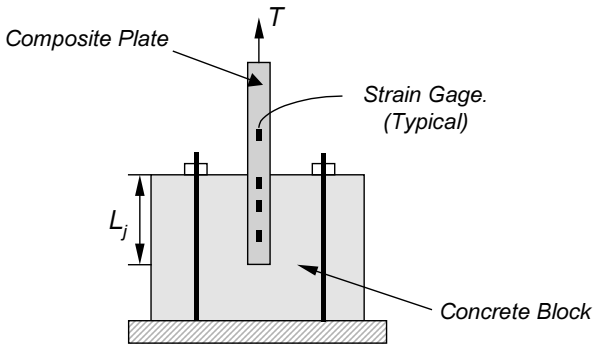

Figure 2.4 Direct Shear Test Apparatus

Bizindavyi and Neale [1999] conducted similar tests of carbon and glass fiber composite laminates bonded to concrete. The effects of multiple plies on the bond transfer characteristics were investigated. Their findings indicate that the maximum strengths of 1-ply and 2-ply, 25-mm CFRP laminates can be developed using bonded lengths equal to 80 and 220 mm, respectively.

Other researchers have investigated the effect of cracking in the distribution of bond stresses along the composite-concrete interface. Iketani and Jinno [1997] used the test specimen illustrated in Figure 2.5 to study the transfer of shear stresses between the surface of the concrete and CFRP composite sheets. This figure illustrates a pair of concrete blocks that are held together through the use of CFRP sheets bonded on both sides. Tension loads were applied through a steel bar that was cast in each concrete block. The CFRP sheets were instrumented using strain gages to quantify the distribution of strain with distance from the concrete discontinuity. The variables investigated included the influence of concrete strength and number of plies on the maximum load that could be applied to the bar pullout specimens.

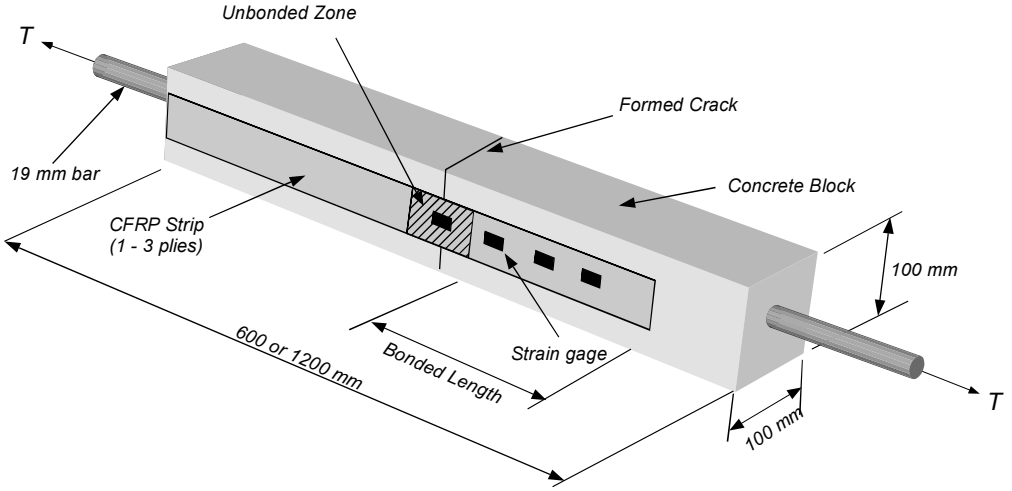

Figure 2.5 Bar-Pullout Bond Test Apparatus [Iketani and Jinno, 1997]

The main conclusions from this study were:

- The concrete strength had little influence on the maximum applied load.
- As the number of layers of CFRP sheets increases, the stiffness of the composite increased and caused shear stresses to be distributed more uniformly along the bonded length.
- Bonded lengths of more than 100 mm did not result in an increase in the maximum measured load.
- Debonding started from the position of the concrete discontinuity and proceeded toward the end of the composites.

From these tests, the variation of shear stress at the interface between the composite and the surface of the concrete with distance from the free edge has been identified. The distribution of shear stresses along the composite-concrete interface is illustrated schematically in Figure 2.6. The distance where the interface shear stresses can be considered negligible varied in the different investigations, but it typically ranged between 100 and 275 mm.

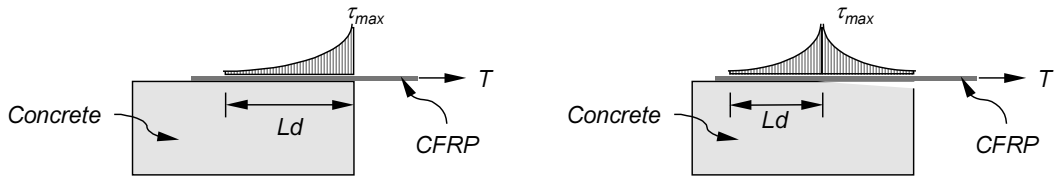

a) Shear stress distribution in uncracked concrete

b) Shear stress distribution in cracked concrete

Figure 2.6 Variation of Interface Shear Stress with Distance [Brosens and VanGemert, 1997]

All the previous research presented in this section focused on the determination of stresses caused by an applied force parallel to the concrete surface. However, the mechanisms involved in an actual strengthened element subjected to bending are diverse and can be caused by several factors. The different phenomena that can initiate peeling along the interface between the composite and the surface of the strengthened element were summarized by Blaschko et al. [1998]. They identified five different modes of peeling that can originate in a strengthened flexural member (Figure 2.7):

- FRP peeling-off at the outermost flexural crack in the uncracked anchorage zone (Mode 1).
- FRP peeling-off at flexural cracks in the area of maximum moment (Mode 2).
- FRP peeling-off at flexural cracks between the outermost crack and the area of maximum moment (Mode 3).
- FRP peeling-off caused by shear cracks (Mode 4).
- FRP peeling-off caused by unevenness of the concrete surface (Mode 5).

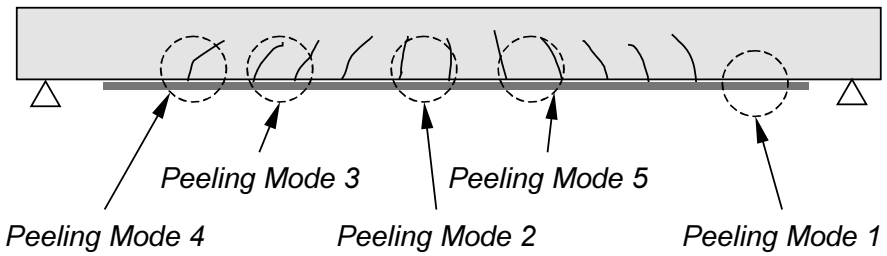

a) Location for different peeling modes

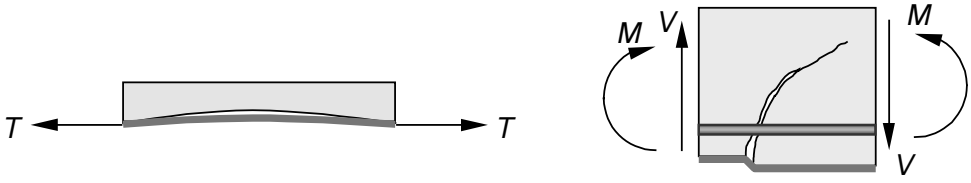

b) Detail for Mode 5

c) Detail for Mode 4

Figure 2.7 Regions in Strengthened Beam where Different Peeling Modes Initiate [Blaschko et al., 1998]

As can be noted from the previous discussion, different failure modes associated with local conditions between the composite and the surface of the concrete can occur in a strengthened element. An efficient way to eliminate the occurrence of these failure modes has not yet been developed; therefore, current efforts should be focused towards delaying debonding of CFRP composites, rather than preventing it entirely.

2.4 BEAMS TESTED UNDER FATIGUE LOAD

The fatigue behavior of strengthened reinforced concrete beams has received much less attention than behavior of beams under static loading. Recently, researchers have reported on the behavior of RC beams strengthened with CFRP composites subjected to repeated loading [Kaiser, 1989; Deuring, 1993; Barnes and Mays, 1999; Shahawy and Beitelman, 1999]. Table 2.6 lists the research groups and number of specimens tested in each of the investigations. Table 2.7 gives a summary of the main characteristics of the specimens tested by the different research groups.

Table 2.6 Summary of Tests of Beams under Fatigue Loading

Test Series	Research Group	Number of Specimens	Cross Sectional Shape	Composite Type
1	Kaiser (1989)	1	Rectangular	Hybrid (33% Carbon/67% E-glass) Sheet
2	Deuring (1993)	1	Tee	CFRP Sheet
3	Barnes and Mays (1999)	5	Rectangular	CFRP Pultruded Plates
4	Shahawy, Beitelman (1999)	6	Tee	CFRP Fabric

In many tests, failure was controlled by fracture of the reinforcement indicating that the performance of the FRP composites was adequate for repeated applications of load. None of the studies reviewed here reported debonding of the composite from the surface of the concrete as a failure mode. However, all the specimens were strengthened using the composites over the entire span of the beams. Additionally, Barnes and Mays [1999] used a steel plate covering the end of the composite plates to prevent peeling at the plate ends. Shahawy and Beitelman [1999] wrapped the composite fabrics to cover the entire stem of the specimens (Figure 2.3) to avoid debonding.

The characteristics of the loading sequence for the different research groups is presented in Table 2.8. The stress ranges that were generated on the reinforcing bars and composites during cycling are also listed in this table. The failure characteristics of the different specimens are listed in Table 2.9. The number of cycles in the table corresponds to the first observed fracture in the reinforcement or composites, although cycling was continued in several specimens.

The main conclusion of the different research groups is that the fatigue performance of the specimens was noticeably improved as compared to the unstrengthened control beams. Additionally, the performance of damaged elements was improved by the application of CFRP composites in the tests by Shahawy and Beitelman [1999]. However, it was also indicated that further tests were required to corroborate these results due to the limited number of tests in the literature.

Table 2.7 Geometry and Reinforcement of Specimens Subjected to Fatigue Loads from Previous Researchers

Test Series	Section Properties								Span Geometry		
	b, in. (mm)	h, in. (mm)	b_f, in. (mm)	t_f, in. (mm)	d, in. (mm)	d', in. (mm)	A_s, in.^{2} (mm^2)	A'_s, in.^{2} (mm^2)	L, in. (mm)	a, in. (mm)	x, in. (mm)
1	12 (300)	10 (250)	-	-	-	-	0.16 (100)	0.16 (100)	79 (2,000)	26 (667)	26 (666)
2	10.2 (260)	20 (500)	35.4 (900)	6.3 (160)	-	-	3.29 (2,124)	0.44 (314)	236 (6,000)	*	*
3	5.2 (130)	9.1 (230)	-	-	8 (205)	-	0.6 (340)	0.16 (100)	82.7 (2,100)	36.2 (920)	10.2 (260)
4	3.6 (91)	17.5 (445)	23 (584)	3.5 (89)	13.5 (342.5)	2 (50)	1.76 (1,135)	0.44 (284)	228 (5,790)	76 (1,930)	76 (1,930)

* Four loads were used along the span of the beam in this test. The distance from the support at each end of the beam to the load points were 53.5 in. (1360 mm) and 74 in. (1880 mm).

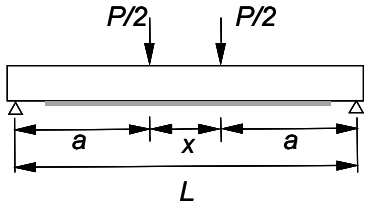

Beam Geometry

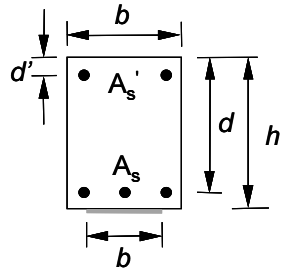

Rectangular Section

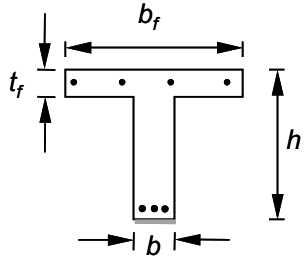

Tee section

Table 2.8 Loading Sequence and Stress Ranges of Specimens Subjected to Fatigue Loads from Previous Researchers

Test Series	Specimen Number	Loading Parameters				Reinforcing Bar Stress, ksi (MPa)		FRP Stress, ksi (MPa)	
		P_{min}, kip (kN)	P_{max}, kip (kN)	P_{max}/P_u	Frequency, Hz	Min	Max	Min	Max
1	-	0.2 (1)	4.3 (19)	-	4	3 (21)	59 (407)	1.6 (11)	29.7 (205)
2	-	28.3 (125.8)	63.8 (283.4)	0.35	-	19 (131)	38 (262)	14.8 (102)	30.4 (210)
3	1	0.9 (4)	9 (40)	0.48	1	4.4 (30)	44 (304)	-	-
	2	0.7 (3)	7.2 (32)	0.39		3 (21)	35.2 (243)		
	3	1.1 (5)	11 (49)	0.39		4.2 (29)	44 (303)		
	4	0.9 (4)	9 (40)	0.32		3.6 (25)	35.8 (247)		
	5	0.7 (2.9)	7.2 (32)	0.26		2.6 (18)	28.7 (198)		
4	C-0L5-FA	11.1 (49.2)	22.1 (98.4)	0.5	1	15 (103.4)	30 (206.9)	-	-
	C-2L5-FB			0.5					
	F-2L5-A			0.37					
	F-2L5-B			0.37					
	F-3L5-A			0.34					
	F-3L5-B			0.34					

Table 2.9 Failure Characteristics of Specimens Subjected to Fatigue Loads from Previous Researchers

Test Series	Specimen Number	Failure Parameters		Notes
		Number of Cycles	Mode of Failure	
1	-	480,000	Steel Fracture	Number of cycles indicates fracture of first reinforcing bar although cycling was continued
2	-	12,000,000	Steel Fracture	After 10.7×10^6 cycles, testing was continued in an environmental chamber at 40ºC and 95% relative humidity
3	1	20,000	Steel Yield	Control
	2	732,600	Steel Yield	Control
	3	508,500	Steel Fracture	Maximum load represented the same percentage of the ultimate load as for specimen 2
	4	1,889,087	Steel Fracture	Stress range in the reinforcement approximately equal to the stress range of specimen 1
	5	>11,968,200	No Failure	-
4	C-0L5-FA	150,000	Steel Fracture	Control; stirrups welded to longitudinal reinforcement
	C-2L5-FB	2,000,000	CFRP Fabric Rupture	Strengthened after applying 150,000 cycles
	F-2L5-A	1,800,000	CFRP Fabric Rupture	Accumulation of damage was characerized by a loss of stiffness in the load-deflection plots after different numbers of cycles
	F-2L5-B	1,756,000	CFRP Fabric Rupture	
	F-3L5-A	3,000,000	CFRP Fabric Rupture	
	F-3L5-B	3,215,000	CFRP Fabric Rupture	

2.5 SUMMARY

The conclusions from previous investigations on the behavior of strengthened reinforced concrete elements using CFRP composites were presented in this chapter. From this review, it is evident that, although the benefits that can be obtained from strengthening flexural members are well identified, there are still areas where further research is required. In particular, most of the previous research was conducted on small-scale specimens where local effects can have a large impact on the global response.

The need to understand the bond behavior between the composite and the surface of the concrete was a consistent conclusion from previous investigations. A summary of previous efforts in this area was also presented. It was found that this phenomenon is highly dependent on local surface and damage conditions and is consequently very difficult to quantify.

Given the limited amount of information available from previous research in the area of strengthening existing members with composites, testing full-scale specimens representative of actual bridges was considered a priority for this research project. Instead of approaching the debonding problem at the local concrete-composite interface level, the approach that was taken in this project was to delay total failure of the strengthened element by using techniques that would control debonding of the composite in an economic manner. For this purpose, a large number of specimens incorporating different strengthening techniques and composite materials were tested in this research project. The results of these tests are presented in the following chapters of this report. Results from the large-scale tests are included in a companion report.

Under fatigue loading, reinforced concrete beams strengthened using CFRP laminates exhibit better performance than reinforced concrete beams. However, fatigue failure of strengthened beams appears to be controlled by fracture of the reinforcing bars in fatigue. Further tests are needed to corroborate the available results and to evaluate the importance of other variables, such as the configuration of the composites.

Chapter 3: Analytical Model to Calculate the Flexural Response of Reinforced Concrete Elements Strengthened Using CFRP Composites

3.1 INTRODUCTION

This chapter describes an analytical procedure that was developed to calculate the moment-curvature and load-deflection response of reinforced concrete members strengthened using CFRP composites. The procedure uses the nonlinear material properties of concrete, steel, and CFRP composites to calculate the internal forces corresponding to equilibrium for a strengthened section. Moment and curvature are then calculated from the internal forces, and deflections along the span are calculated from the moment-curvature relationship.

Procedures used to calculate the moment-curvature response of a strengthened section are described in Section 3.2, and procedures used to calculate deflections are described in Section 3.3. The model is verified in Section 3.4 using published data for reinforced concrete elements strengthened with CFRP composites.

3.2 MOMENT-CURVATURE ANALYSIS OF STRENGTHENED SECTIONS

The analytical procedure described in this chapter is based on a sectional model. Moment-curvature relationships for reinforced concrete sections strengthened with carbon fiber reinforced composites were calculated using nonlinear material properties. Basic assumptions are presented in Section 3.2.1 and the idealized stress-strain curves for the materials are presented in Section 3.2.2.

3.2.1 Assumptions Used in the Sectional Analysis Model

Similarly to most analytical methods used to calculate the flexural response of reinforced concrete elements, the cross section was divided into horizontal slices. The total response of the cross section is obtained by adding the contribution of each slice. Separate slices were used for the different materials; therefore, the idealized behavior of each slice is controlled by the stress-strain relationship for a given material. However, multiple slices may be located at the same position along the depth of the cross section.

The following assumptions, which are consistent with current design practice of reinforced concrete sections, were used in the model:

- Strains increase proportionally with distance from the neutral axis.
- No slip occurs between the steel reinforcement and concrete surrounding it.
- Perfect bond exists between the carbon fiber reinforced composite material and concrete surface.
- Failure is reached when the extreme fiber in compression reaches the maximum usable strain in the concrete (ε_{cu}).

The third assumption was later refined because the CFRP material was observed to slip relative to the concrete surface during the experimental phase of this project. Modifications to the analytical model to include debonding of the CFRP and concrete are discussed in the research report for phase 3 of this project.

3.2.2 Stress-Strain Material Models Used for Sectional Analysis

Three material models were used to calculate the response of the strengthened reinforced concrete sections. The models represent the uniaxial stress-strain behavior of the materials in the cross section. The parameters that are needed to define each material model were based on the measured material properties for concrete and steel, and data from the manufacturers for the CFRP composites (Appendix A).

(a) Concrete

The uniaxial stress-strain behavior of concrete in compression was modeled using the curve proposed by Hognestad [1950]. In this model, the ascending branch of the compressive stress-strain curve is modeled with a parabolic relationship. The maximum concrete stress is defined as f''_c, and the strain corresponding to the maximum stress is called ε_{co}. The peak compressive stress was calculated as the product of a constant k_3, which was set equal to 0.9, and the compressive stress determined from concrete cylinder tests, f'_c. The constant k_3 is defined as the ratio of the compressive stress as determined from compression tests on concrete cylinders to the maximum compressive stress reached in the concrete in the actual member [Hognestad et al., 1955; Rüsch, 1960]. After this point, stresses decrease linearly with increasing strain until the maximum usable strain in the concrete is reached (ε_{cu}). The stress corresponding to the maximum concrete strain is assumed to be equal to 85 percent of the peak stress. The equations that describe the behavior of concrete in compression for the different regions of the stress-strain diagram are presented in Figure 3.1.

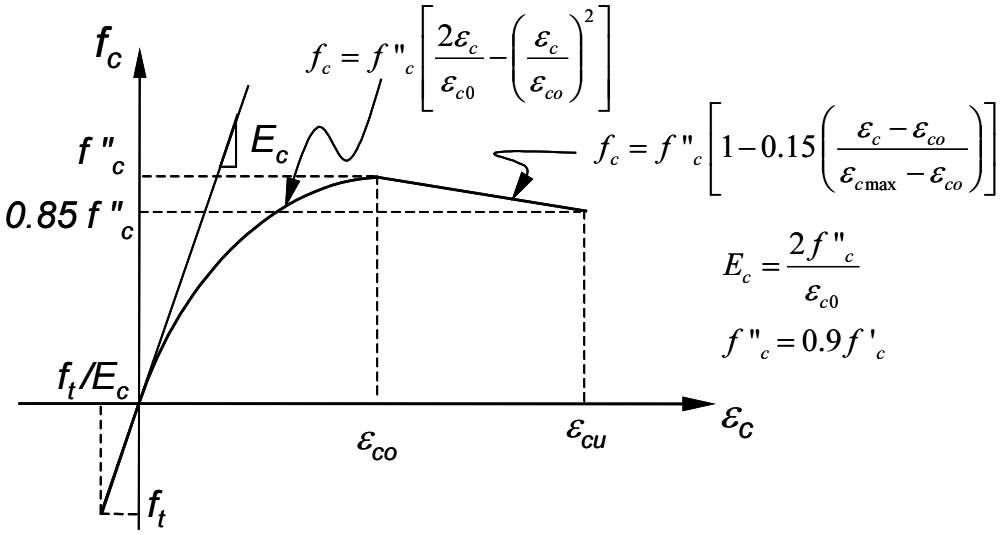

Figure 3.1 Idealized Stress-Strain Relationship for Concrete

Concrete in tension was assumed to behave linearly up to the stress corresponding to its tensile capacity (f_t). After this point, the tensile strength of concrete was assumed to be equal to zero. The slope used for the concrete stress-strain relationship in tension was assumed to be equal to the initial tangent modulus of elasticity in compression (E_c).

Compressive tests of cylinders and split-cylinder tests were used to define the parameters in the concrete model. The concrete cylinders were fabricated using the same concrete mixture that was used for the construction of the specimens. The concrete stress-strain parameters determined for the laboratory specimens are listed in Appendix A. When actual material strengths were not available, f'_c was assumed

to be the specified compressive strength of concrete used for design, f_t was assumed to be equal to $0.1\ f'_c$, and ε_{co} was assumed to be equal to 0.002. The maximum usable strain of concrete, ε_{cu}, was considered to be equal to 0.004.

(b) Reinforcing Steel

The stress-strain relationship for steel reinforcement with a well-defined yield point was idealized using three linear segments. The elastic modulus for the initial slope in the stress-strain curve (E_s) was assumed to be 29,000 ksi. After reaching the yield strain (ε_y), the slope of the stress-strain curve was assumed equal to zero until the strain corresponding to initiation of strain hardening (ε_{sh}) was reached. The strain-hardening behavior of the reinforcement was modeled using a line with a positive slope beginning at ε_{sh}. Details of the material stress-strain model are shown schematically in Figure 3.2.

Steel coupons were tested in tension for the different bar sizes used in the fabrication of the specimens. Using these tests, the values that define the stress-strain parameters for the bars were determined. The slope of the line corresponding to the strain-hardening region, E_{sh}, was calculated as the slope of a line going from the stress at ε_{sh} to the stress at a strain equal to 0.015. If steel with unknown properties was used in the calculations, the E_{sh} was assumed to be equal to 5% of the initial elastic modulus.

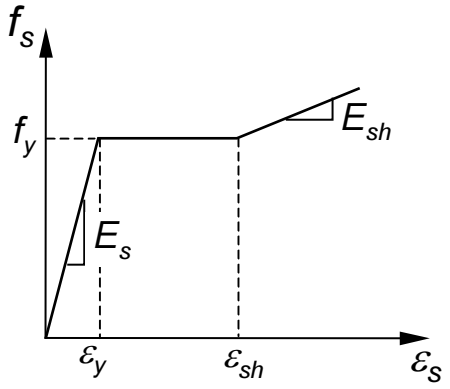

Figure 3.2 Idealized Stress-Strain Relationships for Steel

(c) Fiber Reinforced Polymer Composites

The uniaxial behavior of the carbon fiber reinforced polymer composites (FRP) used in this study was assumed to be linear up to failure (Figure 3.3). Failure in these materials was reached when the strain (ε_{pu}) corresponding to the rupture stress (f_{pu}) was reached.

The properties published by the manufacturers were used to define the material models for the different carbon fiber reinforced polymer materials. The values for these parameters are summarized in Appendix A for the composites used in this research project.

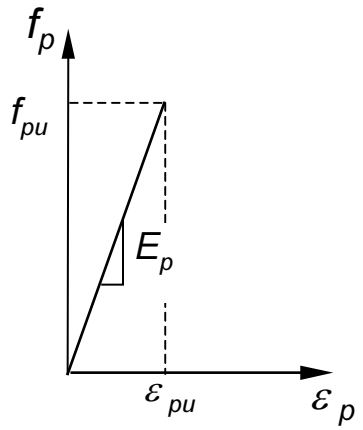

Figure 3.3 Idealized Stress-Strain Relationship for CFRP Composites

3.2.3 Internal Equilibrium of Strengthened Cross Section

The moment-curvature response of a reinforced concrete section strengthened with CFRP composites was calculated by dividing the section into horizontal slices and assigning specific material properties to each slice. The procedures used to calculate the stress and strain in each slice and to calculate the corresponding moment and curvature are described in this section.

Internal force equilibrium was established for a series of maximum concrete compressive strains. Moment and curvature were calculated at each point corresponding to the maximum concrete strain assigned to the extreme fiber under compression.

The procedure used to calculate moment and curvature of a strengthened section is described in the following steps:

- Set the maximum compression strain in the concrete (ε_{cmax}) to a value between zero and the maximum usable concrete strain (ε_{cu}).
- Estimate an initial neutral axis position. The initial neutral axis position was assumed to be h/2 in this study.
- Calculate the strain profile based on the extreme compression fiber strain and the position of the neutral axis and then compute the corresponding internal stress components using the material models discussed in Section 3.2.2.
- Check equilibrium in the horizontal direction using the internal stresses computed in step 3 and the known area of each slice.
- Adjust the neutral axis depth, *c*, until force equilibrium is achieved (repeat steps 1 through 4). A tolerance of 0.05 kip was used in this study.
- Calculate the internal moment and curvature.
- Increase ε_{cmax} and repeat steps 1 through 6 for another point in the moment-curvature response.

The internal stress within each slice was calculated at mid-thickness and was assumed to be constant throughout the slice. The stress distribution was approximated by a series of rectangles having a depth equal to the slice thickness and height equal to the compressive stress calculated from the stress-strain equations. The force contribution from each slice was computed using the width of the cross section at the slice mid-plane (b_i) and the slice thickness (t_{slice}). This is illustrated for sections that have a nonrectangular cross section in Figure 3.4b.

The internal force components were multiplied by their distance to the neutral axis, z_i, to calculate the internal moment (Figure 3.4). Curvature was calculated by dividing the extreme compressive strain by the neutral axis depth:

$$M = \sum_i F_i \, z_i$$
$$\phi = \frac{\varepsilon_{c\ \max}}{c} \tag{3.1}$$

where,

M = Internal moment, kip-in.

ϕ = Curvature, 1/in.

F_i = Internal tensile or compressive force component, kip.

z_i = Distance from neutral axis to internal force component, F_i, in.

$\varepsilon_{c\ max}$ = Strain at the extreme compression fiber.

c = Neutral axis position, in.

The procedure described above was repeated for other points in the moment-curvature diagram of the section until the maximum usable concrete strain was reached in the extreme compression fiber.

The model initially assumed that the CFRP composites remained attached to the concrete surface. Using this assumption, the maximum stress that can be developed in the CFRP is equal to the rupture stress, f_{pu}. The contribution of the CFRP composite to the total tensile force became zero once the rupture stress was reached. However, experimental testing showed that debonding usually occurred before reaching the CFRP rupture stress, and the model was subsequently modified to incorporate this failure mode in the design of the large-scale specimens for phase III of this research project.

The procedure described above to calculate moments and their associated curvatures assumes that the CFRP composites are attached to the reinforced concrete section before any load is applied. However, dead loads are always on a structure before strengthening and this needs to be considered particularly for field applications. A modification to the procedure presented in this section is described in the research report on the large-scale tests. This procedure was implemented to account for the presence of dead loads on the section before bonding the CFRP composites.

3.3 LOAD-DEFLECTION RESPONSE

The calculated moment-curvature relationships for the strengthened members were used to determine deflections. Deflections were calculated using the moment-area method because this method is applicable to members that have a nonlinear moment-curvature relationship.

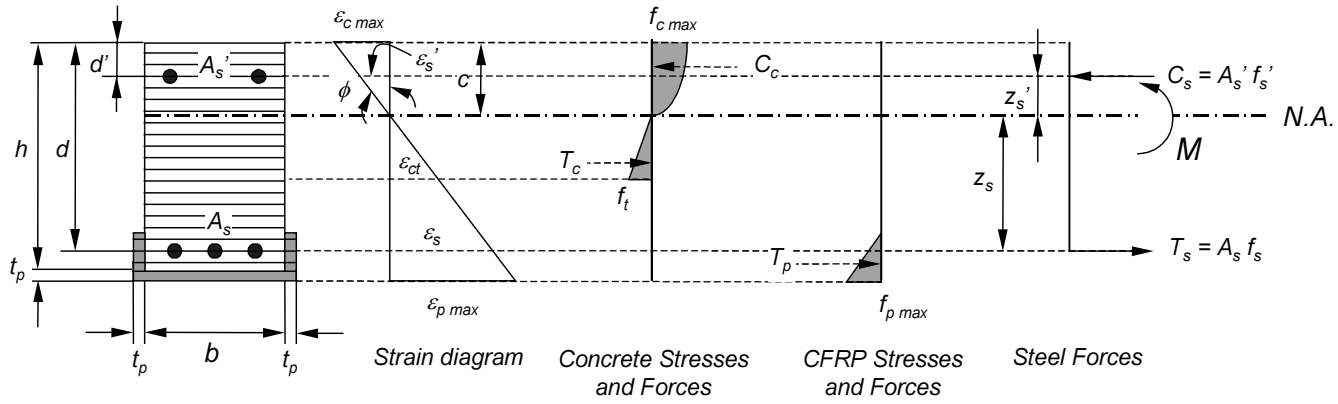

(a) Internal Stresses and Forces in Strengthened Section

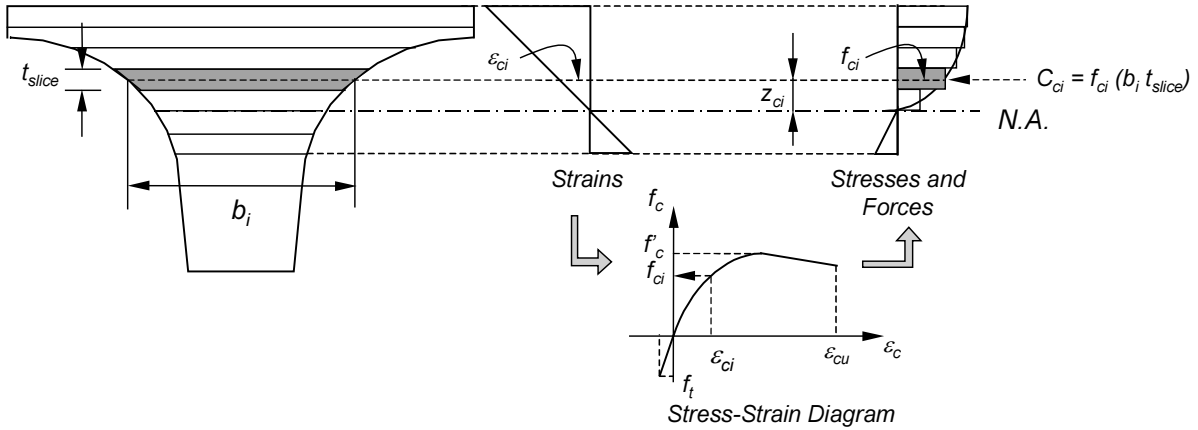

(b) Calculation of Compressive Stresses

Figure 3.4 Schematic Representation of Sectional Response Illustrating the Procedure Used in the Calculations

The moment-area method is summarized in this section (Figure 3.5). First, the moment diagram was calculated for a specific span length and configuration of loading. Then, the curvature at every point along the span was determined using the moment-curvature relationship calculated previously for the cross section.

After determining the curvature diagram along the span, rotations and deflections at any point may be calculated using the moment-area theorems. Numerical integration of the curvature diagram was used to determine the rotations and deflections of tangents to the deflected shape. The change in rotation of the tangents to the deflected shape at two points is determined by computing the area under the curvature diagram between the two points. The vertical distance between two tangents to the deflected curve at a point along the span is determined by calculating the first moment of area of the curvature diagram about the point of interest. Deflections are then determined from geometric considerations.

The procedure used to compute the deflection at point j, δ_j, of an element with a nonlinear moment-curvature relationship using the moment-area theorems is illustrated in Figure 3.5. This procedure can be summarized in the following steps for a simply supported beam:

- Determine the moment and curvature diagrams along the span. Curvatures associated with the moment at each location are obtained from the moment-curvature relationship of the cross section.

- Divide the curvature diagram into sufficient segments (twenty segments were used for this study). The curvature diagram is assumed to be linear within each segment. The curvatures defining an arbitrary segment, ϕ_i and ϕ_{i+1} are shown in Figure 3.5b.

- Calculate the area and centroid of each segment using the trapezoidal rule:

$$A_i = \left(\phi_i + \phi_{i+1}\right) \frac{\Delta x_i}{2}$$
$$\bar{x}_i = \left(\frac{\phi_i + 2\,\phi_{i+1}}{\phi_i + \phi_{i+1}} \right) \frac{\Delta x_i}{3} \qquad (3.2)$$

- Compute the first moment of area of each segment about point j, where the distance between tangents needs to be determined.

- Calculate the deflection at a point from geometric considerations using the tangents to the deflected shape.

The distance between two tangents to the deflected shape of the element is determined by taking moments of each segment about the desired point. For example, the distance between the tangents at points A and B is equal to the sum of the product of the area of each segment from the curvature diagram times the distance from point B to the centroid of each segment (Figure 3.5). The distance between two tangents at points A and j can be calculated similarly by computing the moment of the area of each segment on the curvature diagram about point j. The deflection at point j is calculated using Equation 3.4 after determining the distance y_j from similar triangles (Equation 3.5):

$$\delta_j = y_j - t_{A-j} \qquad (3.3)$$

where:

$$y_j = \frac{t_{A-B}}{l} X_j \tag{3.4}$$

and:

$$\begin{aligned} t_{A-B} &= \sum x_{i-B} A_i \\ t_{A-j} &= \sum x_{i-j} A_i \end{aligned} \tag{3.5}$$

The nomenclature used in Equations 3.4 to 3.6 and in Figure 3.5 is listed below:

δ_j = Vertical deflection at point *j*.

X_j = Horizontal distance from point *A* to point *j*.

y_j = Vertical distance from tangent at *A* to undeformed position at point *j*.

x_{i-B} = Horizontal distance from centroid of segment *i* to point *B*.

x_{i-j} = Horizontal distance from centroid of segment *i* to point *j*.

Ai = Area under the curvature diagram of segment *i.*

t_{A-B} = Vertical distance from tangent at point *A* to tangent at point *B.*

t_{A-j} = Vertical distance from tangent at point A to tangent at point *j*.

3.4 VERIFICATION OF MODEL

The analytical model presented in Sections 3.2 and 3.3 was evaluated using available experimental results. Data from some of the previous experimental investigations were used to validate the analytical model. Four experimental studies were selected for this purpose. All specimens in these studies were strengthened using CFRP systems similar to those used in this research project. Only a brief description and comparisons between the measured and calculated displacement response of these specimens are presented in this section.

Table 3.1 summarizes the dimensions and reinforcement for the specimens that were selected for the comparisons. The measured and assumed material properties are presented in Table 3.2. The CFRP composite was bonded to the tension face of the beams considered.

Debonding of the CFRP composites from the surface of the concrete was not considered as a possible failure mode in this part of the investigation. However, after review of the available data and results from this experimental program, it is clear that this mode of failure often controls the behavior of strengthened reinforced concrete members. A procedure for including debonding of the CFRP composites from the concrete surface is introduced in a separate research report.

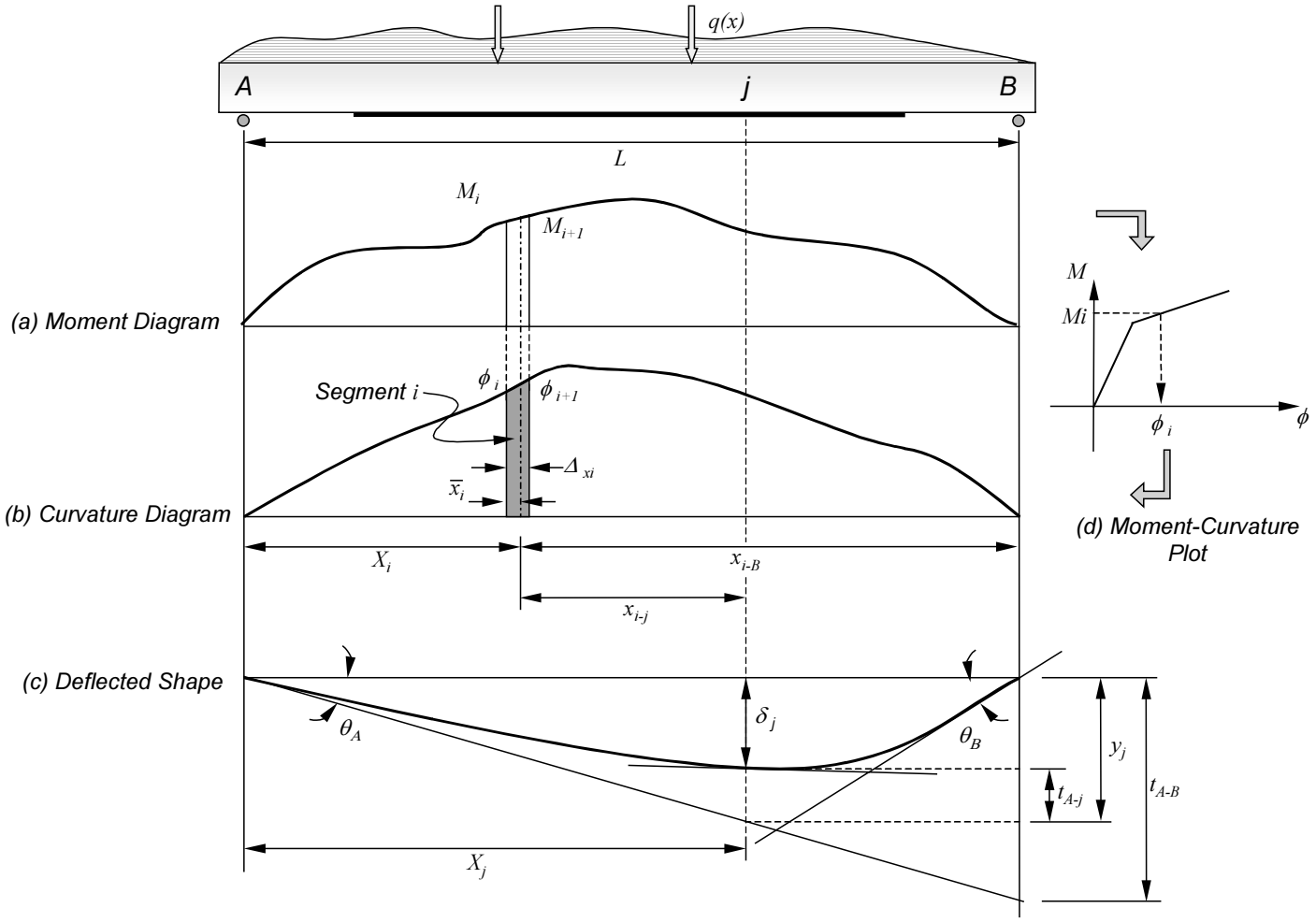

Figure 3.5 Procedure to Calculate Deflections of an Element with a Nonlinear Moment-Curvature Relationship

Table 3.1 Dimensions and Reinforcement of Specimens Reported by Other Researchers

Specimen	b, mm	h, mm	d, mm	d', mm	L, mm	x, mm	a, mm	A_s	A_s'
Spadea et al. (1998)									
A3, A3.3	140	300	275	25	4,800	1,200	1,800	2-16 mm	2-16mm
GangaRao et al. (1998)									
$1A_2$-R, $3B_2$-C	150	300	270	30	2,740	610	1,065	2-19 mm	2-10mm
Arduini et al. (1997)									
B1, B2, B4	300	400	350	50	2,500	300	1,100	3-13mm	2-13mm
Nakamura et al. (1996)									
BL, E24-1P, E24-2P	150	150	120	30	1,200	400	400	2-13mm	2-13mm

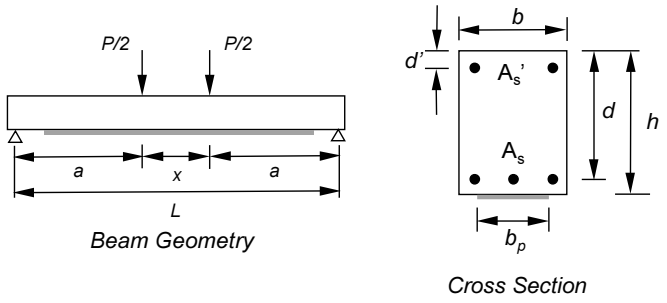

Table 3.2 Material Properties and Dimensions of CFRP Composites of Specimens Reported by Other Researchers

Specimen	f'_c, MPa	f_y, MPa	CFRP Composite				
			t_p, mm	b_p, mm	f_{pu}, MPa	E_p, GPa	Type
Spadea et al. (1998)							
A3	29.5	435	-	-	-	-	-
A3.3	30.5	435	1.2	80	2,300	152	Pultruded Plates
GangaRao et al. (1998)							
$1A_2$-R	50.2	415	-	-	-	-	-
$3B_2$-C	50.2	415	0.33	150	3,100	240	Sheets (3 Plies)
Arduini et al. (1997)							
B1	26	340	-	-	-	-	-
B2	26	340	0.17	300	3,000	400	Sheets (1 Ply)
B4	26	340	0.51	300	3,000	400	Sheets (3 Plies)
Nakamura et al. (1996)							
BL	23.5	410	-	-	-	-	-
E24-1P	23.5	410	0.098	150	3,430	235	Sheets (1 Ply)
E24-2P	23.5	410	0.196	150	3,430	235	Sheets (2 Plies)

Moduli of elasticity for concrete and steel were not reported. The values used in the calculations were:

$E_c = 2\ f'_c/0.002$, $E_s = 200{,}000$ MPa

3.4.1 Tests by Spadea, Bencardino, and Swamy

Spadea et al. (1998) investigated the effect of using steel plates to prevent debonding of the CFRP from the bottom concrete surface. The response of two specimens from their program were compared with the calculations from the analytical model developed in this study: Specimens A3 and A3.3. Specimen A3 was the control beam and Specimen A3.3 was strengthened using a CFRP pultruded plate. The CFRP plate in the strengthened specimen was anchored using steel plates at several locations along the span length. Although the measured strains in the CFRP composite in Specimen A3.3 were the highest in the test series, failure was still controlled by debonding of the CFRP from the concrete surface.

The responses of Specimens A3 and A3.3 are compared with the calculated responses in Figure 3.6. The vertical axis for the calculated response was truncated at 100 kN in order to facilitate comparisons with the measured results.

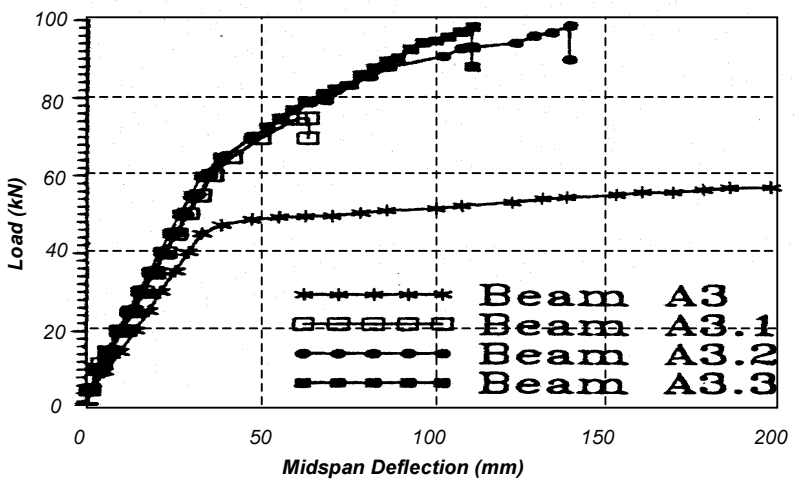

a) Measured Response

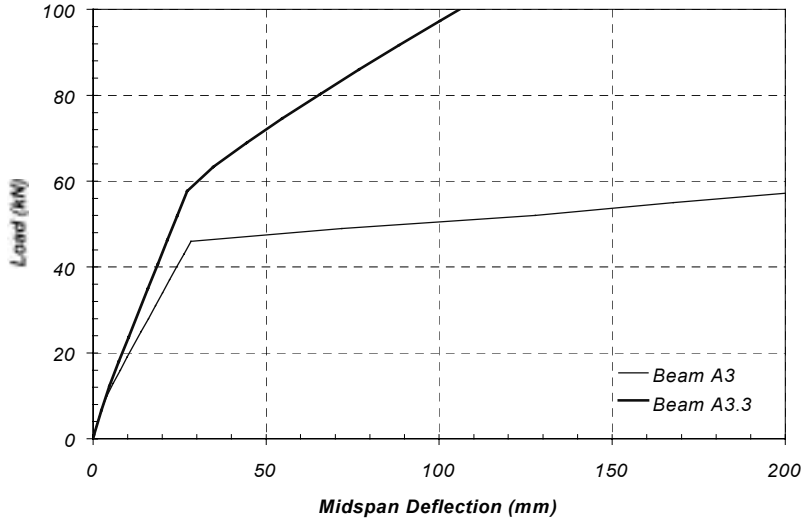

b) Calculated Response

Figure 3.6 Comparison of Load-Deflection Curves for Specimens A.3 and A3.3 Reported by Spadea et al. (1998)

The maximum measured loads are compared with the calculated capacities in Table 3.3. The calculations were based on assumed stress-strain relationships for the steel because these data were not available. A well-defined yield point was assumed. Strain hardening was assumed to begin at a tensile strain of 0.015, and the assumed slope of the stress-strain curve after the onset of strain-hardening portion was 5100 MPa (2.5% E_s). The same material properties were used for both specimens. The ratio of the measured to the calculated capacity was 0.94 for Specimen A3. This 6% difference was believed to be acceptable given the limited available information about the material properties.

Table 3.3 Summary of Results from Published Data and Analytical Model

Test Series	Specimen	P_{test}, kN	P_{calc}, kN	P_{test}/P_{calc}	ε_{calc} [1]	ε_{rupt} [2]	$\varepsilon_{calc}/\varepsilon_{rupt}$
Spadea et al.	A3	57.2	61.0	0.94	-	-	-
	A3.3	98.3	114.3	0.86	0.0112	0.015	0.75
GangaRao et al.	$1A_1$-R	115.7	111.3	1.04	-	-	-
	$3B_2$-C	191.4	185.2	1.03	0.0128	0.013	0.98
Arduini et al.	B1	90 *	85.6	1.05	-	-	-
	B2	170 *	182.7	0.93	0.0066	0.0075	0.88
	B4	270 *	371.8	0.73	0.0048	0.0075	0.60
Nakamura et al.	BL	51.9	54.1	0.96	-	-	-
	E24-1P	73.0	83.4	0.88	0.0093	0.015	0.62
	E24-2P	89.2	102.8	0.87	0.0088	0.015	0.59

***** Values estimated from published load-deflection curves.
[1] Calculated CFRP strain at maximum measured load, P_{test}.
[2] Strain corresponding to CFRP rupture, $\varepsilon_{rupt} = \frac{f_{pu}}{E_p}$.

The calculated capacity of Specimen A3.3 was higher than the maximum measured load. Failure of this specimen was caused by CFRP debonding from the concrete surface. Therefore, it should be expected that the analytical model would calculate a higher load because it assumes perfect bond between the composite and concrete until the composite reaches its rupture stress f_{pu}. In this case, the capacity ratio (P_{test}/P_{calc}) was 0.86.

The calculated strain in the CFRP plate at the maximum measured load in the tests is reported in Table 3.3. The ratio of ε_{calc}, the calculated strain at the measured capacity of the beam, to ε_{rupt}, the rupture strain of the material, gives an indication of the fraction of stress that was developed during the tests compared with the CFRP rupture stress. In this case, the CFRP achieved a stress of 75% of the rupture stress before the specimen failed by debonding.

3.4.2 Tests by GangaRao and Vijay

Two beams from the experimental program reported by GangaRao and Vijay (1988) were used for the comparison with the analytical model: Specimens $1A_2$-R and $3B_2$-C. Specimen $1A_2$-R was the control

beam companion to Specimen $3B_2$-C. The geometry and material properties for these specimens are included in Tables 3.1 and 3.2, respectively.

Specimen $3B_2$-C was strengthened after first cracking the concrete using a CFRP composite fabricated by a wet-layup procedure (Appendix C). This specimen was strengthened using 3 layers (plies) of CFRP sheets bonded to the tension face of the reinforced concrete beam. The sheets were made of unidirectional carbon fibers that were oriented longitudinally along the axis of the beam. An additional CFRP sheet was wrapped around the beam on top of the 3-ply, longitudinal sheets along the entire length to control slip of the CFRP composite.

A comparison of the load-deflection response of the two specimens is presented in Figure 3.7. Failure of both specimens was controlled by concrete crushing in the compression zone. The ratios of maximum measured to calculated loads are included in Table 3.3. The excellent correlation to the model in this case is a result of the failure mode experienced by Specimen $3B_2$-C (concrete crushing). No debonding of the CFRP composite was detected during the test, indicating that wrapping a sheet of CFRP along the entire length of the beam is an effective method of anchoring the sheets.

The ratio of calculated strain at maximum load (ε_{calc}) to CFRP rupture strain (ε_{rupt}) is presented in Table 3.3. This ratio is very close to 1.0 because the failure mode was controlled by crushing of the concrete and not debonding of the CFRP sheets.

3.4.3 Tests by Arduini, Di Tommaso, and Nanni

Arduini et al. (1997) tested square reinforced concrete beams strengthened using CFRP pultruded plates (Series A). They also reported the results of tests performed at Penn State University in 1995 of four rectangular beams strengthened using CFRP flexible sheets (Series B). Three beams from series B: Specimens B1, B2, and B4 were used for comparison to the analytical model in this chapter.

Beam B1 was the control specimen. Beams B2 and B4 were strengthened using 1 and 3 layers of CFRP sheets, respectively, bonded to the tension side of the specimens. These sheets were made with unidirectional carbon fibers and they were oriented longitudinally along the beams. An additional carbon fiber sheet was wrapped around the bottom and sides of Specimen B4 throughout the strengthened portion of the beam to avoid debonding of the longitudinal sheets. Details of the specimen geometry and reinforcement are summarized in Table 3.1. The reported material properties and the characteristics of the CFRP sheets are contained in Table 3.2.

Failure of Specimen B2 was controlled by CFRP rupture at midspan. Specimen B4 failed by concrete crushing at one of the loading points after local debonding of the transverse CFRP sheet was observed at several places.

Measured and calculated responses are compared in Figure 3.8. The plot reported by Arduini et al. (1998) was truncated at a displacement of 12 mm although it is apparent that Specimen B1 experienced larger displacements before failure. The calculated results are plotted to the same scale to facilitate comparisons.

The calculated response of Specimens B1 and B2 show excellent agreement with the measured data. Measured loads corresponding to cracking, yielding, and capacity are reproduced closely with the sectional model for both specimens. The ratio between the measured and calculated capacities for Specimen B2 was 0.93 (Table 3.3). In this case the model estimated the capacity closely because this specimen failed by rupture of the CFRP sheet, rather than debonding.

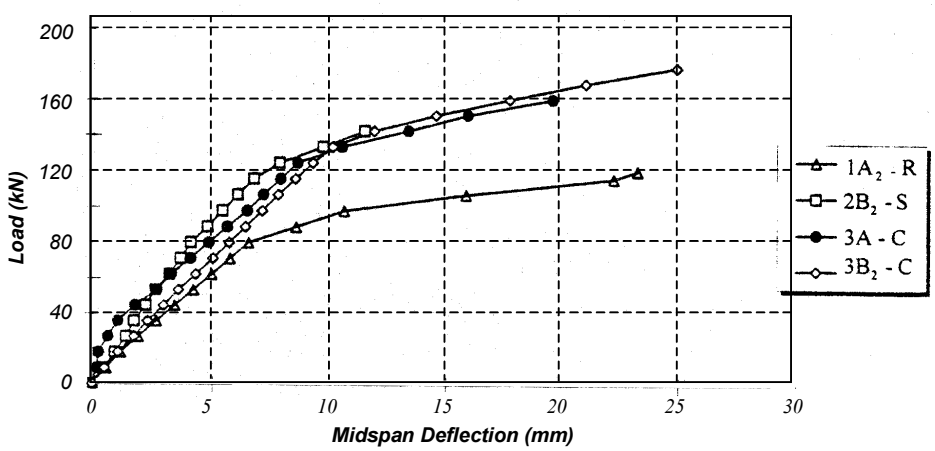

a) Measured Response

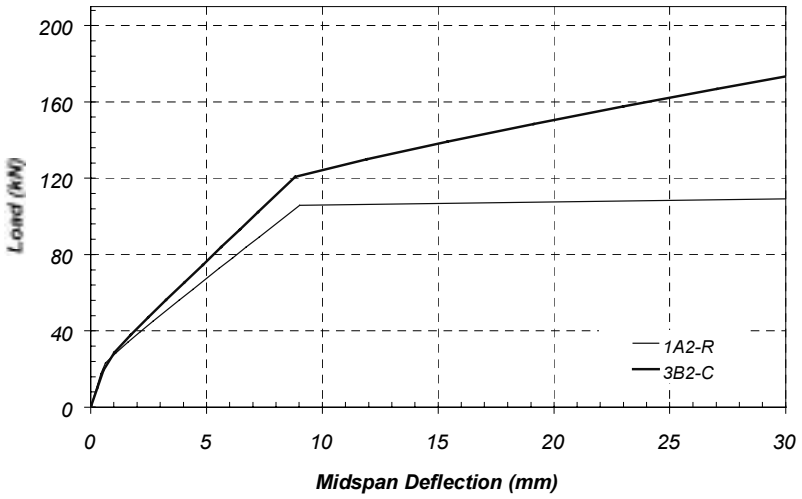

b) Calculated Response

Figure 3.7 Comparison of Load-Deflection Curves for Specimens $1A_2$-R and $3B_2$-C Reported by GangaRao and Vijay (1998)

The calculated and measured responses of Specimen B4 are also shown in Figure 3.8 and Table 3.3. The calculated curve was truncated at a load of 280 kN to facilitate comparison with the measured response, although the calculated capacity was over 370 kN (Table 3.3). The poor correlation with the measured response is due to the failure mode experienced by the specimen (crushing after localized debonding of the transverse sheet).

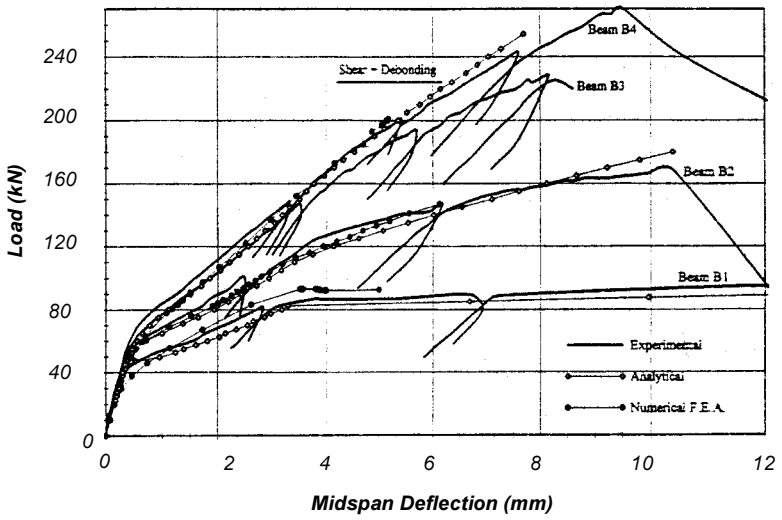

a) Measured Response

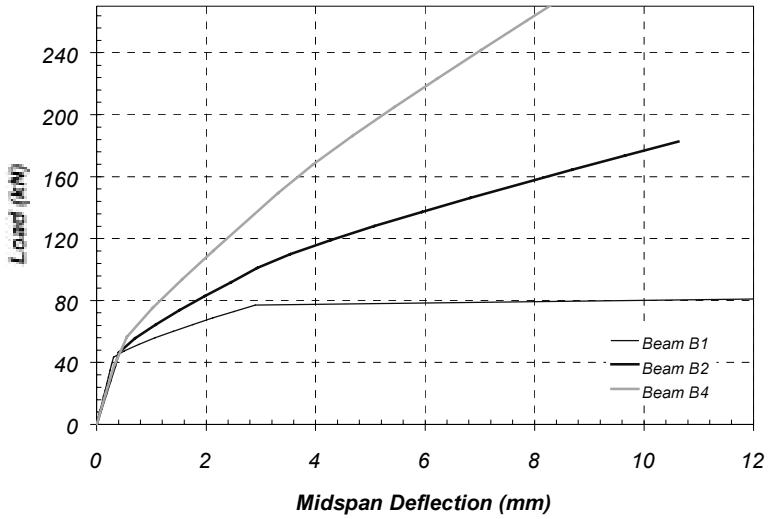

b) Calculated Response

Figure 3.8 Comparison of Load-Deflection Curves for Specimens B1, B2, and B4 Reported by Arduini et al. (1997)

3.4.4 Tests by Nakamura, Sakai, Yagi, and Tanaka

Nakamura et al. (1996) conducted tests on square reinforced concrete beams strengthened with two types of CFRP systems applied using a wet-layup procedure (Appendix C). The two systems had different elastic moduli and strengths (E24 and E64 Series). Only beams from the E24 Series and the control specimens were used for the comparison with the analytical model.

Beams in the E24 Series were strengthened by bonding either 1 or 2 layers of CFRP sheets to the bottom face of the specimens (Specimens E24-1P and E24-2P, respectively). The entire bottom face of the beams was covered with the CFRP sheets. Specimen BL was the control specimen for this series and was constructed with the same materials as the other specimens in this group. The geometry of the specimens

and the loading configuration are summarized in Table 3.1. The properties of the materials used in the specimen fabrication and the characteristics of the CFRP system used in the E24 Series are contained in Table 3.2.

The plots showing the measured and calculated load-deflection response are shown in Figure 3.9. Both strengthened specimens (E24-1P and E24-2P) failed when the CFRP sheets debonded from the concrete surface. Therefore, the analytical model calculated higher loads than those reached during the tests. The measured to calculated ratios are 0.88 and 0.87 for Specimens E24-1P and E24-2P, respectively (Table 3.3). The difference in loads is again due to the assumption of perfect bond between the concrete surface and CFRP composite.

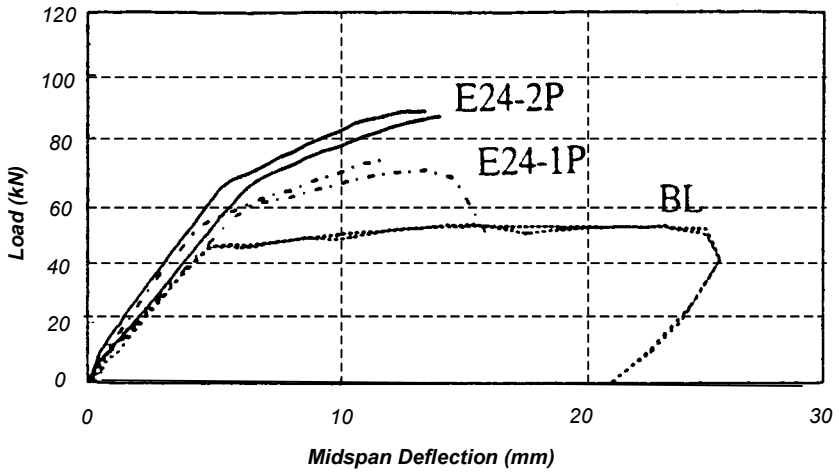

a) Measured Response

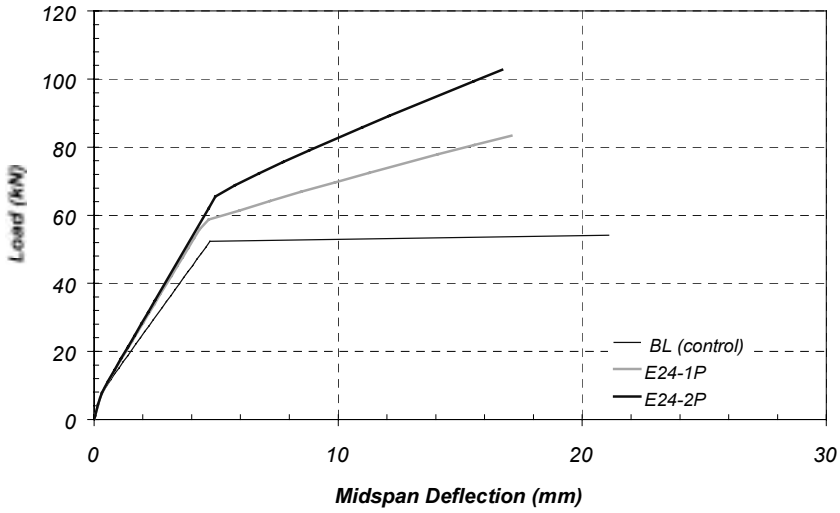

b) Calculated Response

Figure 3.9 Comparison of Load-Deflection Curves for Specimens BL, E24-1P, and E24-2P Reported by Nakamura et al. (1997)

The ratio of calculated to rupture strain indicates that the maximum stress developed in CFRP sheets was about 60% of the maximum rupture stress. No attempt was made to prevent debonding of the CFRP sheets from the beams in these tests.

3.4.5 Summary of Published Data

The analytical model presented in this chapter can reliably reproduce the general behavior of strengthened reinforced concrete specimens using CFRP composites. The shapes of the calculated load-deflection curves follow very closely the measured response reported by other researchers. The agreement between measured and calculated capacity clearly depends on the mode of failure observed during the individual tests. If the composites debond from the concrete surface before reaching their tensile strength, the analytical model will overestimate the capacity of these specimens.

3.5 SUMMARY

An analytical model for calculating the moment-curvature and load-deflection response of reinforced concrete sections strengthened using CFRP composites was presented in this chapter. This model was validated using existing experimental data from reinforced concrete beams using CFRP composites. The model provides an accurate estimate of the observed capacity if the beam fails after rupture of the CFRP composite or crushing of the concrete. However, most beams failed after the CFRP composite debonded from the surface of the concrete, and the analytical model was not capable of reproducing this mode of failure. The model was later refined by adding a limiting composite strain before debonding. The refined model was used to design the composite systems to strengthen the large-scale specimens for this experimental program. A description of the refinements to the analytical model are presented in a separate research report [Breña et al., 2001].

Chapter 4: Description of Laboratory Specimens

4.1 INTRODUCTION

This chapter presents a description of the design and construction of the laboratory specimens tested in this part of the research project. The criteria used to design the laboratory specimens are described in Section 4.2. The calculated capacity of the unstrengthened specimens is presented in Section 4.3. Specimens were strengthened using four different CFRP systems to increase their flexural capacity. A description of the different systems used to strengthen the reinforced concrete beams is presented in Section 4.5, and the calculated capacity of the strengthened specimens is contained in Section 4.6.

Thirty rectangular, reinforced concrete beams were fabricated in the Ferguson Structural Engineering Laboratory at the University of Texas at Austin. Twenty of these beams were subjected to monotically increasing loads after curing for at least 28 days, two were exposed to the environment, including wetting and drying cycles, for approximately 8 months before testing failure, and eight were subjected to repeated loads.

4.2 DESIGN AND CONSTRUCTION OF LABORATORY SPECIMENS

The main objective of this part of the research project was to determine the most suitable configuration of the composite systems to strengthen the reinforced concrete elements. It was hoped that a configuration could be found to utilize the full strength of the composites. The results of this part of the project were expected to be used for the design of the large-scale laboratory specimens in phase 3 of the research project. To facilitate construction and to simplify calculations, simply-supported reinforced concrete beams having a rectangular cross section were selected for these tests. The general trends in the behavior of these specimens were expected to be similar to the behavior of elements with other cross sectional shapes, such as tee or joist sections. Four different composite systems were used to strengthen the reinforced concrete beam specimens. Details of the four different composite systems used in this study are presented in Section 4.5.

The specimens were scaled down from the prototype bridges because it was considered important to be able to study different composite systems and configurations at this stage of the research project. Therefore, a relatively large number of tests were planned to include as many variables as practical. A beam length of approximately one-third of the prototype bridge span was selected as the minimum dimension that could practically be constructed without having to scale aggregate size or longitudinal bar diameters. Once the length of the beams was approximated, the loading configuration and depth of the rectangular beam specimens were selected by choosing a shear-span-to-depth ratio to ensure that the behavior was dominated by flexure. A minimum shear-span-to-depth ratio of approximately three was selected to achieve this goal.

Bonded length of the composite systems was the main parameter studied in this initial set of tests. The beams were designed to avoid failure of the specimens at the CFRP cut-off point at an applied load corresponding to the tensile strength of the composite. The capacity of the cross section was calculated by assuming that the composite did not debond from the surface of the concrete. This assumption was later revised based on the results of the first set of tests as described in Section 4.5. Different bonded lengths were required to develop the maximum flexural capacity of the strengthened beams depending on the strength of the composite system. The length required to develop the full strength of each CFRP

system was determined using the design equations provided by the individual manufacturers, when available [*Master Builders, 1998; Sika, 1997*].

After the distance required to develop the tensile strength of the composite systems was determined, the longitudinal reinforcement was designed to ensure that the flexural capacity of the unstrengthened beam was greater than the applied moment at the CFRP cut-off point. The procedure used for design is illustrated in Figure 4.1. Also, the maximum area of CFRP composite bonded to a specific reinforced concrete section was limited in order to avoid failures by crushing of the concrete in compression.

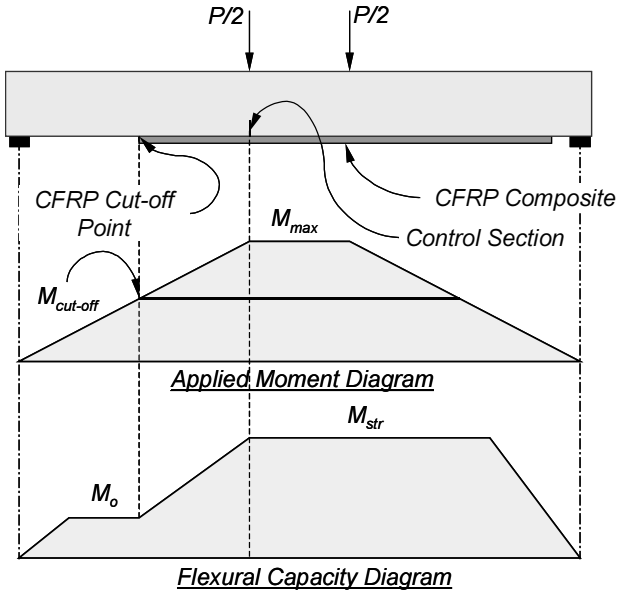

Design Criteria:

$M_{str} \geq M_{max}$

$M_o \geq M_{cut-off}$

where:

M_{max} = Maximum applied moment during tests.

$M_{cut-off}$ = Applied moment at point of CFRP cut-off.

M_{str} = Nominal flexural capacity of strengthened beam.

M_o = Nominal flexural capacity of bare reinforced concrete beam.

Figure 4.1 Moment Diagram Used in the Design of Rectangular Beam Specimens

Two different sizes of beams were required depending on the tensile strength of the composite system (Figure 4.2). All beams were 8-in. wide and either 14-in. or 16-in. deep. The length of the beams was either 9'-6" or 10'-6" to have approximately the same shear-span-to-depth ratio for both beam sizes. All beams were reinforced with two #5 bottom bars, two #3 top bars and No. 6 gage wire stirrups spaced 4 in. on center within the shear span. The top longitudinal reinforcement was used for ease of construction. Stirrup spacing was selected to avoid shear failures in the unstrengthened beams under the maximum applied load that was expected during the tests. A concrete clear cover of approximately 1 in. was provided for all reinforcing bars.

All beams were designed using a nominal 28-day compressive strength of concrete, f'_c, equal to 4,500 psi. The concrete strength was selected based on the estimated strength of the existing concrete in the prototype bridges. Reinforcing bars had a minimum specified yield stress, f_y, equal to 60 ksi. The minimum specified yield stress of the smooth wire was 75 ksi.

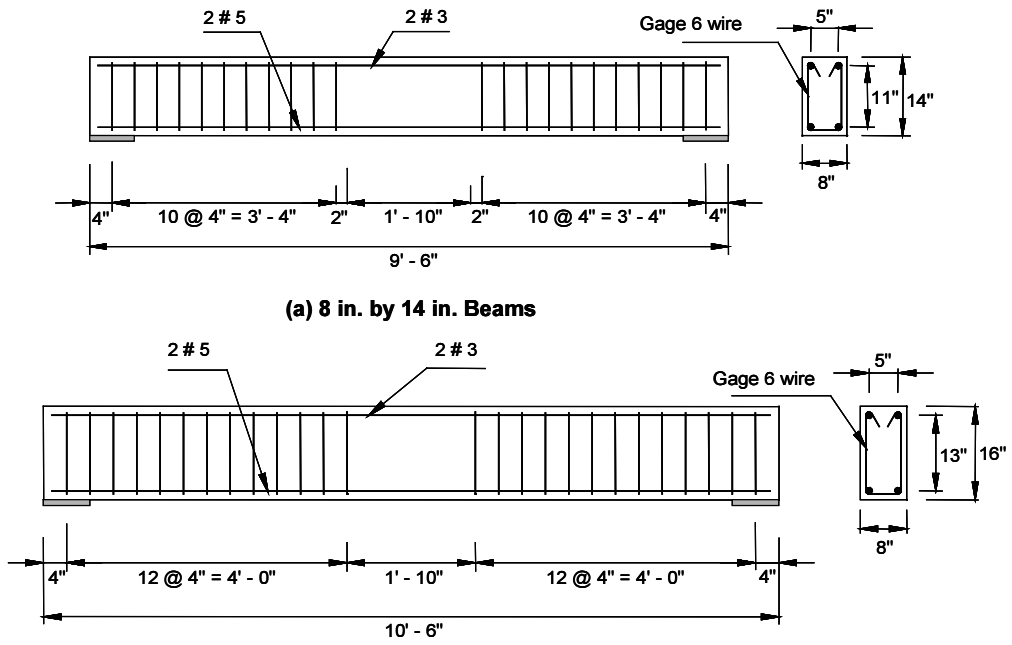

Figure 4.2 Geometry and Reinforcement of Laboratory Specimens

The laboratory specimens were cast using concrete supplied from a local readymix plant. Beams were typically cast in groups of eight specimens. Four 8 by 14 in. and four 8 by 16 in. specimens were cast from one batch of concrete because of space and formwork limitations. Originally, plans had been made to test four reinforced concrete beams with each composite system. Therefore, sixteen beams were initially cast using two different concrete batches and reinforced with bars from the same heat of steel. However, based on the results from the first series of tests, it was decided to expand the number of specimens to include other variables that had not been considered. Therefore, an additional set of six beams was cast in the laboratory using one batch of concrete and steel from a different heat. Finally, to study the effects of repeated loads on the behavior of the rectangular beam specimens, a set of eight beams was fabricated using another batch of concrete and steel from a different heat. Therefore, a total of four different batches of concrete and three different heats of steel were used to fabricate the thirty rectangular beam specimens. Details on the type of composite system, type of test, concrete batch number, and steel heat number are presented in Section 4.5. Pictures illustrating the fabrication process of the rectangular beam specimens in the laboratory are shown in Figure 4.3.

(a) Formwork

(c) Placing concrete in forms

(b) Typical reinforcing cage

(d) Finished set of beams

Figure 4.3 Fabrication Sequence of Rectangular Beams in Laboratory

4.3 CALCULATED CAPACITY OF BARE REINFORCED CONCRETE SPECIMENS

Nominal flexural and shear capacities of the laboratory specimens were calculated in accordance with the current AASHTO *Design Specifications* [AASHTO, 1996]. The measured material properties were used in the calculations. The nominal flexural and shear strengths were calculated using Equations 4.1 and 4.2, respectively:

$$M_n = A_s \, f_y \left(d - \frac{a}{2} \right) \tag{4.1}$$

$$V_n = V_c + V_s \tag{4.2}$$

where

M_n = Nominal flexural strength, lb-in.

$a = \dfrac{A_s f_y}{b\left(0.85 f'_c\right)}$ = depth of equivalent stress block, in.

V_n = Nominal shear strength of member, lb.

$V_c = 2\sqrt{f'_c}\, b\, d$ = concrete contribution to the nominal shear strength of the member, lb.

$V_s = \dfrac{A_v f_y d}{s}$ = stirrup contribution to the nominal shear strength of the member, lb.

A_s = Area of flexural reinforcement, in^2.

A_v = Area of shear reinforcement within a distance s, in^2.

d = Distance from extreme compression fiber to centroid of flexural reinforcement, in.

b = Width of beam, in.

s = Horizontal spacing of shear reinforcement, in.

f_y = Yield stress of flexural or shear reinforcement, psi.

f'_c = Concrete compressive strength, psi.

Four groups of beams were cast using different concrete batches with the same concrete mixture design. The capacities of the unstrengthened beams were calculated for each of the beam groups. Eight beams (four, 14-in. deep and four, 16-in. deep) were cast for groups I, II, and IV, and six beams (four, 14-in. deep and two, 16-in. deep) were cast for group III. The reinforcing steel for beam groups I and II was obtained from the same heat of steel, while the reinforcement for groups III and IV was obtained from different heats.

Concrete cylinders were tested at different ages to determine the variation of concrete strength with time. Although the strength of concrete kept increasing at ages beyond 28 days, the variation of strength was not significant between the dates that the first and last beams within a group of beams were tested (Appendix A). Therefore, the average concrete strength at the time that the last beam within each group was tested was used in the calculations.

4.4 COMPOSITE SYSTEMS USED TO STRENGTHEN THE LABORATORY SPECIMENS

Four different composite systems were used to strengthen the rectangular beam specimens. For the purpose of identification, the different composite systems were labeled using letters A through D. The composite systems were applied to the beams using different strengthening schemes as described in Section 4.5.1. Physical and mechanical properties of the systems are presented in Appendix A.

Composite systems A and B consisted of an epoxy-based matrix reinforced with unidirectional carbon fibers. System C was based on woven unidirectional carbon fibers impregnated in an epoxy-based matrix. The epoxy matrix in systems A through C was also used to bond the systems to the surface of the concrete using the wet-layup technique. System D consisted of pultruded CFRP plates attached to the concrete using an epoxy-based paste. Figures 4.4 through 4.6 illustrate the composite systems being bonded to the tension face of the specimens. As shown in these figures, the specimens were turned upside down in the laboratory to facilitate the strengthening procedure.

Table 4.1 lists the material properties and the flexural and shear capacities for each group of specimens. Beams in groups I through III were subjected to monotonically increasing loads and beams in group IV were subjected to repeated loads.

4.5 COMPOSITE SYSTEMS USED TO STRENGTHEN THE LABORATORY SPECIMENS

Four different composite systems were used to strengthen the rectangular beam specimens. For the purpose of identification, the different composite systems were labeled using letters A through D. The composite systems were applied to the beams using different strengthening schemes as described in Section 4.5.1. Physical and mechanical properties of the systems are presented in Appendix A.

Composite systems A and B consisted of an epoxy-based matrix reinforced with unidirectional carbon fibers. System C was based on woven unidirectional carbon fibers impregnated in an epoxy-based matrix. The epoxy matrix in systems A through C was also used to bond the systems to the surface of the concrete using the wet-layup technique. System D consisted of pultruded CFRP plates attached to the concrete using an epoxy-based paste. Figures 4.4 through 4.6 illustrate the composite systems being bonded to the tension face of the specimens. As shown in these figures, the specimens were turned upside down in the laboratory to facilitate the strengthening procedure.

Table 4.1 Summary of Material Properties and Nominal Capacities of Unstrengthened Rectangular Beam Specimens

Beam Group	f'_c, psi	f_y, ksi (#5 bars)	f_y, ksi (gage 6 wire)	Size	M_n, kip-ft	V_n, kip
Group I	5090	63.8	86.5	8" x 14"	39.3	30.0
				8" x 16"	45.9	34.8
Group II	5390	63.8	86.5	8" x 14"	39.4	30.4
				8" x 16"	46.0	35.2
Group III	4970	63.6	86.5	8" x 14"	39.2	29.8
				8" x 16"	45.7	34.6
Group IV (Fatigue)	5730	62.9	86.5	8" x 14"	39.0	30.8
				8" x 16"	45.5	35.8

Figure 4.4 Composite Systems A and B: Unidirectional Carbon Fibers

Figure 4.5 Composite System C: Woven Unidirectional Carbon Fibers

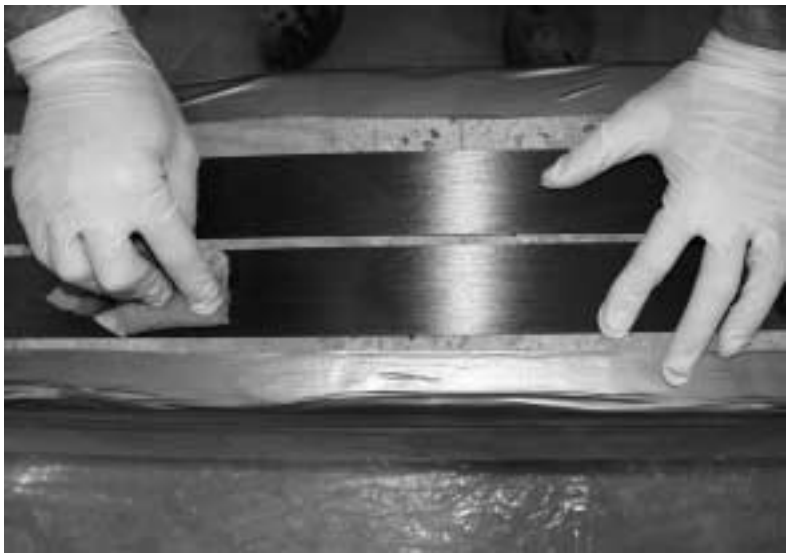

Figure 4.6 Composite System D (Pultruded Plates)

4.5.1 Composite Strengthening Schemes

The initial objective of this phase of the research project was to determine efficient ways of attaching different CFRP composite systems to reinforced concrete sections. Four different composite systems were used to strengthen the rectangular beams that were tested in this phase of the project. The selection of the composite systems was based on their immediate availability for the construction industry. The composite systems were based on either pultruded plates or nonimpregnated carbon fiber sheets or fabrics. Two systems consisted of dry-unidirectional carbon fibers, one consisted of a woven fabric with dry-unidirectional carbon fibers, and one system consisted of pultruded CFRP plates. The dry-fiber systems are bonded to the specimens using a wet-layup process, while the pultruded plate system is

bonded to the surface of the concrete using an epoxy-based paste. Details on the application procedures of each type of system can be found in Appendix C.

After examining the existing information on previous experimental studies, the potential of CFRP debonding was identified as a possible failure mode of the strengthened rectangular beam specimens. In order to create a baseline for comparison of results among the different systems, the first crack was forced to occur at a control section located within the zone of maximum moment. The crack was created by placing a small piece of sheet metal, approximately 0.015 in. thick and extending 0.25 in. deep, across the full width of the beam before casting the concrete for the specimens.

The first series of tests were conducted with the CFRP composites attached to the tension face of the beams. The results obtained from these tests indicated that failure by debonding from the surface of the concrete was not eliminated by simply extending the composite from the section of maximum moment. Therefore, other configurations of the composite systems were used to attempt to eliminate the failure mode by debonding. Other configurations included attaching the composites to the sides of the beams and the use of vertical composite straps to control the propagation of debonding. Figure 4.7 illustrates the composite strengthening schemes that were used in different specimens. A description of each of the strengthening schemes is presented in the following sections.

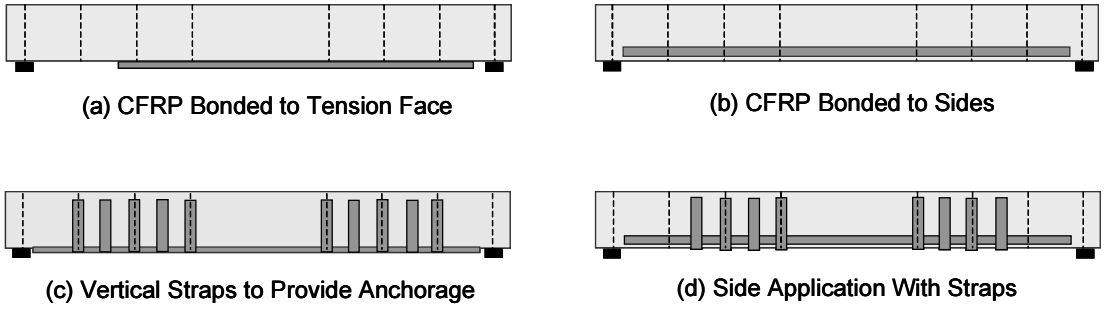

Figure 4.7 Composite Strengthening Schemes Used in Rectangular Beam Specimens

4.5.2 CFRP Bonded to Tension Face of Beams

The four different systems were initially attached to the bottom face of the beams to measure the length required to develop the composite strength. The objective of this type of application was to study the effect of bonded length on the development of stress in the composite systems. Bonded length of the composites was measured from the crack initiator to the end of the composite laminate.

The composites were bonded asymetrically to the tension face of the specimens to force failure by debonding from the surface of the concrete on the short side. The average shear stresses developed along the concrete-composite interface could then be calculated dividing the force developed in the composite system during the test by the width and length of the composite from the critical section. All of the composite systems had a 2 in. width to eliminate variations in behavior introduced by different widths of covered concrete surface. Figure 4.8 illustrates a specimen with a CFRP system attached to the tension face.

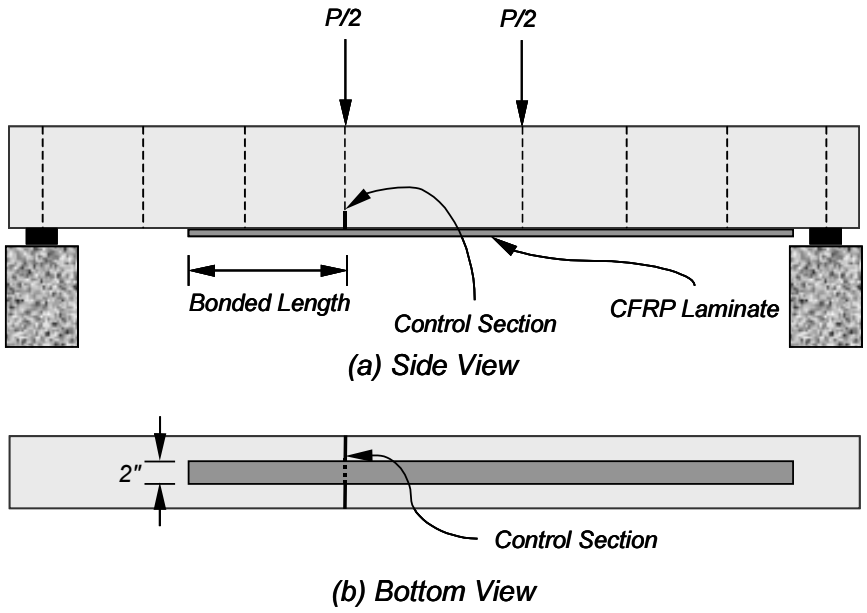

Figure 4.8 Schematic of Specimen with CFRP Bonded to Tension Face

4.5.3 Bottom Application with Transverse Straps

Test specimens with bottom application of the composite tended to fail prematurely because relative vertical displacements at flexural cracks caused local debonding from the bottom surface of the cross section. Debonding quickly propagated to the end of the composite once it had initiated in the vicinity of a crack that exhibited vertical offset. Because specimens with bottom application of the composite did not develop the strength of the composite even when the material was bonded over nearly the entire shear span, some form of anchorage was needed to prevent the composite from debonding prematurely.

Several reaserchers have suggested using bolts to anchor the composite to the concrete cross section [Spadea et al., 1998]. This option was dismissed because all the composites that were used in this project consisted of fibers in the longitudinal direction only. Therefore, the strength of the composites transverse to the fiber direction is very low, which could lead to splitting at the location of the bolts. Other recommendations include clamping the composite with plates and bolts or clamping the composite with transverse composite straps at specified locations. Wrapping a composite sheet throughout the length of the beam was an option that was considered too expensive and therefore was not selected.

Transverse composite straps positioned within the shear span were chosen to control the propagation of debonding from the surface of the specimens (Figure 4.9). The straps were similar to those tested previously to enhance shear strength [Triantafillou, 1998]. The composite straps had a 2-in. width and were placed at discrete locations over the longitudinal composite. They extended on both side faces of the beams and were stopped 3 in. from the top surface of the beam. The center-to-center spacing between straps was equal to half the beam depth to be able to intercept potential diagonal cracks with at least one strap. The straps were intended to allow some debonding between straps but to control the propagation of debonding to the composite ends. Also, their pupose was to restrain shear cracks in order to prevent vertical offsets from occurring along the bottom face of beams.

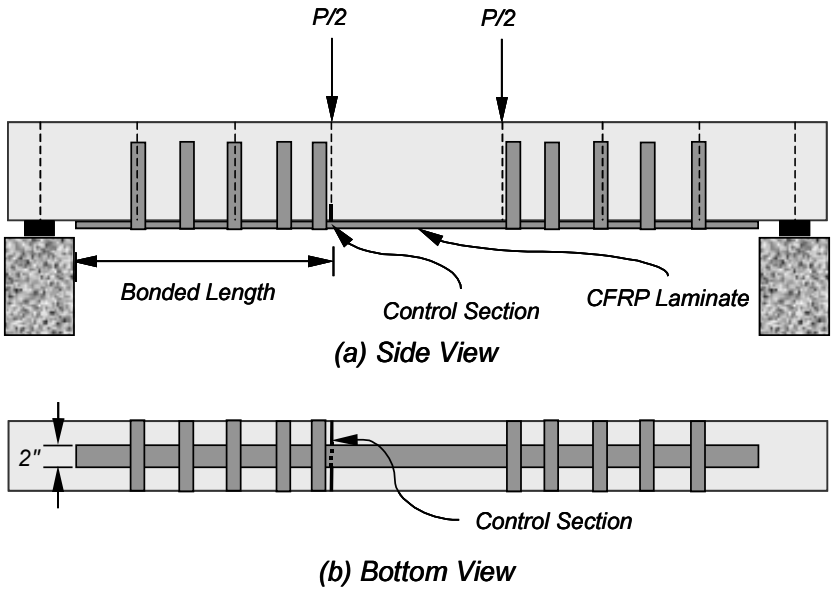

Figure 4.9 Schematic of Specimen with Transverse Straps to Control Debonding

4.5.4 CFRP Bonded to the Sides of Beams

Results from the initial tests of the beams with the composite systems attached to the bottom face of the beams indicated that debonding initiated at flexural crack locations that exhibited vertical offsets. The bond between the composite and the surface of the concrete appeared to be weaker in the direction perpendicular to the surface of the concrete where the composites were attached. Therefore, another approach to control debonding of the composites was selected by attaching the laminates to the sides of the beams and reduce the deformations induced by crack movement. This strengthening scheme is illustrated in Figure 4.10.

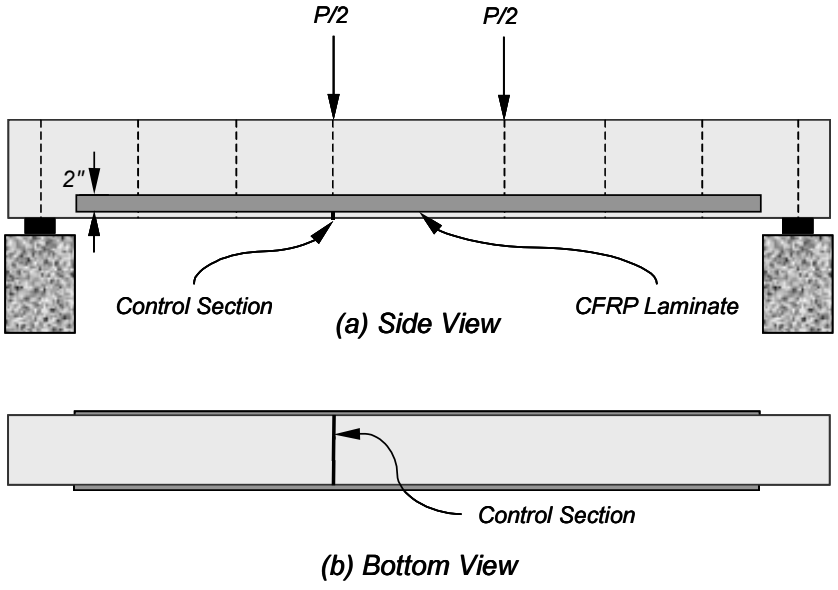

Figure 4.10 Schematic of Specimen with CFRP Bonded to Sides

4.5.5 CFRP Bonded to the Sides of Beams with Straps

Beams with composite material applied to the side faces of the specimens generally failed because of debonding at the interface between the composites and the surface of the concrete. Some specimens failed by rupturing of the cover-concrete of the beams as the composite detached from the surface of the concrete. Transverse straps, similar to those used with the bottom application, were attached to provide additional anchorage for the composites placed longitudinally on the beams (Figure 4.11). In this case, the straps were intended to provide additional bonded area and reduce interface stresses. The composite straps were 2 in. wide and had a center-to-center spacing equal to half the depth of the beams.

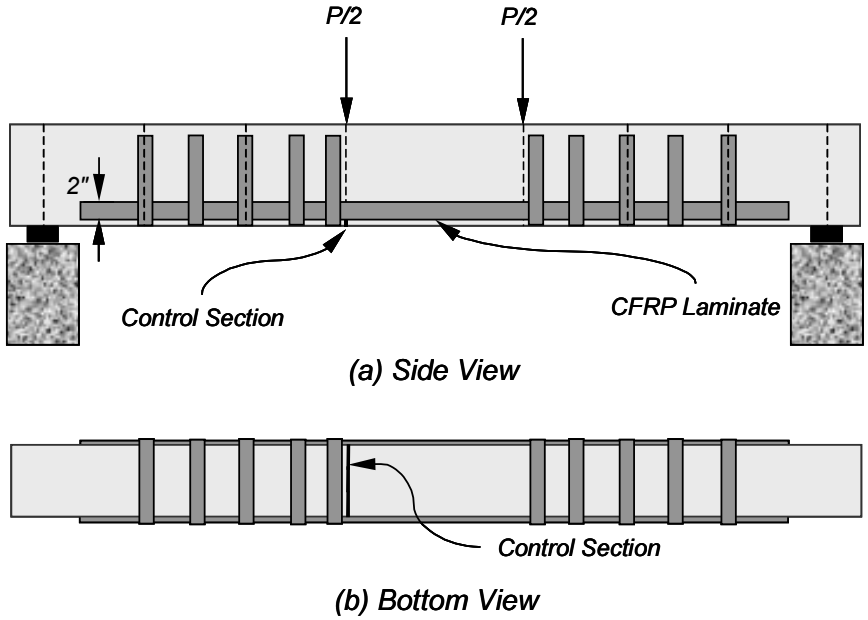

Figure 4.11 Schematic of Specimen with CFRP Bonded to Sides and Anchorage Using Vertical Straps

4.6 CALCULATED CAPACITY OF STRENGTHENED SPECIMENS

The capacity of the strengthened beams was calculated using the procedures described in Chapter 3. The flexural strength was calculated assuming that the CFRP composite systems were perfectly bonded to the surface of the concrete; therefore, a linear distribution of strains across the height of the section was assumed. The flexural capacity of the strengthened sections was assumed to be limited by the rupture strain of the composite systems. The rupture strain for each of the composite systems was obtained from the manufacturer's literature.

The calculated nominal flexural capacity of the strengthened specimens is listed in Table 4.2. The specimens were classified into four different beam groups, depending on the concrete compressive strength and steel yield stress (Table 4.1). Within one beam group, the capacity of the strengthened specimens may be different depending not only on the cross-sectional dimensions, but also on the type of composite and scheme used to strengthen the beams. The types of composite systems and strengthening schemes used for the different beam groups are also listed in Table 4.2. The strength of the specimens was calculated using the measured material properties for the concrete and steel, and the values published in the manufacturer's literature for the composite systems.

Previous investigators have indicated that the use of vertical composite straps can enhance the shear capacity of reinforced concrete sections [Triantafillou, 1998]. However, the shear capacity of the strengthened specimens was not calculated because increase in shear strength was not required for these specimens to achieve the flexural capacity of the strengthened beams.

Table 4.2 Summary of Flexural Capacity of Strengthened Rectangular Beam Specimens

Beam Group	Composite Type	Beam Size	Strengthening Scheme	M_n, kip-ft
Group I	A	8" x 14"	Bottom (Figure 4.8)	53.2
	C	8" x 16"	Bottom (Figure 4.8)	67.7
	C	8" x 16"	Bottom w/straps (Figure 4.9)	67.7
Group II	B	8" x 14"	Bottom (Figure 4.8)	53.2
	B	8" x 14"	Sides (Figure 4.10)	51.5
	C	8" x 16"	Sides (Figure 4.10)	65.7
	D	8" x 16"	Bottom (Figure 4.8)	85.0
	D	8" x 16"	Sides (Figure 4.10)	109.6
Group III	A	8" x 14"	Bottom w/straps (Figure 4.9)	53.0
	D	8" x 16"	Sides w/straps (Figure 4.11)	105.6
Group IV	A	8" x 14"	Bottom w/straps (Figure 4.9)	52.9
	D	8" x 16"	Sides w/straps (Figure 4.11)	107.7

4.7 SUMMARY

The procedures for design and fabrication of the laboratory specimens were presented in this chapter. The flexural and shear capacities of the unstrengthened specimens were calculated using current design equations. The different strengthening schemes using CFRP composites were described and the flexural capacity of the strengthened beams was calculated using the procedure indicated in Chapter 3. A comparison of the calculated flexural strength of the specimens and the measured response is presented in Chapter 6 for the specimens subjected to static loading, and in Chapter 8 for the specimens tested under fatigue loading.

Chapter 5: Description of Laboratory Tests

5.1 INTRODUCTION

Details of the testing program for the rectangular beam specimens are presented in this chapter. The characteristics of the specimens, composite systems used, and strengthening configurations are presented in Section 5.2. The loading sequence during the static tests and details of the loading protocol for the fatigue tests are discussed in Section 5.3. A description of the instrumentation used to monitor the applied load, deflections, and strains is presented in Section 5.4.

5.2 DESCRIPTION OF TESTING PROGRAM

Twenty-two rectangular beam specimens were subjected to monotonically increasing static loads, and eight beams were subjected to fatigue loads. The characteristics of the specimens tested in this part of the experimental program are presented in this section. The number of specimens, type of composite system used for strengthening, and the configuration of the composite system are described.

5.2.1 Static Tests

The main goal of this phase of the testing program was to evaluate the effectiveness of different commercial composite systems for strengthening existing reinforced concrete beams. The effect of strengthening configuration on the response of the specimens was also examined. Two different sizes of rectangular beam specimens were constructed in the laboratory (Chapter 4). A total of twenty-two beams were tested under monotonically applied loads until failure. Two of these beams were tested in an unstrengthened condition to provide a baseline for comparison with the strengthened beams. These beams are called the control specimens. The control specimens were fabricated as part of beam group I (Table 5.1), with 8-in. by 14-in. and 8-in. by 16-in. cross sections. Although other beam groups had different material properties, it was assumed that all specimens could be compared with the corresponding control specimens. The first letter in the nomenclature of the specimens refers to the type of composite that was used to strengthen the beams.

Two plies of carbon fiber sheets or fabrics were used for all the specimens strengthened using composite systems A, B, and C. For the specimens strengthened using composite system D, one plate was used if the composite was applied to the bottom of the beams, and two plates were used if the composites were applied to the sides (D3 through D5).

The composite system manufacturers indicated that the type of surface preparation influences the behavior of the strengthened beams. Therefore, for beams strengthened using composite systems C and D, two different types of surface preparation were examined to evaluate its influence on the behavior of the beams. The surface of the concrete was either prepared by grinding or sandblasting prior to the application of the composite systems to the beams. The rest of the specimens were prepared using an abrasive stone to remove loose particles from the surface of the concrete prior to the application of the composite systems.

Two beams in the static-load test series were subjected to moisture periodically for eight months before loading to failure. The objective of these tests was to evaluate the influence of moisture on the bond between the surface of the concrete and the composite system. The laminates were covered with a water-based latex coating supplied by the manufacturer of the composite system to protect them from

degradation due to ultraviolet radiation [Master Builders, 1999]. The beams were loaded initially to cause cracking corresponding to service load conditions before strengthening. Only composite system A was used to strengthen the beams in these tests, using the bottom application with straps illustrated in Figure 4.9. One of the specimens (A-LT1) was subjected to a sustained load to force flexural cracks to open and facilitate ingress of moisture into the concrete. The sustained load applied to the beam was approximately equal to 20% of the yield load of the strengthened specimen. The other specimen (A-LT2) supported only its self-weight. Figure 5.1 shows a photograph of the two specimens during the eight-month period that they were subjected to periodic moisture cycles. The characteristics of all specimens for the static-load tests are listed in Table 5.1.

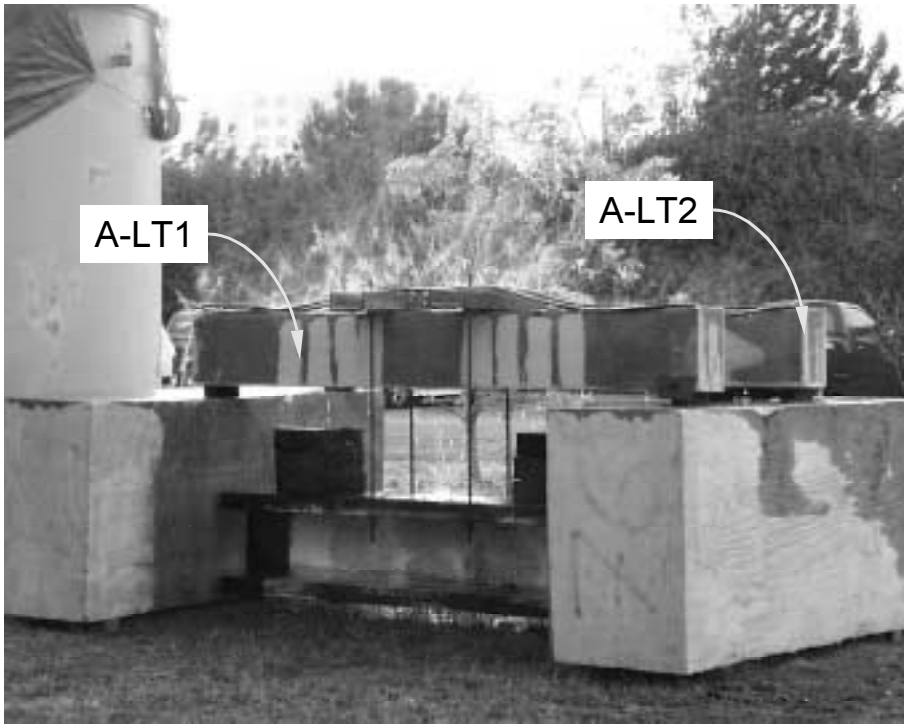

Figure 5.1 Photograph Showing Specimens Subjected to Moisture

5.2.2 Fatigue Tests

The objective of these tests was to evaluate the effects of repeated loads on the behavior of strengthened beams using carbon fiber polymer composites. A group of eight beams was fabricated, strengthened, and subjected to fatigue loads. The strengthening schemes for the fatigue tests were selected based on results from the static-load tests. The 8-in. by 14-in. beams were strengthened using composite system A, using the bottom application with transverse straps (Figure 4.9). The 8-in. by 16-in. beams were strengthened using composite system D applied to the side of the beams with transverse straps (Figure 4.11). Four straps were used along the shear span for all the beams. Table 5.2 summarizes the cross-sectional properties and strengthening configurations of the laboratory specimens for the fatigue-load testing program. The material properties of these specimens were presented in Chapter 4.

Table 5.1 Details of the Specimens in the Static-Load Testing Program [Adapted from Bramblett, 2000]

Specimen	Beam Size, in.	Beam Group	Composite System	Strengthening Scheme	Width of Composite, in.	No. Transverse Straps	Surface Preparation
Control A and B	8 in. by 14 in.	I	None	-	-	-	-
A1			A	Bottom	2	0	Grind
A2				Bottom	2	0	Grind
A3				Bottom	2	0	Grind
A4		II		Bottom	4	0	Grind
B1			B	Bottom	3	0	Grind
B2				Bottom w/Straps	2	6	Grind
B3				Sides	2	0	Grind
B4		III		Bottom w/Straps	2	4	Grind
B5				Bottom w/Straps	2	4	Grind
Control C and D	8 in. by 16 in.	I	None	-	-	-	Grind
C1			C	Bottom	2	0	Grind
C2				Bottom	2	0	Sand-blast
C3				Bottom w/Straps	2	6	Grind
C4		II		Sides	2	0	Grind
D1			D	Bottom	2	0	Grind
D2				Bottom	2	0	Sand-blast
D3				Sides	2	0	Grind
D4		III		Sides w/Straps	2	4	Grind
D5				Sides w/Straps	2	4	Grind
Specimens Exposed to Moisture							
A-LT1	8 in. by 14 in.	III	A	Bottom w/Straps	2	4	Grind
A-LT2				Bottom w/Straps	2	4	Grind

Table 5.2 Details of Laboratory Specimens in the Fatigue-Load Testing Program

Specimen	Beam Size, in.	Composite System	Strengthening Scheme
A-F1	8 in. by 14 in.	A	Bottom Application w/Straps
A-F2			
A-F3			
A-F4			
D-F1	8 in. by 16 in.	D	Side Application w/Straps
D-F2			
D-F3			
D-F4			

5.3 TEST SETUP AND LOADING SEQUENCE

The test setup was designed to apply loads symmetrically about the center of the beams to generate a constant moment region within the span. The loads were applied to the top face of the specimens using steel pins nested on steel cradles. To avoid crushing of the concrete under the points of application of load, elastomeric pads were inserted between the steel cradles and the top surface of the beams. Details of the experimental test setup are shown in Figure 5.2.

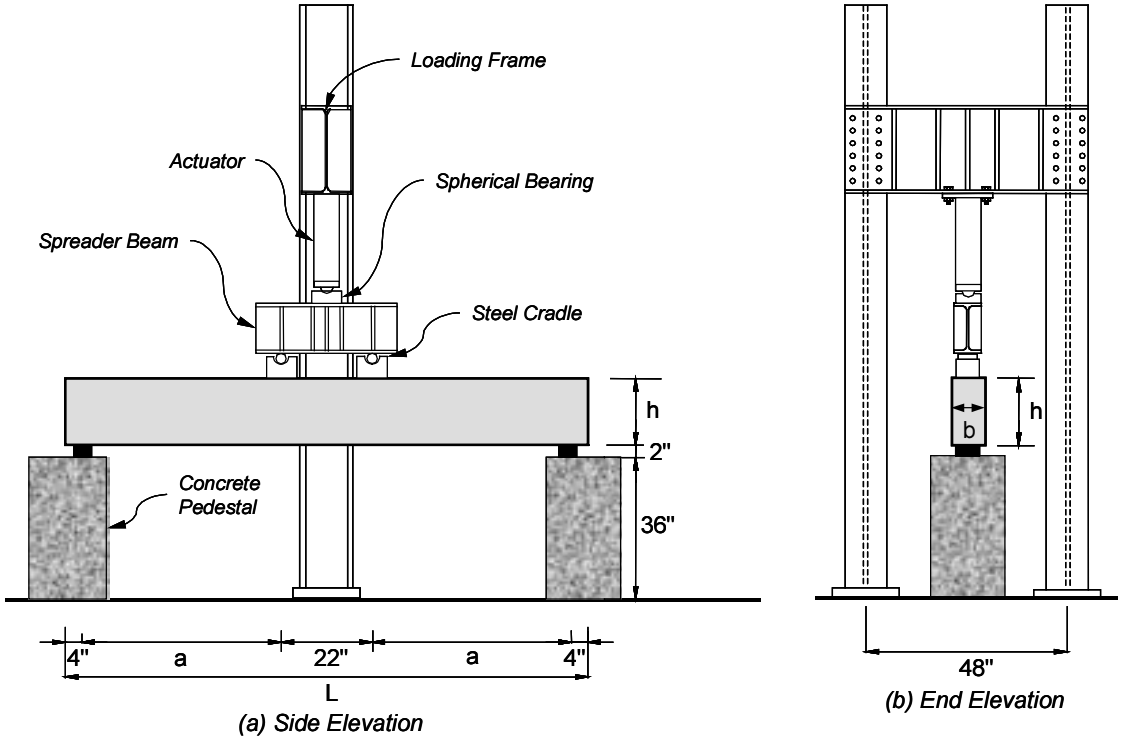

Beam Group	h, in.	b, in.	a, in.	L, in.
A and B	14	8	42	114
C and D	16	8	48	126

Figure 5.2 Test Setup for Rectangular Beam Specimens

The laboratory specimens were positioned on 3-ft tall concrete pedestals so that the research team was able to observe the bottom face of the beams during testing. The pedestals rested on the structural testing floor in the laboratory. Loading was applied using a 120-kip hydraulic actuator that reacted against a steel frame anchored to the testing floor. The actuator was positioned at the centerline of the specimens, and the load from the actuator was distributed to two loading points using a stiffened, steel spreader beam. A spherical bearing was used between the actuator and the spreader beam to apply the load uniformly to the spreader beam. Elastomeric bearing pads were also used at the supports, between the beam specimens and the concrete pedestals, to avoid crushing of the concrete. Figure 5.2 illustrates the experimental setup.

The same loading frame and support system was used for the static and the fatigue tests. For the static tests, a hand-operated hydraulic pump was used to supply fluid to the actuator. For the fatigue tests, a closed-loop system was used to control the frequency and amplitude of the applied load. The details on the loading sequence used for the tests are described in the following sections.

5.3.1 Static Tests

Each beam was loaded incrementally to failure. The loading sequence for the static-load tests was either controlled by force or displacement. Force-control was used for loads up to yielding of the longitudinal reinforcement. During this stage of testing, loads were applied in approximately 3-kip increments. The specimens were inspected visually for cracking or debonding of the CFRP composites between load increments. After yielding of the longitudinal reinforcement, testing was monitored using displacement control. The displacement of the specimens at midspan was increased in approximately 0.15 in. increments until failure. During the time between loading increments, leakage of the hydraulic fluid occurred so the specimens had to be re-loaded to the maximum load applied previously before proceeding to the following load or displacement increment.

5.3.2 Fatigue Tests

The amplitude of the applied load varied for the different tests. The maximum loads (Figure 5.3) were determined based on the measured response of companion specimens that were subjected to monotonically increasing loads. Five of the beams (A-F1, A-F2, A-F3, D-F1, and D-F2) were tested under fatigue loads representative of service-load conditions, and three beams (A-F4, D-F3, and D-F4) were tested under fatigue loads representative of overload conditions.

The maximum repeated loads for specimens strengthened using composite system A were determined from the measured response of specimen B4. The maximum load for specimens A-F1 and A-F2 corresponded to measured strains in specimen B4 of 33% of the yield strain. The maximum load for specimen A-F3 corresponded to measured strains in specimen B4 equal to 50% of the yield strain, and the maximum load for specimen A-F4 corresponded to measured strains of 90% of the yield strain.

The maximum repeated loads for specimens strengthened using composite system D were determined from the measured response of specimen D5. The maximum loads for specimens D-F1, D-F2, and D-F3 corresponded to measured strains in specimen D5 of 33%, 50%, and 90% of the yield strain, respectively. The maximum load for specimen D-F4 corresponded to 110% of the measured yield load for specimen D5.

The minimum repeated load for all specimens was approximately 1 kip (Figure 5.3). The minimum load was selected to ensure that the bearing pads would remain in compression throughout the fatigue tests.

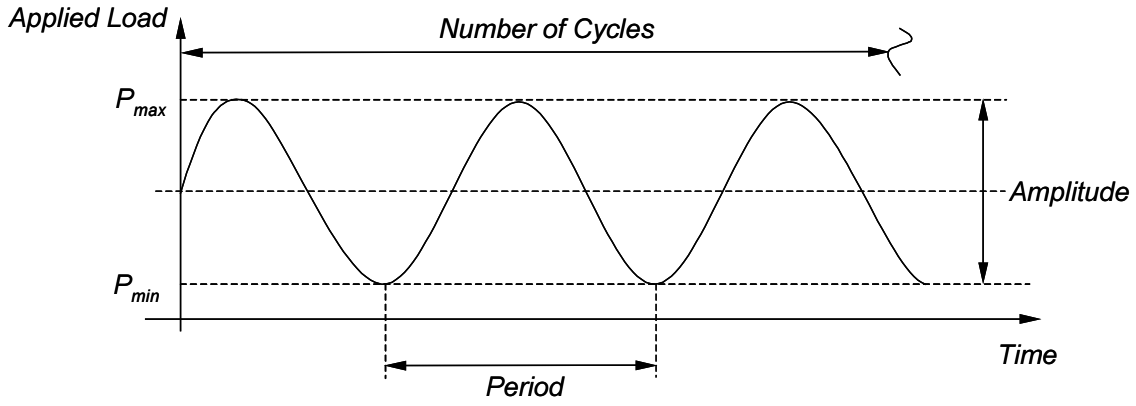

Figure 5.3 Schematic of Loading Protocol for Fatigue Tests

The number of cycles applied to the specimens tested in this part of the program varied. The beams tested under simulated service-load conditions were subjected to either 10,000 or 1,000,000 cycles of load. After the application of the fatigue loads, these specimens were then tested statically to failure following the procedure described in Section 5.2.1. The beams tested under simulated overload conditions were subjected to cyclic loads until failure of the specimens. Table 5.3 lists details of the loading protocol used for the specimens in the fatigue tests.

Table 5.3 Summary of Fatigue Testing Program

Specimen	P_{max}, kip	P_{max}/P_y	Amplitude, kip	Frequency, Hz	Number of Cycles
A-F1	8	0.33	7	2	10,000
A-F2	8	0.33	7	2	1,000,000
A-F3	12.5	0.50	11.5	2	1,000,000
A-F4	21	0.90	20	1.75	155,950
D-F1	12	0.33	11	2	1,000,000
D-F2	17	0.50	16	2	1,000,000
D-F3	28	0.90	27	1.75	55,490
D-F4	33	1.10	32	0.5	8,990

5.4 SPECIMEN INSTRUMENTATION AND DATA ACQUISITION

The instrumentation was designed to be able to determine the relationships between load and strain, and load and deflection at specified locations during testing. Electrical resistance strain gages, linear potentiometers, and one load cell were used to instrument the beams.

The strain gage positions were selected to measure strains in the different materials and determine the strain profile at the instrumented sections. Strain gages were bonded to steel reinforcing bars, on the side faces of the beam in the concrete compression zone, and on the carbon fiber composites. The main instrumented section corresponded to the location of the crack initiator, defined as the critical section in Chapter 4. This section was at the end or within the constant moment region of the specimens. The critical section was located directly below the south load point for the 8-in. by 14-in. beams, and 2 in. from the south load point within the constant moment region for the 8-in. by 16-in. beams. A section approximately half way between the critical section and the end of the composite was also instrumented

in some of the beam specimens (beam groups III and IV). The location of instrumented sections is shown in Figure 5.4. The strain gage characteristics used for the different materials are listed in Table 5.4.

The distance from the support to the instrumented sections (sections 1 and 2), and the bonded length of CFRP composite are listed in Table 5.5. The bonded length was measured from the critical section of the specimens to the south end of the composite laminate.

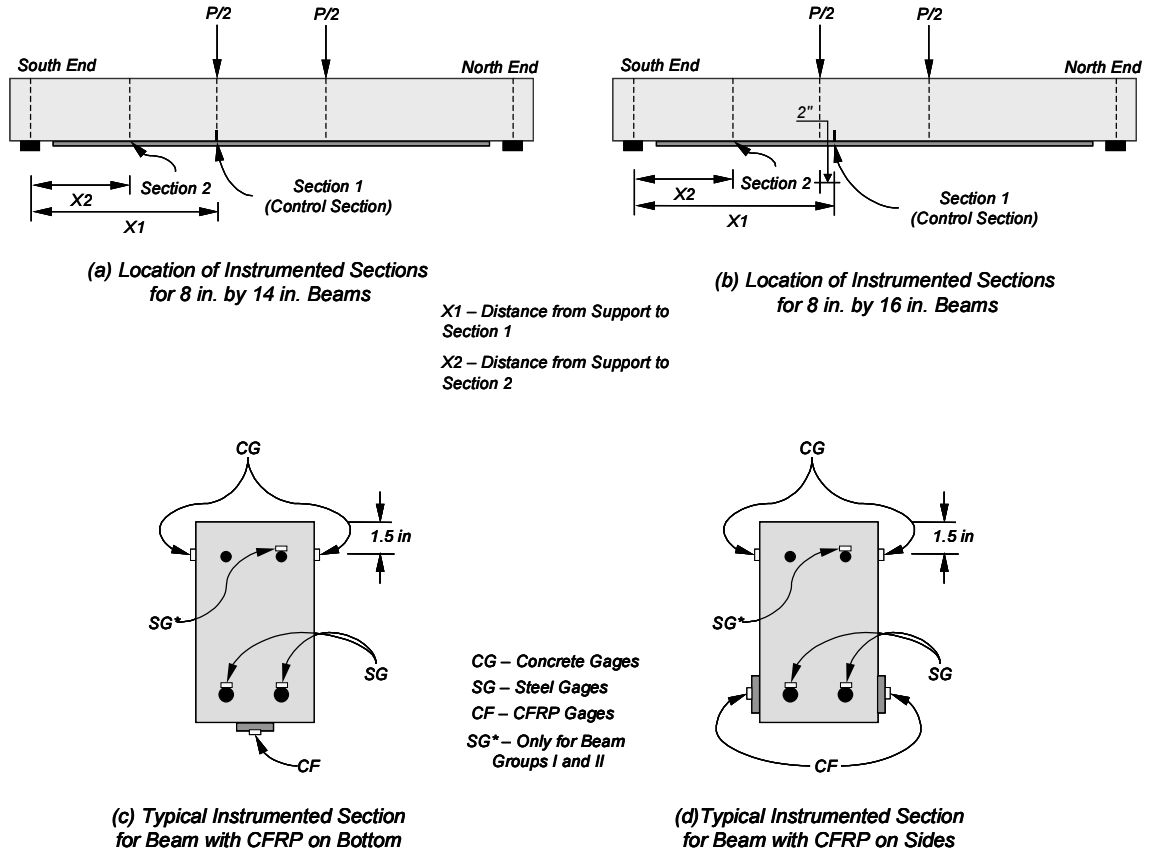

Figure 5.4 Location of Instruments in Rectangular Beam Specimens

Table 5.4 Characteristics of Strain Gages

Material	Strain Gage Type	Resistance, Ohm	Gage Length, mm
Reinforcing Steel	Foil	120	5 or 6*
CFRP Composite	Foil	120	6
Concrete Surface	Wire	120	60

*Gage length varied depending on availability

Table 5.5 Position of Instrumented Sections for Rectangular Beam Specimens

Specimen	X1, in.	X2, in.	CFRP Bonded Length, in.
Specimens Subjected to Static Loads			
Control A and B	42	Not Instrumented	-
A1			10
A2			14
A3			30
A4			15
B1			35
B2			35
B3			35
B4		26	35
B5		30	24
Control C and D	50	Not Instrumented	-
C1			45
C2			45
C3			45
C4			45
D1			45
D2			45
D3			45
D4		26	45
D5		38	30
A-LT1	42	30	35
A-LT2			35
Specimens Subjected to Fatigue Loads			
A-F1	42	26	35
A-F2			35
A-F3			35
A-F4			35
D-F1	50	38	30
D-F2			30
D-F3			30
D-F4			30

Five 2-in. linear displacement potentiometers were used to measure displacements of the specimens. Potentiometers were placed within the beam span and at the supports (Figure 5.5). The potentiometers at the supports were used to subtract the support deformation caused by the flexibility of the elastomeric pads from the displacement readings within the span. Because only one potentiometer was used at each support, they were positioned at diametrically opposite sides of the beams to account for possible twisting of the specimens during testing caused by misalignment of the actuator.

Total applied load was measured using a fatigue-rated Strainsense load cell placed between the spherical bearing and the steel wide-flange spreader beam used to apply load at two points on the beam. The load cell had a maximum capacity equal to 50 kip. Electronic readings from the instruments were collected every 2 seconds during loading using a Hewlett Packard 75000 scanner and were stored in spreadsheet format on a personal computer.

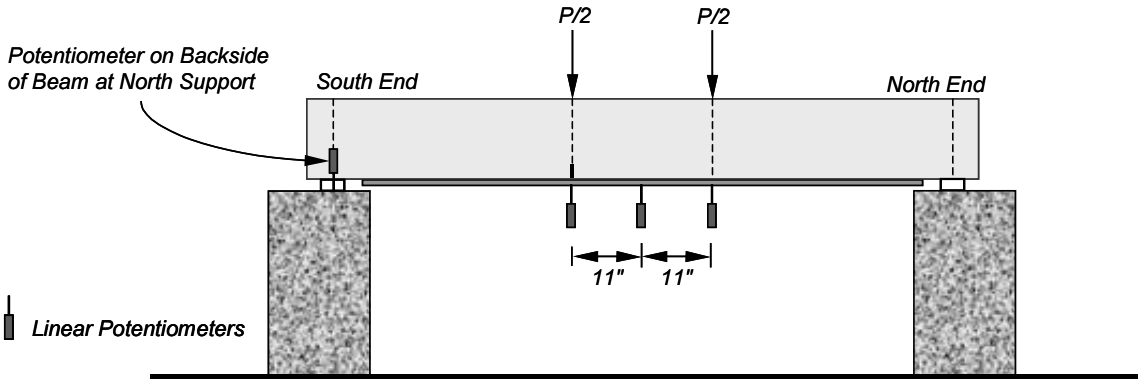

Figure 5.5 Position of Linear Potentiometers on Laboratory Specimens

5.5 SUMMARY

Details on the characteristics of the specimens including the type and configuration of composite system used for strengthening were presented in this chapter. The testing procedures were also discussed. Details on the instrumentation and data acquisition were also presented. The measured response of the laboratory specimens is presented in Chapter 6.

Chapter 6: Measured Response of Beams Subjected to Static Loads

6.1 INTRODUCTION

The response of the specimens subjected to static loads is presented in this chapter. The observed behavior of the specimens during the tests is presented in Section 6.2. The differences in behavior caused by the use of different strengthening schemes are discussed. The mechanisms that led to failure of the specimens are also presented and discussed in this section. A discussion of the measured load-deflection response of the different groups of beams is presented in Section 6.3. The variables that were included in each of the different groups are presented, and their effect on the measured response is discussed. Finally, the typical measured strain response of the specimens is presented in Section 6.4. The discussion presented in this section centers about the response of one of the specimens because similar features were observed in all the specimens. Measured load-strain plots for all the specimens are presented in Appendix D.

6.2 OBSERVED RESPONSE OF SPECIMENS DURING TESTING

The observed response of the specimens during the static tests are presented in this section. Although the trends in the global behavior of all the strengthened specimens were similar regardless of which composite system was used for strengthening, the propagation of debonding of the CFRP composites was significantly different depending on the strengthening scheme. Because of this, it was considered important to include a description of the sequence of debonding for each of the strengthening schemes. A qualitative description of the global response of the specimens is presented in Section 6.2.5.

Crack formation and crack widths were monitored and measured throughout testing to assess the behavior of the strengthened specimens in comparison with the behavior of the unstrengthened control beams. However, no significant differences in the cracking patterns and crack widths were observed between the specimens strengthened using different CFRP schemes. Therefore, the cracking patterns for the specimens are not discussed here. Only the formation of cracks that led to debonding of the composites from the surface of the concrete are discussed in this section. The crack patterns and widths of all the specimens at failure are presented in Appendix B.

6.2.1 Beams Strengthened Using CFRP Bonded to the Tension Face

The observed response of all the strengthened specimens was similar up to the yield load. No evidence of debonding of the CFRP composites was observed until after yielding of the reinforcement. The formation of secondary cracks adjacent to existing flexural cracks was an indication of initiation of debonding of the composite laminates. These cracks were followed by the formation of longitudinal debonding cracks along the sides of the CFRP composites (Figure 6.1). These cracks propagated toward the end of the composite laminates and caused total debonding of the composites from the surface of the concrete. The load required to cause propagation of the debonding cracks to the end of the CFRP composites varied depending on the strengthening configuration.

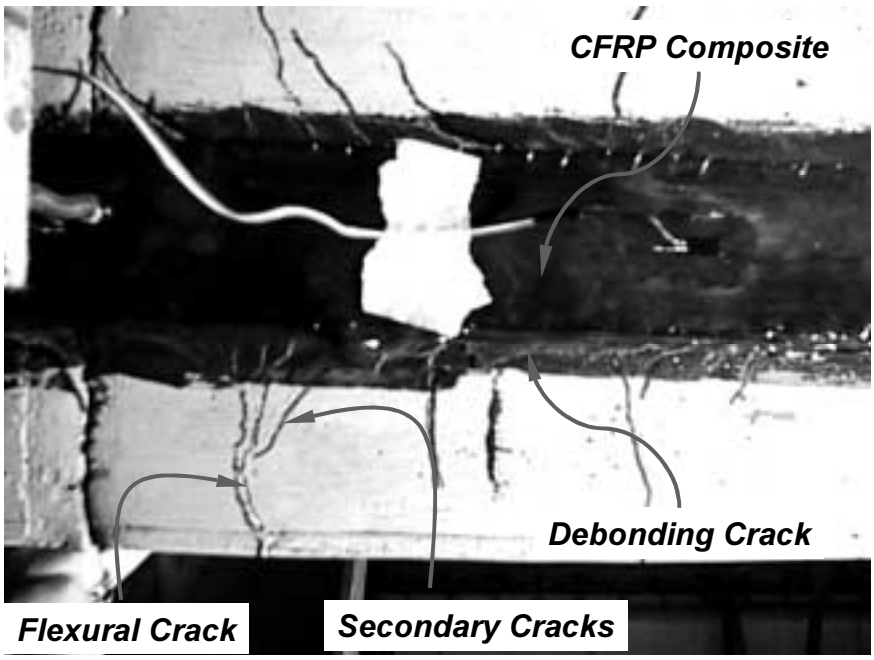

Figure 6.1 View of Bottom of Specimen A2 Showing the Formation of Secondary Cracks and Debonding Cracks Along Both Sides of the CFRP Composite

As could have been expected, the specimens that were strengthened using short lengths of CFRP composites were not able to withstand a significant increase in load beyond the load that caused the formation of the initial debonding cracks. Debonding of the CFRP composites from the surface of the concrete in these specimens occurred shortly after yielding of the reinforcement. Debonding in these cases was very sudden and the only indication of incipient failure was a few popping sounds as the debonding cracks propagated quickly to the end of the composites. Specimens A1, A2, and A4 exhibited this type of behavior. The bonded length in these specimens was 10 in., 14 in., and 15 in., respectively. The bonded length in these specimens is less than or approximately equal to the depth of the specimens. Figure 6.2 shows a photograph of specimen A1 after debonding of the CFRP composite. Secondary cracks at the critical section can also be seen in this photo.

Subsequently, the specimens were strengthened using significantly longer bonded lengths because of the sudden mode of failure observed in the first series of tests. The CFRP composites were extended as close as practical to the supports of the strengthened beams. The bonded length measured from the critical section to the end of the composite was approximately equal to 2.5 to 3 times the depth of the beams. This had an effect on the debonding sequence observed in these specimens.

Because the length of the composites extended a distance greater than the depth of the specimens, several flexural cracks that formed within the shear span of the beams crossed the laminates at different locations. The width of the cracks that formed within the shear span increased as the magnitude of the applied moment increased, and the beams experienced a relative vertical displacement from one side of these cracks to the other due to the presence of shear. The vertical offset triggered debonding of the CFRP composites from the surface of the concrete in the vicinity of the flexural-shear crack. Debonding generally initiated at the location of the flexural-shear crack within the shear span that formed closest to the critical section. A comparison of the mechanisms involved in the opening of cracks that form within the constant moment region and within the shear span of a strengthened beam is presented in Figure 6.3. Initiation of CFRP debonding caused by relative displacement of a flexural-shear crack in specimen B1 is shown in Figure 6.4.

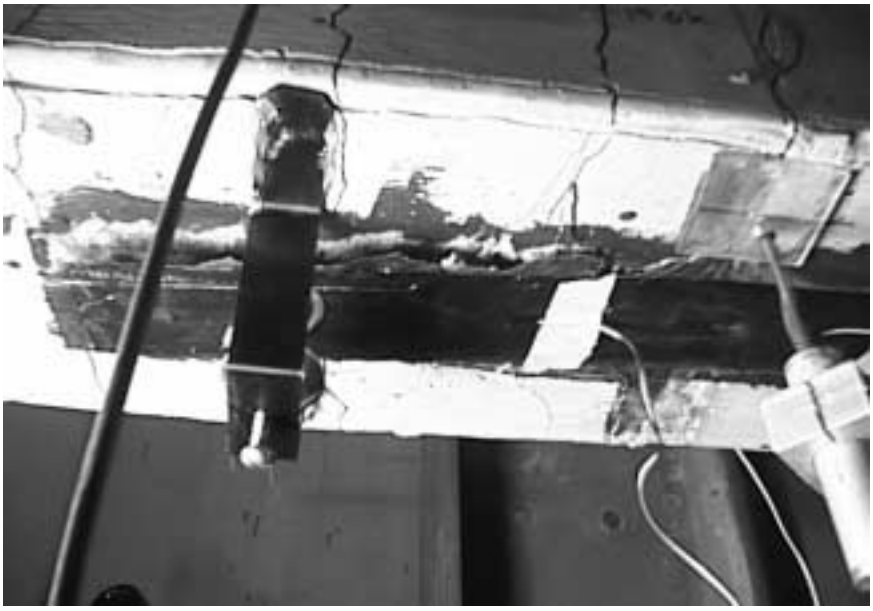

Figure 6.2 View of the Bottom Face of Specimen A1 after Debonding of the CFRP Composite

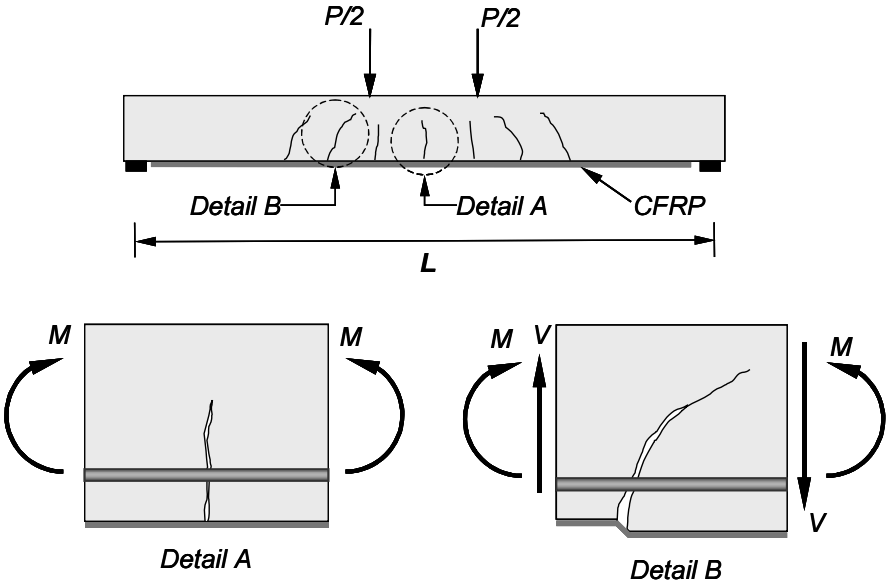

Figure 6.3 Schematic Representation of Cracking Mechanisms at Different Locations of a Strengthened Beam

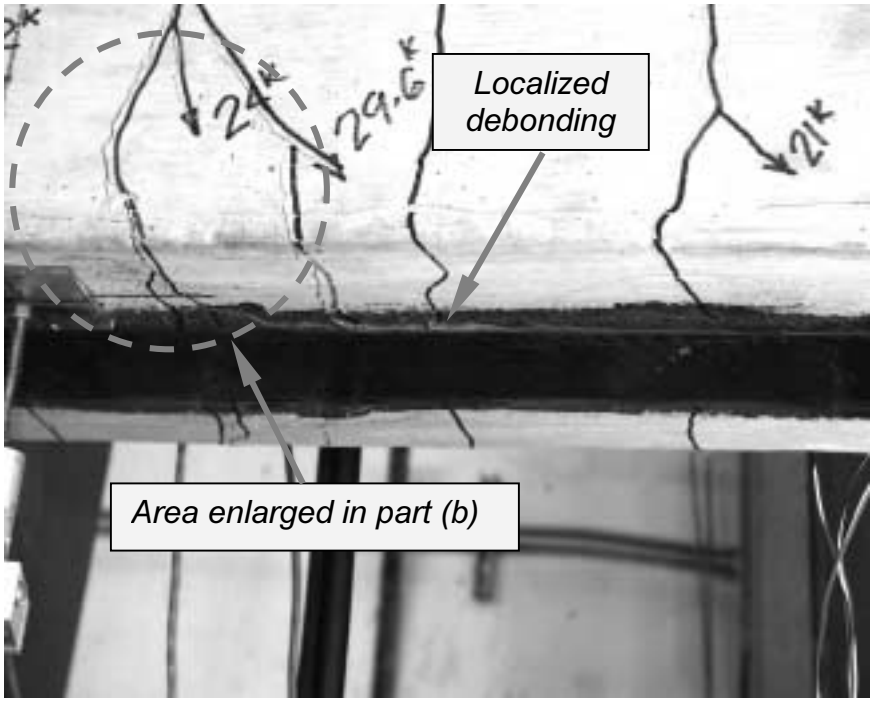

(a) Localized debonding in the vicinity of crack

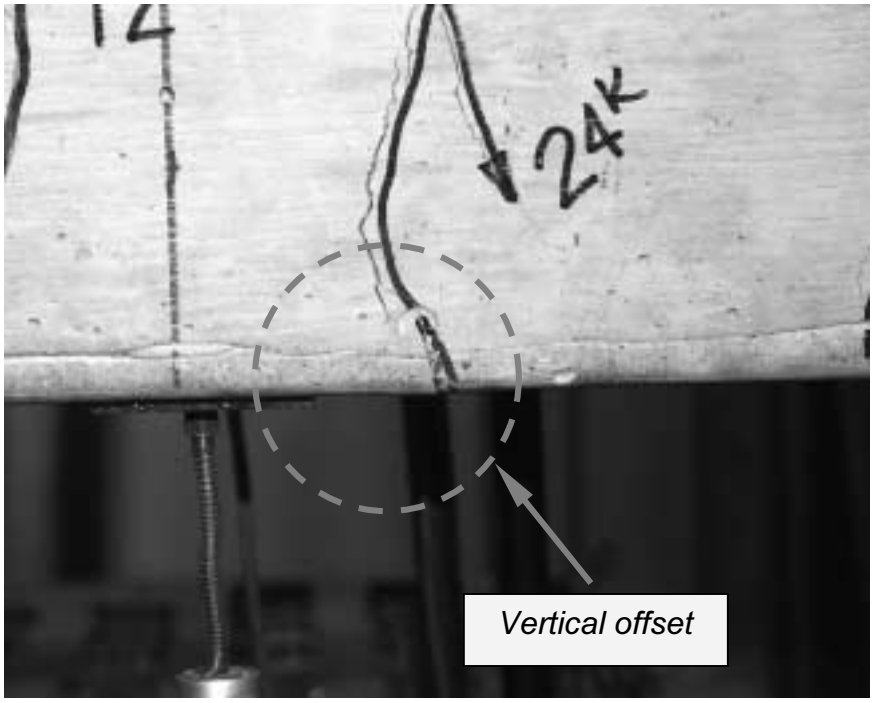

(b) Vertical movement across critical crack within shear span

Figure 6.4 Initiation of Debonding Caused by Vertical Offset at Crack Location (Specimen B1)

Concrete was pulled-off from the surface of the beam in the form of a wedge in the region where debonding of the composite laminate initiated. A detail of the surface of the concrete after debonding of the CFRP composite for specimen B1 is shown in Figure 6.5. The characteristics of the debonding sequence for specimens A3, C1, C2, D1, and D2 were similar to the ones described in this section. In these specimens the bonded length of the CFRP composites was larger than 2.5 times the depth of the beams.

Figure 6.5 Bottom View of Specimen B1 Showing the Surface of the Concrete in the Area where CFRP Debonding Initiated

The effect of surface preparation was examined in some specimens strengthened using the bottom application technique. The type of surface preparation on beams strengthened using composite systems C (specimens C1 and C2) and D (specimens D1 and D2) was varied to evaluate if the observed mode of failure would change. The surface of the concrete was abraded by grinding or by pressure sand blasting (Table 5.1). The sequence of debonding was not affected by the use of different techniques of surface preparation. The effect on the load-deflection will be discussed in Section 6.2.5.

Additionally, the surface of the composites was examined after the laminates debonded from these specimens. The amount of concrete that remained attached to the composites after debonding varied depending on the type of surface preparation that was used. No significant difference in the amount of concrete that remained attached to the surface of the composite laminate for composite type C was observed after debonding. Figure 6.6 shows the surface of the concrete and CFRP composite of specimen C2 after failure. On the other hand, the surface of the composite plate for beams strengthened using composite type D showed more concrete after failure when the beam surface was prepared by sand blasting (Figure 6.7). Therefore, no clear trend could be established based on the limited number of tests that were conducted. Grinding was therefore used to prepare the surface of the concrete for all subsequent specimens.

Figure 6.6 Concrete Pulled-off from Surface of Specimen C2 after Debonding

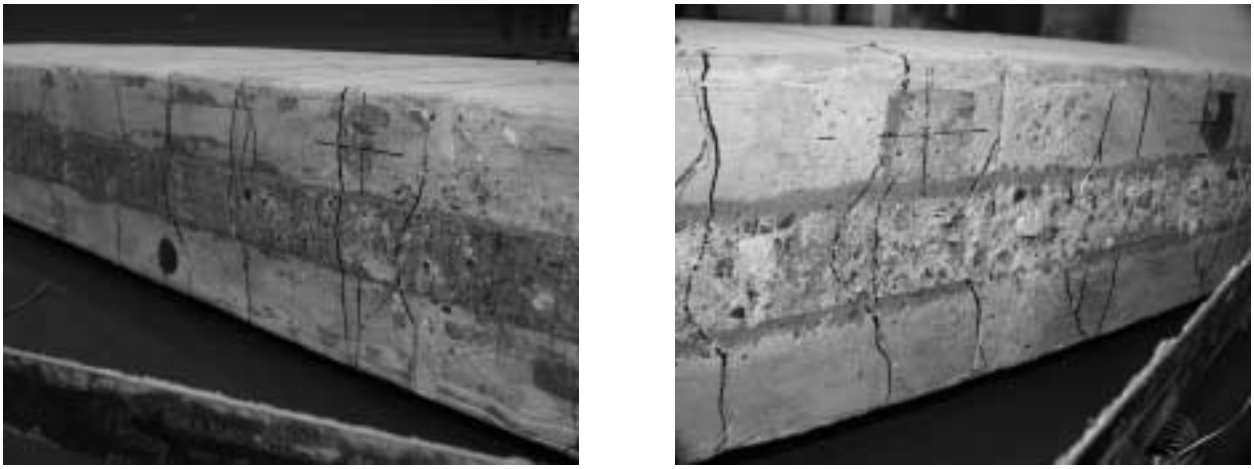

(a) Specimen D1
(Surface Prepared by Grinding)

(b) Specimen D2
(Surface Prepared by Sand Blasting)

Figure 6.7 Comparison of Bottom Surface of Concrete after Debonding of CFRP for Specimens D1 and D2

6.2.2 Beams Strengthened Using CFRP Bottom Application and Straps

The specimens strengthened using CFRP applied to the bottom with straps behaved in a different manner than the specimens where the composites were applied only to the bottom. The addition of straps was intended to arrest the debonding cracks that were observed to propagate on both sides of the composites. Also, the use of vertical straps at discrete locations along the composites was intended to control the vertical offset observed at the location of flexural-shear cracks.

The specimens in this category did not exhibit any signs of debonding before reaching the yield load. After yielding, local debonding initiated either at the critical section (crack initiator) or at the location of

flexural cracks. Although localized debonding triggered the formation of debonding cracks along the composites, the straps were effective in arresting the crack propagation (Figure 6.8). Therefore, the specimens exhibited larger deflections and were able to sustain higher loads than similar specimens that were strengthened without using straps. In most cases, failure was reached when the composites ruptured at the control section although debonding had proceeded toward the ends of the beam (Figure 6.9).

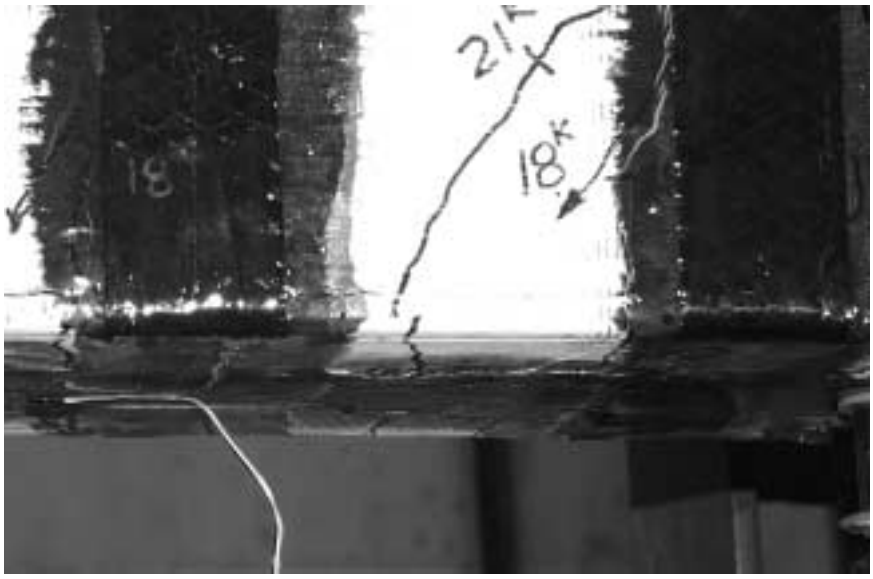

Figure 6.8 Localized Debonding Arrested by Vertical Straps in Specimen B2

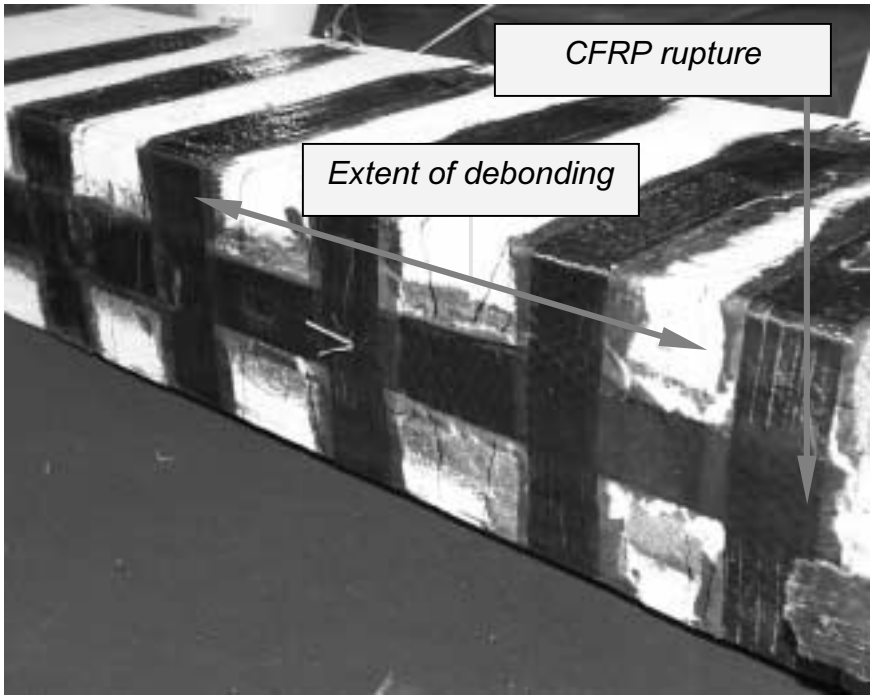

Figure 6.9 Extent of Debonding and Rupture of CFRP Composite in Specimen B2

Different configurations of straps and bonded lengths were examined using this strengthening scheme. Specimens B2 and C3 had six straps within the shear span placed along the entire bonded length of the CFRP composites. The bonded length in these specimens was 35 in. and 45 in., respectively. Both specimens failed by rupture of the composite laminate at the critical section (Figure 6.9). Therefore, it was decided to investigate whether reducing the number of straps within the shear span would have any effect on the behavior of the specimens. Specimen B4 was tested with the same bonded length as B2 but with only four straps placed along the shear span. Failure of specimen B4 was also characterized by CFRP rupture near the critical section after debonding had propagated toward the end of the composite laminate (Figure 6.10). Finally, both the number of straps and bonded length of the composite were modified in specimen B5. The bonded length was reduced to 24 in. from the critical section. Four straps were placed along the shear span of the specimen. The mode of failure of this specimen was by debonding of the CFRP composite from the surface of the concrete (Figure 6.11). Although the failure mode of specimen B5 was different from other cases that used this strengthening scheme, the observed behavior of the specimen was similar to other beams strengthened using this strengthening scheme. From these tests, it can be concluded that straps were effective in arresting the debonding cracks from propagating suddenly toward the end of the composites. However, when the debonding cracks were close to the end of the composite, failure by debonding was not eliminated.

Figure 6.10 Rupture of CFRP Composite in Specimen B4

Figure 6.11 Bottom View of Specimen B5 after Debonding

6.2.3 Beams Strengthened Using CFRP Bonded to Sides

Several specimens were strengthened with the CFRP composites bonded to the sides of the beams. This strengthening configuration was chosen to eliminate the effect of local debonding of the composites caused by the relative vertical displacement of the surface of the concrete at crack locations (Figure 6.3). Composite systems B, C, and D were used to strengthen the beams with this scheme.

No local debonding was observed up to the yield load of the specimens. After yielding, secondary cracks formed adjacent to existing flexural cracks (Figure 6.12). Some of these cracks propagated horizontally following the upper edge of the CFRP composites and eventually caused debonding in some of the specimens (specimen C4 and D3). One of the specimens strengthened using this scheme failed by CFRP composite rupture at the critical section (specimen B3). The concrete cover was pulled-off from this specimen after rupture of the CFRP composite (Figure 6.13).

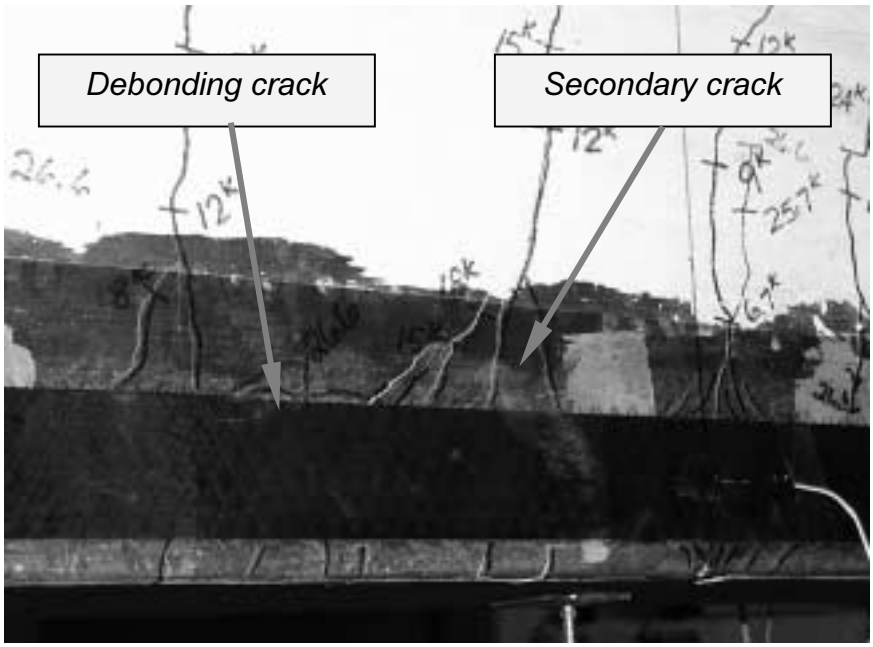

Figure 6.12 Propagation of Secondary Cracks into a Debonding Crack in Specimen B3

Specimen D3 also exhibited formation of secondary cracks that formed from existing flexural cracks. However, the cracks that propagated horizonally along the top edge of the composite plates caused debonding from the surface of the concrete at failure. The formation of secondary and debonding cracks during testing of specimen D3 is shown in Figure 6.14. Debonding of the CFRP composite from the surface of the concrete from specimen D3 is shown in Figure 6.15. Diagonal cracks that formed on the bottom surface of the beam as a result of debonding of the composite plates can be observed in this figure.

The results from these series of tests indicated that failure by debonding of the CFRP composites from the surface of the concrete was eliminated in some specimens by placing the the laminates on the sides of the beams. However, debonding still occurred in the specimens strengthened using composite system D but the propagation of debonding did not occur as suddenly as for the beams with composites bonded to the tension face. Because of this, vertical straps were also used in some specimens to evaluate if debonding was delayed with the use of straps.

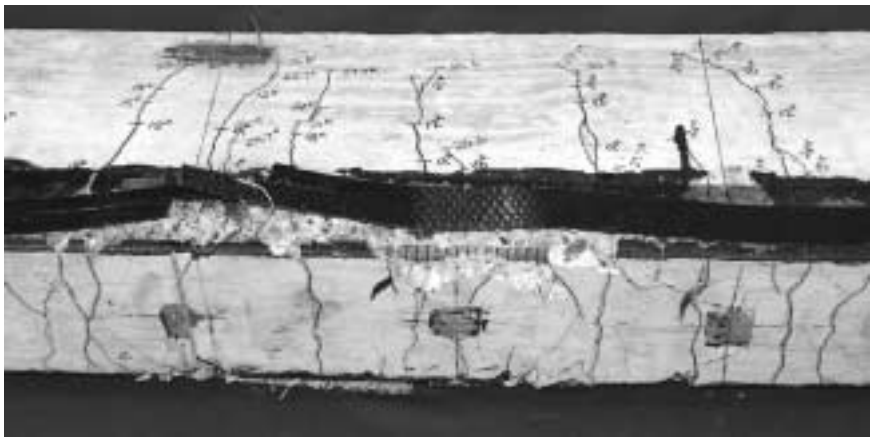

Figure 6.13 Rupture of CFRP Composite in Specimen B3 after Failure

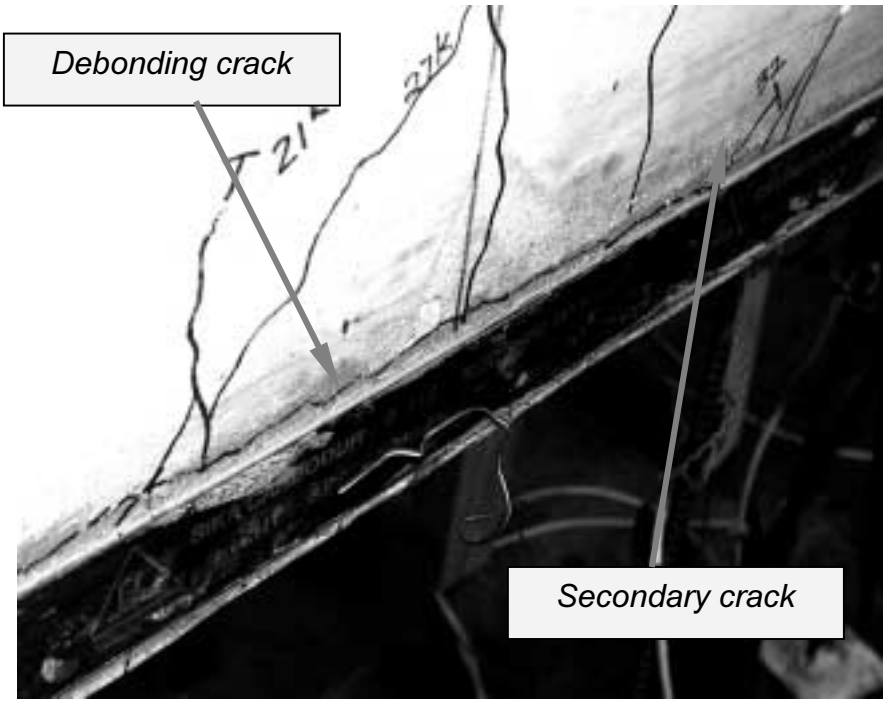

Figure 6.14 Close-up of Debonding Crack that Originated from a Secondary Crack in Specimen D3

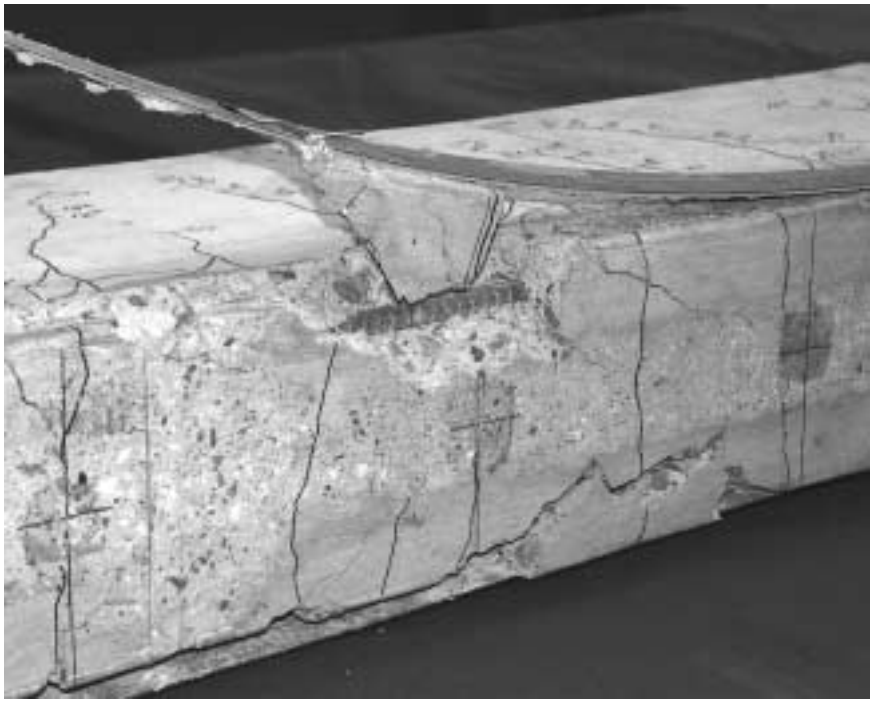

Figure 6.15 Bottom View of Specimen D3 Showing Exposed Reinforcement after Debonding of CFRP Plates

6.2.4 Beams Strengthened Using CFRP on Sides with Straps

Specimens D4 and D5 were strengthened using the CFRP composites bonded to the sides of the beams with the addition of straps throughout the entire length of the composites. The lengths of the composite plates measured from the critical section were 45 in. and 30 in. for specimens D4 and D5, respectively. The observed behavior of both specimens was similar, so only specimen D4 will be discussed here.

Evidence of debonding in these specimens was not observed for loads below the yield load of the specimens. Beyond yield, secondary cracks formed and turned horizontally into debonding cracks as for the specimens described in the previous section. However, the debonding cracks were arrested at every strap location and delayed debonding of the CFRP plates. The vertical straps restrained the composite plates from separating from the surface of the concrete and therefore controlled the propagation of the debonding cracks. Figure 6.16 shows the formation of secondary cracks and the propagation of debonding cracks that was delayed by the presence of vertical straps in specimen D4. Debonding also occurred at the end of the CFRP composite plates in specimen D4 prior to total debonding from the surface of the concrete (Figure 6.17). This can be attributed to the propagation of a flexural-shear at the end of the composites caused by the higher load that was applied to this specimen. The strengthening scheme was effective in delaying the propagation of debonding but failure was also characterized by debonding of the longitudinal composite plates followed by shearing or debonding of the transverse composite straps (Figure 6.18).

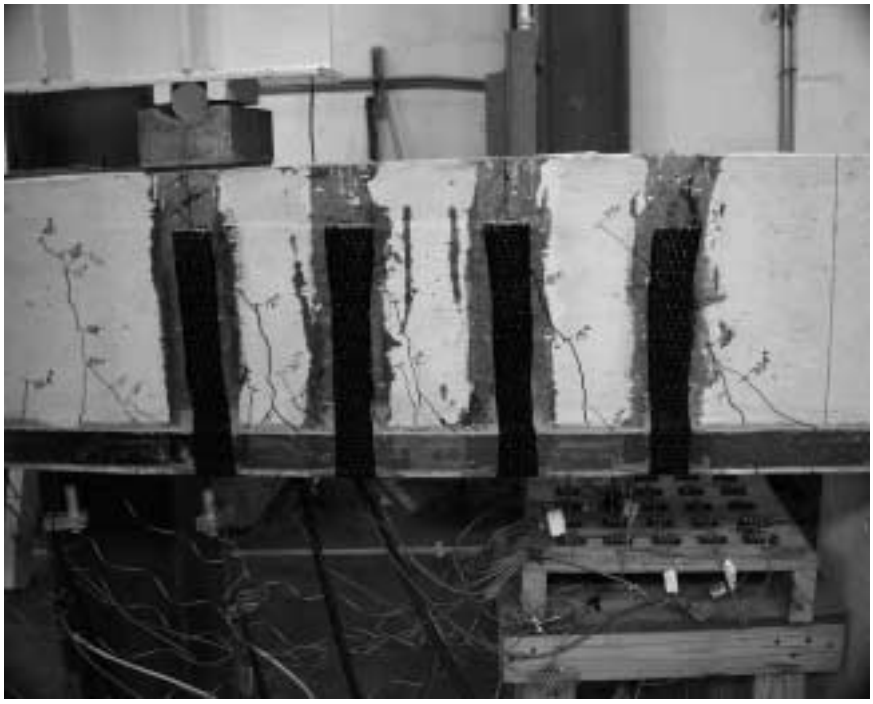

Figure 6.16 Formation of Debonding Cracks in Specimen D4

Figure 6.17 Debonding at the End of the CFRP Composite Plate in Specimen D4

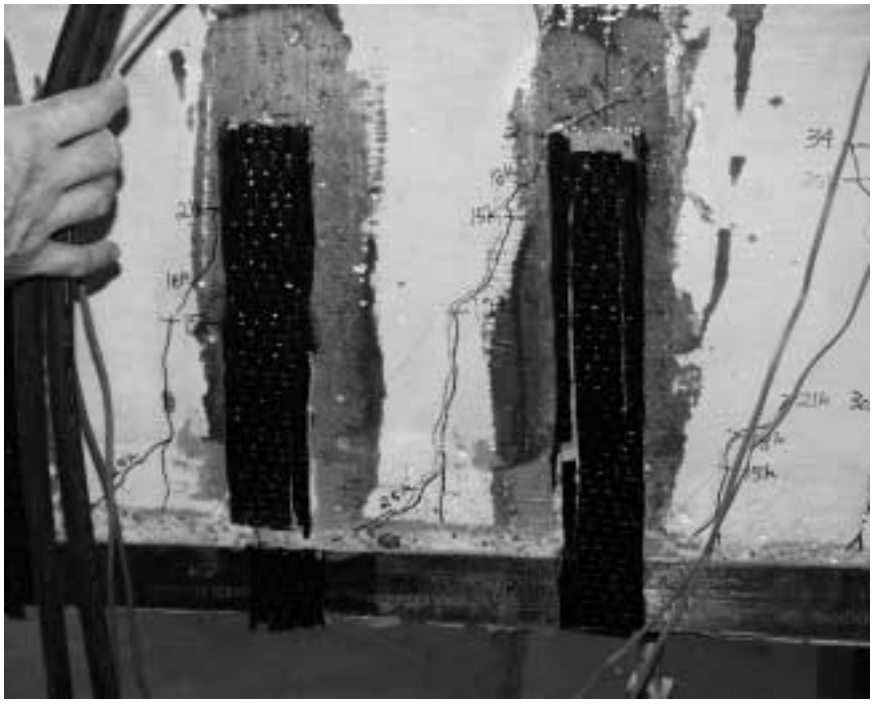

Figure 6.18 Shearing of Transverse Composite Straps after Debonding of CFRP Composites in Specimen D4

6.2.5 Beams Subjected to Cycles of Moisture and Environmental Exposure

Specimens A-LT1 and A-LT2 were strengthened using the same strengthening scheme as specimen B4. These beams were cracked before the application of the composite system. After the beams were strengthened, they were placed outside the laboratory to subject them to periodic moisture and exposure to the environment. Specimen A-LT2 was also subjected to a sustained load approximately equal to 20% of the yield load of the strengthened specimen. After 8 months of exposure, the beams were then tested statically to failure inside the laboratory.

The observed response of the beams during testing was similar to the response of specimen B4. No evidence of debonding was observable at load levels below the yield load. Debonding cracks formed at each of the existing flexural cracks and were arrested at every strap location along the shear span. Both specimens failed by rupture of the CFRP composite at or near the maximum moment section. At failure, debonding of the CFRP composite from the surface of the concrete had propagated approximately 14 in. toward the supports. The load at failure of specimen A-LT2 was slightly lower than the failure load of specimen A-LT1. The differences in the measured load-deflection response between these specimens will be discussed in Section 6.3. The cracking patterns and crack widths of the specimens at failure are presented in Appendix B. Figure 6.19 shows specimen A-LT1 after rupture of the CFRP composite. Figure 6.20 shows specimen A-LT2 after failure. In this case, failure of the specimen was characterized by longitudinal splitting of the CFRP composite and fiber rupture at the sections of maximum moment.

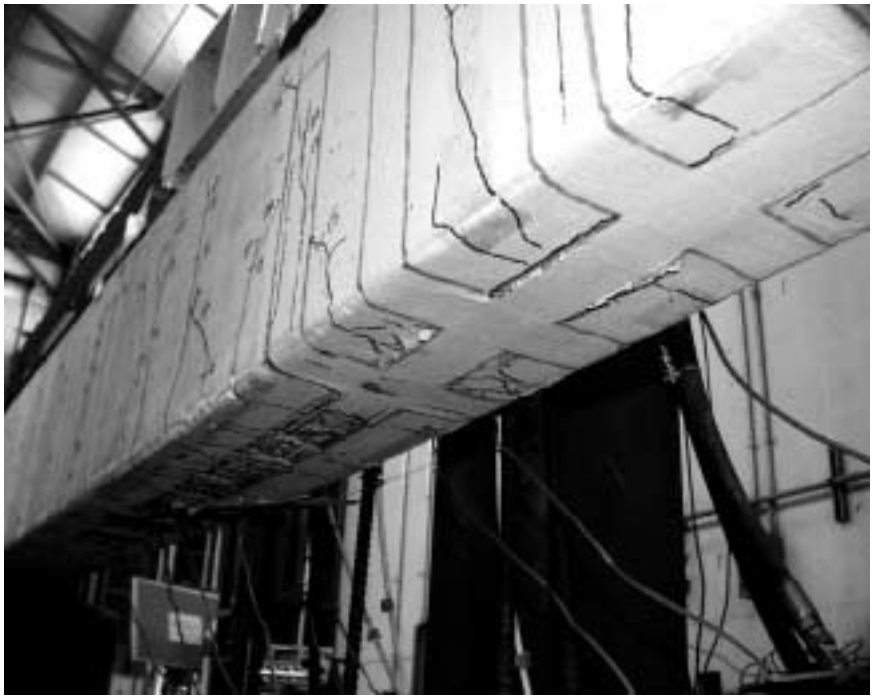

Figure 6.19 Bottom View of Specimen A-LT1 after Rupture of the CFRP Composite

Figure 6.20 Bottom View of Specimen A-LT2 after Rupture of the CFRP Composite

6.3 MEASURED LOAD-DEFLECTION RESPONSE

The measured load-deflection response of the specimens is presented in this section. A qualitative description of the load-deflection behavior observed in all the specimens is presented in Section 6.3.1. The measured load-deflection response of each group of specimens strengthened using the different composite systems is then compared in Section 6.3.2. The type of composite and the strengthening scheme influenced the behavior of the specimens. The differences in behavior that were observed from the examination of the load-deflection response of the specimens are also discussed in this section.

6.3.1 Qualitative Response of Strengthened Specimens

The general trends in the load-deflection response that were observed during testing of the strengthened specimens are presented in this section. The typical load-deflection response of the strengthened specimens is described with reference to Figure 6.21. In this figure, three distinct regions can be observed. Each region is represented qualitatively by a line with a slope that depends on the flexural stiffness of the strengthened specimen. The first region in the load-deflection response of the strengthened beams (region A) ends at the load corresponding to cracking. The second region (region B) is bounded by the load corresponding to cracking and the yield load. Finally, the yield load and the maximum load of the strengthened specimens bound the third region (region C) in the load-deflection behavior.

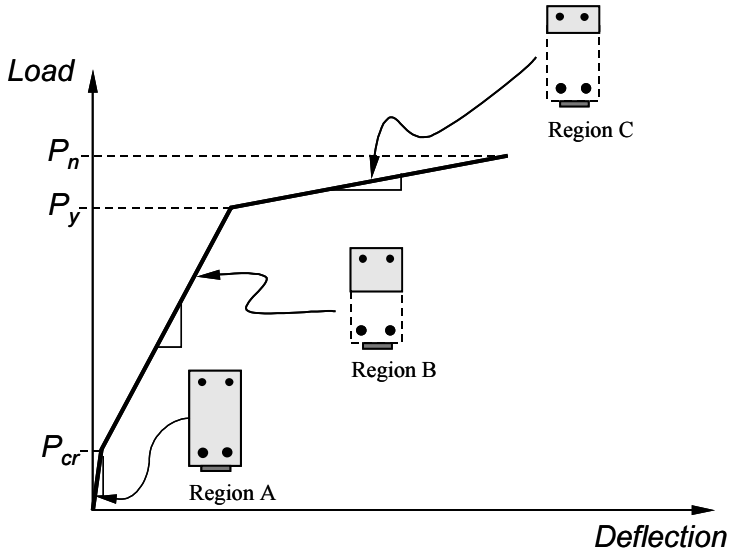

Region	Material Behavior		
	Concrete	Reinforcement	CFRP
A	Uncracked	Elastic	Elastic
B	Cracked	Elastic	Elastic
C	Cracked	Yielding	Elastic

Figure 6.21 Qualitative Representation of the Load-Deflection Response of the Strengthened Specimens

The slope of the load-deflection curve in each of the regions was controlled by the stiffness of the specimens. In region A, the specimens remained uncracked and the flexural stiffness could be calculated by using gross cross-sectional properties of the specimens. The flexural stiffness of the specimens in region B corresponds to cracked concrete and elastic behavior of the reinforcement and CFRP laminates. The slope of the load-deflection curve in this region is controlled by the amount of reinforcement and CFRP composites on the cross section. Finally, the flexural stiffness in region C is controlled by the stiffness of the CFRP composites and the straw-hardening stiffness of the reinforcement. The behavior described in this section is similar to the behavior of unstrengthened reinforced concrete elements. However, the slope of the load-deflection curves in Region C was larger for the strengthened beams due to the stiffness of the CFRP composites. The length and slope of the load-deflection curves of the strengthened specimens varied depending on the type and area of composite system that was used to strengthen the beams. The measured load-deflection response of all specimens is presented and discussed in Section 6.2.5.

6.3.2 Measured Load-Deflection Response of Different Groups of Specimens

The load-deflection response of the specimens was used initially to evaluate the differences in global response of all the beams. Because the beams were strengthened using different composite systems and schemes, the response was only compared within beams strengthened using the same composite system. In this way, the effect of using the different schemes was evaluated without introducing variations caused by the differences in the mechanical properties of the different composite systems. However, as discussed in the previous section, the trends in the load-deflection response were similar for the different composite systems, so the main differences in behavior can be attributed to the strengthening scheme and not the composite system. A brief description of the variables included in each group of beams is provided first, followed by a comparison of the load-deflection response of the beams within each group.

(a) Beams Strengthened Using Composite System A

Four specimens were strengthened using composite system A applied to the tension face of the specimens. The main variable that was investigated in this series of beams was the bonded length beyond the critical section. The specimens were strengthened using two plies of CFRP composites with a 2 in. width. Specimen A4 was strengthened using 1 ply of CFRP composite with a 4 in. width. Table 6.1 summarizes the variations of the composite configuration of this group of specimens and the observed failure modes.

Table 6.1 Summary of Parameters and Failure Modes for Specimens Strengthened Using Composite System A

Specimen	Composite Width, in.	Number of Plies	Bond Length, in.	Failure Mode
A1	2	2	10	CFRP Debonding
A2	2	2	14	CFRP Debonding
A3	2	2	30	CFRP Debonding
A4	4	1	15	CFRP Debonding

The load-deflection response of this group of specimens is shown in Figure 6.22. The response of the strengthened specimens is compared in each chart with the response of the control specimen. The response of the specimens was clearly affected by the bonded length of the composite system beyond the critical section. The behavior of all the specimens was similar before yielding. The slope in the load-deflection diagram of the strengthened specimens followed closely the slope of the control specimen, indicating that stiffness of the beams was not increased significantly by the CFRP composite. Specimen

A4 exhibited the largest increase in cracking load from the cracking load of the control specimen. However, this difference can be attributed to the difference in strength of the concrete that was used in the fabrication of the specimens.

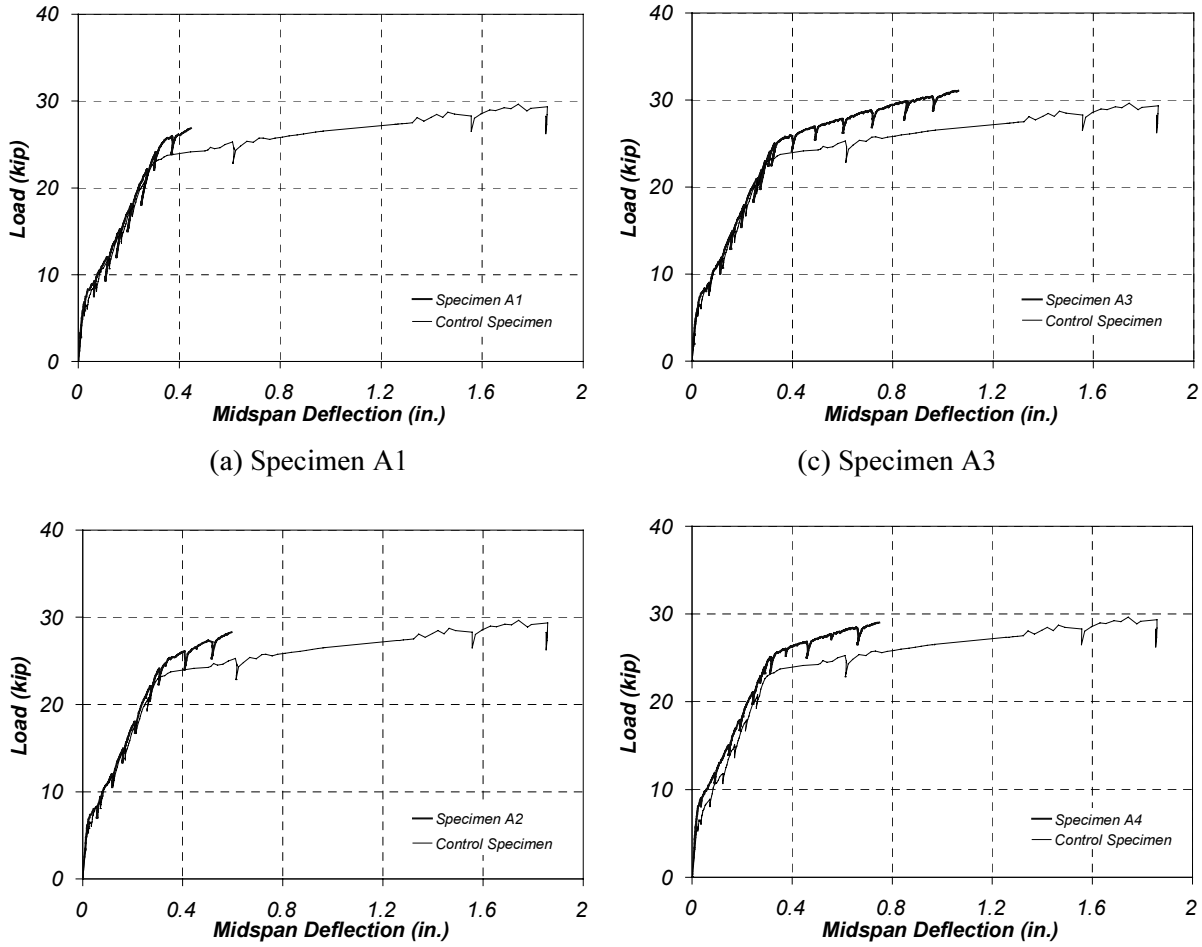

(a) Specimen A1 (c) Specimen A3

(b) Specimen A2 (d) Specimen A4

Figure 6.22 Comparison of the Load-Deflection Response of Specimens Strengthened Using Composite System A

The yield load of the strengthened specimens was approximately 10% larger than the yield load of the control specimen. After yielding, the behavior of the specimens was influenced by the length of the composite laminates. The deformation capacity of the specimens before debonding of the CFRP composite from the surface of the concrete increased with bonded length as evidenced from these load-deflection plots. However the slope of the load-deflection diagrams was approximately the same for all the specimens. The main parameters of the measured load-deflection curves are listed in Table 6.2.

Table 6.2 Summary of Response of Specimens Subjected to Static Loads

Specimen	P_{cr}, kip	Δ_{cr}, in.	P_y, kip	Δ_y, in.	P_{max}, kip	Δ_{max}, in.
Control A and B	6.6	0.037	22.6	0.292	29.4	1.858
A1	8.3	0.038	23.7	0.299	26.9	0.446
A2	7.8	0.048	24.1	0.306	28.3	0.595
A3	7.6	0.044	23.9	0.314	31.1	1.062
A4	8.4	0.030	24.9	0.316	29.0	0.748
B1	8.4	0.040	24.8	0.310	29.8	0.809
B2	8.5	0.033	24.9	0.309	31.9	1.077
B3	8.1	0.032	24.3	0.311	30.8	1.128
B4	7.5	0.030	23.9	0.307	29.8	1.066
B5	7.5	0.030	24.4	0.302	29.2	0.907
Control C and D	9.0	0.070	22.1	0.300	28.3	2.247
C1*	-	-	27.3	0.403	32.3	0.903
C2	9.8	0.075	25.4	0.345	28.3	0.665
C3	9.4	0.042	27.1	0.358	33.5	0.980
C4	9.7	0.048	25.8	0.332	29.8	0.931
D1	9.9	0.053	26.7	0.335	28.8	0.431
D2	9.5	0.044	27.1	0.333	30.1	0.549
D3	9.9	0.037	29.9	0.352	35.7	0.650
D4	9.8	0.048	31.4	0.372	42.3	0.906
D5	8.8	0.052	30.8	0.373	40.6	0.843
Specimens Exposed to Moisture						
A-LT1**	8.1	0.032	24.8	0.298	32.0	1.171
A-LT2**	-	-	23.4	0.260	29.6	0.837

*Specimen was cracked during handling in the laboratory before strengthening.
** Specimens were loaded to 9 kip before strengthening to cause cracking.

Specimens A3 and A4 were tested to evaluate equations contained as part of the literature from the manufacturer of composite system A. These design guidelines contain equations to calculate the required length for the CFRP composite to reach the rupture strength of the laminate [Master Builders, 1998]. The design guidelines recommend the use of Equation 6.1 to calculate the required length of the composites to reach the rupture stress. Equation 6.1 is a function of the rupture stress of the composite, thickness of the laminate, and the concrete strength. Applying Equation 6.1 to calculate the required length of the composite for specimens A3 and A4 results in bond lengths approximately equal to 30 in. and 15 in., respectively. Although the strength of the composites in specimens A3 and A4 was equal, the deformation capacity of the specimens was different. Specimen A4 failed at a load approximately 8% lower than specimen A3. Also, the midspan deflection of specimen A4 was approximately 25% smaller than specimen A3. This result indicated that the use of Equation 6.1 might lead to unconservative designs for particular configurations of CFRP composites.

$$l_{dp} = \frac{f_{pu}\, t_p\, n}{3\sqrt{f'_c}} \tag{6.1}$$

where:

l_{pd} = Bond length, in.
f_{pu} = Rupture stress of the composite, psi
t_p = Design thickness of the composite, in.
n = Number of plies
f'_c = Compressive strength of concrete, psi

(b) Beams Strengthened Using Composite System B

Five specimens were strengthened using composite system B. The composites were bonded symmetrically about the centerline of the beams. The results from the tests of beams strengthened using composite system A indicated that the strength of the composites was not reached before debonding, even when the laminates extended nearly the entire length of the span. Therefore, the composite laminates in the first four specimens in this group extended 35 in. from the critical section. The longitudinal composites were formed using two plies of unidirectional carbon fibers. Three different schemes were used to strengthen the beams. Therefore, the main variable investigated in these tests was the strengthening scheme. Only specimen B5 was strengthened using a bond length equal to 24 in. after observing that specimens B2 through B4 failed by rupture of the CFRP composite. Table 6.2 summarizes the main parameters of the specimens in this group and the observed failure modes.

Table 6.3 Summary of Parameters and Failure Modes for Specimens Strengthened Using Composite System B

Specimen	Bond Length, in.	Width of CFRP, in.	Number of Straps*	Composite Scheme	Failure Mode
B1	35	3	-	CFRP applied to the tension face	CFRP Debonding
B2	35	2	6	Bottom application with straps	CFRP Rupture
B3	35	2	-	CFRP applied to sides of beam	CFRP Rupture
B4	35	2	4	Bottom application with straps	CFRP Rupture
B5	24	2	4	Bottom application with straps	CFRP Debonding

*Number of straps placed along the shear span of the beams.

The measured load-deflection response of this group of specimens is presented in Figure 6.23. The measured response is compared with the load-deflection response of the control specimen. A summary of the main parameters obtained from the load-deflection response is listed in Table 6.2. The response of the strengthened specimens is similar to the response of the control beam at load levels below the yield load (25 kip). After yielding, the behavior of the specimens was controlled by the performance of the strengthening scheme.

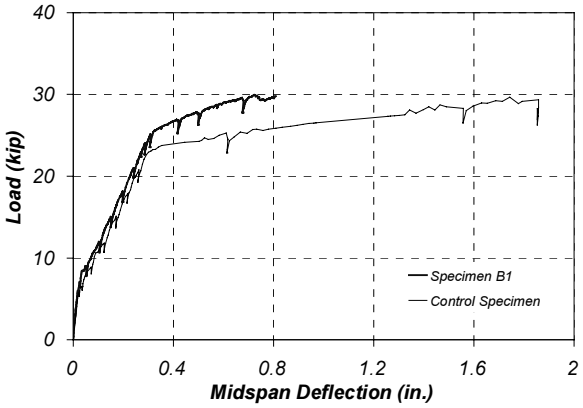

(a) Specimen B1

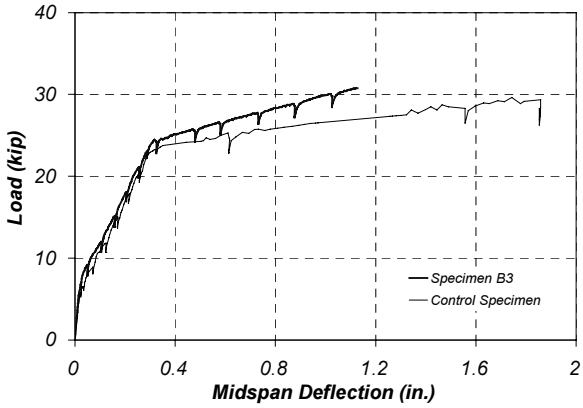

(c) Specimen B3

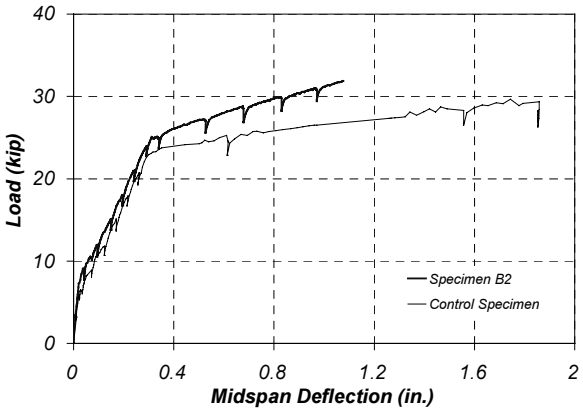

(b) Specimen B2

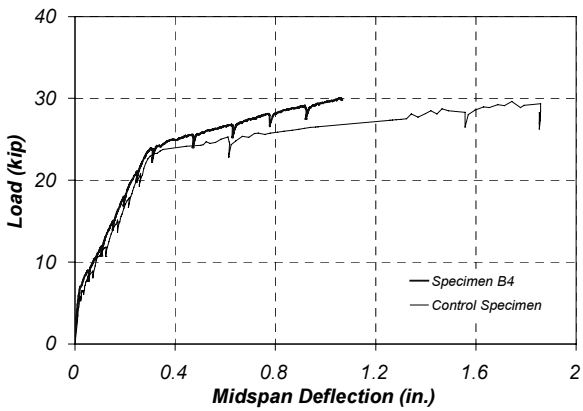

(d) Specimen B4

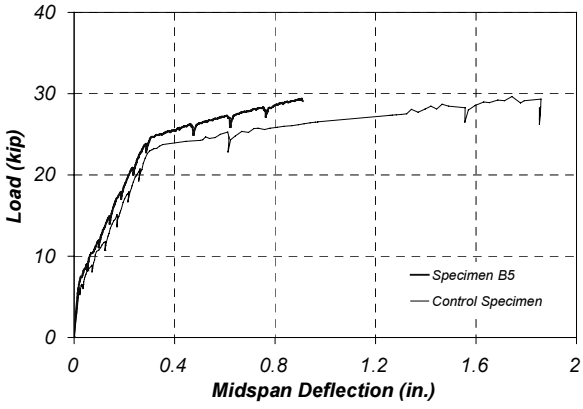

(e) Specimen B5

Figure 6.23 Comparison of the Load-Deflection Response of Specimens Strengthened Using Composite System B

Specimen B1 showed the smallest deflection at failure of this group of specimens (approximately 0.8 in.). As observed, the deflection at failure was significantly increased in specimens B2 and B3 with the addition of straps or by placing the composites on the sides, respectively. Also, failure of specimens B2 and B3 was characterized by composite rupture instead of debonding from the surface of the concrete. The maximum measured midspan deflection of specimens B2 and B3 was approximately 1.1 in. The beams reached higher ultimate loads by increasing the deformation capacity of the specimens.

Specimens B4 and B5 were fabricated using a different heat of steel than specimens B1 through B3. The yield stress of the reinforcing bars of these specimens was slightly lower than the yield stress of the bars used in specimens B1 to B3. Therefore, the slight difference in the slope of the load-deflection response of these specimens after yielding as compared to specimens B1 to B3 can be attributed to this factor rather than to differences in the performance of the composite system. The deformation capacity of specimens B4 and B5 was approximately 1.1 in. and 0.9 in., respectively (Table 6.2). Therefore, reducing the bond length of the composite in specimen B5 affected the deformation capacity of the specimen and the mode of failure.

(c) Beams Strengthened Using Composite System C

Four specimens were strengthened using composite system C. The composites were bonded symmetrically about the centerline of the beams using a 45-in. bonded length. The composites were 2 in. wide and were formed using two plies of unidirectional carbon fiber woven fabric. Three different strengthening schemes were used to strengthen the beams. In this group of tests, the variables investigated were the type of preparation of the surface of the concrete and the strengthening scheme. Table 6.4 summarizes the main parameters of the strengthened beams in this group and the observed failure modes.

Table 6.4 Summary of Parameters and Failure Modes for Specimens Strengthened Using Composite System C

Specimen	Bond Length, in.	Number of Straps*	Surface Preparation	Composite Scheme	Failure Mode
C1	45	-	Grinding	CFRP applied to the tension face	CFRP Debonding
C2	45	-	Sandblasting	CFRP applied to the tension face	CFRP Debonding
C3	45	6	Grinding	Bottom application with straps	CFRP Rupture
C4	45	-	Grinding	CFRP applied to sides of beam	CFRP Debonding

*Number of straps placed along the shear span of the beams.

Figure 6.24 shows the measured load-deflection response of the beams strengthened using composite system C. The response of the specimens are also compared with the response of the control specimen in this figure. Similarly to the beams strengthened using composite systems A and B, the slope of the load-deflection curve at load levels below the yield load is similar to the slope of the control specimen. The yield load of the strengthened specimens, however, was approximately 15% higher than the yield load of the control specimen (Table 6.2). After yielding, the slope in the load-deflection diagram of the strengthened specimens was steeper than the control specimen. Therefore, it is evident that the response of the specimens beyond yield was controlled by the strength and stiffness of the CFRP composites.

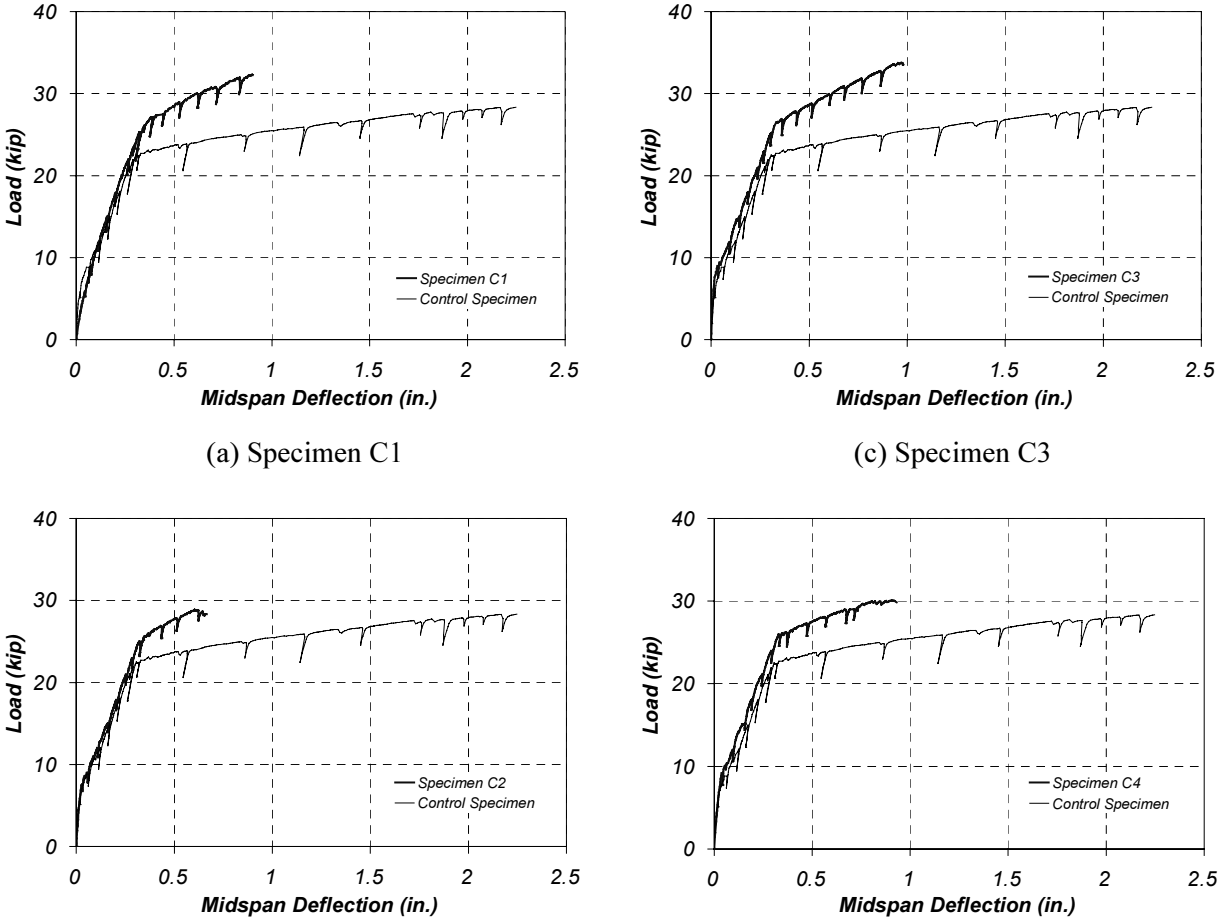

(a) Specimen C1

(c) Specimen C3

(b) Specimen C2

(d) Specimen C4

Figure 6.24 Comparison of the Load-Deflection Response of Specimens Strengthened Using Composite System C

The effect of the type of surface preparation on the load-deflection behavior of these specimens can be observed by comparing the response of specimens C1 and C2. The surface of the concrete in specimen C1 was prepared by grinding before bonding the CFRP system, whereas the surface in specimen C2 was prepared by sand blasting. Although sand blasting created a rougher concrete surface than grinding, the bond strength of the composite in specimen C2 was not increased with the use of this technique. The maximum midspan deflection of specimen C2 was approximately 0.65 in. while the maximum measured deflection of specimen C1 was approximately 0.9 in. Therefore, specimen C1 was able to sustain a higher load than specimen C2.

Specimen C3 exhibited the largest displacement capacity and load of this group of beams. The maximum midspan deflection of specimen C3 was approximately 1.0 in. at a load equal to 33.5 kip. This specimen was the only specimen in the group that failed by rupture of the composite laminate. The effect of placing the composite system on the sides of the beam is shown in the response curve for specimen C4. In this case, this strengthening scheme was not as effective as in the case of specimen B3. The maximum deflection at failure of the specimen was not significantly larger than the maximum measured displacement of specimen C1. Also, as a consequence of reducing the lever arm of the composite by placing it on the sides of the beam, the maximum measured load was lower than the maximum measured load of specimen C1 (Table 6.2).

(d) Beams Strengthened Using Composite System D

Composite system D was used to strengthen five specimens using different schemes. The composites were bonded symmetrically about the centerline of the beams using a 45 in. bond length, except for specimen D5 where a 30-in. bonded length was used. The composite system consisted of pultruded carbon composite plates that were approximately 2 in. wide. Three different strengthening schemes were tested using this group of beams. The main variables that were investigated were the type of preparation of the surface of the concrete and the strengthening scheme. Table 6.5 summarizes the main parameters of the strengthened beams in this group and the observed failure modes.

Table 6.5 Summary of Parameters and Failure Modes for Specimens Strengthened Using Composite System D

Specimen	Bond Length, in.	Number of Straps*	Surface Preparation	Composite Scheme	Failure Mode
D1	45	-	Grinding	CFRP applied to the tension face	CFRP Debonding
D2	45	-	Sandblasting	CFRP applied to the tension face	CFRP Debonding
D3	45	-	Grinding	CFRP applied to sides of beam	CFRP Debonding
D4	45	4	Grinding	CFRP applied to sides of beam with straps	CFRP Debonding
D5	30	4	Grinding	CFRP applied to sides of beam with straps	CFRP Debonding

*Number of straps placed along the shear span of the beams.

The comparison of the measured load-deflection response of this group of beams with the control specimen is presented in Figure 6.25. The main parameters obtained from the load-deflection curves are contained in Table 6.2. The slopes of the load-deflection curves of the strengthened specimens are consistently steeper than the control specimen. This phenomenon was not as apparent in the other groups of beams and is attributed to the strength properties of composite system D. The yield load was also higher in the strengthened specimens than the control beam. The increase in yield load depended on the configuration of the composite system (Table 6.2). In this case the area of composite plates was doubled when the system was applied to the sides of the beams because the system consisted of prefabricated plates that were not cut to match the strength of the 2 in. plate bonded on the tension face of the beams.

Specimens D1 and D2 were strengthened using the composite system applied to the tension face of the beams. The surface of the concrete in specimens D1 and D2 was prepared by grinding and sand blasting, respectively. Specimen D2 exhibited a larger deformation capacity and higher ultimate load than specimen D1. However, only a minor improvement in the load-deflection response was observed.

On the other hand, placing the composite system on the sides of the beams resulted in a significant increase in the maximum measured deflections. This technique was used in specimens D3 to D5. The maximum measured loads cannot be compared directly with the ultimate load of specimen D1 because the areas of composites were different. The maximum deflection of specimen D3 was approximately 50% higher than specimen D1. Similarly, maximum midspan deflections of specimens D4 and D5 were approximately 110% and 95% higher then the measured deflection of specimen D1. In these specimens, the straps bonded along the shear span of the composite plates restrained the propagation of the cracks that caused debonding of the plates. It should be noted, however, that although improved behavior was

observed by applying some of the more involved strengthening techniques, failure was always initiated by debonding of the composites from the surface of the concrete.

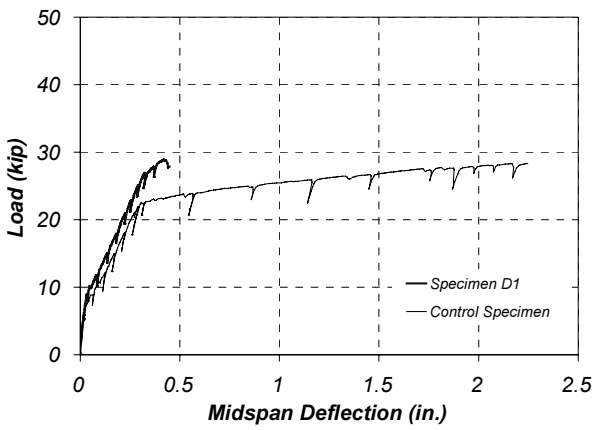

(a) Specimen D1

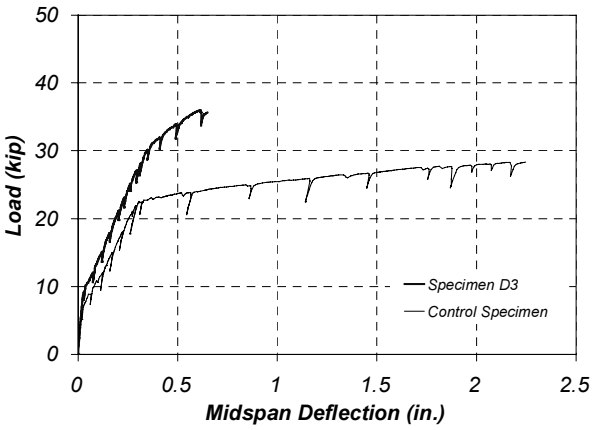

(c) Specimen D3

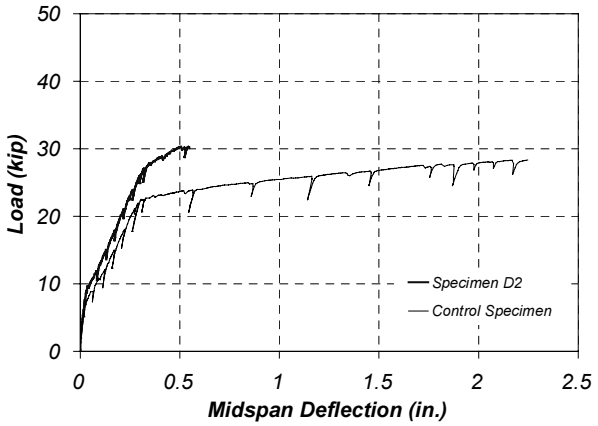

(b) Specimen D2

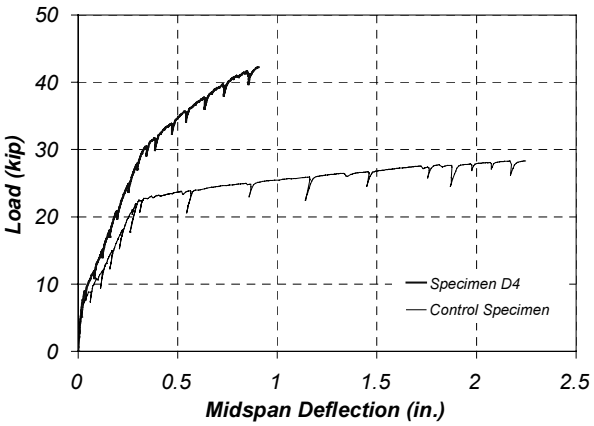

(d) Specimen D4

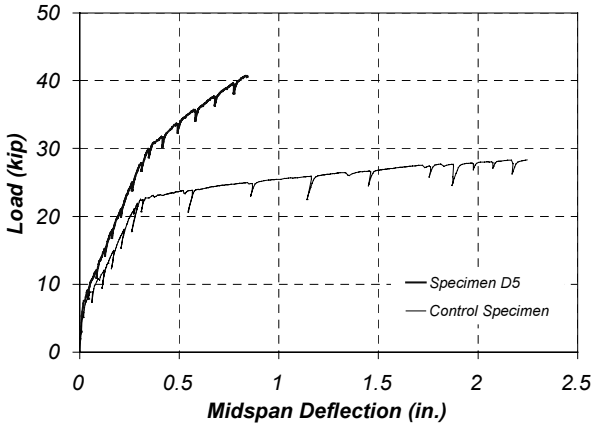

(e) Specimen D5

Figure 6.25 Comparison of the Load-Deflection Response of Specimens Strengthened Using Composite System D

(e) Beams Subjected to Cycles of Moisture and Environmental Exposure

Two beams strengthened using composite system A were tested after being subjected to periodic cycles of moisture and exposure to environmental conditions for approximately 8 months. These beams were strengthened using the same scheme as specimen B4, but using composite system A. Composite systems A and B had essentially the same published mechanical properties (Appendix A) and were therefore considered to have equivalent effects on strengthening of the reinforced concrete beams. In addition to being subjected to moisture, specimen A-LT2 was subjected to a sustained load approximately equal to 20% of the yield load of the strengthened beam. Table 6.6 gives a summary of the main parameters examined during the test of specimens A-LT1 and A-LT2.

Table 6.6 Summary of Parameters and Failure Modes for Specimens Tested after Periodic Exposure to Moisture

Specimen	Composite Width, in.	Number of plies	Bond Length, in.	Sustained Load, P/Py	Failure Mode
A-LT1	2	2	35	0	CFRP Rupture
A-LT2	2	2	35	0.2	CFRP Rupture

The measured load-deflection response of this group of beams is shown in Figure 6.26. The response of the beams is compared with the response of the control specimen in this figure. Because specimens A-LT1 and A-LT2 were strengthened using the same scheme as specimen B4, the measured load-deflection response of these specimens is also compared to the measured response of specimen B4.

Although both specimens were loaded to cause cracking before applying the CFRP composite system, specimen A-LT1 exhibited a load-deflection behavior similar to uncracked-strengthened specimens. To facilitate the composite strengthening procedure, the specimens were turned upside down, which may have caused the cracks to close before the application of the composites. For the case of specimen A-LT2, the cracks possibly opened again when the sustained load was applied on the specimen. Therefore, the load-deflection response of specimen A-LT2 does not exhibit the characteristic change in stiffness corresponding to cracking.

After yielding, the measured response of specimens A-LT1 and A-LT2 was similar. The slope of the load-deflection curve of both specimens was approximately equal to the slope in the response curve of specimen B4. The maximum measured deflection of specimen A-LT1 was larger than the measured deflection of specimen B4. On the other hand, the maximum measured deflection of specimen A-LT2 was smaller than that for specimen B4. Similarly, the ultimate load for specimen A-LT1 was higher than for specimen B4, and the ultimate load for specimen A-LT2 was slightly lower than the ultimate load of specimen B4. Although only a very small number of tests were included in this series, there seems to be no significant effect in the response of these beams after being subjected to moisture. However, the differences in the maximum displacement and ultimate load between specimens A-LT1 and A-LT2 may be due to the application of sustained loading on only one of the specimens.

Similarly to specimen B4, both specimens failed by rupture of the CFRP composites. Therefore, no apparent degradation of the bond between the CFRP composites and the surface of the concrete occurred by the exposure to moisture.

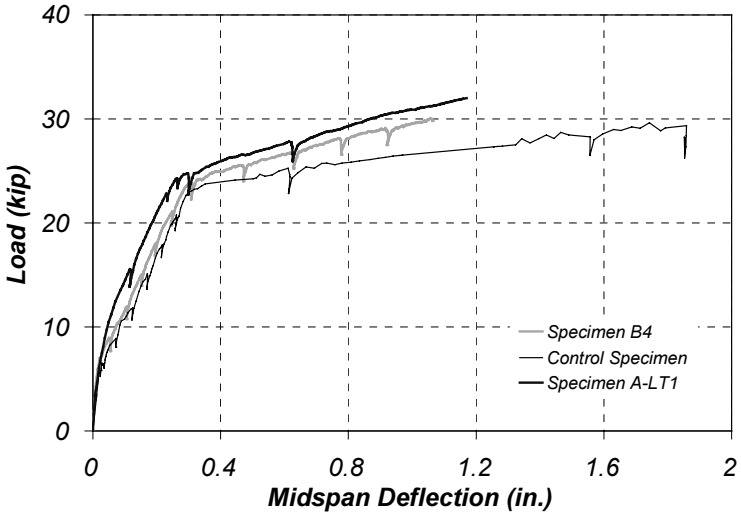

(a) Specimen A-LT1

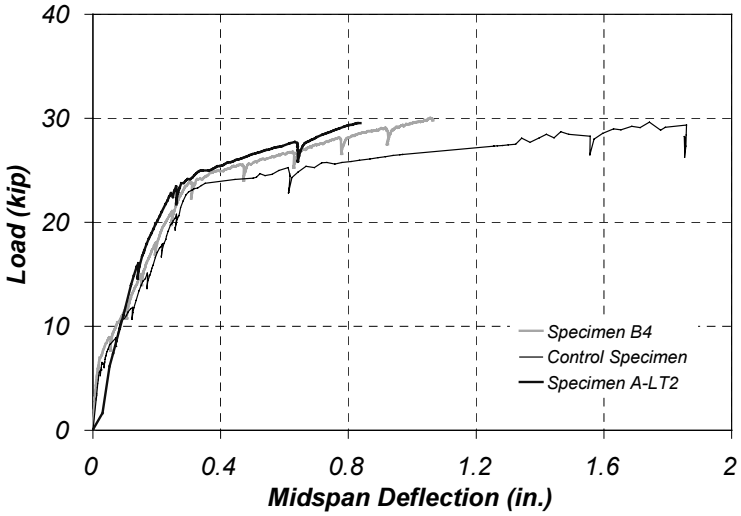

(b) Specimen A-LT2

Figure 6.26 Load-Deflection Response of Specimens Subjected to Long-Term Exposure to Cycles of Moisture

6.4 MEASURED STRAINS

The specimens were instrumented using strain gages to calculate stresses in the reinforcing bars, in the concrete, and in the CFRP laminates. The strain gages were attached to the reinforcing bars before casting the concrete. The strain gages on the surface of the concrete and CFRP composites were bonded after the specimens were positioned on the support blocks before loading. The effects of the self-weight of the specimens on the strains measured on the reinforcing bars were considered to be negligible. Therefore, the reinforcing bars were assumed to have zero strain at the beginning of the tests.

The observed strain response of the specimens is discussed in this section. The characteristics of the strain response of all the specimens were similar. Therefore, only a discussion of the typical characteristics is presented in this section. The average measured strains in the different materials for all

the specimens at yield and ultimate loads are listed in Table 6.7. The ultimate load is considered to be the load corresponding to rupture or debonding of the CFRP composites. Load-strain plots for all the specimens are presented in Appendix D. The positions of the strain gages on the reinforcing bars, on the surface of the concrete, and on the surface of the CFRP composites are illustrated in Figure 5.4 and are listed in Table 5.5.

The general characteristics of the measured strain response of the beams tested under static load are discussed in this section. Although the values of the measured strains varied with the type of composite system and strengthening scheme, the trends in the behavior were similar. Therefore, only the general trends in the strain response are discussed here. The average measured strains for specimen B4 were considered representative of all the specimens and are therefore used for the discussion of the trends in the strain response of all the specimens. Table 6.7 lists the average measured strains at the yield and ultimate loads in the reinforcing bars, surface of the concrete, and composite system at the critical section (section 1) for all the specimens. Appendix D contains the measured load-strain plots for all the beams tested under static loading.

Figure 6.27a shows the average reinforcement strains in specimen B4. The two linear portions in the initial part of the load-strain curve correspond to uncracked and cracked behavior of the specimen, respectively. The change in slope that is observed in this initial part of the curve corresponds to the load that caused cracking of the specimen (7 kip, approximately). Yielding of the reinforcing bars was observed at a load approximately equal to 24 kip. At this load, strains in the reinforcing bars grew significantly as the bars yielded. In this specimen, yielding caused the average strain in the bars to increase to approximately 0.015. The accumulation of strain on the bars was an indication of crack opening at the critical section and local debonding of the CFRP composite. If the CFRP composite had remained perfectly bonded to the surface of the concrete, it would have restrained the accumulation of strains in the reinforcement. The strain at which the reinforcing bar strains stabilized after yielding varied for the different specimens depending on the extent of local debonding that the CFRP composites sustained during yielding of the reinforcing bars.

Figure 6.27b shows the average measured strain on the surface of the CFRP composite in specimen B4. The initial portion of the curve ends at the load corresponding to cracking of the specimen. At this point, a significant reduction of the slope in the load-strain curve is observed. After cracking, the strains in the CFRP composite laminate increase without significant increase in load up to a load of approximately 8 kip. After this point, the slope in the curve becomes steeper and is approximately linear up to the yield point. This behavior after cracking and before yielding of the reinforcement is possibly caused by the different rates at which the cracks open along the beam. After yielding (24 kip), the CFRP strains increased to approximately 0.005 without an increase in load. The difference between this strain and the measured strains in the reinforcement at the end of the horizontal portion of the curve indicates local debonding of the CFRP composites. Subsequently, the load-strain curve exhibited a positive slope again as the strains in the CFRP composite increased with loading. The maximum measured strain in this beam was approximately equal to 0.012 at 30 kip. The length of the ascending portion after yielding on the load-strain curve varied for each specimen and was influenced by the strengthening scheme.

Finally, the average measured strains on the surface of the concrete of specimen B4 are shown in Figure 6.27c. In this figure, compressive strains are plotted as negative strains. The strains on the concrete decrease approximately linearly up to the yield load. After yielding, the strains on the concrete increased and turned into tensile strains at a load approximately equal to 28 kip. The strain gages were bonded 1.5 in. below the top surface of the beam. As the flexural cracks grew and widened after yielding, the neutral axis shifted toward the top of the beam. The measured concrete strains turned into tensile strains once the position of the neutral axis was above the location of the strain gages on the surface of the beam.

Figure 6.28 shows the average measured strains at section 2 in specimen B4. The strains in the reinforcement and the surface of the concrete are shown in Figures 6.28a and 6.28c, respectively. The strain response was essentially linear after cracking in these plots. However, the measured strain in the CFRP composites increased substantially at a load approximately equal to 28 kip. This phenomenon can be the consequence of propagation of debonding toward the end of the composite laminates. As debonding of the CFRP composite reached section 2, the value increased to the strain at a section closer to the maximum moment region. The magnitude of this increase depended on the extent of debonding at section 2.

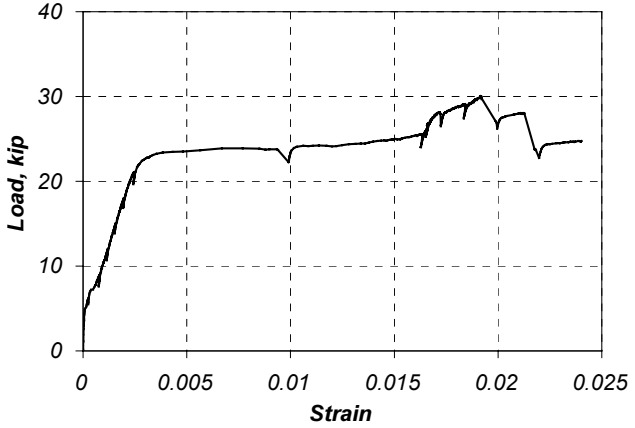

(a) Average #5 Reinforcing Bar Strains

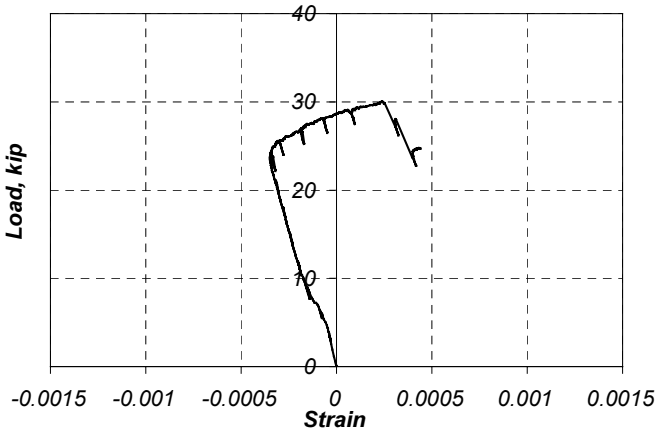

(c) Average Concrete Strains

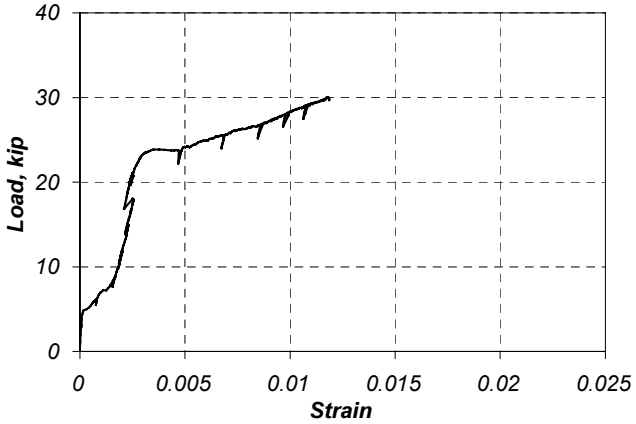

(b) Average CFRP Composite Strains

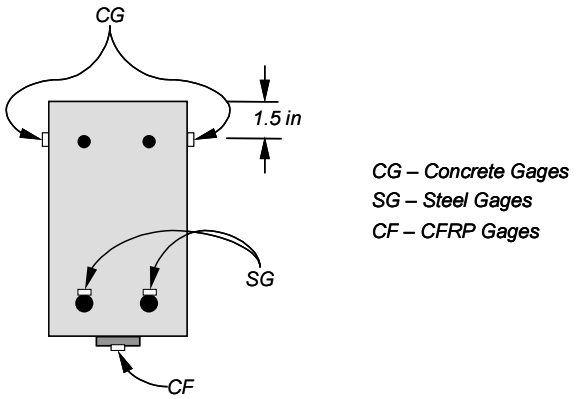

(d) Position of Strain Gages

Figure 6.27 Average Measured Strains in Specimen B4 (Section 1)

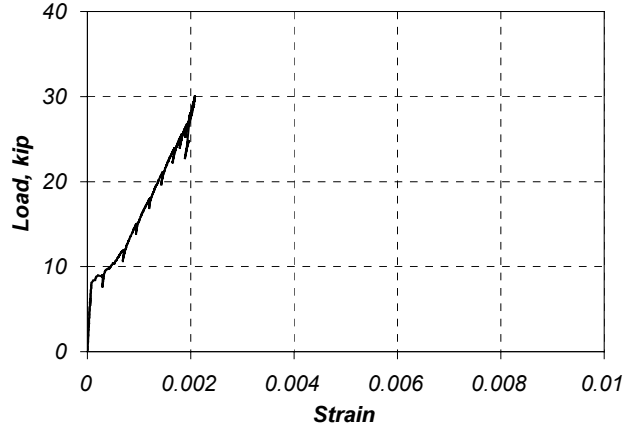

(a) Average #5 Reinforcing Bar Strains

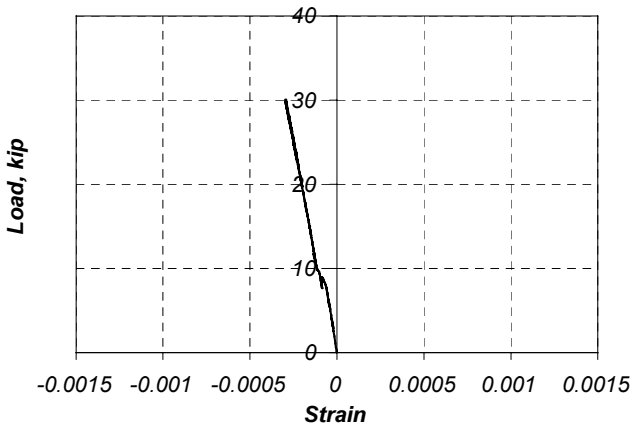

(c) Average Concrete Strains

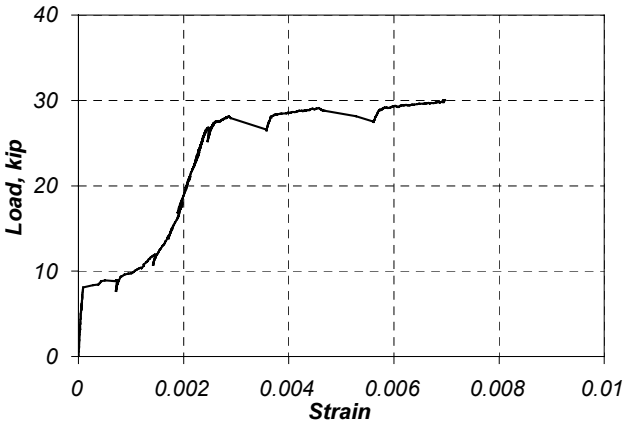

(b) Average CFRP Composite Strains

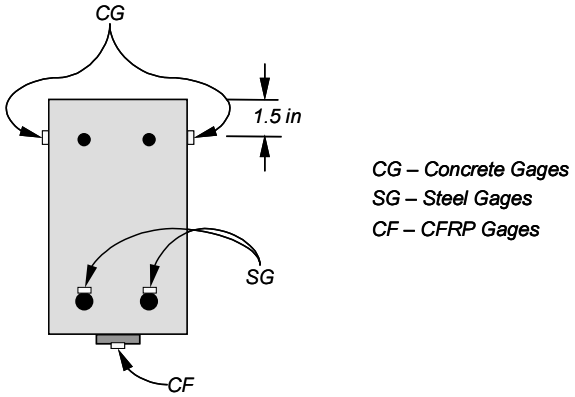

(d) Position of Strain Gages

Figure 6.28 Average Measured Strains in Specimen B4 (Section 2)

Table 6.7 Average Measured Strains for Specimens Subjected to Static Loads

Specimen	Average Measured Strains at Yield Load (Microstrain)			Average Measured Strains at Capacity (Microstrain)		
	Steel	Concrete**	CFRP	Steel	Concrete**	CFRP
Control A and B	2,900	-350	-	28,400	-150	-
A1	2,800	-340	3,800	12,600	-290	7,900
A2	2,800	-360	2,800	15,900	-270	6,100
A3	2,800	-360	3,200	16,800	600	10,200
A4	2,800	-420	2,800	12,100	-150	7,800
B1	2,900	-410	2,900	13,300	-300	7,200
B2	2,800	-390	3,000	17,900	240	11,300
B3	2,800	-340	2,900	16,400	790	10,700
B4	2,700	-340	3,500	19,200	240	11,900
B5	2,900	-340	4,000	13,900	240	13,200
Control C and D	2,700	-380	-	21,400	40	-
C1	2,800	-480	2,600	11,100	-400	7,600
C2	3,000	-400	3,900	11,600	-400	7,000
C3	2,900	-490	2,100	11,900	-100	7,500
C4	2,900	-380	2,500	Damaged	Damaged	Damaged
D1	2,800	-420	2,300	9,500	-390	3,500
D2	2,700	-470	2,900	10,300	-450	4,800
D3	3,000	-510	2,600	9,600	-560	4,400
D4	2,800	-480	2,600	11,700	-580	6,500
D5	2,900	-550	2,500	12,800	-550	6,200
A-LT1	2,200	-600*	2,800	13,700	-1,700*	11,100
A-LT2	2,200	-630*	4,300	16,700	-1,800*	11,800

*Strains measured at the top surface of the specimens.
**Negative values indicate compressive strains.

6.5 SUMMARY

The observed and measured response of the specimens subjected to static loads were presented in this chapter. The different mechanisms that led to failure of the specimens were presented and discussed in Section 6.2. The measured load-deflection response was compared within the different groups of specimens in Section 6.3. The effects of the different variables that were included in each of the groups of beams were also discussed. Finally, the features of the strain response that were characteristic of all the specimens were presented in Section 6.4. The average measured strains at yielding and ultimate of all the specimens were summarized in this section. Chapter 7 presents a comparison of the response of several specimens with the calculated response using the analytical model developed in Chapter 3.

Chapter 7: Evaluation of Measured Response of Beams Subjected to Static Loads

7.1 INTRODUCTION

The measured response of the specimens that were subjected to monotonically increasing loads are evaluated in this chapter. Only the response of representative specimens from each group of beams are discussed because the trends in the behavior were similar, as discussed in Chapter 6. Average measured strain profiles are plotted for different stages of loading in Section 7.2 to evaluate the assumption of a linear strain distribution with depth. The average measured strains are compared with the strains calculated using the analytical model presented in Chapter 3. The differences between the measured strains and the calculated strains are discussed in Section 7.3. The load-deflection response of the beams are also compared with the calculated response in Section 7.4.

When discussing the measured response of the test specimens, beams A1, B3, B4, C3, and D5 are considered throughout this chapter. At least one specimen strengthened with each of the composite systems was selected for the evaluation. Specimen A1 was selected because it gives insight into the behavior of specimens strengthened using a very short bonded length beyond the critical section. Therefore, it was considered important to compare the response of this specimen with other specimens with longer bonded lengths. Specimens B3 and B4 were selected to compare the influence of the strengthening scheme on the measured response of the specimen. Specimen B3 was strengthened using the side application technique while specimen B4 was strengthened by attaching the composite to the tension face and using transverse straps. Specimens C3 and D5 were selected because these specimens sustained the highest load within their group and gave ample indications of incipient failure.

7.2 MEASURED STRAIN PROFILES

The analytical model presented in Chapter 3 was based on several assumptions that are commonly used in the design of reinforced concrete flexural members. One of the assumptions considers that the distribution of strains is proportional to the distance from the neutral axis. This assumption has been verified experimentally only for reinforced concrete members and may not be valid for the composite materials that are bonded to the surface of the concrete. Therefore, it was considered important to validate the assumption of linear strains using the strains measured during testing.

The average measured strains in the different materials were plotted over the height of the cross section. The strain profiles were obtained for several load levels to investigate the behavior of the specimens before and after yielding. The load levels are indicated in the corresponding plots. Because debonding of the composites initiated in the vicinity of the critical section (section 1), only the measured strains at the critical section (section 1) are included in this discussion.

Figures 7.1 through 7.5 show the strain distribution with depth for the five representative beams. Tensile strains are plotted as positive values in these figures. The average measured strains were considered to vary linearly within the reinforced concrete section. Therefore the measured strains on the surface of the concrete and the reinforcing bars were joined by straight lines in these plots. Any departure of the measured strains on the composite laminates from the straight line joining the concrete and reinforcing bar strains would therefore give an indication initiation of debonding.

The strain profile for specimen A1 is shown in Figure 7.1. In this specimen, the composite extended only 10 in. beyond the critical section. It can be observed that the strain profiles obtained for loads below yield

are approximately linear throughout the cross section. However, at loads above yield, the measured strain in the composite laminate does not follow the linear distribution that was assumed for the reinforced concrete section. This change in behavior is attributed to local debonding of the composite from the surface of the concrete at the critical section. The specimen failed at a load slightly higher than yield, due to debonding of the composite laminate. The failure load was limited by the relatively short development length beyond the critical section. It is interesting to note that at load levels that were slightly higher than the observed yield load, the strain profiles depart significantly from the straight-line assumption. Therefore, it can be concluded that debonding of the composites from the surface of the concrete took place after yielding of the reinforcing bars occurred.

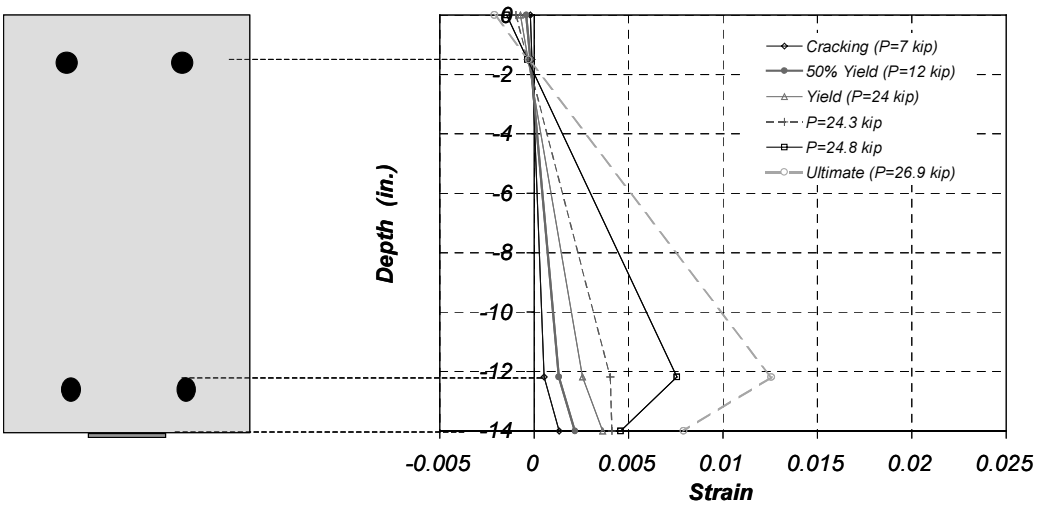

Figure 7.1 Strain Profiles for Specimen A1 (Section 1)

Other specimens included in this discussion were selected because the observed global behavior of the strengthened beams was significantly different than specimen A1. In these specimens, the strengthening configurations were selected to preclude failure by debonding of the composites from the surface of the concrete and reach the rupture strength of the composite materials.

The strain profiles for specimens B3, B4, C3, and D5 are presented in Figures 7.2 through 7.5, respectively. These specimens are representative of different composite systems and strengthening schemes. Failure in specimens B3, B4, and C3 was characterized by rupture of the carbon fiber composites, whereas failure in specimen D5 was by debonding of the composites from the surface of the concrete. It can be observed that the behavior after yielding of the reinforcing bars in all the specimens is similar to the behavior of specimen A1 although the observed global behavior and failure mode of the specimens were significantly different. At load levels slightly above yield, the measured strain on the surface of the composite laminates departs significantly from the assumption of linear strains with depth. The strain plots give an indication of the local behavior at the critical section of the specimens and not the overall response. Although local debonding of the composite is observed after yielding in these plots, the composites remained attached to the surface of the concrete at other locations and the beams were able to sustain loads well beyond the yield load.

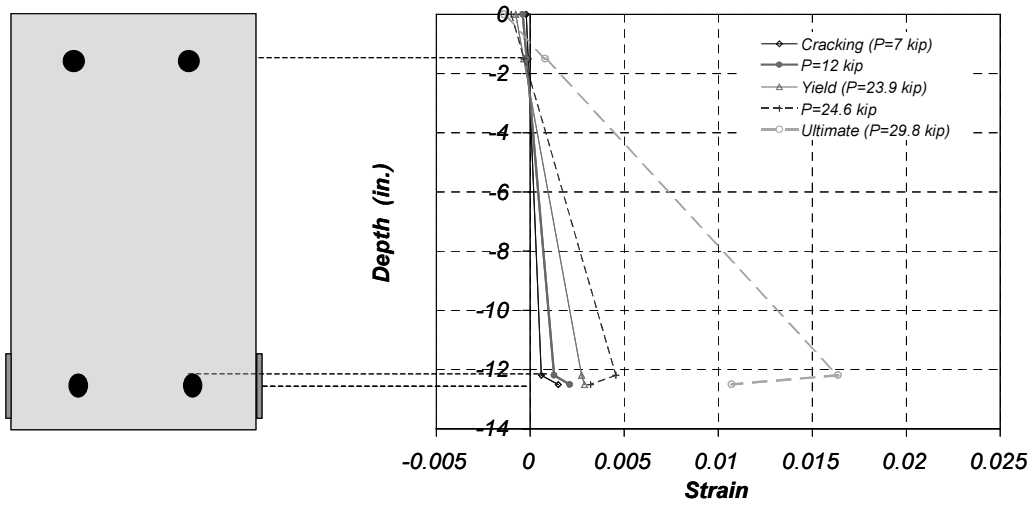

Figure 7.2 Strain Profiles for Specimen B3 (Section 1)

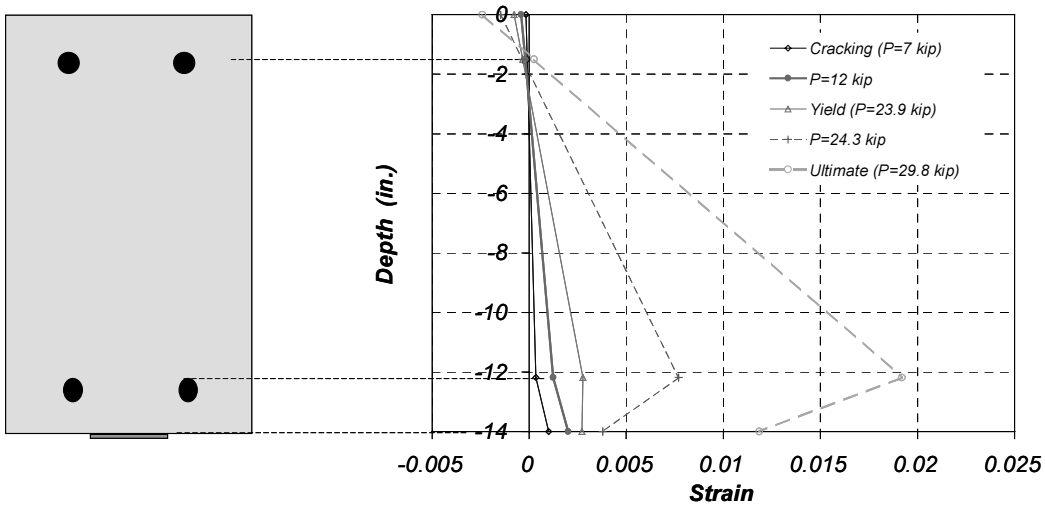

Figure 7.3 Strain Profiles for Specimen B4 (Section 1)

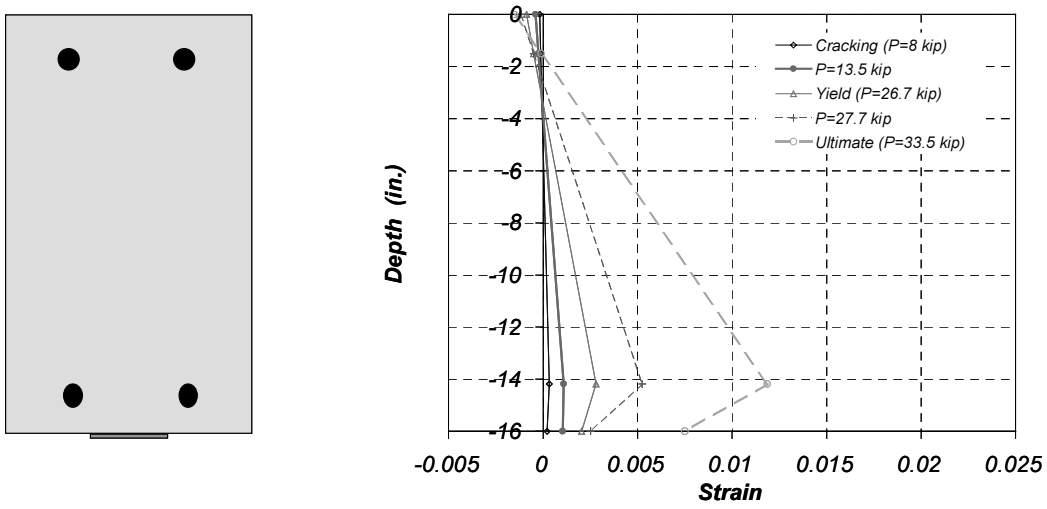

Figure 7.4 Strain Profiles for Specimen C3 (Section 1)

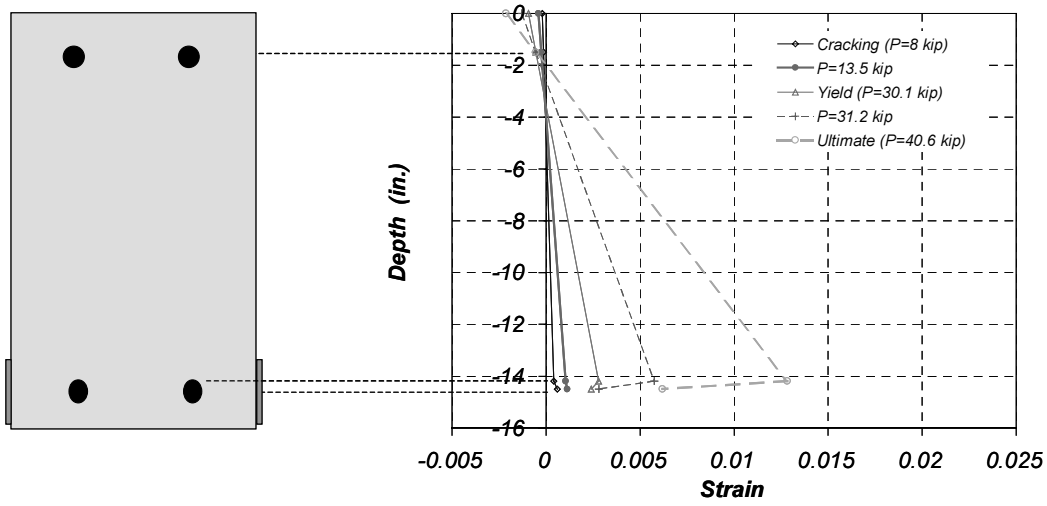

Figure 7.5 Strain Profiles for Specimen D5 (Section 1)

7.3 COMPARISON OF MEASURED AND CALCULATED STRAINS

As discussed in the previous section, the assumption of a linear strain distribution with depth was not observed in the test specimens, particularly for loads above the yield load. The analytical model presented in Chapter 3 was based on the assumption of a linear strain distribution with depth, so it was important to compare the measured strains in the different materials with the calculated values.

The average measured strains in the reinforcing bars, in CFRP laminates, and on the surface of the concrete are compared with the calculated strains in Figures 7.6 through 7.10. These figures show load-strain plots obtained at the critical section of specimens A1, B3, B4, C3, and D5, respectively. Again the general trends in the plots are similar and therefore the discussion will be presented generically instead of particularly for each specimen.

The average measured strain in the reinforcing bars is compared with the calculated strain in Figures 7.6a through 7.10a. The calculated strain in the reinforcing bars approximate the measured values for load levels below yield. After yielding, the analytical model does not capture the measured strain response because local debonding at the crack locations was not included in the model. Widening of cracks after yielding of the reinforcement causes an increase of reinforcing bar strain under constant load. The applied load in the specimens increased only after some debonding of the composites had occurred in the vicinity of the cracks. The composites were not able to restrain the cracks from widening at yielding because of local debonding.

Figures 7.6b through 7.10b show a comparison of the calculated strain and measured strain on the surface of the composite laminates. After cracking, the calculated strains at load levels below yield were smaller than the measured values in specimens A1, B3, and B4. On the other hand, the calculated values in specimens C3 and D5 are approximately equal to the measured strains. This difference in the post-cracking behavior can be caused by the variability in the tensile strength of concrete that causes the cracks to widen and propagate differently after cracking for the different specimens. After yielding of the specimens, however, the measured strains are in close agreement with the calculated strains. It is interesting to note that because local debonding took place after yielding, the measured strains on the surface of the composite did not increase although the cracks widened during yielding of the reinforcement. A schematic representation of the strain distribution on the composite laminates as local debonding occurs is presented in Figure 7.11. It can be seen that local debonding causes the strain in the composite to increase in the vicinity of a crack that widens during yielding of the reinforcement. This behavior is consistent with the measured strains at the critical section of the laboratory specimens.

Finally, a comparison of the measured and calculated strains on the surface of the concrete is presented in Figures 7.6c through 7.10c. The calculated response agrees closely with the measured strains for load levels below yield. The peak compressive strains were reached at yielding. After yielding, the measured compressive strains decreased and in some specimens turned into tensile strains as a consequence of cracks propagating toward the top of the specimens. This behavior was not observed in the plots of the calculated strains because of the assumption of perfect bond between the composite and the surface of the concrete. Crack propagation was restrained in the analytical model because the composites remained attached to the surface of the concrete.

A summary of the maximum measured strains on the surface of the composites is listed in Table 7.1. The strain at rupture as published by the different manufacturers of the composite materials is also listed in this table. The published rupture strains were used in the analytical model to define failure of the strengthened beams. The ratio of measured to published strains is included in the table to give a measure of the efficiency of the strengthening scheme. It can be observed that although several specimens failed by rupture of the CFRP composites, the published rupture strains were not achieved in any of the tests. The average of the maximum strains developed for different strengthening schemes within the different groups of beams are included in the table. These values were used to select a conservative value of CFRP strain to design the strengthening scheme for specimens in the third phase of this research project.

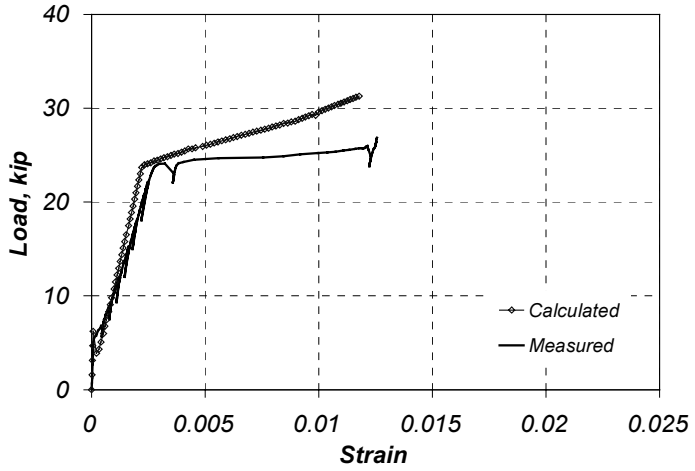

(a) Reinforcing Bar Strains

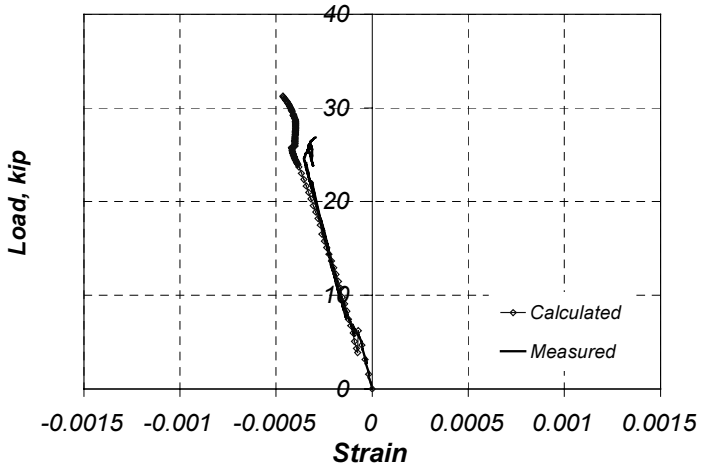

(c) Concrete Strains

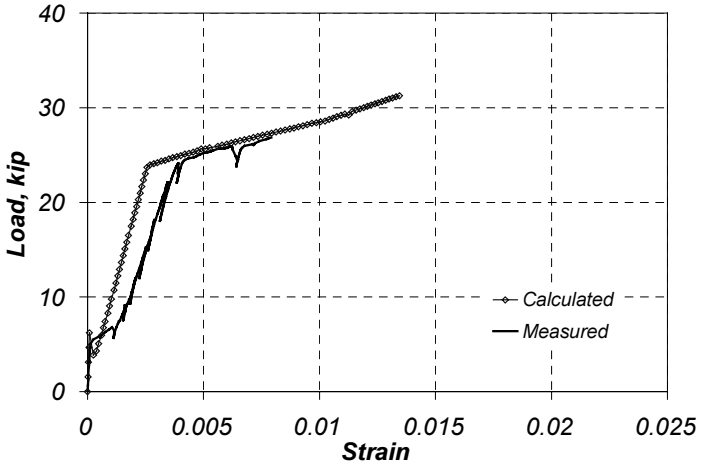

(b) CFRP Strains

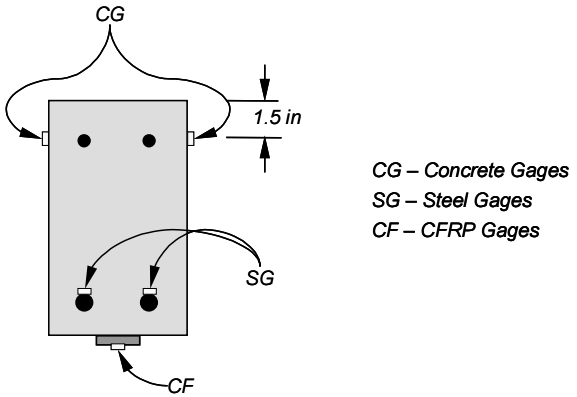

(d) Location of Strain Gages

Figure 7.6 Comparison of Measured and Calculated Strains in Specimen A1 (Section 1)

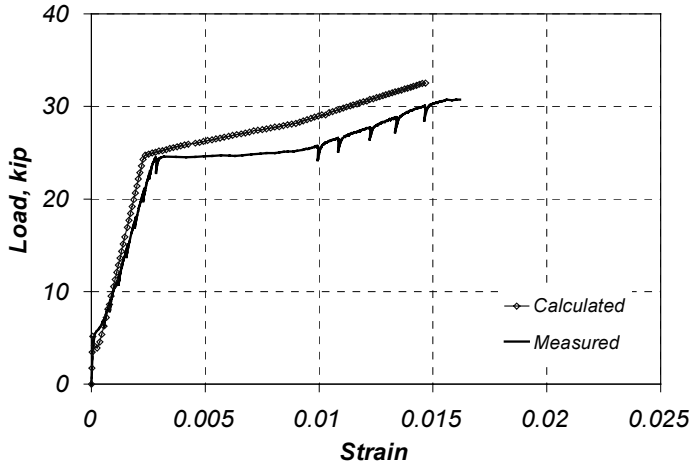

(a) Reinforcing Bar Strains

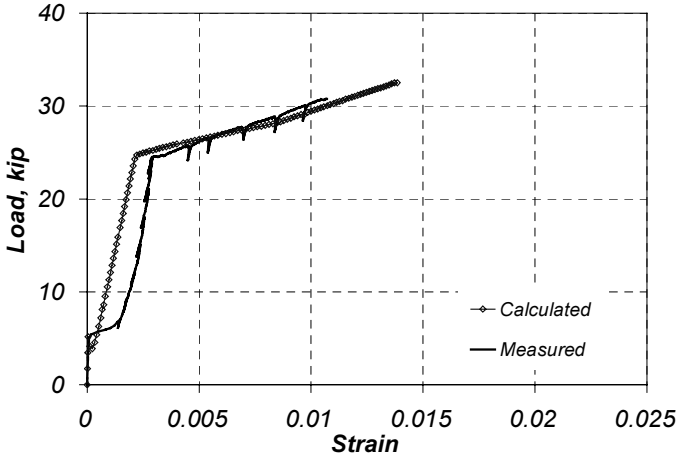

(b) CFRP Strains

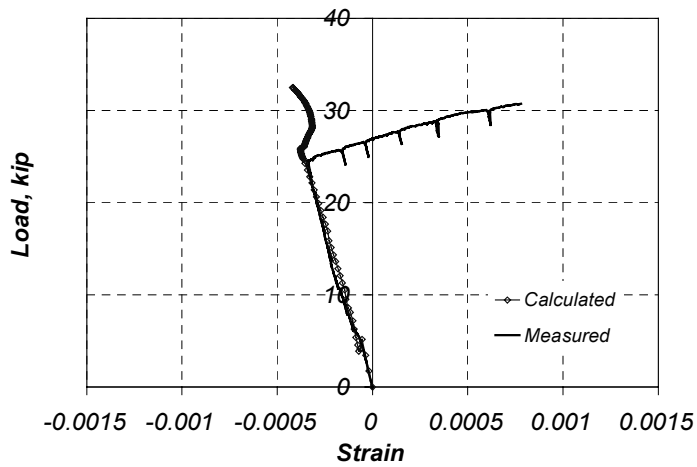

(c) Concrete Strains

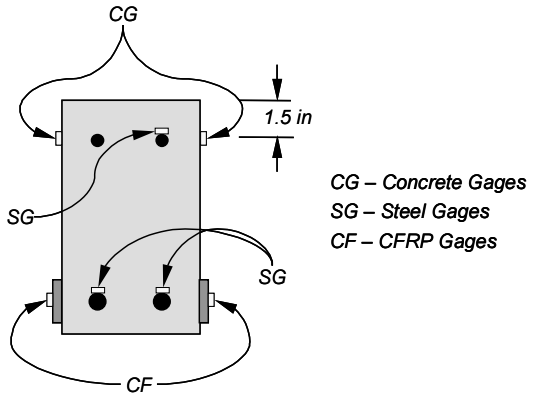

(d) Location of Strain Gages

Figure 7.7 Comparison of Measured and Calculated Strains in Specimen B3 (Section 1)

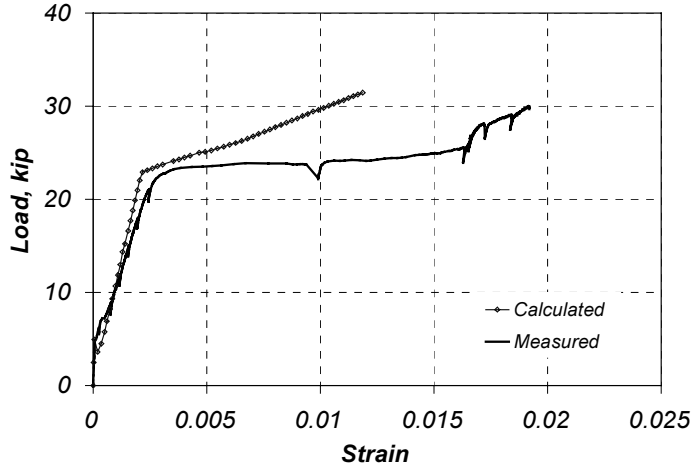

(a) Reinforcing Bar Strains

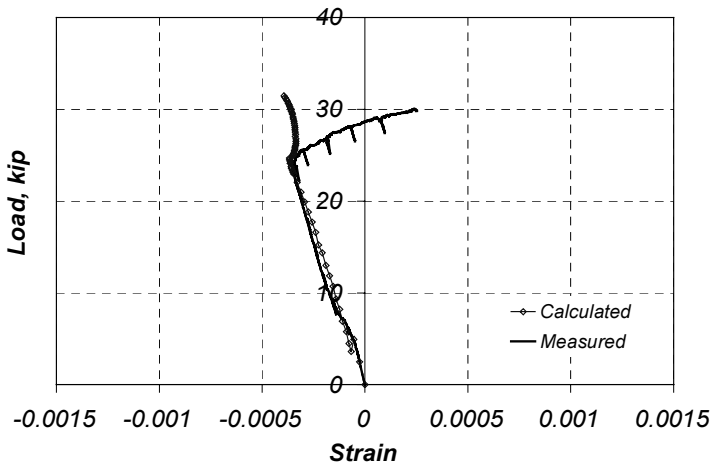

(c) Concrete Strains

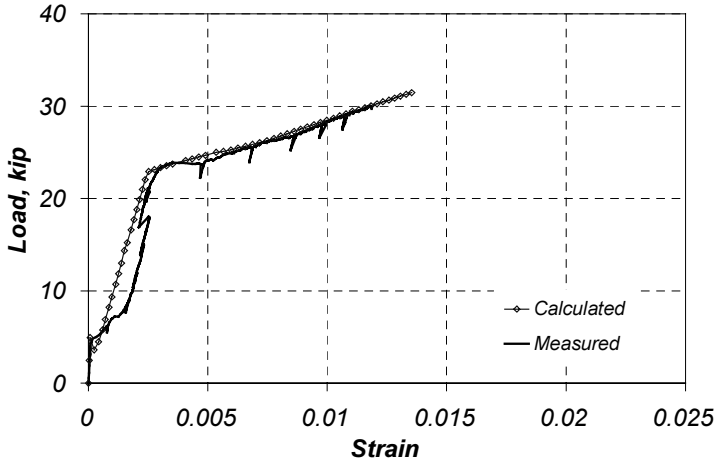

(b) CFRP Strains

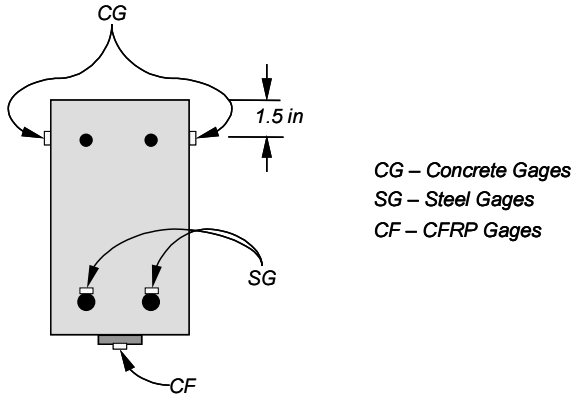

(d) Location of Strain Gages

Figure 7.8 Comparison of Measured and Calculated Strains in Specimen B4 (Section 1)

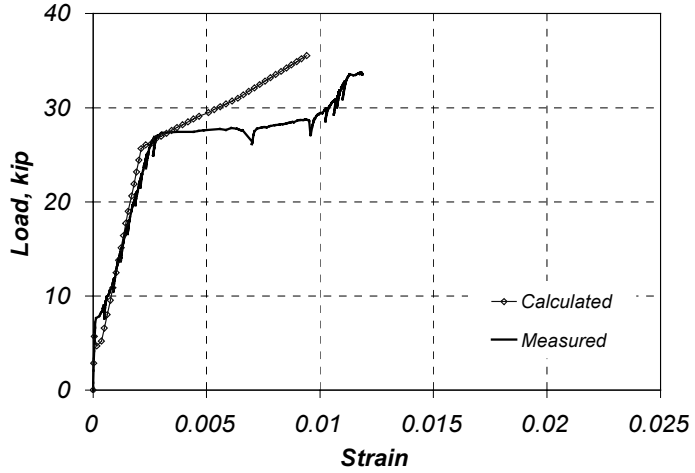

(a) Reinforcing Bar Strains

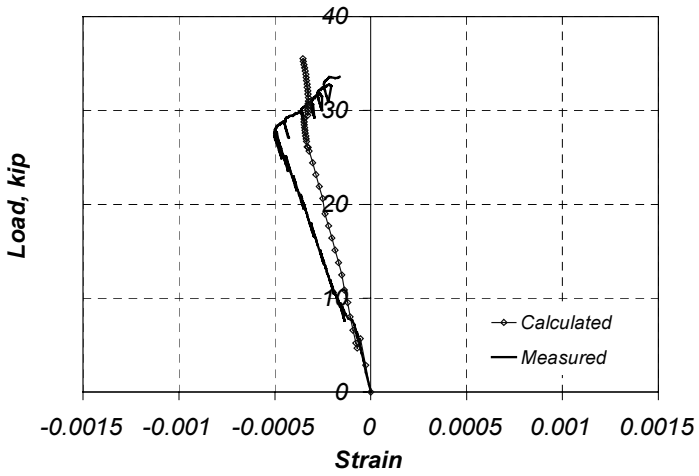

(c) Concrete Strains

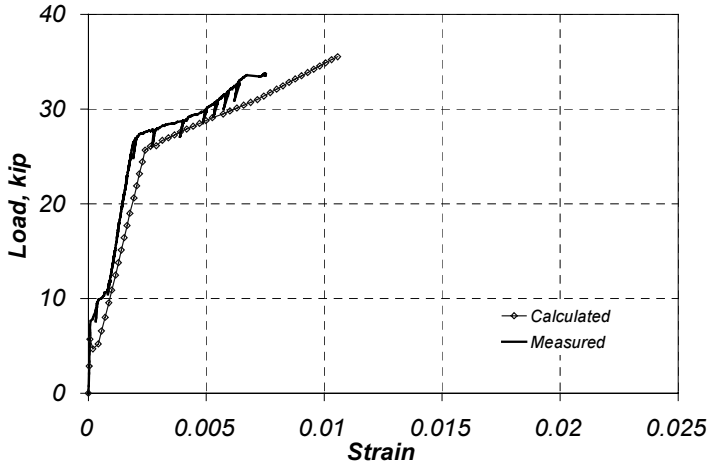

(b) CFRP Strains

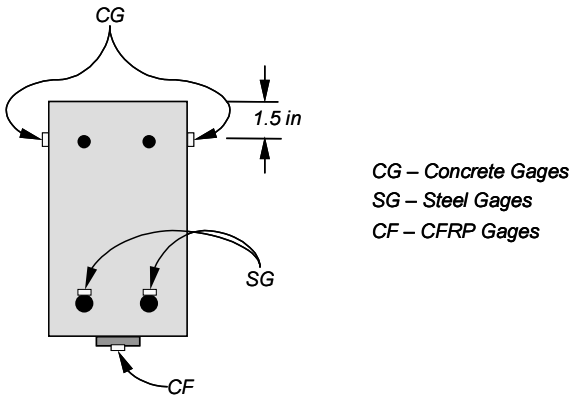

(d) Location of Strain Gages

Figure 7.9 Comparison of Measured and Calculated Strains in Specimen C3 (Section 1)

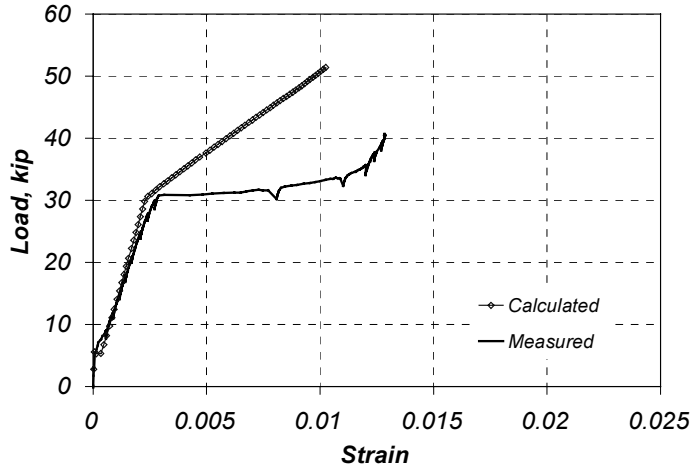

(a) Reinforcing Bar Strains

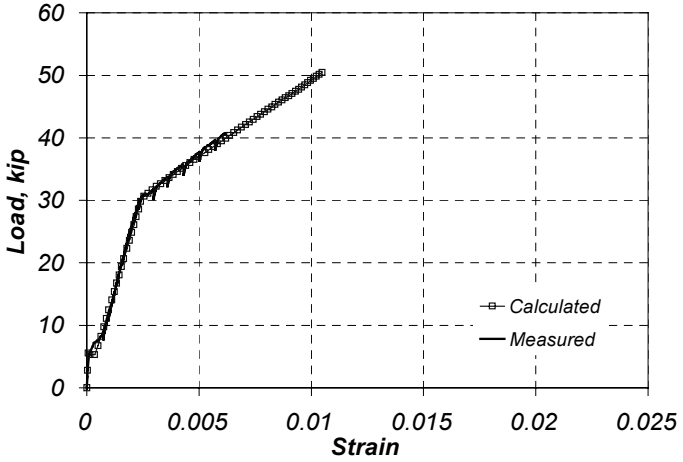

(b) CFRP Strains

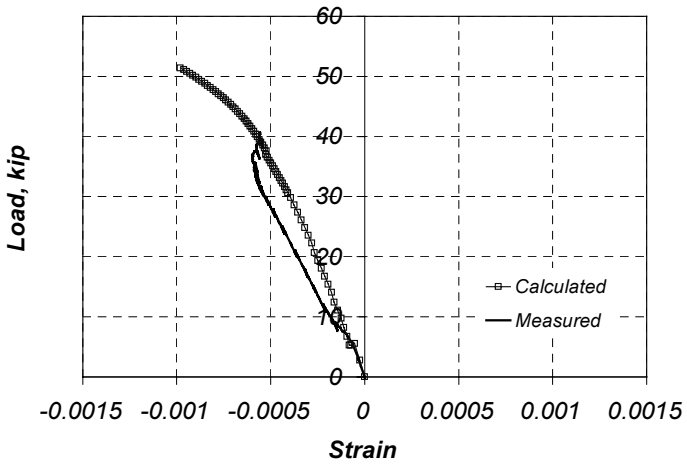

(c) Concrete Strains

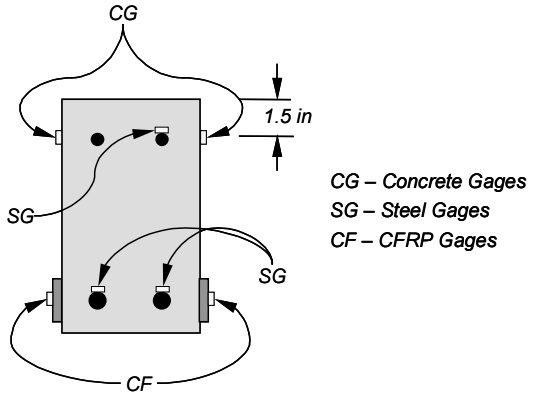

(d) Location of Strain Gages

Figure 7.10 Comparison of Measured and Calculated Strains in Specimen D5 (Section 1)

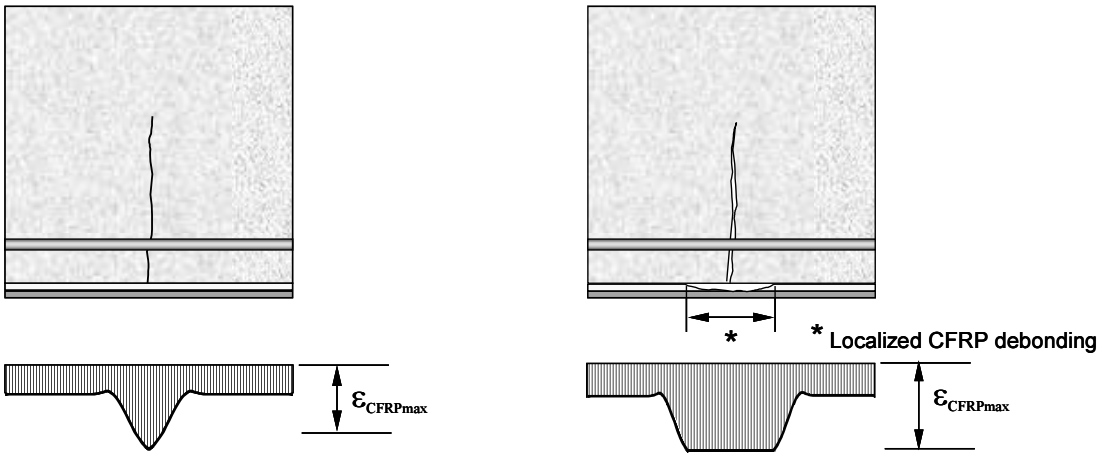

(a) Perfect Bond Between CFRP and Surface of Concrete

(b) Local Debonding Between CFRP and Surface of Concrete

Figure 7.11 Schematic Distribution of Strains on the Surface of the CFRP Composites

7.4 COMPARISON OF MEASURED AND CALCULATED DEFLECTIONS

The load-deflection behavior of the strengthened specimens was also compared with the calculated response using the procedure described in Chapter 3. The load-deflection response was calculated for the same specimens that were discussed in the previous section. The same specimens were selected not only because they are representative of each composite system, but also because it was considered important to evaluate whether the differences in the measured and analytical strain responses would have any effect on the global load-deflection response of the specimens.

A comparison between the measured and calculated load-deflection response of specimen A1 is shown in Figure 7.12. The calculated response approximates very closely the measured response of the specimen at load levels below the yield load. After yielding, the specimen failed at a much lower load than the calculated capacity. This difference is attributable to debonding of the CFRP composite immediately after yielding of the reinforcement during the laboratory test. While failure in the analytical model is defined by carbon fiber rupture, failure during the test was by CFRP debonding from the surface of the concrete.

Table 7.1 Comparison of Maximum Measured and Published Strains on the CFRP Laminates

Specimen	$\varepsilon_{CFRPtest}$	$\varepsilon_{CFRPpubl}$	$\varepsilon_{CFRPtest}/\varepsilon_{CFRPpubl}$	Failure Mode	Average Measured CFRP Strain for Different Schemes
A1	0.0079	0.015	0.53	CFRP Debonding	0.0085
A2	0.0061		0.41		
A3	0.0120		0.80		
A4	0.0078		0.52		
B1	0.0072		0.48		0.0072
B2	0.0113		0.75	CFRP Rupture	0.0118
B3	0.0107		0.71		
B4	0.0119		0.79		
B5	0.0132		0.88		
C1	0.0076	0.012	0.63	CFRP Debonding	0.0073
C2	0.0070		0.58		
C3	0.0075		0.63	CFRP Rupture	0.0075
C4	Unavailable		-	CFRP Debonding	-
D1	0.0035	0.015*	0.23	CFRP Debonding	0.0042
D2	0.0048		0.32		
D3	0.0044		0.29		0.0057
D4	0.0065		0.43		
D5	0.0062		0.41		
A-LT1	0.0111	0.015	0.74	CFRP Rupture	0.011
A-LT2	0.0118		0.79		

*Calculated from $\varepsilon_{CFRP} = f_{pu}/E_{pu}$, where f_{pu} and E_{pu} are the rupture stress and modulus of elasticity of the composite, respectively.

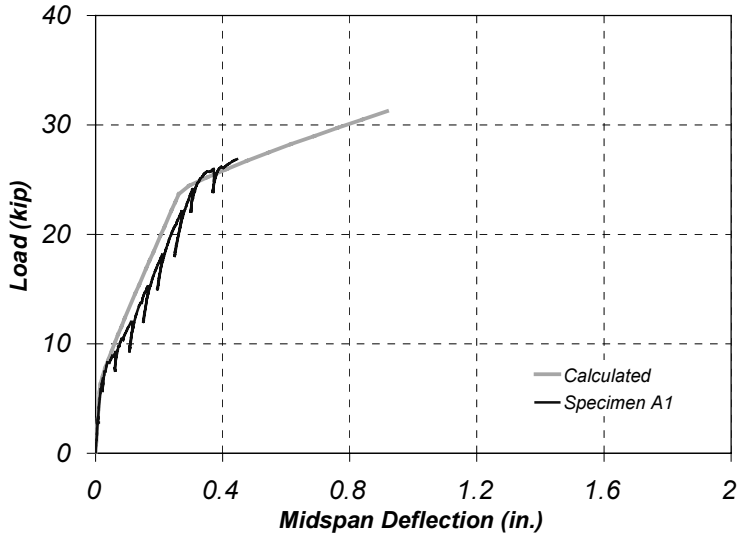

Figure 7.12 Comparison of Measured and Calculated Load-Deflection Response of Specimen A1

The measured and calculated responses of specimens B3, B4, C3, and D5 with the calculated response are presented in Figures 7.13 through 7.16. The load-deflection behavior in these specimens was similar and was considered representative of other specimens within their respective beam groups. The primary difference in behavior was observed in the post-yield region of the load-deflection curves. The slope and the length of the post-yield region of the measured load-deflection curves varied for the different specimens subjected to monotonically increasing loads.

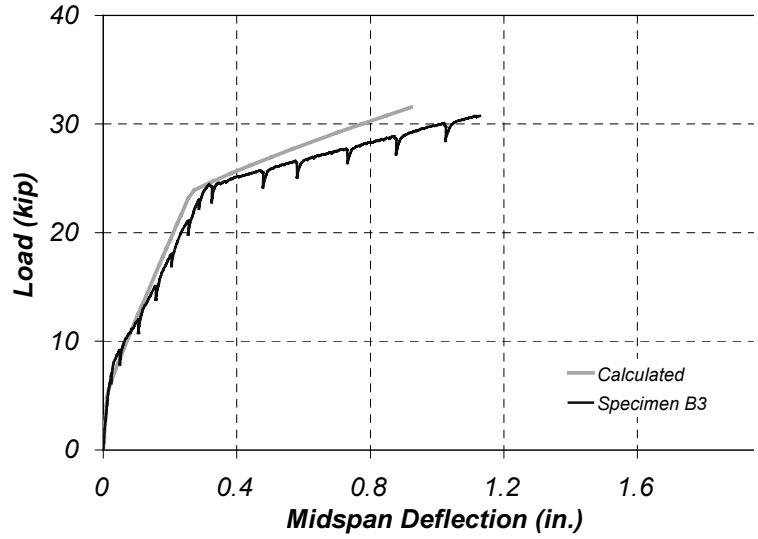

Figure 7.13 Comparison of Measured and Calculated Load-Deflection Response of Specimen B3

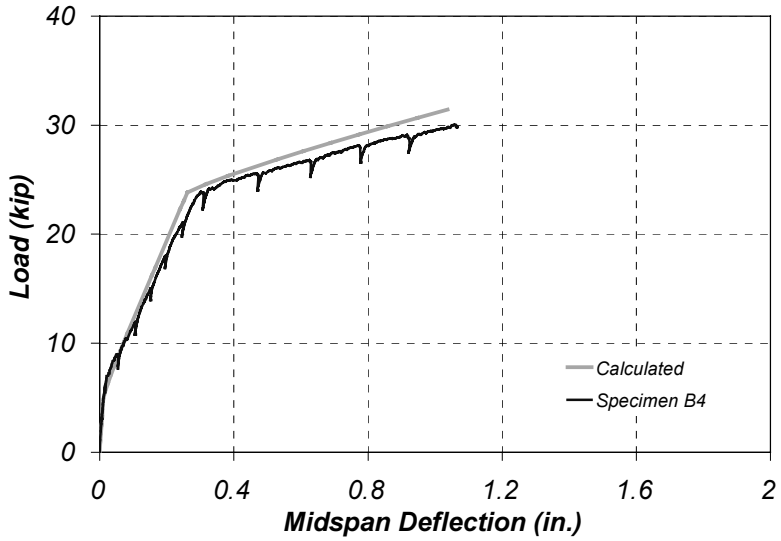

Figure 7.14 Comparison of Measured and Calculated Load-Deflection Response of Specimen B4

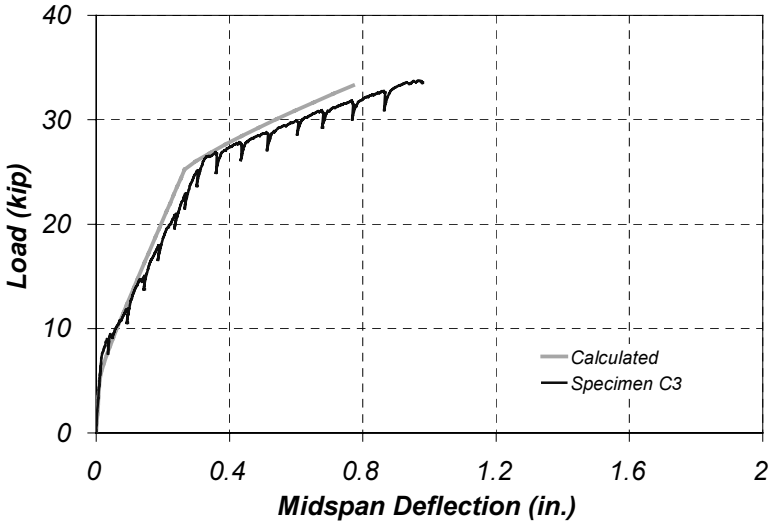

Figure 7.15 Comparison of Measured and Calculated Load-Deflection Response of Specimen C3

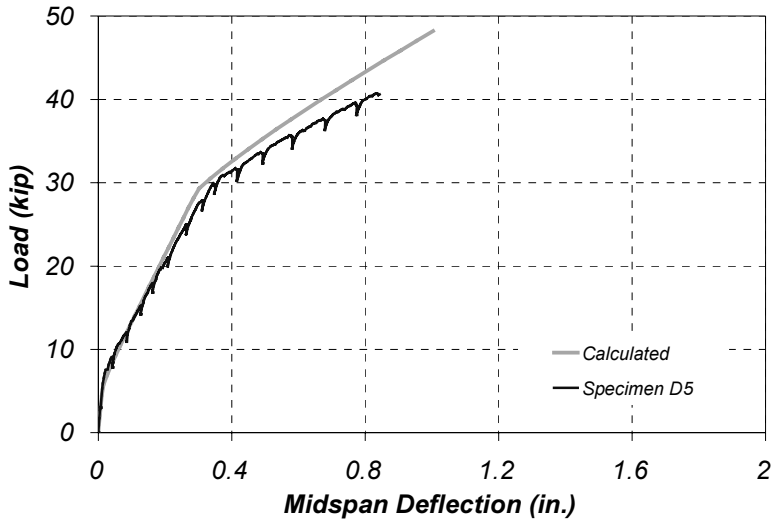

Figure 7.16 Comparison of Measured and Calculated Load-Deflection Response of Specimen D5

Figures 7.13 through 7.16 also indicate that the maximum calculated load was approximately equal to the maximum measured load for specimens B3, B4, and C3 because failure was characterized by CFRP rupture. However, the calculated failure load of specimen D5 was higher than the measured load during the test. This specimen failed by debonding of the composite from the surface of the concrete and was therefore unable to develop the rupture strain of the composite material. Table 7.2 lists the maximum measured and calculated loads as well as the maximum calculated and measured displacements for all the specimens in the static-load testing program. It can be seen that the analytical model provided accurate estimates of the maximum measured load for specimens where failure was by rupture of the CFRP composites. On the other hand, for specimens where failure was caused by debonding of the composites from the surface of the concrete, the calculated load was about 30% higher than the measured value. Midspan deflections were not calculated accurately using the analytical model even for cases when failure was caused by rupture of the composites primarily because of the differences in the calculated and measured post-yield stiffness of the beams.

In general, the calculated load-deflection curves are steeper than the measured response curves after yielding. However, the slope varied depending on the composite system and strengthening configuration. The shallower measured load-deflection curves may be an indication of a reduction in stiffness of the specimens caused by local debonding at the critical crack location. Because the analytical model is based on the assumption of perfect bond between the composite and the surface of the concrete, the calculated tensile stresses on the concrete are expected to be lower than the tensile stresses generated during a test. For this reason, the cracks should be expected to be longer in the test specimens than the lengths calculated with the analytical model.

Table 7.2 Comparison of Calculated and Measured Load-Deflection Response

Specimen	Maximum Measured Parameters		Maximum Calculated Parameters		P_{test}/P_{calc}	$\Delta_{test}/\Delta_{calc}$
	P_{test}, kip	Δ_{test}, in.	P_{calc}, kip	Δ_{calc}, in.		
A1	26.9	0.446	31.2	0.918	0.86	0.49
A2	28.3	0.595	31.2	0.918	0.91	0.65
A3	31.1	1.062	31.2	0.918	1.00	1.16
A4	29.0	0.748	31.2	0.918	0.93	0.81
B1	29.8	0.809	31.4	1.037	0.95	0.78
B2	31.9	1.077	31.4	1.037	1.02	1.04
B3	30.8	1.128	31.5	0.923	0.98	1.22
B4	29.8	1.066	31.4	1.037	0.95	1.03
B5	29.2	0.907	31.4	1.037	0.93	0.87
C1	32.3	0.903	33.3	0.771	0.97	1.17
C2	28.3	0.665	33.3	0.771	0.85	0.86
C3	33.5	0.980	33.3	0.771	1.01	1.27
C4	29.8	0.931	33.3	0.889	0.89	1.05
D1	28.8	0.431	41.2	1.030	0.70	0.42
D2	30.1	0.549	41.2	1.030	0.73	0.53
D3	35.7	0.650	48.2	1.003	0.74	0.65
D4	42.3	0.906	48.2	1.003	0.88	0.90
D5	40.6	0.843	48.2	1.003	0.84	0.84
A-LT1	32.0	1.171	31.4	1.037	1.02	1.13
A-LT2	29.6	0.837	31.4	1.037	0.94	0.81

7.5 SUMMARY

The measured response of the beams subjected to monotonically increasing loads was evaluated in this chapter. Strain profiles were obtained for representative specimens in Section 7.2 to evaluate the assumption of a linear distribution of strains with depth of the cross section. It was concluded that the strains did not follow a linear distribution particularly after yielding of the reinforcement because of local debonding of the composites from the surface of the concrete. A comparison between measured and calculated strains on the different materials was presented in Section 7.3. For load levels below the yield load, the calculated strains were reasonably closed to the measured values. After yielding, however, the calculated strains did not provide an accurate representation of the measured strains because of the occurrence of local debonding in the vicinity of the critical section. In particular, the analytical model did not capture the accumulation of plastic strains on the reinforcement after yielding. Finally, the measured load-deflection response of the specimens was compared with the calculated response in Section 7.4. Only representative specimens from each of the beam groups were used for the comparison because the general trends in the response were similar for all the tests. It was found that although not all the characteristics of the strain response were captured using the analytical model, the global response of the specimens was well represented.

Chapter 8: Measured Response of Beams Subjected to Fatigue Loading

8.1 INTRODUCTION

The measured response of the specimens subjected to fatigue loads are presented in this chapter. The observed behavior of the specimens during the tests is presented in Section 8.2. The observed response during cycling and during the subsequent monotonically increasing loads to failure of some of the specimens is presented in detail in this section. A discussion of the measured load-deflection response of the two groups of beams tested under fatigue loading is presented in Section 8.3. The measured load-deflection response is compared with the response of companion specimens subjected to static loads. Finally, the measured strain response of the specimens is presented in Section 8.4. The effects of cycling on the load-strain response of the specimens are also discussed in this section.

8.2 OBSERVED RESPONSE OF SPECIMENS DURING TESTING

The observed response of the specimens during testing is presented in this section. The application of cyclic loads was stopped periodically during testing to conduct a static-load cycle and collect readings from the instrumentation connected to the specimens. During the static-load cycles, cracks were also marked and measured to relate the extension of cracks caused by the application of repeated loads to specimen failure. Typical sequences of crack growths are presented in the description of each of the beam groups that were tested in this part of the research program. The cracking patterns and crack width sequences of all the specimens are presented in Appendix B.

The specimens were also examined during the static-load cycles to observe if any debonding cracks were formed at different stages in the cyclic load history. The discussion in this section concentrates therefore on the observed differences in the behavior of the specimens among the beams within each group. The differences in the measured load-deflection response and the measured strain response are discussed in Sections 8.3 and 8.4, respectively.

Two composite systems were used to strengthen the beams that were subjected to fatigue loads. The beams were subjected to different load amplitudes and number of cycles. Beams that were subjected to amplitudes of loading approximately equal to 33% or 50% of the measured yield load of companion strengthened specimens were tested statically to failure after being subjected to one million cycles. Beams subjected to load amplitudes of approximately 90% or 110% of the measured yield load were subjected to fatigue loading until failure. A detailed discussion of the specimen characteristics and loading schemes were presented in Chapter 5.

8.2.1 Beams Strengthened Using Composite System A

The specimens in this group were strengthened using the strengthening scheme used for specimen B4 in the static-load tests. The strengthening configuration was chosen because failure in specimen B4 was characterized by CFRP rupture accompanied by significant deflections. Therefore, the observed response of the specimens in this group were compared with the response of specimen B4 to evaluate the influence of repeated loading on the behavior of the beams. Specimens A-F1, A-F2, and A-F3 were subjected to load amplitudes representative of service-load conditions, whereas specimen A-F4 was subjected to loads representative of overload conditions on a bridge. Specimens A-F1 through A-F3 were subjected to a static-load test to failure after the application of 10,000 or one million loading cycles.

Specimens A-F1 and A-F2 were subjected to maximum cyclic loads equivalent to 33% of the yield load of the strengthened specimen. The specimens were subjected to 10,000 and one million loading cycles, respectively, prior to being tested statically to failure. The observed behavior of specimens A-F1 and A-F2 was similar. The specimens did not exhibit any signs of debonding or excessive crack growth during cycling. During the subsequent tests to failure, the behavior of these specimens was similar to the behavior of specimen B4. No debonding cracks were observed before yielding of the reinforcement. After yielding, debonding cracks formed along the edges of the CFRP composites and propagated toward the end of the beam. However, debonding did not initiate at the critical section but in a region of the beam that had a surface imperfection built into the specimen during construction caused by the deformation of the formwork (Figure 8.1). Failure of both specimens was characterized by debonding of the CFRP composite from the surface of the concrete after the debonding crack propagated to the end of the composite laminate. Also, the vertical straps ruptured after the composite debonded from the tension face of the specimen. Figure 8.2 shows a picture of the bottom of specimen A-F2 after failure.

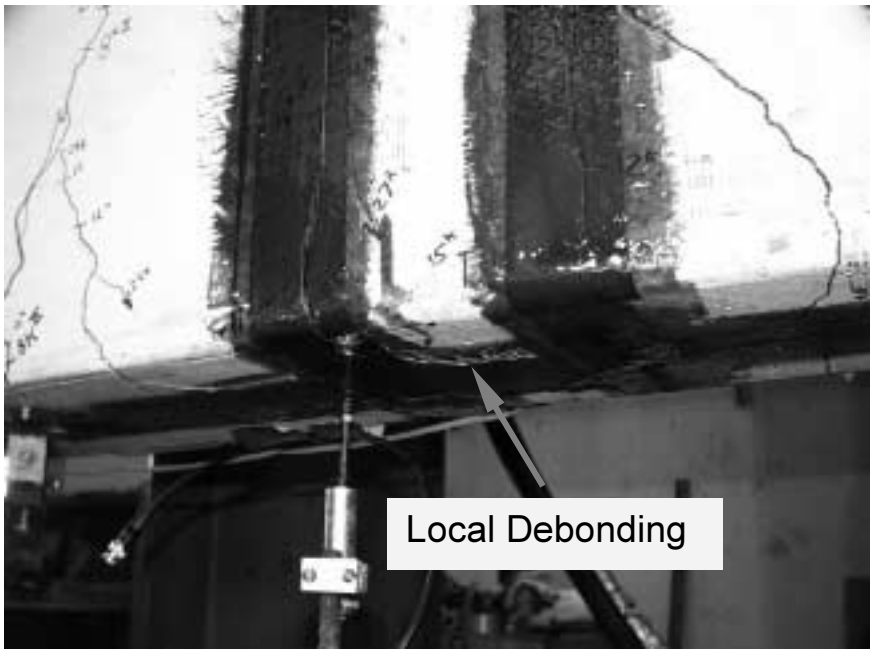

Figure 8.1 Initiation of Debonding of Specimen A-F1

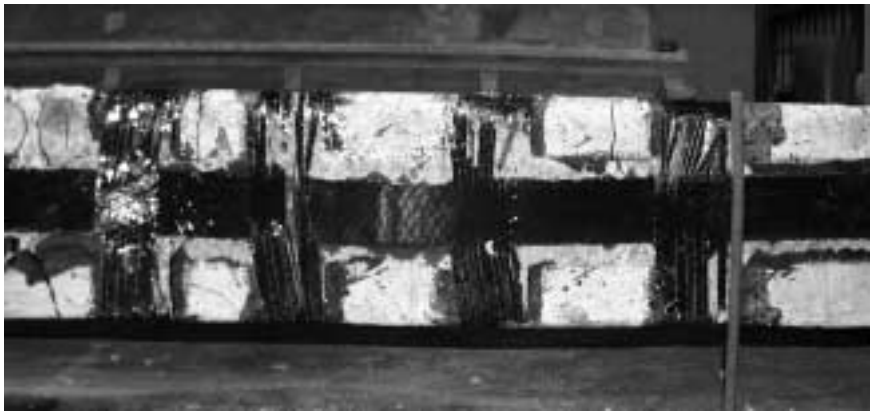

Figure 8.2 View of Tension Face of Specimen A-F2 after Debonding

Specimen A-F3 was subjected to maximum fatigue loads equivalent to 50% of the yield load of the strengthened specimen. The specimen was subjected to 1,000,000 cycles before testing statically to failure. The accumulation of damage with cycling was more pronounced in this specimen than for specimens A-F1 or A-F2. Cracking and extension of cracks with cycling was considered to be an indication of accumulation of damage in the specimens. Only the cracking behavior of specimen A-F3 is discussed in this section because specimens A-F1 and A-F2 exhibited similar behavior. The influence of cycling with the cracking patterns of all the specimens in this group is contained in Appendix B. The effect of the number of load cycles on the extension of cracking in specimen AF-3 is shown in Figure 8.3. Only a few new cracks were generated after the application of one million load cycles (Figure 8.3b). The crack widths during cycling remained below 0.002 in. and therefore are not indicated in the figure. Also, the crack widths at yield during the static-load test to failure were similar to the crack widths measured for the specimens in the static-load testing program. Therefore, no significant influence of load cycling on the cracking behavior of the specimens was observed.

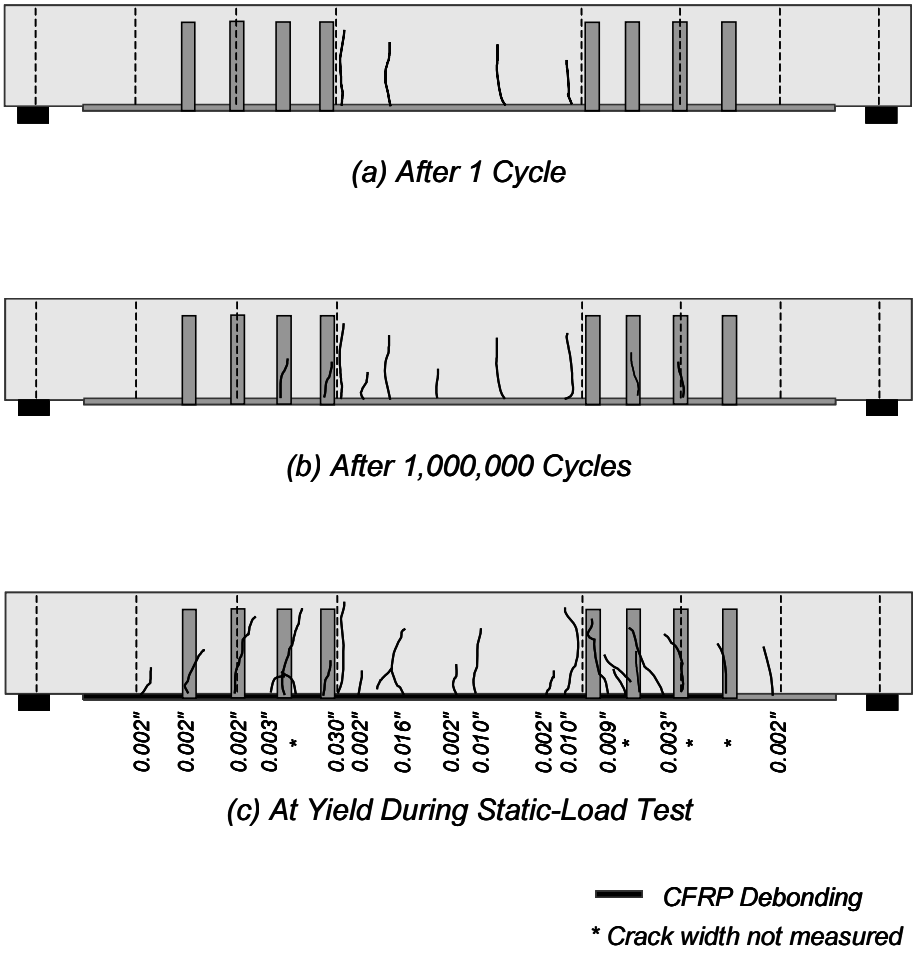

Figure 8.3 Extension of Cracks during Cycling of Specimen A-F3

After the application of 100,000 cycles, local debonding of the CFRP composite was observed in the vicinity of the critical section in specimen A-F3 (Figure 8.4). Apparently, debonding was triggered by an irregularity on the surface of the concrete near the crack initiator. However, debonding did not propagate during cycling and the global behavior of the specimen was not affected by this phenomenon. It can be concluded, therefore, that the condition of the surface of the concrete has an important effect on the local bond behavior of the composites.

Figure 8.4 Local Debonding of CFRP Composite after 100,000 Cycles of Loading in Specimen A-F3

Failure of specimen A-F3 was caused by debonding of the CFRP composite from the surface of the concrete. The extent of CFRP debonding after failure is indicated in Figure 8.3c. After debonding, the vertical straps split in the direction perpendicular to the orientation of the carbon fibers. Figure 8.5 shows the propagation of debonding between straps and the initiation of splitting of straps on the side of composite laminate that remained attached to the surface of the concrete after failure of the specimen.

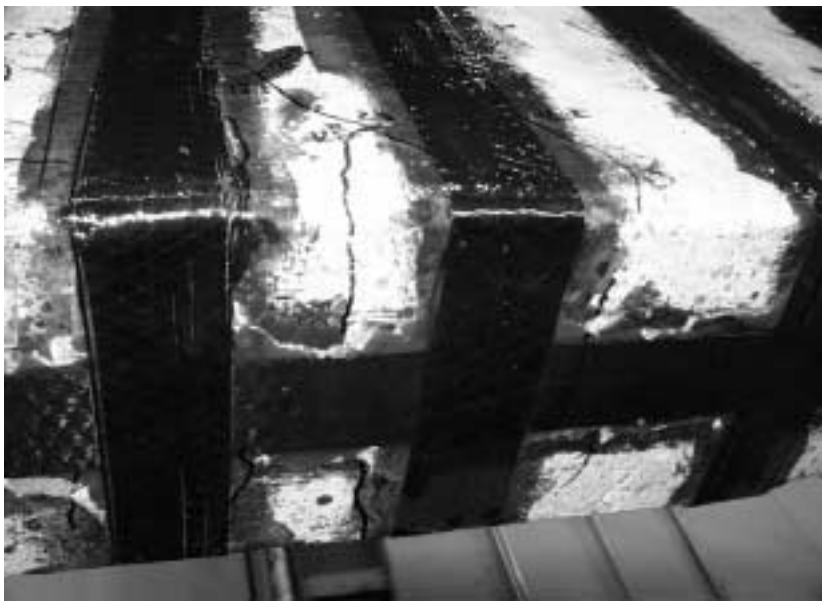

Figure 8.5 Propagation of Debonding and Initiation of Strap Splitting after Failure of Specimen A-F3

Specimen A-F4 was subjected to maximum cyclic loads equivalent to 90% of the yield load of the strengthened specimen. Due to the larger amplitude of cycling, the cracks were significantly wider than the cracks measured during cycling of specimens A-F1 through A-F3. Also, the accumulation of damage was more pronounced in this case and was apparent after fewer cycles of applied load. Figure 8.6 illustrates the observed crack growth of specimen A-F4 after 10,000 cycles of loading. Similarly to other specimens in this group, new cracks formed with cycling but the crack widths did not change.

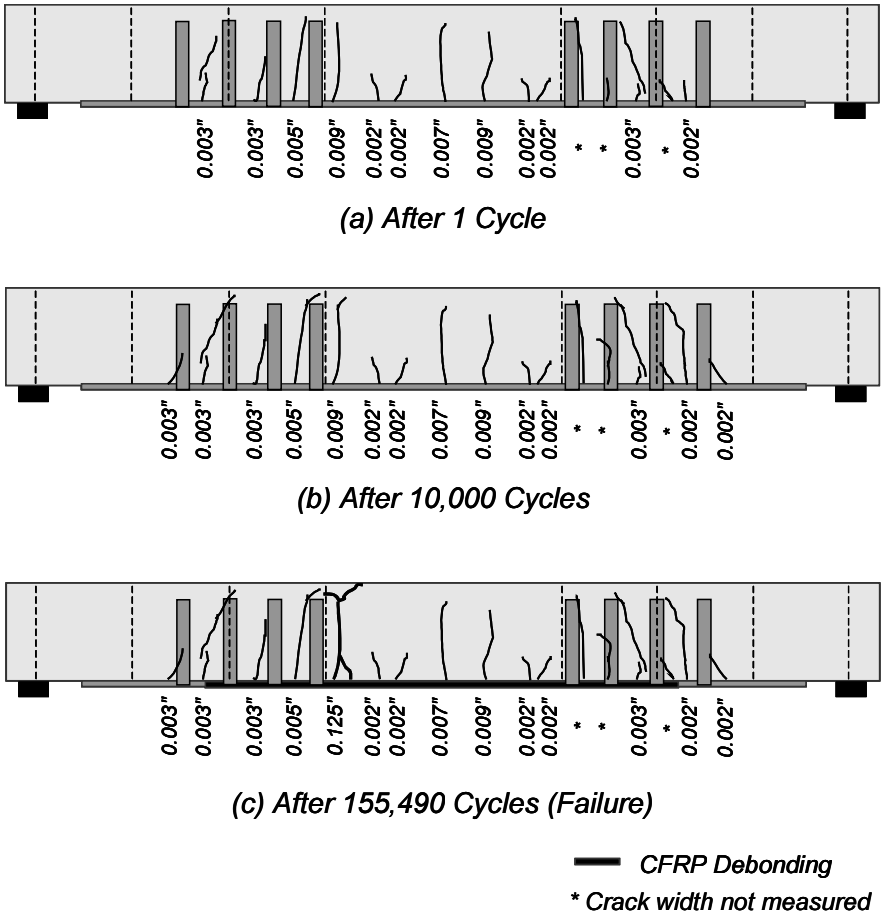

Figure 8.6 Extension of Cracks during Cycling of Specimen A-F4

Local debonding in the vicinity of the crack initiator was observed after 25,000 cycles. Also, secondary cracks formed adjacent to existing flexural cracks indicating the initiation of local debonding of the CFRP composites from the surface of the concrete (Figure 8.7). However, these cracks did not propagate beyond the location of the first transverse strap with subsequent cycling.

Failure of specimen A-F4 was caused by fatigue fracture of the reinforcing bars approximately 2 in. from the crack initiator after approximately 155,500 cycles. However, no indication of incipient failure of the beam was observed prior to fracture of the reinforcement. Excessive crack widening or substantial debonding of the CFRP composite was not observed prior to failure. After fracture of the reinforcement, the CFRP composite debonded from the surface of the concrete symmetrically about the centerline of the specimen as indicated in Figure 8.6c. However, debonding did not propagate to the end of the composite laminate, as was characteristic of debonding failures. Figure 8.8 shows a detail of the reinforcing bar fracture after removal of the concrete cover in specimen A-F4. The performance of this specimen

indicated that the bond between the composite laminate and the surface of the concrete exhibited a better fatigue performance than the reinforcing bars.

Figure 8.7 Bottom View of Specimen A-F4 Showing the Formation of Secondary Cracks during Cycling in the Vicinity of the Crack Initiator

Figure 8.8 Detail Showing Fatigue Fracture of Reinforcing Bar in Specimen A-F4

8.2.2 Beams Strengthened Using Composite System D

The specimens in this group were strengthened using the same strengthening scheme as specimen D4 in the static-load testing program. Specimens D-F1 and D-F2 were subjected to a load amplitude representative of service-load conditions whereas specimens D-F3 and D-F4 were subjected to load amplitudes representative of overload conditions for a bridge. Specimens D-F1 and D-F2 were subjected to a static-load test to failure after one million loading cycles.

The behavior of specimens D-F1 and D-F2 was similar during fatigue cycling and during the static-load test to failure. Therefore, only the behavior of specimen D-F2 will be discussed. Accumulation of damage to specimen D-F2 as inferred from the extension of cracks with cycling was not evident after one million cycles of loading. Although new cracks formed during cycling and existing cracks lengthened, the crack widths did not exceed 0.002 in. However, the extent of cracking in specimen D-F2 was more widespread than in specimen D-F1 because of the difference in the amplitude of loading. The formation and extension of cracks with cycling in specimen D-F2 is presented in Figure 8.9. After 250,000 cycles, local debonding was observed on the top edge of the CFRP plate between the first and second straps on one end of the beam (Figure 8.10). However, debonding did not propagate past the second vertical strap with subsequent cycling (Figure 8.9b).

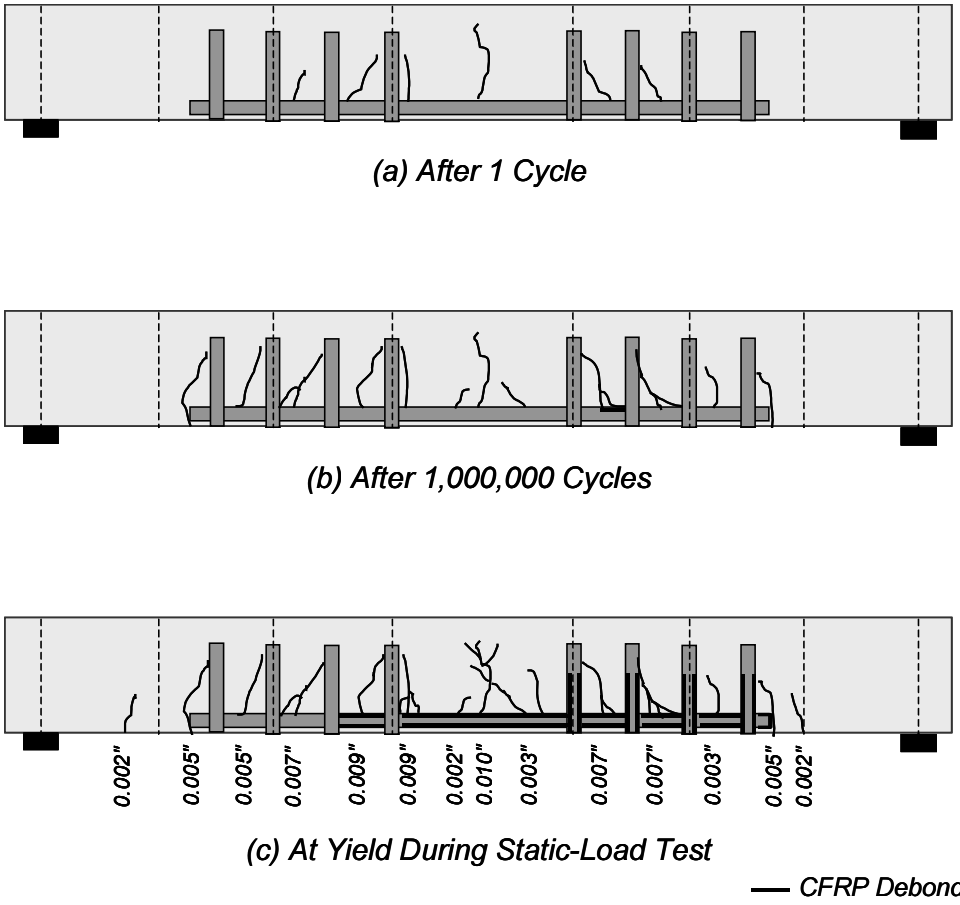

Figure 8.9 Formation and Extension of Crack Lengths as a Function of Load Cycling in Specimen D-F2

Figure 8.10 Local Debonding of CFRP Plate on Specimen D-F2 during Fatigue Cycling

During the static-load test to failure, no propagation of debonding was observable for loads below the yield load of the specimens. After yield, debonding initiated from secondary cracks that formed from existing flexural cracks and turned horizontally along the top edge of the composite plates. The plate debonding initiated in the midspan region of the specimens and propagated toward the end of the plates. As for the specimens tested in the static-load testing program, the debonding cracks were arrested at every strap location therefore delaying total debonding of the CFRP plates. Figure 8.11 shows the formation of debonding cracks in the maximum moment region of specimen D-F2. Failure of this specimen was characterized by debonding of the longitudinal composite plates followed by vertical splitting of the transverse composite straps (Figures 8.12 and 8.13). The behavior of specimens D-F1 and D-F2 was not substantially different from the behavior of specimen D4 during the static-load test to failure. It can be concluded, therefore, that load cycling did not degrade the bond between the composite and the surface of the concrete.

Specimen D-F3 was subjected to maximum cyclic loads with an amplitude approximately equal to 90% of the yield load of the strengthened specimen (specimen D4). During the first excursion to the peak load, extensive cracking took place along the beam (Figure 8.13). Initiation of debonding at several locations along the CFRP plates was observed after only 100 cycles of loading. Subsequently, a shear crack formed on one end of the beam after 1,000 cycles and propagated toward the compression face of the beam after further cycling (Figure 8.14). Although there were concerns of fatigue fracture of the stirrups during testing, the shear reinforcement within the shear span of the specimen was adequate to prevent this crack from causing failure.

Failure of specimen D-F3 was caused by debonding of the CFRP plate on one side of the specimen after approximately 55,000 load cycles. CFRP debonding originated in the region of maximum moment of the beam and propagated to the end of the plate (Figure 8.13c). Only the plate on one side of the beam debonded fully from the surface of the concrete. The asymmetric debonding of the CFRP plate generated a stress concentration in the diagonally opposite corner of the specimen and caused crushing of the concrete in compression within the region of maximum moment of the beam (Figure 8.15). Therefore, repeated load cycling deteriorated the bond between the composite plate and the surface of the concrete in this specimen. However, it should be noted that the amplitude of loading used in this specimen does not occur commonly throughout the lifetime of a bridge structure.

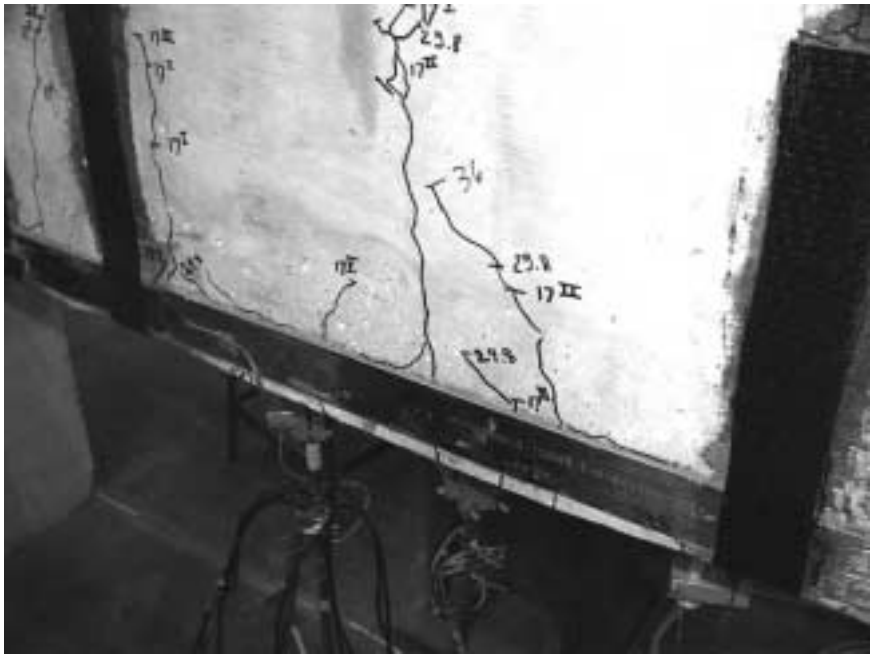

Figure 8.11 Formation of Debonding Cracks in Specimen D-F2

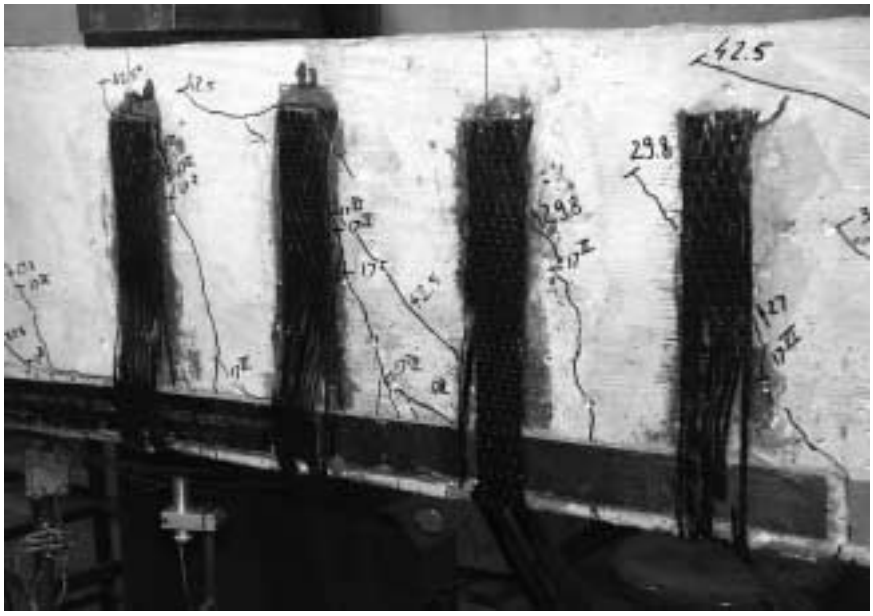

Figure 8.12 Debonding at the End of the CFRP Composite Plate in Specimen D-F2

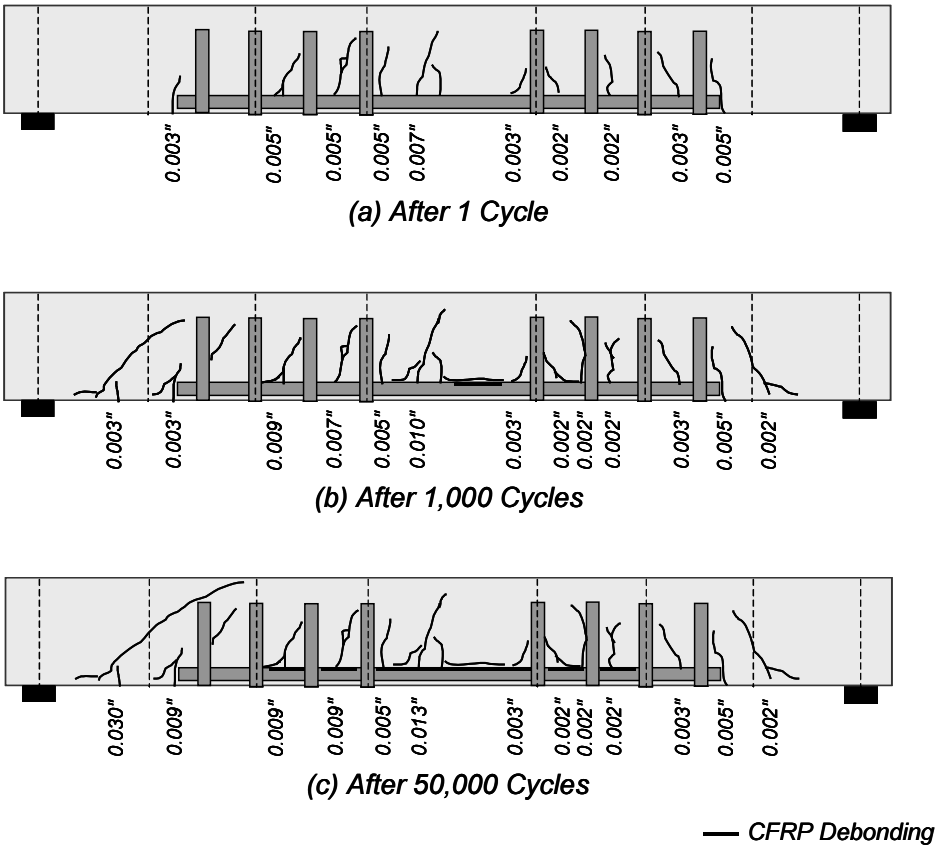

Figure 8.13 Formation and Extension of Crack Lengths as a Function of Load Cycling in Specimen D-F3

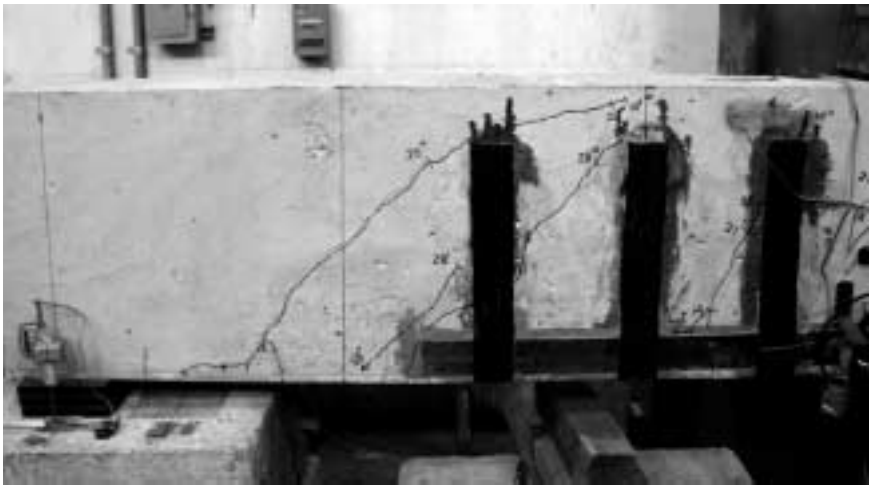

Figure 8.14 Shear Crack that Formed During Cycling of Specimen D-F3

Figure 8.15 Crushing of the Concrete in the Compression Zone after Debonding of the CFRP Plate on the Opposite Side of Specimen D-F3

During the first loading cycle, extensive cracking occurred on the beam. Because the loading amplitude was beyond the yield load of the specimen, flexural cracks widened during cycling (Figure 8.16). Also, debonding cracks appeared on the top edge of the composite plates during the first cycle of loading and propagated toward the end of the composite laminate with load cycling (Figure 8.17). After 5,000 cycles of loading, debonding had progressed from midspan to the end of the composite plates. Also, some flexure-shear cracks extended toward the compression face of the specimens causing the vertical straps to debond from the surface of the concrete (Figure 8.18). Failure of the specimen was controlled by debonding of the CFRP composite from the surface of the concrete after approximately 9,000 cycles. The propagation of debonding as a consequence of cycling eventually caused total debonding of the composites at a lower load than was applied to specimen D4 in the static-load testing program.

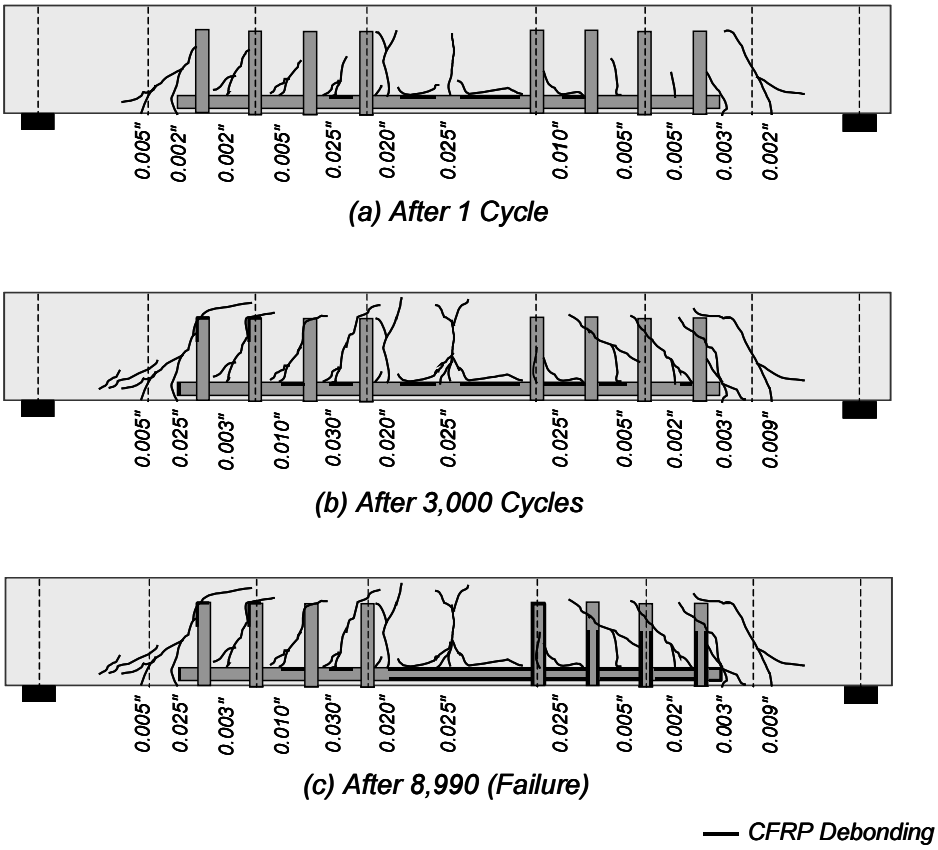

Figure 8.16 Formation and Extension of Crack Lengths as a Function of Load Cycling in Specimen D-F4

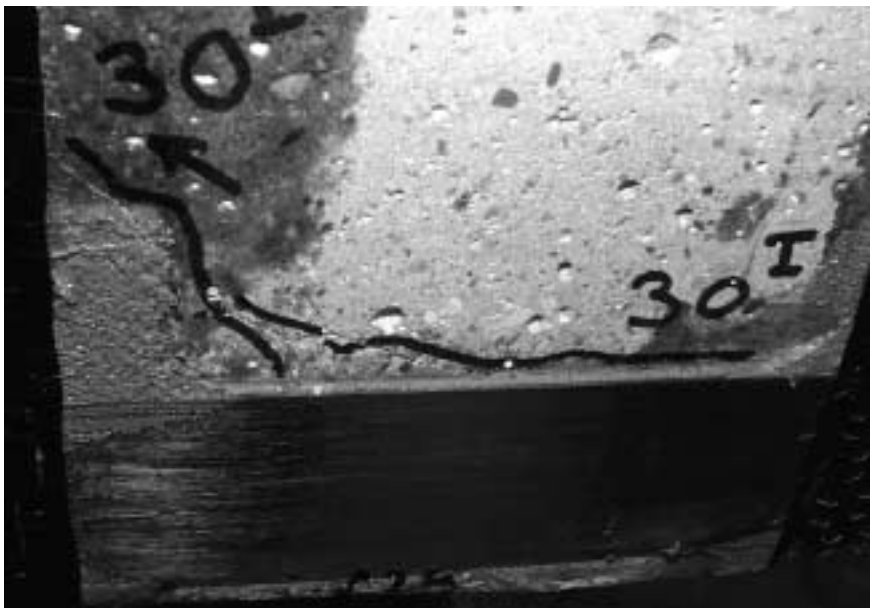

Figure 8.17 Detail Showing Propagation of Debonding Along the Top Edge of the Composite Laminate in Specimen D-F4 during the First Cycle of Loading

Figure 8.18 Debonding of Vertical Composite Straps During Cycling of Specimen D-F4

8.3 MEASURED LOAD-DEFLECTION RESPONSE

The measured load-deflection response of the specimens subjected to fatigue loads is presented in this section. The measured load-deflection response of each group of specimens is discussed in Sections 8.3.1 and 8.3.2. The number of cycles and amplitude of loading affected the response of the specimens to different extents. The load-deflection response of the specimens is also compared with the load-deflection response of companion specimens tested in the static-load testing program. The differences in the measured behavior are discussed in this section.

8.3.1 Beams Strengthened Using Composite System A

Four specimens were strengthened using composite system A. These specimens were strengthened using the same scheme as specimen B4. Because the mechanical properties of composite systems A and B were nearly identical, the response of the specimens in this group was compared with specimen B4. The specimens were subjected to different numbers of cycles of load and load ranges as indicated in Table 8.1. The specimens were subjected to a maximum of one million load cycles and then tested statically to failure whenever this number of cycles was reached. Specimen A-F1 was tested statically to failure after only 10,000 load cycles. Only specimen A-F4 failed before reaching one million cycles of load. Table 8.1 also lists the failure modes that were observed in this series of tests.

Table 8.1 Observed Failure Modes of Specimens Strengthened Using Composite System A

Specimen	Number of Cycles	Load Range, kip	Loading Regime at Failure	Failure Mode
A-F1	10,000	7	Static-Load Test	CFRP Debonding
A-F2	1,000,000	7	Static-Load Test	CFRP Debonding
A-F3	1,000,000	11.5	Fatigue	CFRP Debonding
A-F4	155,950	20	Fatigue	Reinforcement Fatigue Fracture

The load-deflection response of this group of specimens is shown in Figure 8.19, and the main parameters obtained from the measured load-deflection curves are listed in Table 8.3. The response of the strengthened specimens is compared in each chart to the response of specimen B4 and to the response of the control specimen. Figure 8.19a shows that the response of specimen A-F1 was similar to the response of specimen B4. Because specimen A-F1 was subjected to a very small number of load cycles, no deterioration of strength or stiffness was observed after cycling. The slopes in the load-deflection curves for both specimens before and after yielding are approximately equal.

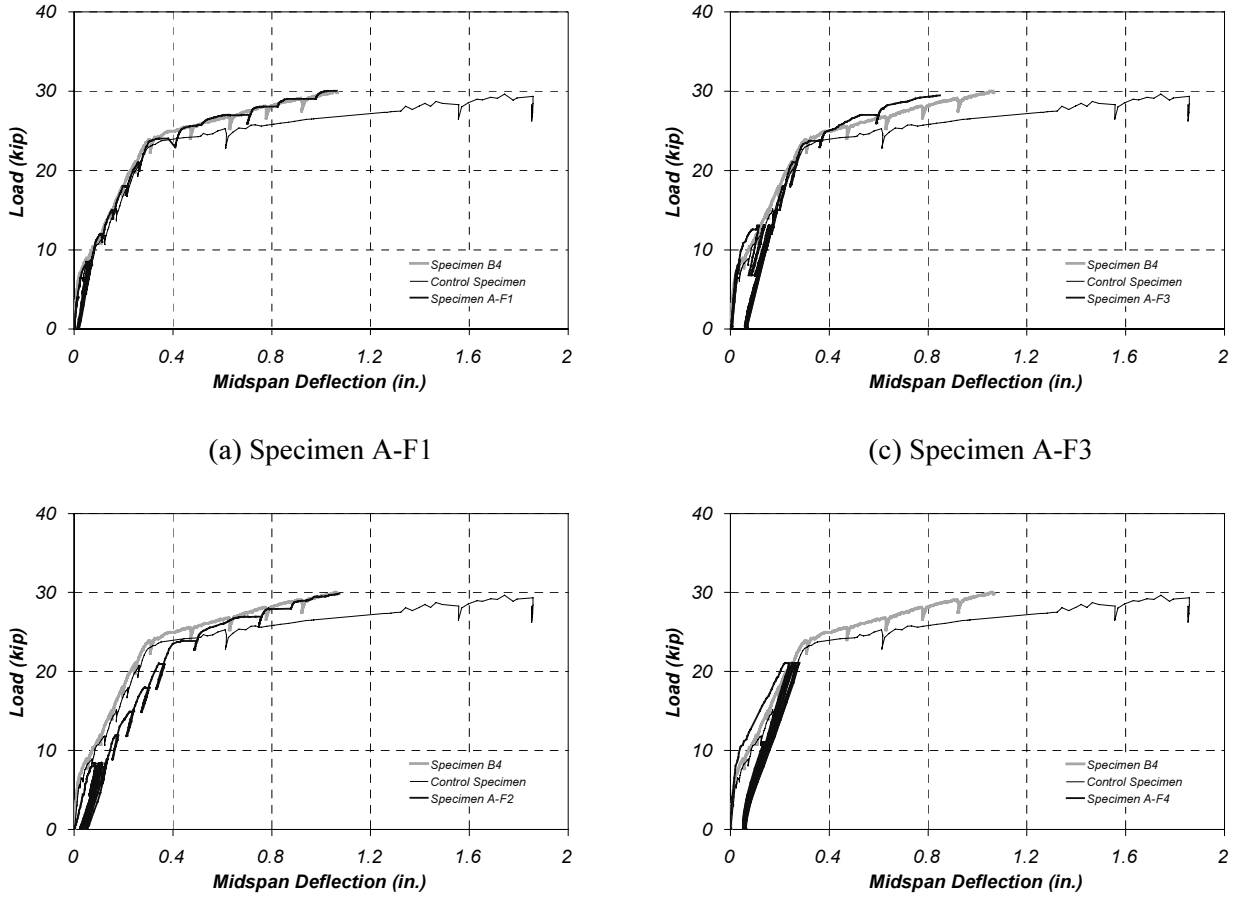

(a) Specimen A-F1

(c) Specimen A-F3

(b) Specimen A-F2

(d) Specimen A-F4

Figure 8.19 Comparison of the Load-Deflection Response of Specimens Strengthened Using Composite System A

Specimen A-F2 was subjected to the same load range as specimen A-F1. However, the number of cycles was increased to one million after observing that specimen A-F1 did not exhibit any apparent degradation of strength or stiffness. The midspan deflection of specimen A-F2 increased during cycling as can be observed in Figure 8.19b. During the static test to failure, the specimen did not exhibit a cracking point in the load-deflection response curve. Therefore, the slope in the initial portion of the load-deflection curve resembled the slope of a pre-cracked specimen. Although the yield load of specimen A-F2 and specimen B4 were approximately equal, the yield displacement of specimen A-F2 was higher because of the accumulation of deflection with cycling. The load-deflection curve for specimen A-F2 joined the curve for specimen B4 in the post-yield region before failure. The load at failure of specimen A-F2 was approximately equal to the capacity of specimen B4. This result indicates that cycling at approximately 33% of the yield load did not affect the ultimate behavior of the specimen.

Specimen A-F3 was subjected to one million cycles to a load approximately equal to 50% of the yield load in the strengthened specimen. The behavior of the specimen during cycling was similar to specimen A-F2. During the static test to failure, the specimen also behaved similarly to a pre-cracked specimen. The measured load-deflection curve for this specimen approximated the load-deflection curve for specimen B4 after yielding. Similarly to other specimens in this group, the behavior beyond the yield load was similar to the behavior of specimen B4. In this case, the specimen failed at a load slightly lower than the capacity of specimen B4, but specimen variability rather than fatigue loading probably caused this slight difference.

Finally, specimen A-F4 was subjected to cyclic loads with amplitudes approximately equal to 90% of the yield load of the strengthened specimen. The specimen exhibited a slightly higher initial stiffness during the first loading cycle to the peak load as can be observed in Figure 8.19d. Midspan deflections also increased with cycling in this case. Failure of this specimen was controlled by fracture of the reinforcing bars near the critical section although no signs of degradation were apparent from the load-deflection curve.

8.3.2 Beams Strengthened Using Composite System D

Four specimens were strengthened using composite system D. The beams were strengthened by attaching the composites to the sides of the beams and placing straps along the shear span. This strengthening scheme was identical to the one used for specimen D5. The load-deflection response of the specimens in this series of tests was compared with the response of specimen D5. The beams were subjected to varying numbers of cycles and load ranges. Table 8.2 summarizes the main parameters that were studied in this group of specimens and the observed failure modes. A detailed discussion of the loading sequence was presented in Section 5.3 and summarized in Table 5.3.

Table 8.2 Observed Failure Modes of Specimens Strengthened Using Composite System D

Specimen	Number of Cycles	Load Range, kip	Load Sequence at Failure	Failure Mode
D-F1	1,000,000	11	Static-Load Test	CFRP Debonding
D-F2	1,000,000	16	Static-Load Test	CFRP Debonding
D-F3	55,490	27	Fatigue	CFRP Debonding
D-F4	8,990	32	Fatigue	CFRP Debonding

Data were collected periodically during load cycling by applying a cycle of loading statically. The deflection at midspan was measured at loads corresponding to the maximum and minimum loads that defined the sequence of cycling. The comparison of the measured load-deflection response of this group of beams to specimen D5 is presented in Figure 8.20. The load-deflection response is also compared with the control specimen to compare the maximum applied load during cycling to the capacity of the unstrengthened specimen. Table 8.3 lists some of the important parameters that were obtained from the load-deflection curves.

Specimens D-F1 and D-F2 were tested statically to failure after the specimens had been subjected to one million cycles. The peak loads in these specimens were determined to represent service load conditions of a bridge. Two load levels were used to simulate unstrengthened and strengthened service load conditions. Using these two load-levels, the strains generated on the reinforcing bars on specimens D-F1 and D-F2 corresponded approximately to 33% and 50% of the yield load, respectively.

During the static test, specimen D-F1 exhibited a behavior that was almost identical to the load-deflection behavior of specimen D5. Although there was a slight increase of midspan deflection with cycling (Table 8.3), the specimen rejoined the measured load-deflection curve of specimen D5 before yielding. Specimen D-F1 failed at a slightly lower load than specimen D5 but the global behavior during the static test was almost identical. It can be concluded, therefore, that cycling at a stress level of approximately 33% of the yield load did not affect the behavior of the strengthened specimen.

The load-deflection response of specimen D-F2 was also very similar to the response of specimen D5. However, the midspan deflection increased more during cycling than specimen D-F1 because the specimen was subjected to higher peak loads (Table 8.3). At the initiation of the static test to failure, the load-deflection curve for specimen D-F2 was significantly different from the curve measured for specimen D5. This difference was caused by the accumulation of damage that specimen D-F2 had sustained during cycling. However, the trends in the load-deflection curves for the two specimens were similar, particularly after yielding. Specimen D-F2 failed at a higher load than specimen D5, indicating that although there was accumulation of damage during cycling, it did not affect the ultimate load of the specimen.

Specimens D-F3 and D-F4 were subjected to peak loads representative of significant overloads on a bridge. The load magnitude was selected to generate failure by fatigue after a relatively small number of cycles. The purpose of these tests was to determine whether fatigue failure of the reinforcing bars or the bond between the composites and the surface of the concrete would be the controlling failure mode.

Specimen D-F3 was subjected to a peak load of approximately 90% of the yield load of the strengthened specimen. The slope of the loading branch for the first load cycle was approximately equal to the initial slope in the load-deflection curve of specimen D5 (Figure 8.20c). Midspan deflections increased during cycling as can be observed from this figure and Table 8.3. The increase of deflections indicated the degradation of stiffness as damage was accumulated with cycling.

The peak load used in specimen D-F4 had a magnitude of approximately 110% of the yield load of the strengthened specimen (specimen D5). The load-deflection curve for this specimen also followed the curve for specimen D5 very closely during the first loading cycle to the maximum load. There was a significant increase in the midspan deflection during cycling for this specimen (Figure 8.20d).

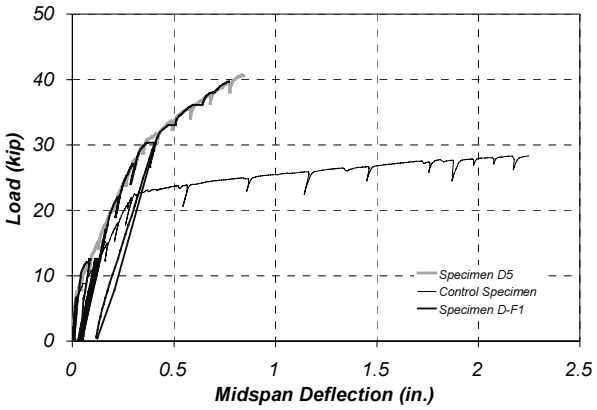

(a) Specimen D-F1

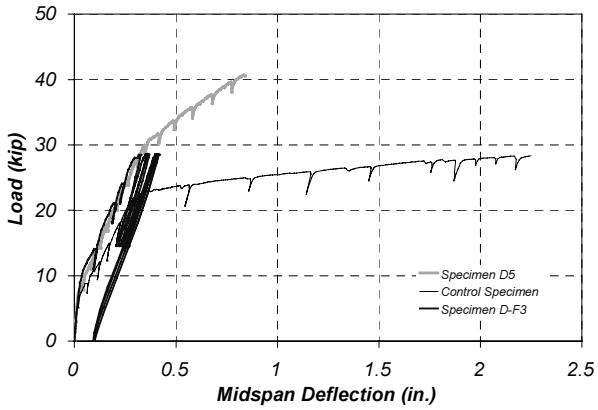

(c) Specimen D-F3

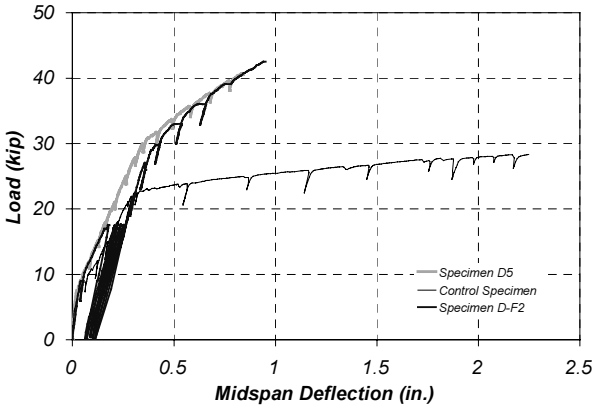

(b) Specimen D-F2

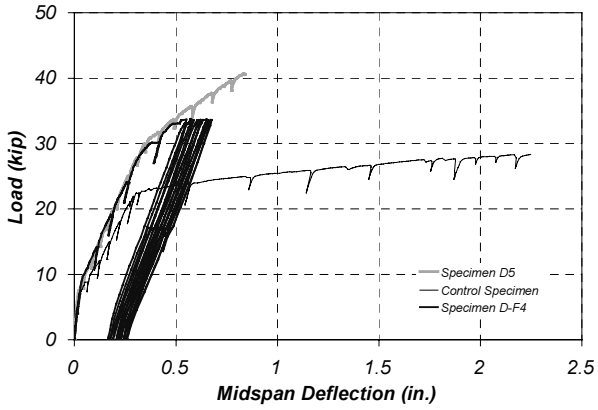

(d) Specimen D-F4

Figure 8.20 Comparison of the Load-Deflection Response of Specimens Strengthened Using Composite System D

8.4 MEASURED STRAINS

The specimens were instrumented using strain gages to calculate stresses in the reinforcing bars, in the concrete, and in the CFRP laminates. The strain gages were attached to the reinforcing bars before casting the concrete. The strain gages on the surface of the concrete and CFRP composites were bonded after the specimens were positioned on the support blocks before loading. The effects of the self-weight of the specimens on the strains measured on the reinforcing bars were considered negligible. Therefore, the reinforcing bars were assumed to have zero strain at the beginning of the tests.

Table 8.3 Summary of Results from Load-Deflection Response of Specimens in the Fatigue-Load Testing Program

Specimen	Parameters Measured During Fatigue Loads			Parameters Measured During First Excursion Beyond Yield			
	P_{peak}, kip	Δ_1, in.	Δ_N, in.	P_y, kip	Δ_y, in.	P_{max}, kip	Δ_{max}, in.
A-F1	8	0.057	0.072	23.7	0.309	26.9	0.446
A-F2	8	0.085	0.131	23.5	0.398	28.3	0.595
A-F3	12.5	0.114	0.174	23.7	0.321	31.1	1.062
A-F4	21	0.238	0.276	-	-	*	*
D-F1	12	0.086	0.134	30.3	0.376	28.8	0.431
D-F2	17	0.178	0.264	29.8	0.424	30.1	0.549
D-F3	28	0.326	0.416	-	-	*	*
D-F4	33	0.551	0.673	30.1	0.393	*	*

Δ_1 represents the midspan deflection measured at the peak load on the first cycle of loading.
Δ_N represents the midspan deflection measured at the peak load after the last cycle of loading.

* Failure occurred during fatigue loads.

The observed strain response of the specimens is discussed in this section. The strain response of the specimens that were tested statically to failure after fatigue loading is compared with the response of companion specimens tested monotonically to failure. Also, the variation in average measured strains with cycling is presented here. The characteristics of the strain response of all the specimens were very similar. Therefore, only a discussion of these typical characteristics is presented in this section. Table 8.4 lists a comparison of the average measured strains during the first cycle and last cycles of loading to the peak load on the different materials. The average measured strains in the different materials for the specimens at yield and ultimate loads are listed and compared with the companion specimens subjected to static loads in Table 8.5. Load-strain plots for all the specimens are presented in Appendix D. The location of the instrumented sections for all the specimens was indicated in Table 5.5. The position of the strain gages on the reinforcing bars, on the surface of the concrete, and on the surface of the CFRP composites was illustrated in Figure 5.4.

8.4.1 Measured Strain Response of Specimens Tested Under Static Loading

The general characteristics of the measured strain response of the beams tested during the static-load test to failure are discussed in this section. Only the specimens that were subjected to load amplitudes representative of service-load conditions were tested statically to failure after the application of cyclic loads. Therefore, the discussion presented here refers to only these specimens. Specimens subjected to conditions representative of overloads on bridges failed during the fatigue cycles, so a static test was not conducted for these specimens. The type of loading at failure of the specimens was presented in Section 8.3.

The behavior of the specimens tested statically to failure after fatigue loading was similar to the companion specimens tested monotonically to failure. The general trends in the strain response for the specimens tested statically to failure in the fatigue-load testing program are discussed here. The average measured strains for specimens A-F3 and D-F2 were chosen for this discussion. These specimens were subjected to load amplitudes approximately equal to 50% of the yield load of the strengthened specimens. The load amplitude in these specimens was considered representative of the loads expected on the strengthened bridges studied in this research project. Table 8.5 lists the average measured strains at the yield and ultimate loads on the reinforcing bars, surface of the concrete, and composite system at the critical section (section 1) for all the specimens. Appendix D contains the measured load-strain plots for all the beams tested in the static-load testing program.

Figure 8.21a shows the average measured strains on the reinforcing bars in specimen A-F3. The two linear portions in the initial part of the load-strain curve correspond to uncracked and cracked behavior of the specimen, respectively, during the initial loading to the peak load. During the static-load test to failure, the steeper slope representative of uncracked behavior was no longer observed because the specimen was subjected to load amplitudes that were greater than the load corresponding to cracking. Yielding of the reinforcing bars was observed at a load approximately equal to 24 kip. At this load, strains on the reinforcing bars grew significantly as the bars yielded. In this specimen, yielding caused the average strain on the bars to increase to approximately 0.01. The final slope in the load-strain curve is indicative of the strength of the composites being mobilized after yielding of the reinforcement stabilized.

Figure 8.21b shows the average measured strain on the surface of the CFRP composite in specimen A-F3. As for the curve for the reinforcing bars, a change in the initial slope of the load-strain curve was only observed during the first loading cycle. The curve for the static-load test to failure initiated at a strain of approximately 0.0007. This permanent strain was probably caused by the cracks remaining partially open after cycling. Therefore, the load-strain curve during the static-load test to failure exhibited a constant slope until yielding. After yielding (24 kip), the CFRP strains increased to approximately 0.008 without an increase in load. The difference between this strain and the measured strains on the reinforcement at

the end of the horizontal portion of the curve indicates local debonding of the CFRP composites. Subsequently, the load-strain curve exhibited a positive slope again as the strains in the CFRP composite increased with loading. The maximum measured strain in this beam was approximately equal to 0.012 at 30 kip.

The average measured strains on the surface of the concrete of specimen A-F3 are shown in Figure 8.21c. In this figure, compressive strains are plotted as negative strains. The strains on the concrete decrease approximately linearly up to the yield load. After yielding, the strains on the concrete increased slightly as the neutral axis shifted toward the top of the beam after yielding.

Figure 8.22 shows the average measured strains in specimen D-F2. The strain gages on the reinforcing bars debonded during load cycling and therefore no information was available during the static-load test to failure. The measured strains on the surface of the composite plates show different characteristics from the measured response of specimen A-F3. At the load corresponding to yielding of the reinforcement, the slope on the measured strain curve for the composite plates decreases without becoming horizontal (Figure 8.22b). Because all the specimens in the fatigue-load testing program were fabricated using the same heat of steel, it is expected that the load-strain behavior of the reinforcing bars would have been similar to specimen A-F3. Therefore, the fact that a horizontal slope is not observed on the load-strain curve for the composite plates indicates that local debonding took place because the composite strains do not follow the general shape of the load-strain curve for the reinforcement. However, the measured strains in the composite plates are similar to the measured strains of the companion specimen (specimen D5) in the static-load testing program (Appendix D). The measured strains on the surface of the concrete exhibited similar characteristics to the response of specimen A-F3 and are therefore not discussed further.

The measured strains in the different materials varied during load cycling. Figures 8.23 through 8.26 show the variation of strain with number of load cycles for all the specimens tested in the fatigue-load testing program. Figures 8.23 and 8.25 show the variation of strain with load at the critical section (section 1). The strains in all the specimens increased at an approximately constant rate with cycling. However, the rate of increase was a function of the magnitude of the load amplitude. In general, the strains in specimens subjected to load amplitudes corresponding to service-load conditions (specimens A-F1 through A-F3, and D-F1 through D-F2) increased at lower rates than the specimens subjected to higher load amplitudes.

Figures 8.24 and 8.26 show the variation of strain in the different materials for all the specimens at section 2. In this case, the rate of change of strain with cycling varied for the different specimens and materials. This effect was probably caused by the redistribution of strains that took place after cracks formed during cycling of the specimens. Cracks forming in the vicinity of the location of the strain gages would cause the strains to increase suddenly after a specific number of cycles. On the other hand, a decrease in the measured strains with increasing number of cycles can be the result of cracks forming far from the location of the strain gage. This phenomenon was not observed in the plots for section 1 because in those cases a crack always formed in the vicinity of the strain gages because of the presence of the crack initiator.

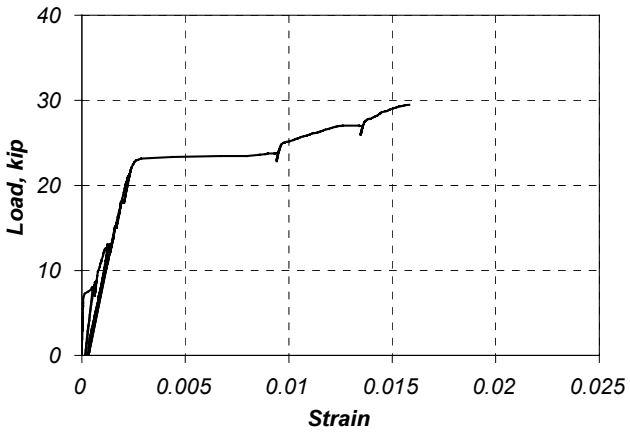

(a) Average #5 Reinforcing Bar Strains

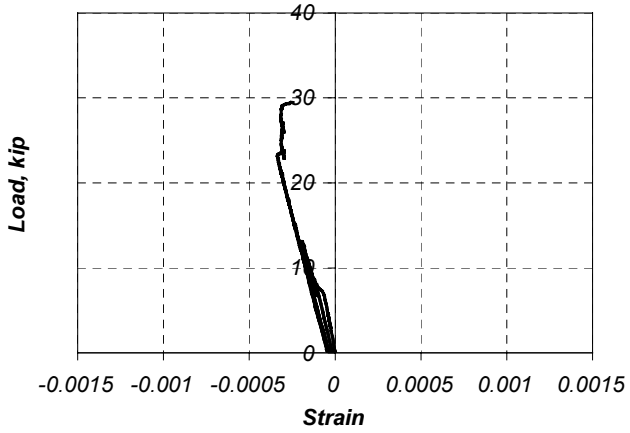

(c) Average Concrete Strains

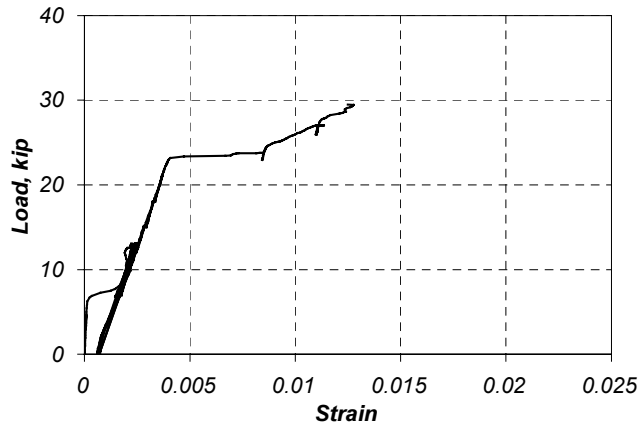

(b) Average CFRP Composite Strains

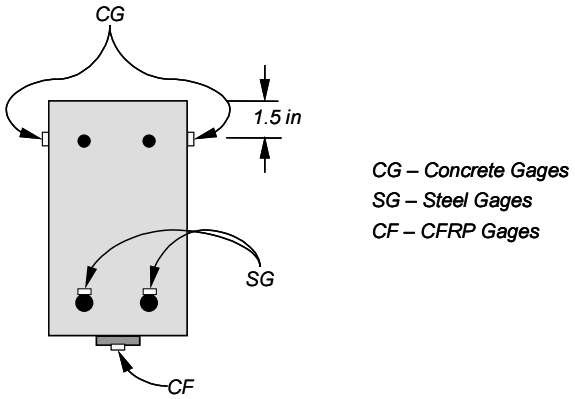

(d) Position of Strain Gages

Figure 8.21 Average Measured Strains in Specimen A-F3 during Static-Load Test to Failure (Section 1)

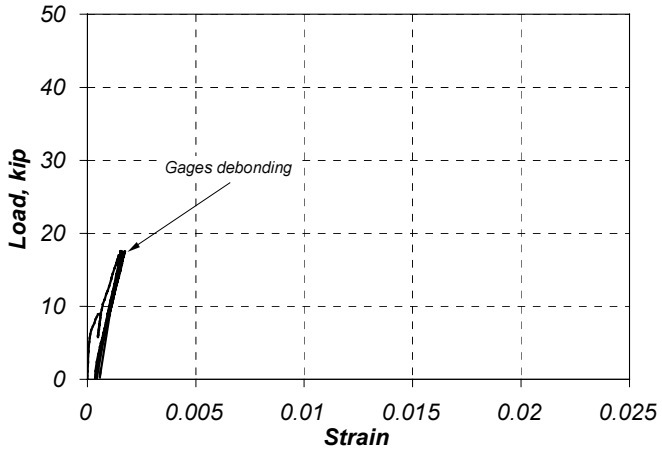

(a) Average #5 Reinforcing Bar Strains

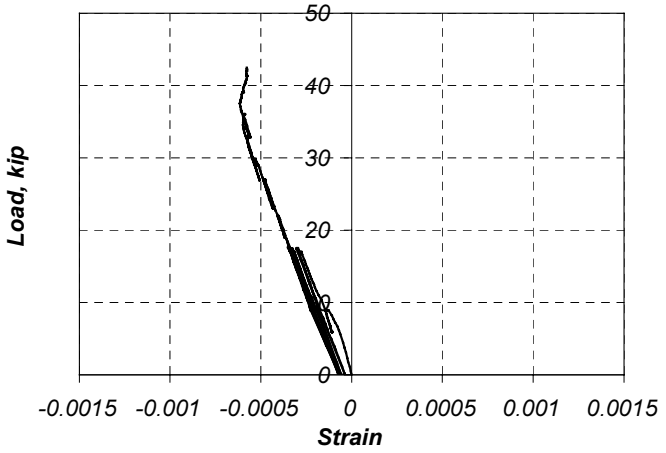

(c) Average Concrete Strains

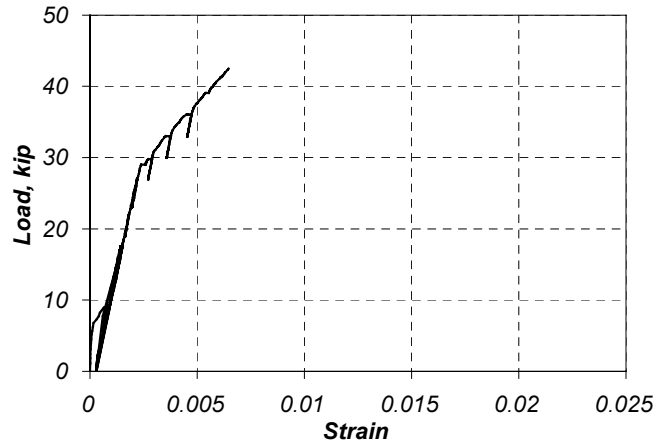

(b) Average CFRP Composite Strains

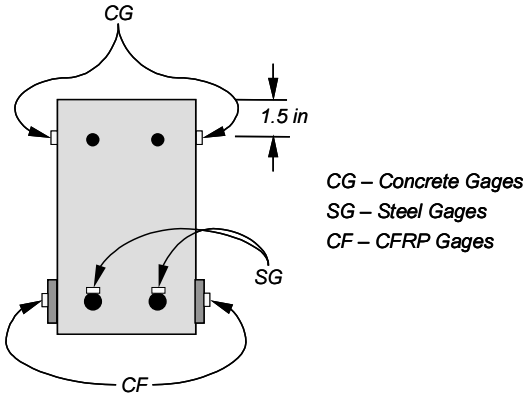

(d) Position of Strain Gages

Figure 8.22 Average Measured Strains in Specimen D-F2 during Static-Load Test to Failure (Section 1)

Table 8.4 Average Measured Strain at Different Load Cycles for the Specimens in the Fatigue-Load Testing Program

Specimen	Peak Load, kip	Average Measured Strain During First Cycle at the Peak Load (Microstrain)			Average Measured Strain During Last Cycle at Peak Load (Microstrain)		
		Steel	Concrete**	CFRP	Steel	Concrete**	CFRP
A-F1	8	560	-120	1,300	720	-130	1,600
A-F2	8	660	-120	Malfunction	850	-170	Malfunction
A-F3	12.5	1,200	-190	2,100	1,400	-200	2,500
A-F4	21	2,300	-470	5,200	2,700	-550	5,700
D-F1	12	1,000	-210	1,100	1,200*	-260	1,100
D-F2	17	1,500	-300	1,400	1,700*	-340	1,500
D-F3	28	8,500	-470	2,300	11,400	-520	2,900
D-F4	33	10,700	-590	4,300	11,300*	-660	5,200

*The reading was taken before the last load cycle because of strain gage malfunction.
**Negative values indicate compressive strains.

Table 8.5 Average Measured Strain in Fatigue Specimens and Static-Load Specimens During Static-Load Test to Failure

Specimen	Average Measured Strain at Yield Load (Microstrain)			Average Measured Strain at Ultimate Load (Microstrain)		
	Steel	Concrete**	CFRP	Steel	Concrete**	CFRP
A-F1	2,500	-360	3,500	14,900	-350	10,600
A-F2	2,600	-370	Malfunction	14,300	-290	Malfunction
A-F3	2,600	-340	4,000	15,800	-250	12,800
B4	2,700	-340	3,500	19,200	240	11,900
D-F1	Malfunction	-550	2,300	Malfunction	-580	6,200
D-F2	Malfunction	-550	2,500	Malfunction	-580	6,500
D5	2,900	-550	2,500	12,800	-550	6,200

**Negative values indicate compressive strains.

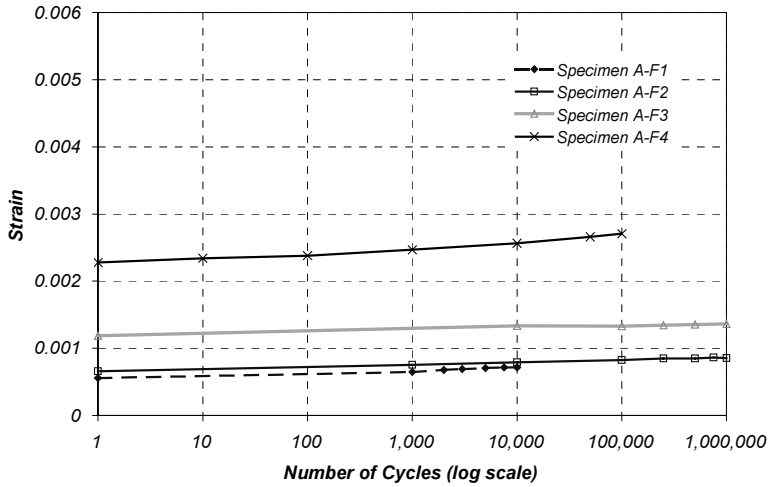

(a) Reinforcing Bar Strains

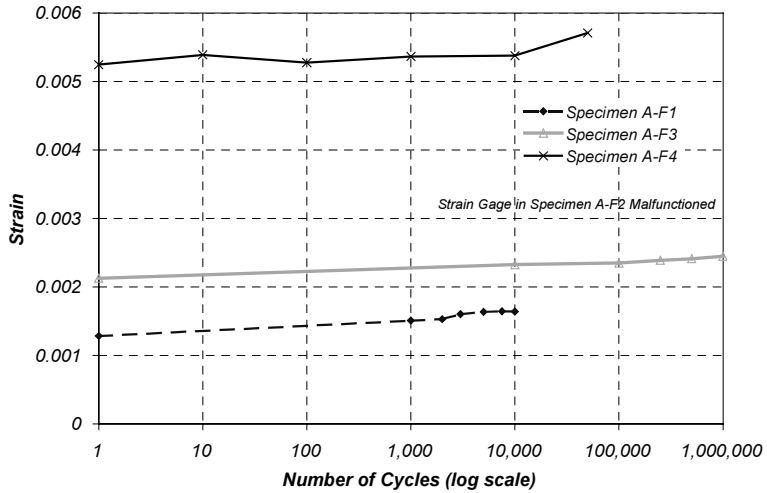

(b) CFRP Strains

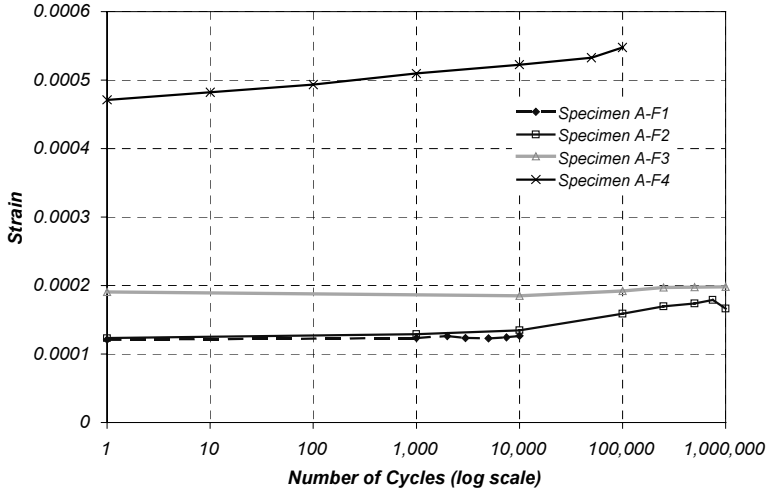

(c) Concrete Strains

Figure 8.23 Variation of Average Measured Strains with Number of Cycles for Specimens Strengthened Using Composite System A (Section 1)

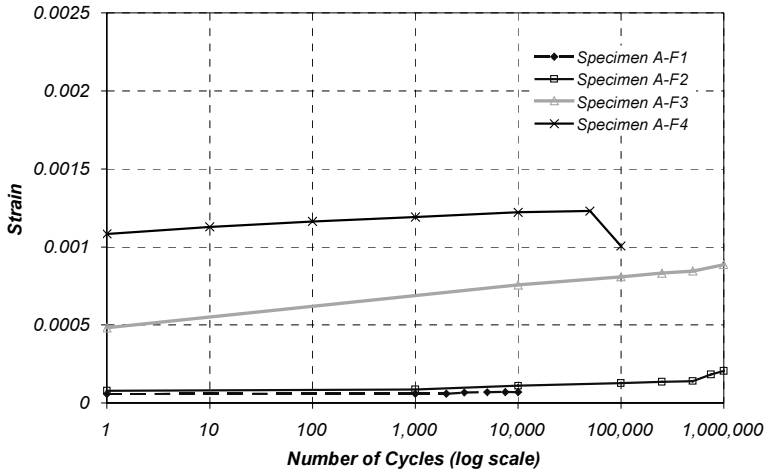

(a) Reinforcing Bar Strains

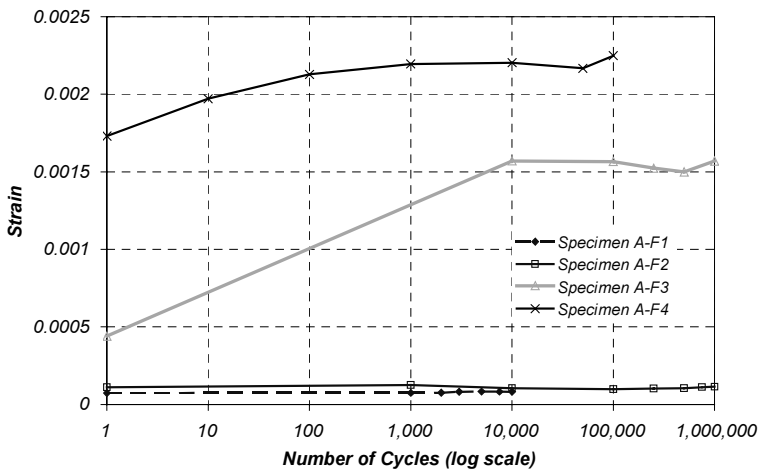

(b) CFRP Strains

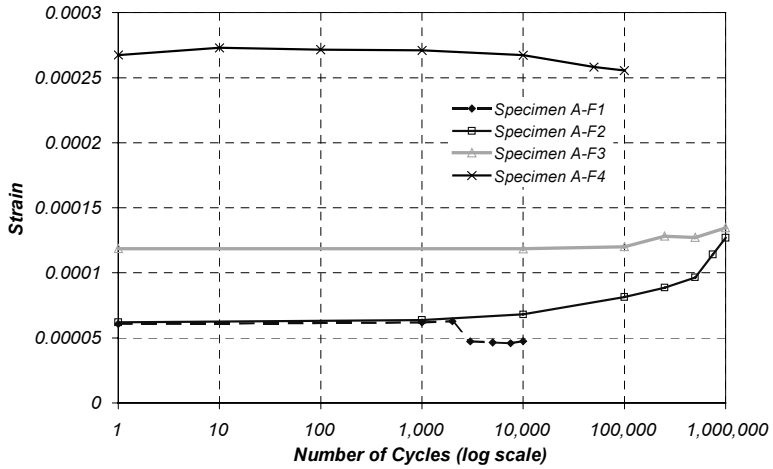

(c) Concrete Strains

Figure 8.24 Variation of Average Measured Strains with Number of Cycles for Specimens Strengthened Using Composite System A (Section 2)

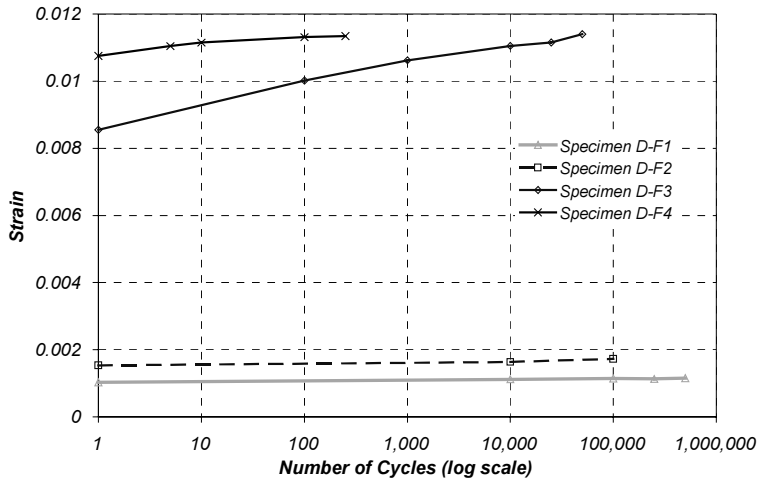

(a) Reinforcing Bar Strains

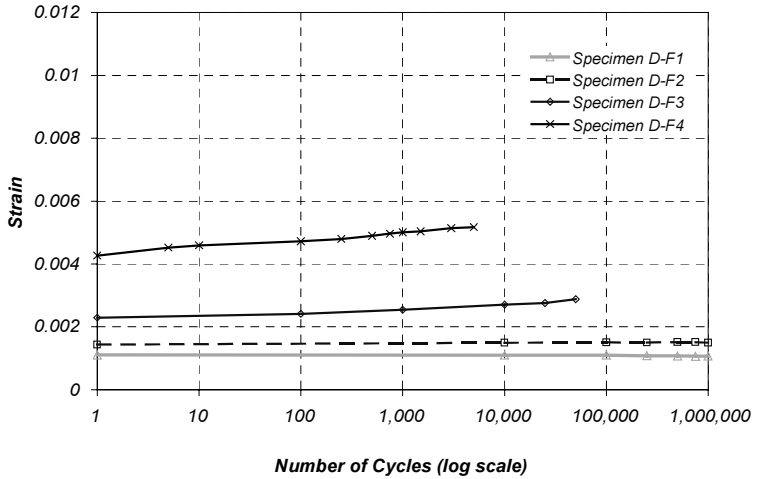

(b) CFRP Strains

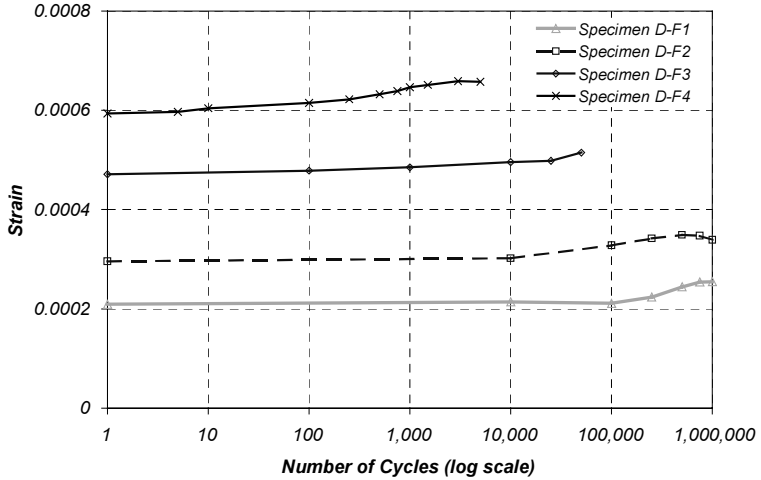

(c) Concrete Strains

Figure 8.25 Variation of Average Measured Strains with Number of Cycles for Specimens Strengthened Using Composite System D (Section 1)

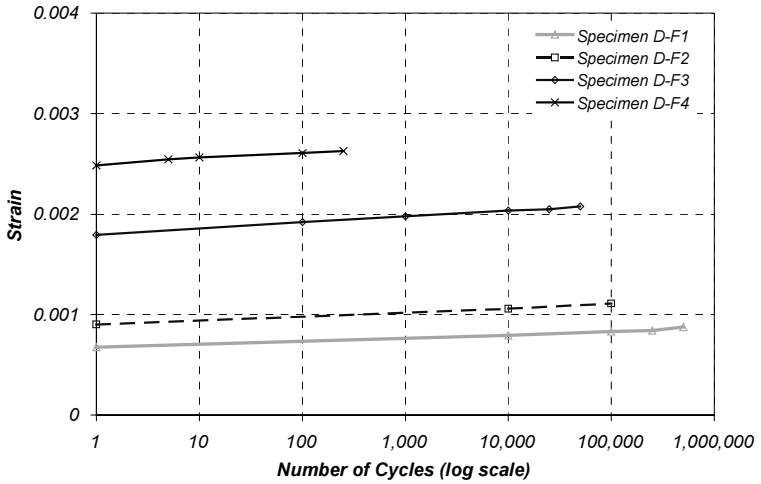

(a) Reinforcing Bar Strains

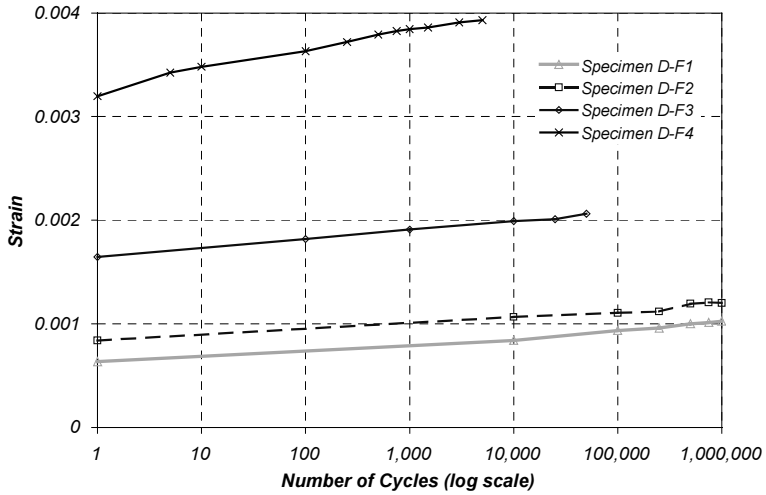

(b) CFRP Strains

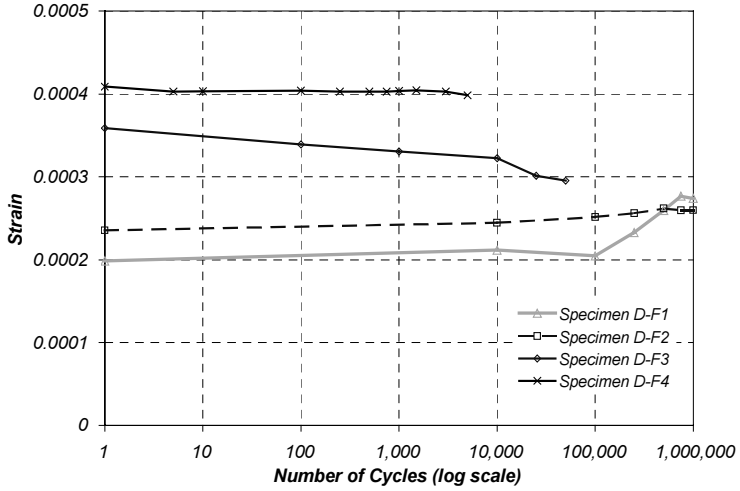

(c) Concrete Strains

Figure 8.26 Variation of Average Measured Strains with Number of Cycles for Specimens Strengthened Using Composite System D (Section 2)

8.5 SUMMARY

The observed and measured response of the specimens subjected to fatigue loads was presented in this chapter. The observed response of the specimens during the fatigue tests was presented in Section 8.2 and the accumulation of damage with cycling was described. The measured load-deflection response of the different groups of specimens was presented in Section 8.3. Finally, the characteristics of the measured strain response of all the specimens was discussed for the two groups of specimens in Section 8.4. The average measured strains at yielding and ultimate of all the specimens and the variation of strains as a function of the number of applied load cycles were summarized in this section.

Chapter 9: Summary and Conclusions

9.1 SUMMARY

The objective of the research project was to investigate the effects of strengthening existing reinforced concrete bridges using composites and to develop reliable design procedures for these systems. Available fiber types were determined at the onset of the work and carbon fiber composites were selected as a result of the initial literature review. The research project was divided into three phases to investigate the behavior of strengthened elements. The first two phases of the research project were discussed in this report.

The first phase of the research project included testing 22 rectangular beam specimens strengthened using different types of CFRP composite systems. The main goal of this part of the research project was to identify strengthening schemes to develop the rupture strength of the composite systems. The beams were tested monotonically to failure. Twenty specimens were tested as soon as the composite systems had cured for a period of seven days. Two specimens were subjected to periodic cycles of moisture for approximately 8 months before loading the beams to failure.

Four different manufacturers provided the composite systems tested in these specimens. Initially, the composites were attached to the tension face of the beams using different bonded lengths. Subsequently, the composites were applied along the entire beam span on the bottom face or sides of the beams. Additionally, vertical straps along the shear span of the specimens were used to delay the onset of debonding of the composite systems from the surface of the concrete.

The predominant failure mode in this series of tests was characterized by debonding of the composite from the surface of the concrete. However, the use of transverse straps along the shear span, and the application of the composite to the side surface of the beams delayed or precluded debonding in some of the specimens. The average measured strain in the composite laminates at the critical section at failure depended on the type of strengthening scheme and composite system. However, the measured values were generally lower than the values published by the manufacturers of the composite systems even for specimens that failed by rupture of the composite laminates.

The second phase of the research project consisted of evaluating the fatigue performance of strengthened specimens using two of the composite strengthening schemes identified from phase 1. Eight specimens were tested under various stress ranges representative of service-load and overload conditions on a bridge. Monotonic tests to failure were conducted on five specimens after they had undergone a repeated loading sequence to a maximum of 1,000,000 cycles. The amplitude of loading during the repeated loading sequence for these specimens generated stresses representative of service load conditions in the reinforcing bars. Three specimens were subjected to loading amplitudes that generated stresses in the reinforcement that were representative of overload conditions.

All the beams that were tested monotonically to failure after the repeated load sequence failed by debonding of the composites from the surface of the concrete. The observed behavior was not substantially different from the companion specimens tested in phase 1. The beams subjected to cyclic overload conditions failed during the fatigue-load cycles. Two of these beams failed by fatigue of the interface between the composite and the surface of the concrete. One specimen failed by fracture of the reinforcing bars during the repeated-load sequence.

The degree of accumulation of damage differed depending on the amplitude of loading. Increases in deflection and loss of initial stiffness observed during cycling resulted in permanent deformations. This phenomenon is consistent with the behavior of reinforced concrete structures subjected to cyclic loads. Therefore, this does not necessarily reflect the influence of the CFRP composite materials bonded for strengthening. Under service-load conditions, no visual evidence of damage propagation at the concrete-composite bond interface was observed. However, for the specimens subjected to cycles representative of overload conditions, debonding propagated as the number of load cycles increased.

9.2 CONCLUSIONS FROM SPECIMENS SUBJECTED TO STATIC LOADS

The results of this phase of the investigation demonstrated that CFRP composites represent a viable means of increasing the flexural strength of reinforced concrete beams. The four different CFRP systems that were investigated in the first two phases performed satisfactorily. The general trends in the behavior of the strengthened specimens were nominally identical regardless of the composite system. Therefore, any of the CFRP composite systems tested in this part of the research project should be considered seriously for strengthening existing reinforced concrete bridges.

On the other hand, the strengthening scheme affected the observed and measured behavior of the specimens substantially. While most of the strengthened beams failed after the CFRP composites debonded from the surface of the concrete, this mode of failure was delayed by using transverse CFRP straps. In addition, placement of the longitudinal CFRP on the sides of the cross section, rather than on the bottom face, reduced the tendency of the CRFP composites to pry off the surface of the concrete at locations where the laminates crossed existing cracks. Therefore, the application of composites to the tension face of beams only should not be used for bridge applications. The addition of straps to arrest the cracks propagating to the end of the beams during debonding is recommended to improve the deformation capacity of the strengthened beams.

The beams that were subjected to periodic moisture for a period of 8 months did not give indications of degradation of the bond between the composites and the surface of the concrete. It should be noted that the composites were protected from the attack of ultraviolet radiation using the protective coating provided by the manufacturer of the composite system [Master Builders, 1998b]. The characteristics of the response of these beams were similar to other specimens tested monotonically to failure. For the limited number of beams subjected to moisture and environmental actions, no detrimental effects were observed on the bond between the composite and the surface of the concrete.

The analytical model developed during this phase of the research was adequate to estimate the global characteristics of the response of the beams. However, the local response was not reproduced accurately because the model did not account for local debonding of the composites from the surface of the concrete. During testing, it was observed that local debonding did not significantly affect the global behavior of the strengthened beams. For this reason, the analytical procedure was considered adequate to calculate the response of strengthened elements. In order to account for the possibility of composite debonding, the analytical procedure was modified slightly to design the large-scale specimens that were tested during the third phase of this research project. A detailed discussion of the modifications that were required is presented in a companion report [Breña et al., 2001].

9.3 CONCLUSIONS FROM SPECIMENS SUBJECTED TO FATIGUE LOADS

Fatigue loading in specimens subjected to cycles representative of service-load conditions did not affect the observed behavior of the strengthened beams during the subsequent monotonic tests to failure. The

capacity of the specimens was apparently not affected by the fatigue loading. However, the deformations of the strengthened beams increased with cycling.

On the other hand, the behavior of specimens subjected to loads representative of overload conditions was affected significantly by load cycling. The capacity of the specimens was controlled by the fatigue performance of the composite-concrete interface or the reinforcing bars. At this load level, damage at the bond interface propagated toward the end of the composite with increasing number of cycles and fatigue failure occurred by sudden debonding of the laminate in two of the specimens. One specimen failed by fracture of the reinforcement indicating that the bond between the surface of the concrete and the composite exceeded the fatigue life of the reinforcement.

None of the specimens tested under fatigue loading at different stress levels failed by rupture of the fibers in the composite laminates. Bond fatigue was only observed in two specimens during fatigue cycling at extremely high stress levels. Therefore, it can be concluded that the fatigue performance of strengthened specimens will be at least equivalent to that of reinforced concrete elements.

9.4 LARGE-SCALE TESTS OF STRENGTHENED BRIDGE COMPONENTS

The last phase of this research project included laboratory tests of selected strengthening schemes on full-scale bridge components. The results of the first two phases of the research project, presented in this research report, were used to design and detail the strengthening schemes for the large-scale tests of bridge components. Details of phase 3 are discussed in detail in a companion research report [Breña et al., 2001].

References

American Association of State Highway and Transportation Officials (AASHTO 1994), *Manual for Condition Evaluation of Bridges*, Washington, D.C., 1994.

American Association of State Highway and Transportation Officials (AASHTO 1996), *Standard Specifications for Highway Bridges*, 16th Edition, Washington, D.C., 1996.

American Concrete Institute (ACI 318-99), *Building Code Requirements for Structural Concrete (318-99) and Commentary (318R-99)*, Farmington Hills, Michigan, 1999.

American Society of Civil Engineers (1984), *Structural Plastics Design Manual*, ASCE Manuals and Reports on Engineering Practice No. 63, New York, 1984.

American Society of Mechanical Engineers (1992), *Reinforced Thermoset Plastic Corrosion Resistant Equipment,* ASME RTP-1, New York, 1992.

American Society of Mechanical Engineers (1998), *Fiber-Reinforced Plastic Pressure Vessels,* Reported by ASME Boiler and Pressure Vessel Committee, New York, 1998.

American Society for Testing and Materials (1996), *Standard Test Method for Compressive Properties of Rigid Plastics,* Annual Book of ASTM Standards, Vol. 08.01, Designation: D 695-96, 1996.

American Society for Testing and Materials (2000a), *Standard Test Method for Tensile Properties of Plastics, Annual Book of* ASTM Standards, Vol. 08.01, Designation: D 638-99, 2000.

American Society for Testing and Materials (2000b), *Standard Test Methods for Flexural Properties of Unreinforced and Reinforced Plastics and Electrical Insulating Materials,* Annual Book of ASTM Standards, Vol. 08.01, Designation: D 790-99, 2000.

Arduini, M., Di Tommaso, A., and Nanni, A. (1997), "Brittle Failure in FRP Plate and Sheet Bonded Beams," *ACI Structural Journal*, Vol. 94, No. 4, July-August 1997.

Arduini, M. and Nanni, A. (1997), "Parametric Study of Beams with Externally Bonded FRP Reinforcement," *ACI Structural Journal*, Vol. 94, No. 5, September-October 1997.

Barnes, R. A. and Mayes, G. C. (1999), "Fatigue Performance of Concrete Beams Strengthened with CFRP Plates," *Journal of Composites for Construction*, Vol. 3, No. 2, May 1999, pp. 63-72.

Benouaich, M.A. (2000), *Fatigue Loading of Reinforced Concrete Members Strengthened Using Carbon Fiber Reinforced Polymer Composites,* Thesis presented to the Department of Civil Engineering in partial fulfillment of the requirements for the Diploma of Civil Engineer, Swiss Federal Institute of Technology at Lausanne, March 2000.

Bizindavyi, L. and Neale, K.W. (1999), "Transfer Lengths and Bond Strengths for Composites Bonded to Concrete," *Journal of Composites for Construction*, Vol. 3, No. 4, November 1999, pp. 153-160.

Blaschko, M., Niedermeier, R., and Zilch, K. (1998), "Bond Failure Modes of Flexural Members Strengthened with FRP," *Second International Conference for Composites in Infrastructure*, Vol. 1, Ehsani and Saadatmanesh, Editors, Tucson, AZ, 1998.

Bramblett, R. M. (2000), *Strengthening of Reinforced Concrete Beams Using Carbon Fiber Reinforced Polymer Composites*, Thesis presented to the Graduate School in partial fulfillment of the requirements for the degree of Master of Science in Engineering, The University of Texas at Austin, August 2000.

Breña, S. F., Wood, S. L., and Kreger, M. E., (2001), "Increasing the Flexural Capacity of Typical Reinforced Concrete Bridges in Texas Using Carbon Fiber Reinforced Polymer Composites."

Brosens, K. and VanGemert, D. (1997), "Anchoring Stresses between Concrete and Carbon Fibre Reinforced Laminates," *International Conference: Composite Construction – Conventional and Innovative*, Innsbruck, 1997, pp. 181-186.

Chajes, M.J., Finch, W.W., Januszka, T.F., and Thomson, T.A., "Bond and Force Transfer of Composite Material Plates Bonded to Concrete," *ACI Structural Journal*, Vol. 93, No. 2, March-April 1996, pp. 208-217.

David, E., Djelal, C., and Buyle-Bodin, F. (1997), "Repair and Strengthening of Reinforced Concrete Beams using Composite Materials," *Proceedings of the Seventh International Conference on Structural Faults and Repair*, Vol. 2, Engineering Technics Press, University of Edinburgh, Scotland, 1997, pp. 169-173.

Deuring, M. (1993), *Post-strengthening of Concrete Structures with Pretensioned Advanced Composites*, Research Report No. 224, EMPA Duebendorf, Duebendorf, Switzerland.

Ferguson, P.M., *Reinforced Concrete Fundamentals*, 3rd Ed., John Wiley & Sons, 1958.

Federal Highway Administration (1997), *FHWA Study for Advanced Composites in Bridges in Europe and Japan*, United States Department of Transportation, December 1997.

Federal Highway Administration (1999), *Strategic Goals for Deficient Bridges*, Memorandum http://www.fhwa.dot.gov/bridge/defbrid.htm, July 1999.

Fyfe, Co. LLC (1997), *Comparative Properties of Composite Material Systems*, December 1997.

GangaRao, H.V.S. and Vijay, P.V. (1998), "Bending Behavior of Concrete Beams Wrapped with Carbon Fabric," *Journal of Structural Engineering*, Vol. 124, No. 1, January 1998, pp. 3-10.

Garden, H.N. and Hollaway, L.C. (1998), "An Experimental Study on the Influence of Plate End Anchorage of Carbon Fibre Composite Plates Used to Strengthen Reinforced Concrete Beams," *Composite Structures*, Vol. 42, No. 2, June 1998, pp. 175-188.

Grace, N.F., Sayed, G.A., Soliman, A.K., and Saleh, K.R. (1999), "Strengthening Reinforced Concrete Beams Using Fiber Reinforced Polymer (FRP) Laminates," *ACI Structural Journal*, Vol. 96, No. 5, September-October 1999, pp. 865-874.

He, J.H., Pilakoutas, K., and Waldron, P. (1997), "CFRP Plate Strengthening of RC Beams," *Proceedings of the Seventh International Conference on Structural Faults and Repair*, Vol. 2, Engineering Technics Press, University of Edinburgh, Scotland, 1997, pp. 119-127.

Hognestad, E. (1950), *An Experimental Study of Combined Bending and Axial Load in Reinforced Concrete Members*, University of Illinois, Engineering Experiment Station, October 1950.

Hognestad, E., Hanson, N.W., and McHenry D. (1955), "Concrete Stress Distribution in Ultimate Strength Design," *Journal of the American Concrete Institute*, Vol. 27, No. 4, December 1955, pp. 455-479.

Hollaway, L.C. and Leeming, M.B., Editors (1999), *Strengthening of Reinforced Concrete Structures Using Externally-Bonded FRP Composites in Structural and Civil Engineering*, CRC Press LLC, 1999.

Iketani, J. and Jinno, Y. (1997), "Adhesive Properties of a Carbon Fiber Blanket on to the Concrete Surfaces," *Proceedings of the 42nd International SAMPE Symposium*, May 1997, pp. 109-116.

Kaiser, H.P. (1989), *Strengthening of Reinforced Concrete with Epoxy-Bonded Carbon-Fiber Plastics (In German),* Doctoral Thesis, Diss. ETH No. 8918, ETH Zurich, Switzerland, 1989.

Mallick, P.K. (1993), *Fiber-Reinforced Composites: Materials, Manufacturing and Design*, 2nd Ed., Marcel Dekker, Inc., 1993.

Master Builders, Inc. (1998a), *MBrace™ Composite Strengthening System-Engineering Design Guidelines,* Cleveland, OH, 1998.

Master Builders, Inc. (1998b), *MBrace™ Composite Strengthening System – Data Sheet*, Cleveland, OH, 1998.

Master Builders, Inc. (1999), *MBrace™ Topcoat – Data Sheet*, Cleveland, OH, 1999.

Meier, U., Deuring, M., Meier, H., and Schwegler, G. (1992), "Strengthening of Structures with CFRP Laminates: Research and Applications in Switzerland", *Advanced Composite Materials in Bridges and Structures*, Canadian Society for Civil Engineering, 1992.

Meier, U. and Winistörfer, A. (1995), "Retrofitting of Structures through External Bonding of CFRP Sheets," *Non-metallic (FRP) Reinforcement for Concrete Structures*, Ed. L. Taerwe, 1995, pp. 465-472.

Mitsubishi Chemical Corp. (1999), *Technical Manual for REPLARK™ System,* Japan, January 1999.

Nakamura, M., Sakai, H., Yagi, K., and Tanaka T., (1996), "Experimental Studies on the Flexural Reinforcement Effect of Carbon Fiber Sheet Bonded to Reinforced Concrete Beam," *1st International Conference on Composites in Infrastructure*, Tuczon, Arizona, 1996, pp. 760-773.

Norris, T., Saadatmanesh, H., and Ehsani, M.R. (1997), "Shear and Flexural Strengthening of R/C Beams with Carbon Fiber Sheets," *Journal of Structural Engineering*, Vol. 123, No. 7, July 1997, pp. 903-911.

Ritchie, P.A., Thomas, D.A., Lu, L., and Connelly G.M. (1991), "External Reinforcement of Concrete Beams using Fiber Reinforced Plastics," *ACI Structural Journal*, Vol. 88, No. 4, July-August 1991, pp. 490-500.

Ross, C.A., Jerome D.M., Tedesco, J.W., and Hughes, M.L. (1999), "Strengthening of Reinforced Concrete Beams with Externally Bonded Composite Laminates," *ACI Structural Journal*, Vol. 96, No. 2, March-April 1999, pp. 212-220.

Saadatmanesh, H. and Ehsani, M.R. (1991), "RC Beams Strengthened with GFRP Plates. I: Experimental Study," *Journal of Structural Engineering*, Vol. 117, No. 4, November 1991, pp. 3417-3433.

Shahawy, M.A. and Beitelman, T. (1996), "Flexural Behavior of Reinforced Concrete Beams Strengthened with Advanced Composite Materials," *41st International SAMPE Symposium*, 1996, pp. 1015-1025.

Shahawy, M.A. and Beitelman, T. (1999), "Static and Fatigue Performance of RC Beams Strengthened with CFRP Laminates," *Journal of Composites for Construction*, Vol. 125, No. 6, 1999, pp. 613-621.

Shijie, W. and Ruixian, Z. (1993), "Study of Fiber Composite Plates for Strengthening Reinforced Bridges," *Proceedings, 9th International Conference on Composite Materials*, Madrid, Spain, 1993.

Sika Corporation (1997), *Engineering Guidelines for the Use of CarboDur® (CFRP) Laminates for Structural Engineering,* Lyndhurst, NJ, 1997.

Sika Corporation (1999), *Sika Carbodur®– Structural Strengthening Systems*, Lyndhurst, NJ, 1999.

Spadea, G., Bencardino, F., and Swamy, R.N. (1998), "Structural Behavior of Composite RC Beams with Externally Bonded CFRP," *Journal of Composites for Construction*, Vol. 2, No. 3, August 1998, pp. 132-137.

Texas Department of Transportation (TxDOT 1999), Bridge Inventory, Inspection, and Appraisal Program (BRINSAP) Load Rating Spreadsheet, 1999.

Appendix A: Measured Material Properties

This appendix contains information on the material properties for the specimens tested under static and repeated loading. The appendix is divided into three sections. Concrete material properties are summarized in Section A.1, reinforcing steel properties are summarized in Section A.2, and CFRP properties are summarized in Section A.3. Concrete cylinders and steel coupons were tested as part of this research program to determine the material properties. Material properties reported by the manufacturers are summarized for the composite material systems.

A.1 CONCRETE

Concrete cylinders (6 in. diameter by 12 in. in height) were fabricated using standard ASTM procedures as specified in ASTM C-40 [ASTM, 1996]. The concrete cylinders were extracted from their molds at the time the rectangular beams were removed from the forms to subject the concrete to similar conditions. The concrete cylinders were cured under ambient conditions in the laboratory next to the beams. Three concrete batches were required to fabricate all the rectangular beam specimens subjected to static loads, and one concrete batch was required to fabricate the specimens tested for the repeated-load testing program. All the concrete batches used the same mix design and were supplied by a local ready-mix plant. Two or three cylinders were tested in compression 3, 7, 14, and 28 days after casting to evaluate the change in strength with time for the concrete used in each batch. Due to the limited number of cylinders for each batch, compression tests were conducted after testing the first and last beams within a group, while split cylinder tests were conducted after testing the last beam of each group.

A.1.1 Beam Specimens Tested under Static Loading

Twenty rectangular beam specimens were fabricated using three different concrete batches. Batches 1 and 2 were used to fabricate eight, 8-in. by 14-in. and eight, 8-in. by 16-in. beam specimens. Four, 8-in. by 14-in. specimens and two, 8-in. by 16-in. specimens were fabricated with concrete batch 3. Two of the 8 by 14-in. beams from batch 3 were tested after 8 months of exposure to periods of moist and dry conditions. The batch number corresponding to each of the beam specimens tested under static loading was summarized in Table 3.1.

Concrete compressive strength versus time curves for batches 1, 2, and 3 are shown in Figure A.1, Figure A.2, and Figure A.3, respectively. The figures show the points when the first and last beam specimens were tested within each group. The concrete age at the time of testing the beam specimens varied for each of the concrete batches. However, very little variation of concrete strength was experienced at ages beyond 28 days, so the average compressive strength measured after the last beam specimen was tested in each group was used in all calculations.

Stress-strain curves for concrete were measured for the concrete from batch 3 (Figure A.4). The curves were determined at ages of 70 and 306 days. The 70-day test corresponds to the last beam tested in this beam group, while the 306-day test corresponds to the last beam test conducted after environmental exposure. Cylinder strains were measured using a compressometer with an 8-in. gage length. The cylinders were tested under force control using a 600-kip Forney testing machine at an average loading rate of 800 lb/sec.

The concrete model [Hognestad, 1950] used to calculate internal compressive stresses for all specimens is superimposed to the cylinder test data in Figure A.4. The stress-strain parameters used in the material model for batch 3 are reported in Table A.1. These values were obtained from the concrete cylinder tests after testing the last beam in the group.

Split-cylinder tests were also conducted for the concrete from batches 1 and 2. The results are summarized in Table A.2.

A.1.2 Beam Specimens Tested under Repeated Loading

Eight rectangular beams were fabricated for the repeated-load testing series using concrete from a single batch. Four, 8-in. by 14-in. beams and four, 8-in. by 16-in. beams were fabricated using batch 4. The 28-day compressive strength of the concrete from batch 4 was significantly higher than the strength developed by the batches used for the static tests, even though the same concrete mix was used. This can be attributed to different ambient conditions at the time of casting.

The concrete compressive strength versus time curve for batch 4 is shown in Figure A.5. The age of testing the first and last specimens in this group is also indicated in the figure. The concrete strength showed a small variation beyond the 28-day compressive strength, except for the test conducted at 104 days. This variation can be attributed to experimental error rather than increase in concrete strength due to the limited number of tests conducted at each age. Therefore, the compressive strength of concrete at 142 days was used in all calculations.

Stress-strain curves for concrete were measured for the concrete from batch 4 (Figure A.6). The curves were determined at an age of 69 days. The curve corresponding to the material model for this concrete batch is superimposed on the test data in Figure A.6. The parameters used for the concrete model are listed in Table A.1.

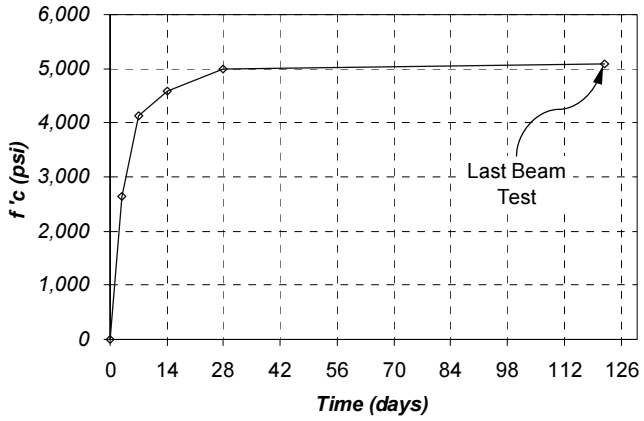

Figure A.1 Variation of Concrete Compressive Strength with Time for Batch 1

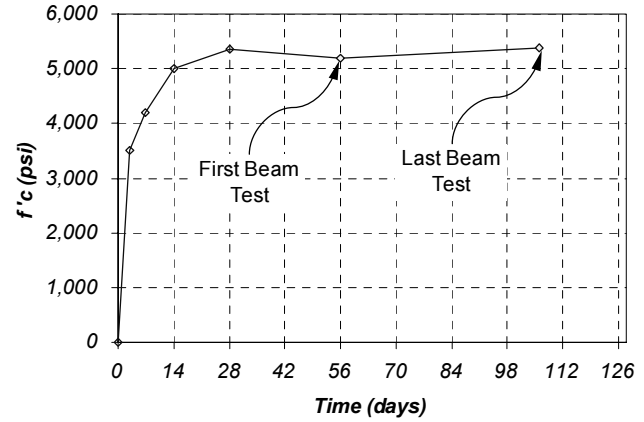

Figure A.2 Variation of Concrete Compressive Strength with Time for Batch 2

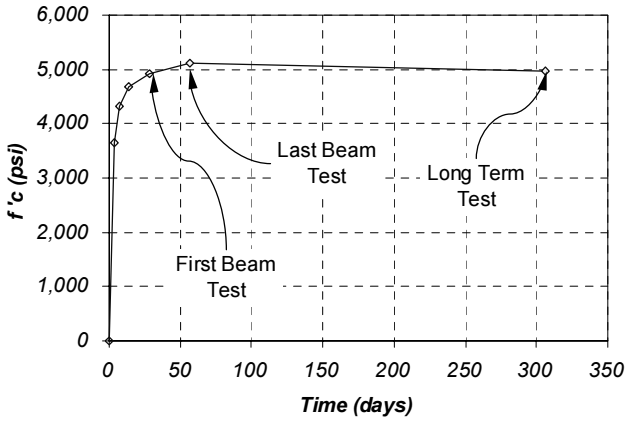

Figure A.3 Variation of Concrete Compressive Strength with Time for Batch 3

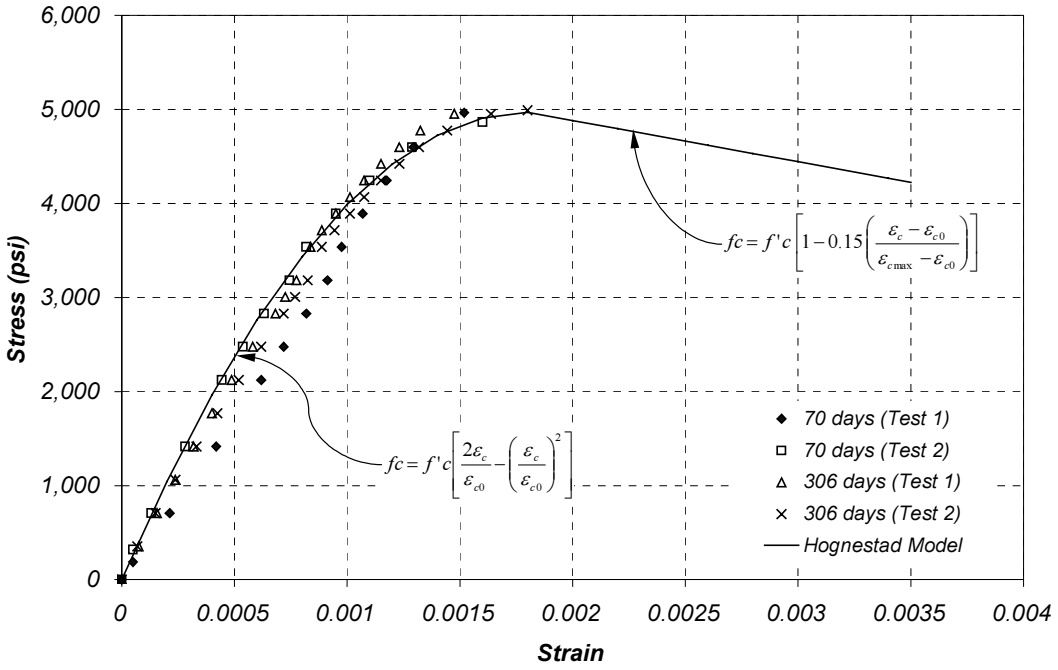

Figure A.4 Concrete Stress-Strain Curve for Batch 3

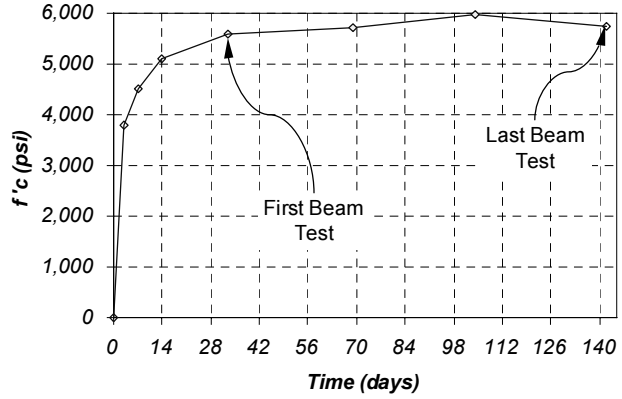

Figure A.5 Variation of Concrete Compressive Strength with Time for Batch 4 (Repeated Load Tests)

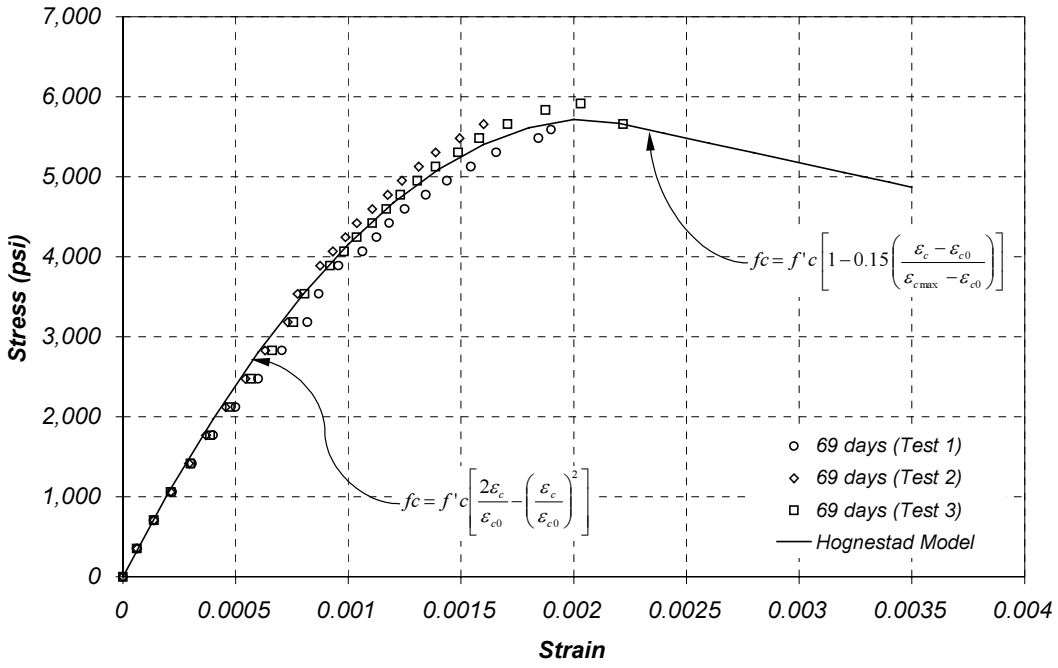

Figure A.6 Concrete Stress-Strain Curve for Batch 4 (Repeated Load Tests)

Table A.1 Concrete Compression Tests and Parameters Used for Material Models

Concrete Batch	Age, days	Compressive Strength, psi			Avg. f'_c, psi	Std. Dev., psi	ε_{co}
		Test 1	Test 2	Test 3			
1	122	5,170	5,010	-	5,090	114	-
2	106	5,620	5,160	-	5,390	320	-
3	306	4,950	4,990	-	4,970	26	0.0018
4	142	5,570	5,730	5,900	5,730	168	0.0021

Table A.2 Tensile Strength of Concrete Determined from Split Cylinder Tests

Concrete Batch	Age, days	Tensile Strength, psi			Average f_t, psi	Standard Dev., psi
		Test 1	Test 2	Test 3		
1	122	450	465	450	455	10
2	106	450	370	480	430	59

A.2 REINFORCING STEEL

The results of the reinforcing bar tests are presented in this section. Tension tests were performed to determine the yield stress and strength of the reinforcing bars used to fabricate the specimens. Stress-strain curves were determined for the bottom longitudinal bars because these were the only bars expected to yield during the tests. The specimens were fabricated using reinforcing bars from three different heats. Specimens cast using concrete batches 1 and 2 used bars from heat 1, whereas specimens cast using batch 3 used reinforcing steel from heat 2. The specimens in the repeated-load testing program used reinforcing bars from heat 3.

Bar elongation was measured using a clip-on extensometer with an 8-in. gage length. The bars were tested in a 120-kip Tinius Olsen testing machine at a strain rate of 0.00125/min. The extensometer was removed from the bars at a strain of approximately 0.04 to avoid damage.

Two different sizes of reinforcing bars were used to fabricate the specimens. The longitudinal reinforcement consisted of deformed #5 bars for the bottom bars and #3 bars for the top bars. Stirrups were fabricated using No. 6 gage smooth wire. Figure A.7 shows stress-strain curves for the longitudinal reinforcement used in the beams tested under static loads (steel heats 1 and 2). Figure A.8 shows the stress-strain relationship for the #5 bars used in the beams for the repeated load testing program. As observed in these figures, all the bars exhibited a well-defined yield point. Therefore, a tri-linear model was used to model the stress-strain behavior of the reinforcing bars in the calculations.

Table A.3 summarizes measured yield stress and tensile strength for the reinforcing bars. Table A.5 lists the parameters required to define the material model used to calculate the response of the beams.

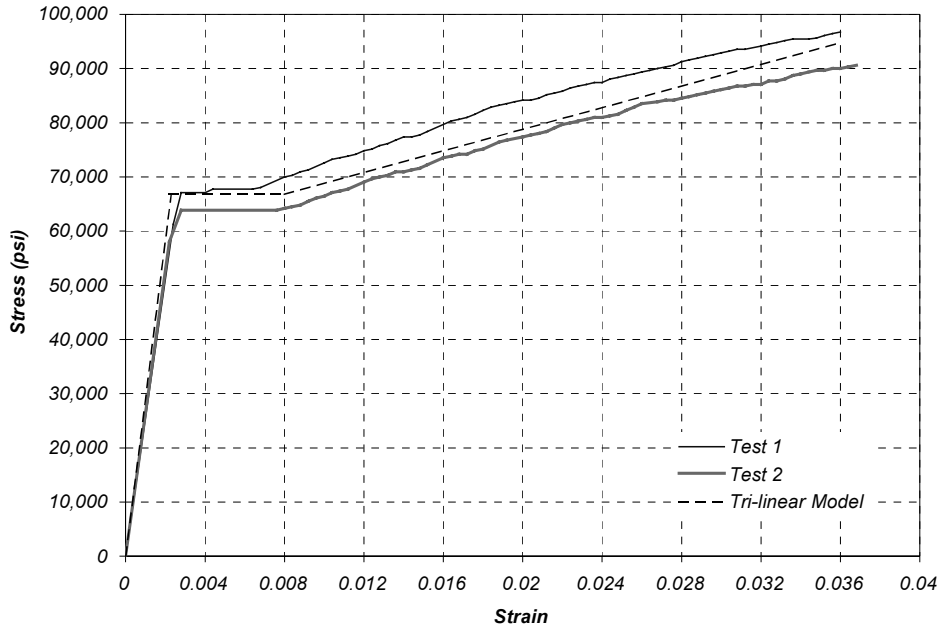

a) Heat 1 - #5 Reinforcing Bars

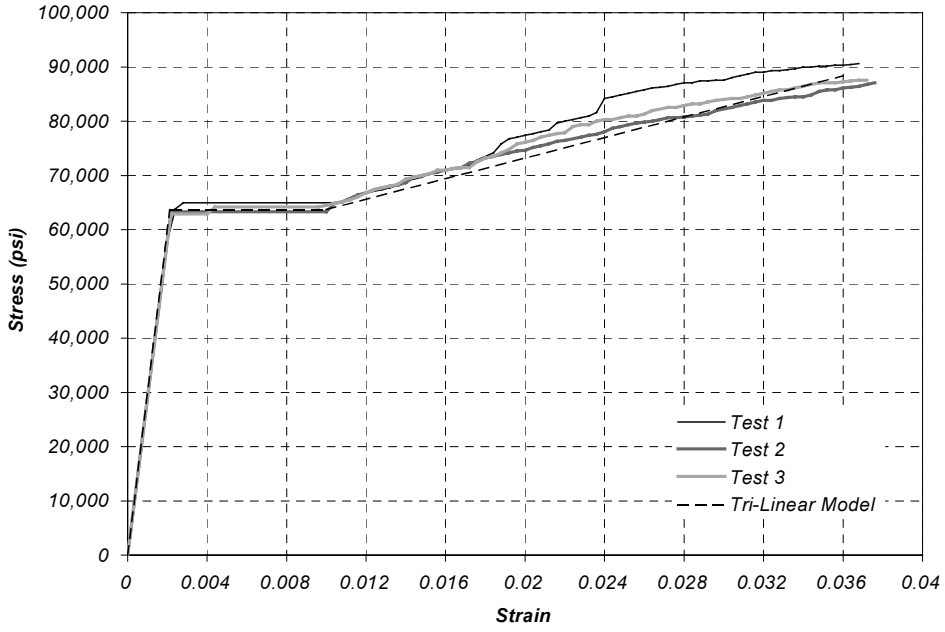

b) Heat 2 - #5 Reinforcing Bars

Figure A.7 Stress-Strain Curves for #5 Bars in Beams Tested Under Static Load

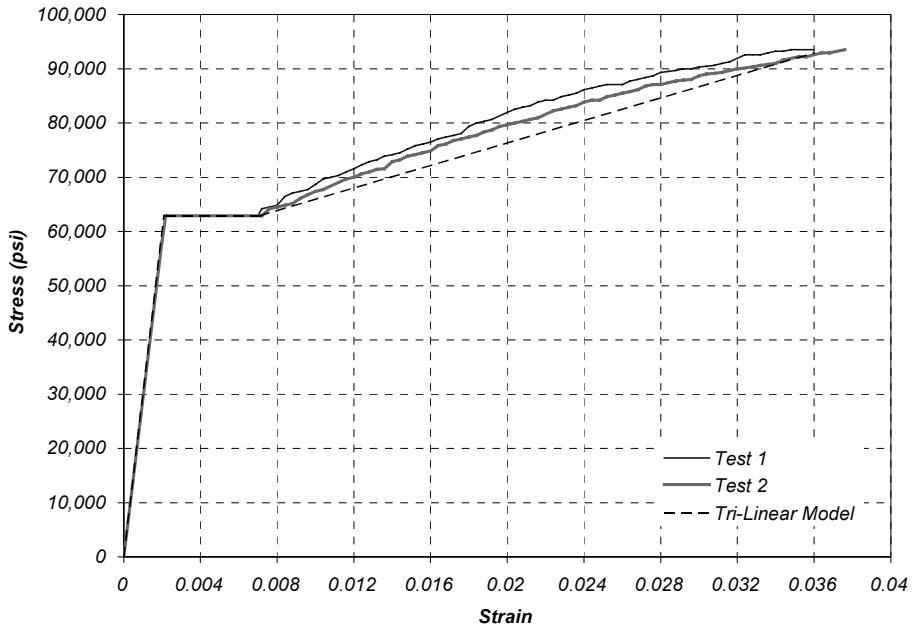

Figure A.8 Stress-Strain Curves for #5 Bars in Beams Tested Under Repeated Load

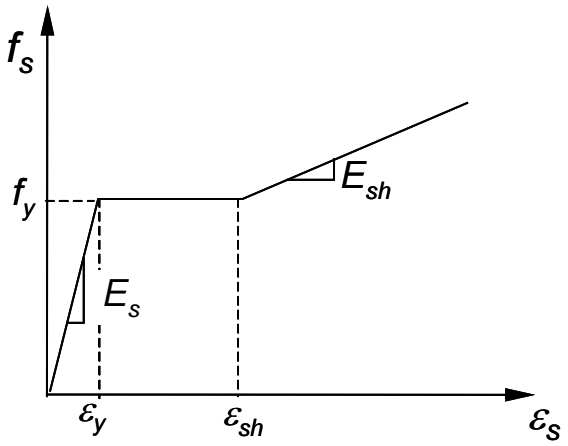

Figure A.9 Parameters in Tri-Linear Material Model for Reinforcing Bars

Table A.3 Measured Yield Stress and Tensile Strength of Reinforcing Bars

Bar No.	f_y, ksi				$f_{y\ avg}$, ksi	Std Dev, ksi	f_u, ksi				$f_{u\ avg}$, ksi	Std Dev, ksi
	Test 1	Test 2	Test 3	Test 4			Test 1	Test 2	Test 3	Test 4		
Heat 1												
#5	62.9	62.3	63.9*	67.7*	63.8	1.8	100.3	98.7	101.3	105.2	101.4	2.7
#3	60.0	62.0	66.5	66.2	63.7	3.2	88.0	92.7	96.5	95.6	93.2	3.8
Heat 2												
#5	63.2	65.0*	63.3*	62.9*	63.6	0.9	97.4	99.4	97.7	97.7	98.1	0.9
#3	69.6	70.9	-	-	70.3	0.9	112.0	113.5	-	-	112.7	1.0
Heat 3												
#5	62.9*	62.9*	-	-	62.9	0.0	104.5	104.8	-	-	104.7	0.2
#3	61.8	61.8	-	-	61.8	0.0	100.0	100.9	-		100.5	0.6
Smooth Wire (Stirrups)												
Gage 6	84.8	88.9	85.9	-	86.5	2.1	90.3	91.7	92.1	-	91.4	0.9

* Indicates tests where the stress-strain curves were obtained.

Table A.4 Parameters Used to Model the Stress-Strain Relationship for the #5 Reinforcing Bars

Heat No.	f_y, ksi	ε_y	ε_{sh}	E, ksi	E_{sh}, ksi
1	66.8	0.0022	0.0090	29,000	1,000
2	63.7	0.0021	0.0100	29,000	950
3	62.9	0.0021	0.0071	29,000	1,040

A.3 CFRP SYSTEMS

Properties for the CFRP systems were not determined in the laboratory. However, it is recommended that the CFRP systems be tested in future laboratory experiments. Coupons can be removed from the strengthened specimens after failure to determine the actual properties of the complete CFRP/epoxy system.

The values that were used in calculations are listed in Table A.7 and are the values reported by each of the manufacturers. The systems used in this research project are proprietary, so only the mechanical properties of the composites were available. For the composites formed using unidirectional carbon fibers, the manufacturer publishes the stress-strain parameters based on the dimensions of the fibers only and not on the thickness of the formed composite (see bottom row in Table A.7). This is the reason that the thickness of this system is smaller than the thicknesses of the other two types of composites listed in the table.

The mechanical properties for the resins used to impregnate and bond two of the composite systems to the surface of the concrete are listed in Tables A.5 through A.7. These data were obtained from the available information about the proprietary systems indicated in each table.

Table A.5 Properties of CFRP Composite Systems Published by Manufacturers [Fyfe, 1997; Master Builders, 1998; Mitsubishi, 1999; Sika, 1997]

System*	Composite Type	Manufacturer	t_p, in.	f_{pu}, ksi	E_p, ksi	ε_{max} (rupture)
D	Pultruded	Sika, Corp. (Sika® Carbodur®)	0.047	348	22,500	0.015
D	Woven Fabric	Sika/Hexcel (SikaWrap® Hex 103 C)	0.040	139	10,600	0.013
C	Woven Fabric	Fyfe, Co. (Tyfo® SCH-41)	0.041	110	9,000	0.012
A	Unidirectional Fiber	Master Builders (Mbrace™ CF 130)	0.0065**	505	33,000	0.015
B	Unidirectional Fiber	Mitsubishi Chemical (Replark™ 30)	0.0066**	493	33,400	0.015

* The system identification refers to the nomenclature used throughout this report.
** Thickness used for design calculations. Actual thickness after fabrication ranged from 0.03 to 0.06 in. per ply.

Table A.6 Mechanical Properties of Resin (Mbrace™ Saturant) used for Mbrace™ System [Master Builders, 1998]

Property	Tension[1]	Flexure[2]	Compression[3]
Maximum Stress (psi)	8,000	20,000	12,500
Stress at Yield (psi)	7,800	20,000	12,500
Stress at Rupture (psi)	7,900	18,000	-
Strain at Maximum Stress	0.030	0.042	0.050
Strain at Yield	0.025	0.038	0.050
Strain at Rupture	0.035	0.050	-
Elastic Modulus (ksi)	440	540	380
Poisson's Ratio	0.40	-	-

Notes: Properties determined at 72° F and 40% relative humidity after curing for 7 days.
[1]ASTM D-638 [ASTM, 2000a]
[2]ASTM D-790 [ASTM, 2000b]
[3]ASTM D-695 [ASTM, 1996]

Table A.7 Mechanical Properties of Epoxy Paste (SikaDur® 30) Used to Bond Pultruded Plates [Sika, 1997]

Property	Tension[1]	Flexure[2]	Compression[3]
Maximum Stress (psi)	3,600	6,800	8,600
Strain at Maximum Stress	0.010	-	-
Elastic Modulus (ksi)	650	1,700	390

Notes: Properties determined at 73° F and 50% relative humidity after curing for 7 days.
[1]ASTM D-638 [ASTM, 2000a]
[2]ASTM D-790 [ASTM, 2000b]
[3]ASTM D-695 [ASTM, 1996]

Table A.8 Mechanical Properties of Impregnating Resin (SikaDur® Hex 300/306) for SikaWrap® Hex 103 C Woven Fabric [Sika, 1999]

Property	Tension[1]	Flexure[2]
Maximum Stress (psi)	10,500	17,900
Strain at Maximum Stress	0.048	-
Elastic Modulus (ksi)	459	452

Notes: Properties determined at 73° F and 50% relative humidity after curing for 7 days.
[1]ASTM D-638 [ASTM, 2000a]
[2]ASTM D-790 [ASTM, 2000b]
[3]ASTM D-695 [ASTM, 1996]

Appendix B: Crack Patterns

B.1 SPECIMENS SUBJECTED TO STATIC LOADS

Observed crack patterns in each of the specimens subjected to static loads are presented in this section. The crack widths indicated in the figures correspond to loads immediately before failure of the specimens.

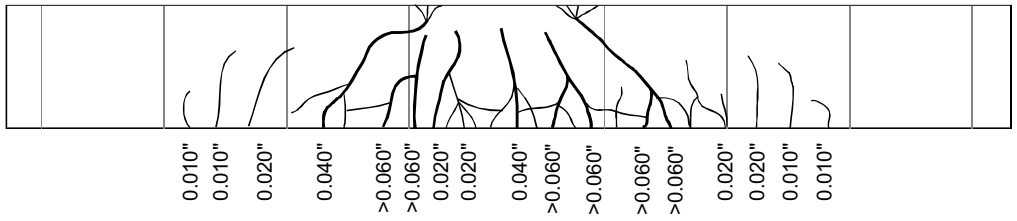

Control A & B

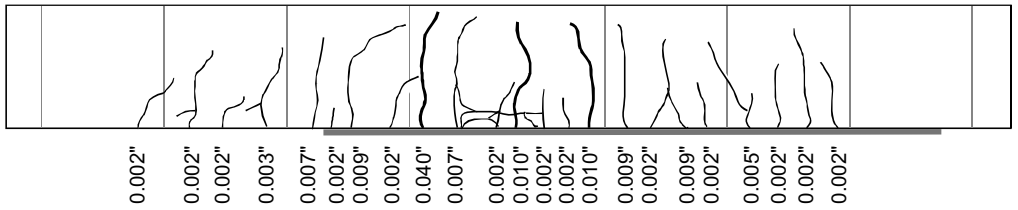

A1

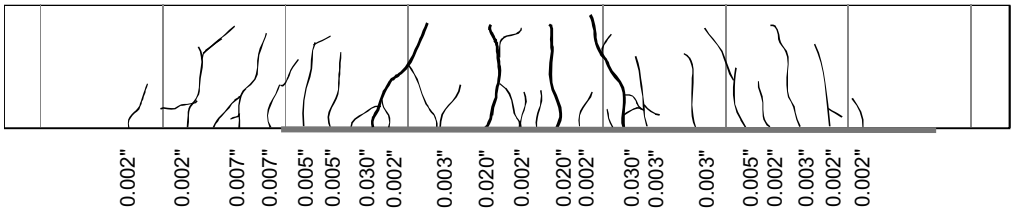

A2

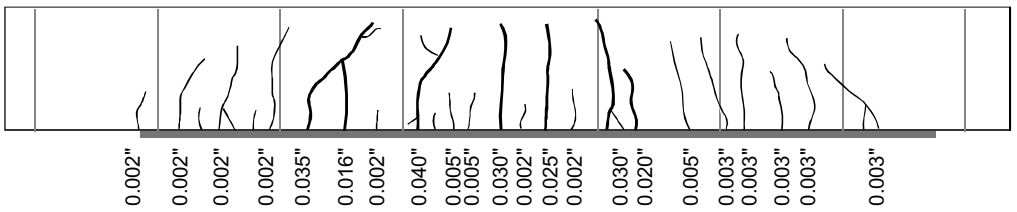

A3

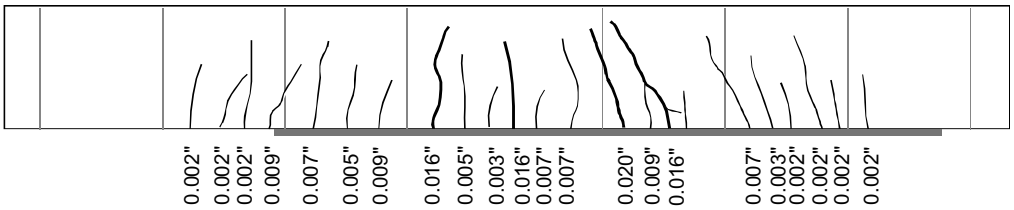
0.002"
0.002"
0.002"
0.009"
0.007"
0.005"
0.009"
0.016"
0.005"
0.003"
0.016"
0.007"
0.007"
0.020"
0.009"
0.016"
0.007"
0.003"
0.002"
0.002"
0.002"
0.002"

A4

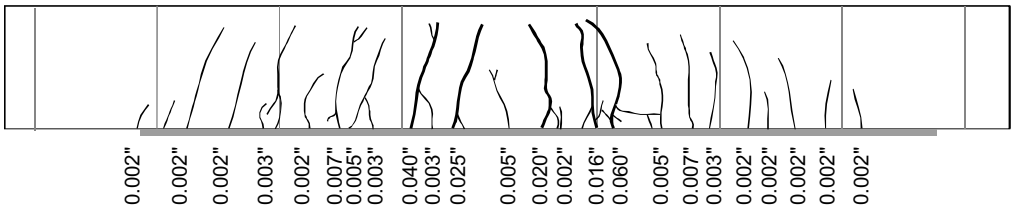
0.002"
0.002"
0.002"
0.003"
0.002"
0.007"
0.005"
0.003"
0.040"
0.003"
0.025"
0.005"
0.020"
0.002"
0.016"
0.060"
0.005"
0.007"
0.003"
0.002"
0.002"
0.002"
0.002"
0.002"

B1

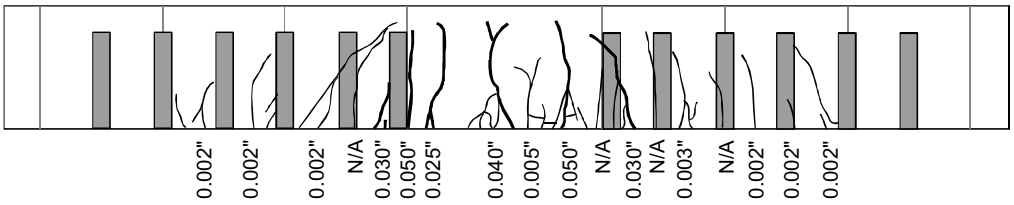
0.002"
0.002"
0.002"
N/A
0.030"
0.050"
0.025"
0.040"
0.005"
0.050"
N/A
0.030"
N/A
0.003"
N/A
0.002"
0.002"
0.002"

B2

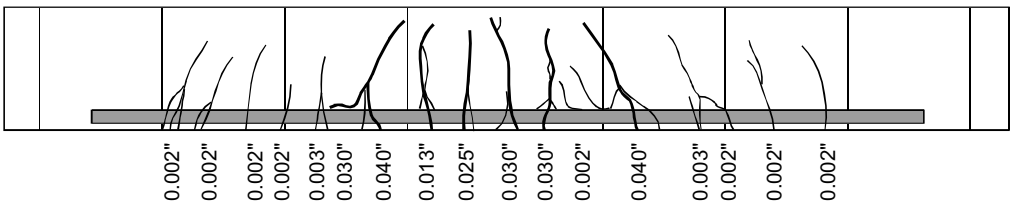
0.002"
0.002"
0.002"
0.002"
0.003"
0.030"
0.040"
0.013"
0.025"
0.030"
0.030"
0.002"
0.040"
0.003"
0.002"
0.002"
0.002"

B3

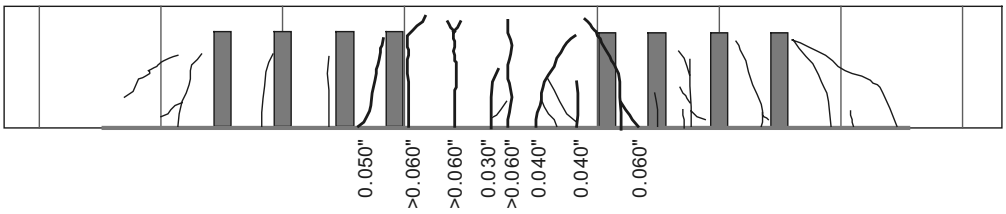

B4

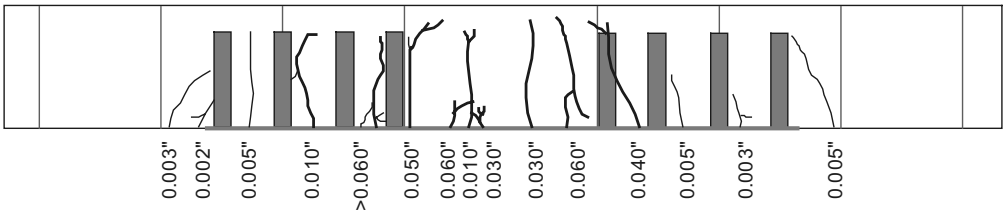

B5

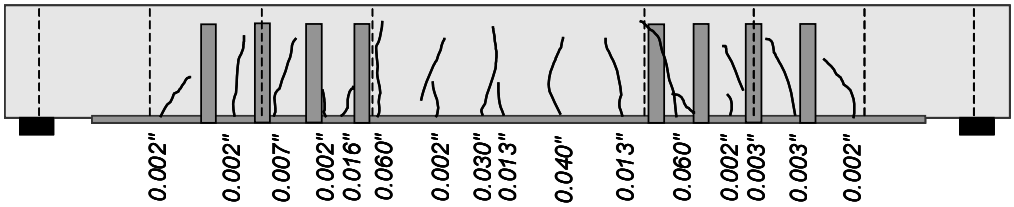

A-LT1

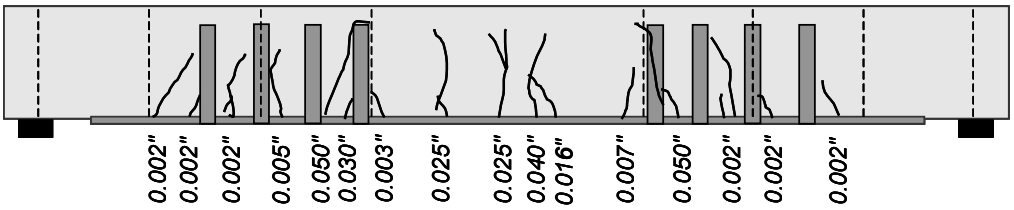

A-LT2

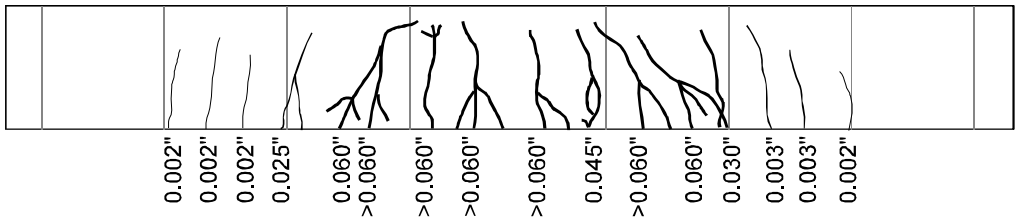

Control C & D

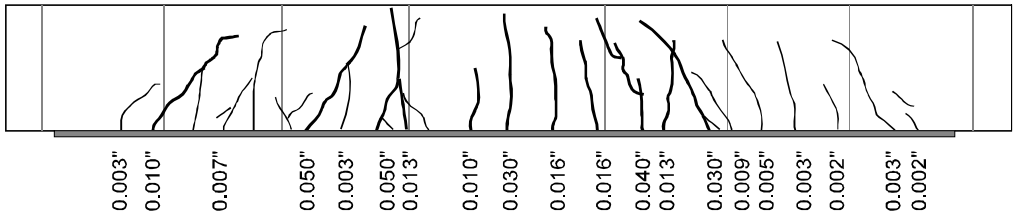

C1

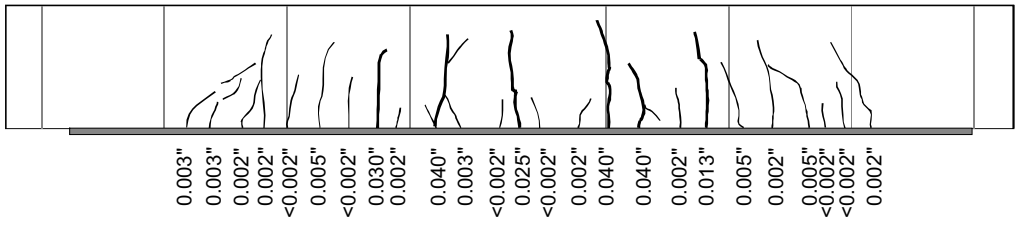

C2

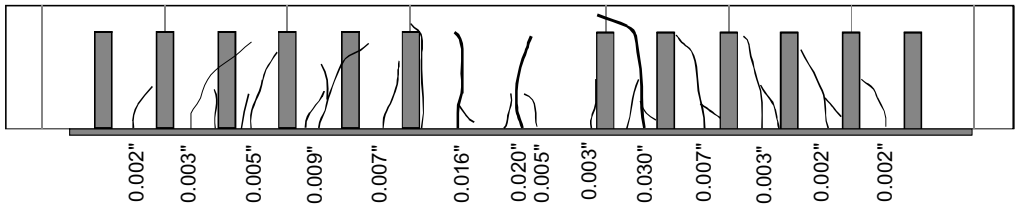

C3

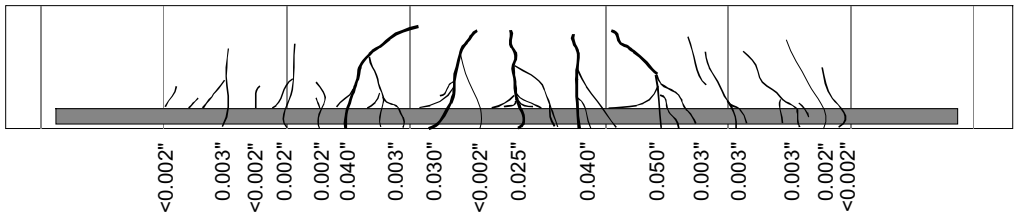

C4

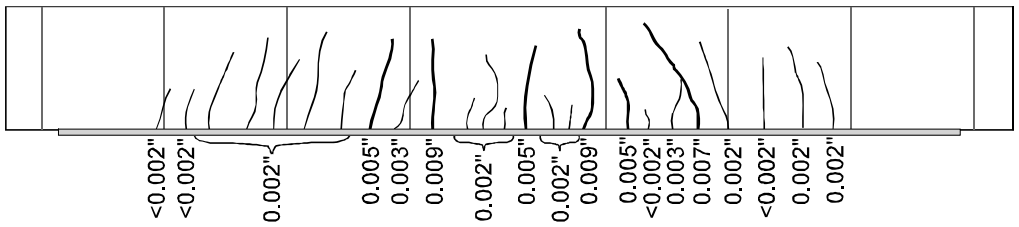

D1

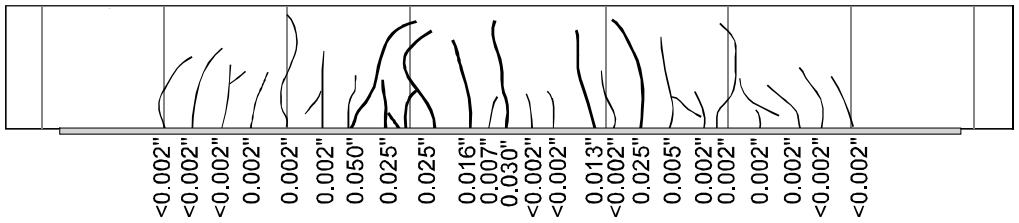

D2

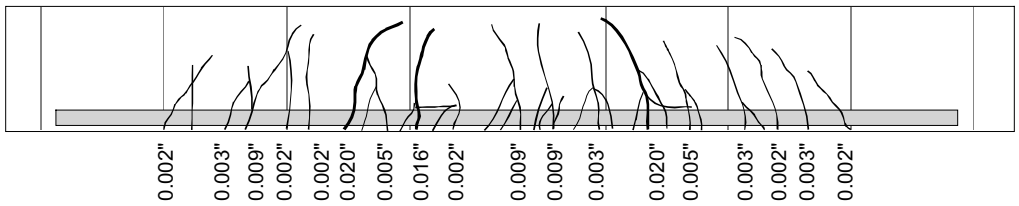

D3

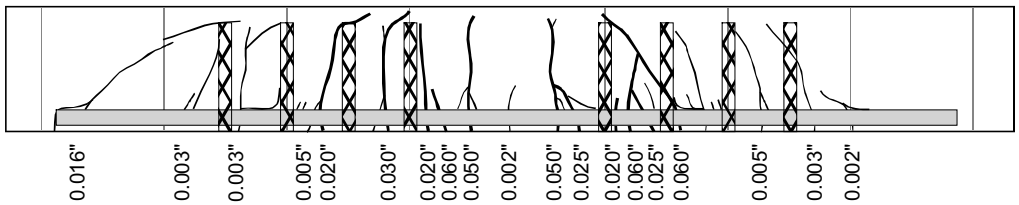

D4

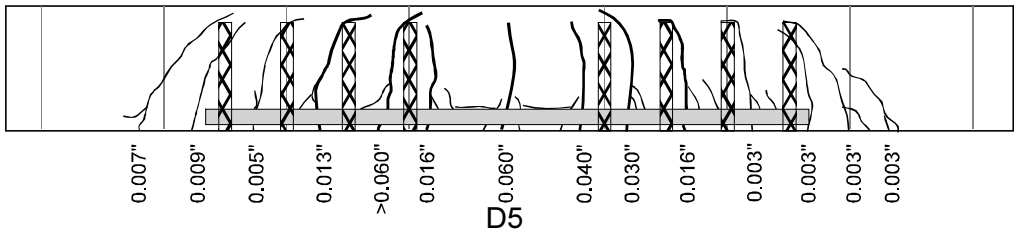

D5

B.2 SPECIMENS SUBJECTED TO FATIGUE LOADS

Crack patterns in each of the specimens subjected to fatigue loads are presented in this section. The figures indicate the extent of cracking after several numbers of cycles of fatigue loading. For the specimens subjected to load amplitudes representative of service load conditions, the crack widths were measured only at yield (specimens A-F1 through A-F3, and specimens D-F1 through D-F2). Crack widths were measured at several load cycles for the specimens subjected to loads representing overload conditions on a bridge (specimens A-F4, D-F3, and D-F4).

(a) After 1 Cycle

(b) After 10,000 Cycles

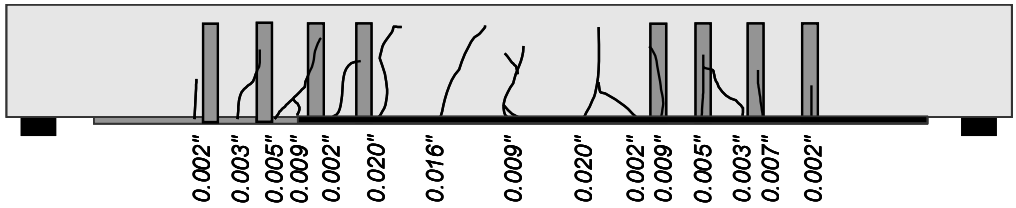

(c) At Yield During Static-Load Test

CFRP Debonding

** Crack width not measured*

Specimen A-F1

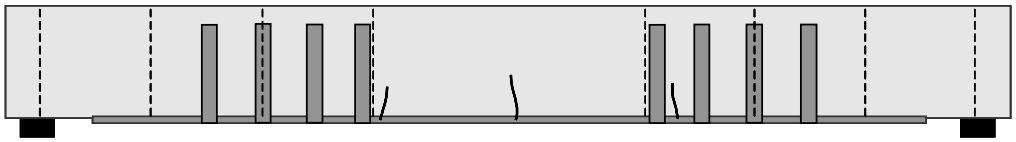

(a) After 1 Cycle

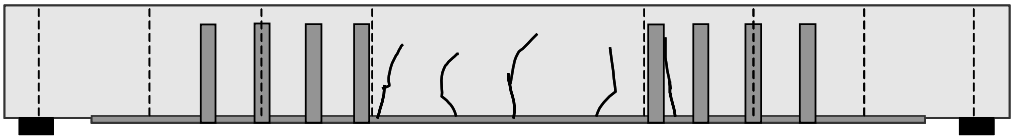

(b) After 1,000,000 Cycles

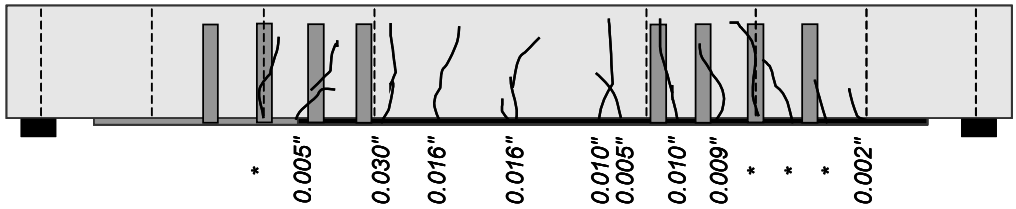

(c) At Yield During Static-Load Test

CFRP Debonding

** Crack width not measured*

Specimen A-F2

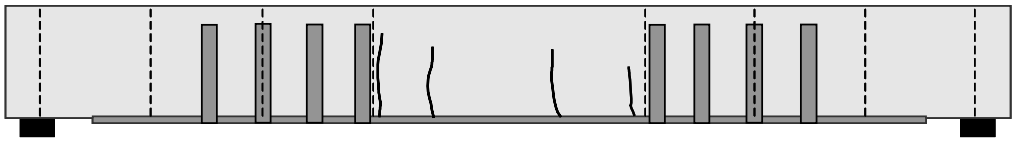

(a) After 1 Cycle

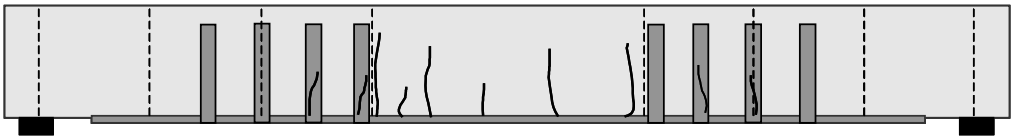

(b) After 1,000,000 Cycles

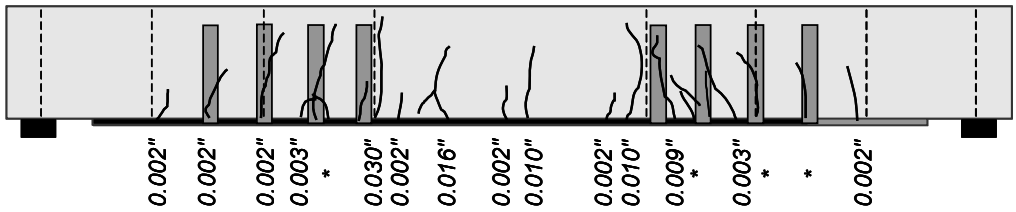

(c) At Yield During Static-Load Test

CFRP Debonding

** Crack width not measured*

Specimen A-F3

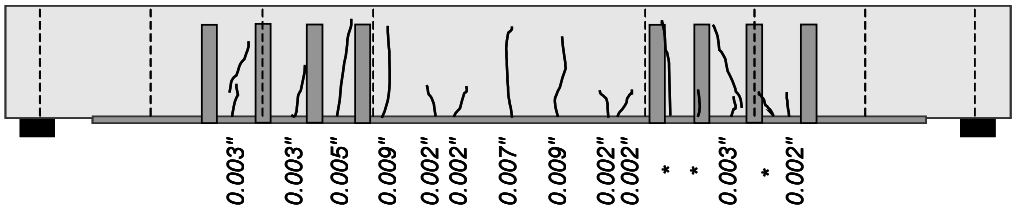

(a) After 1 Cycle

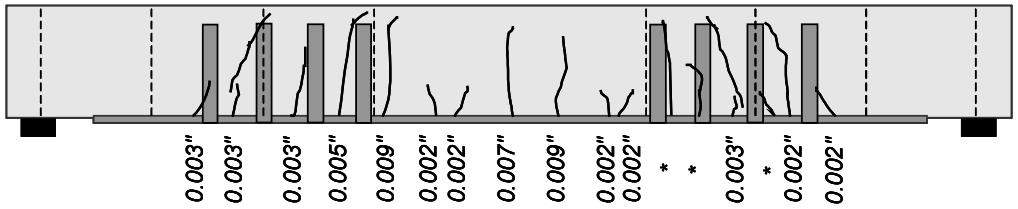

(b) After 10,000 Cycles

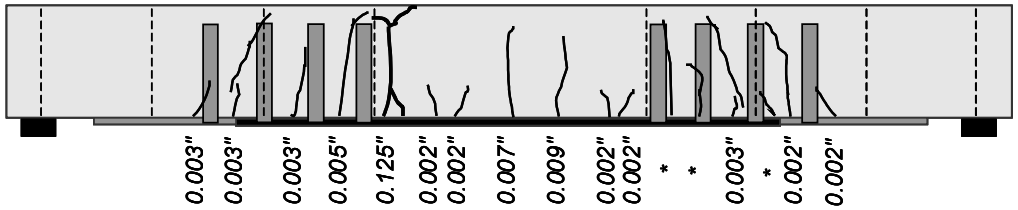

(c) After 155,490 Cycles (Failure)

CFRP Debonding

** Crack width not measured*

Specimen A-F4

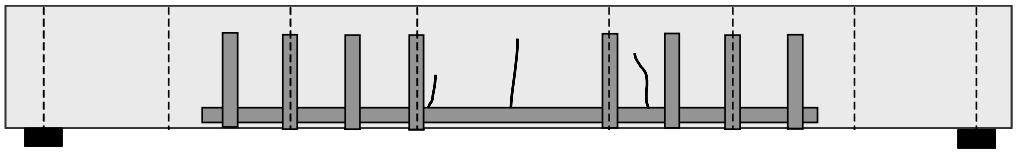

(a) After 1 Cycle

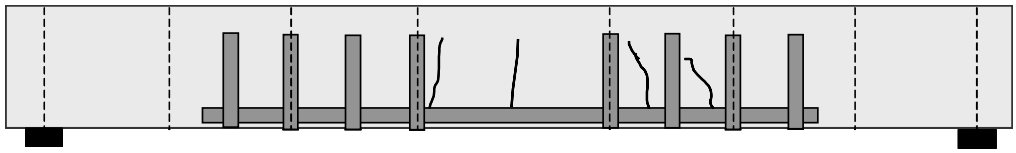

(b) After 1,000,000 Cycles

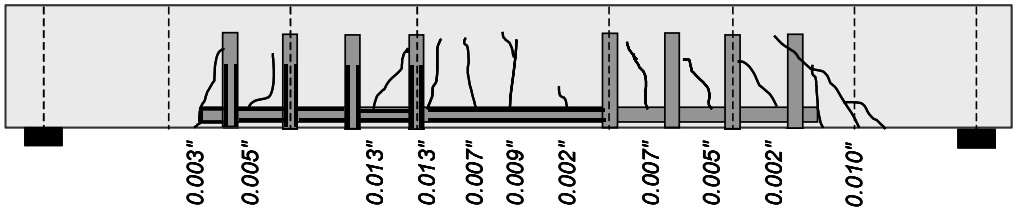

(c) At Yield During Static-Load Test

— *CFRP Debonding*

Specimen D-F1

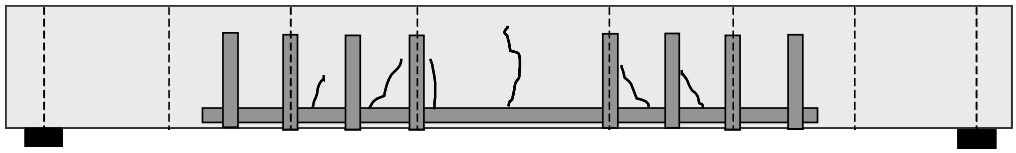

(a) After 1 Cycle

(b) After 1,000,000 Cycles

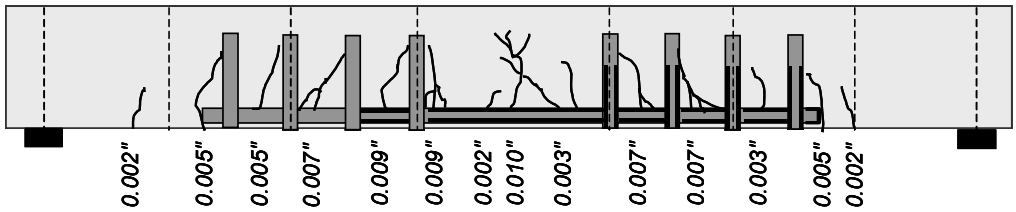

(c) At Yield During Static-Load Test

— *CFRP Debonding*

Specimen D-F2

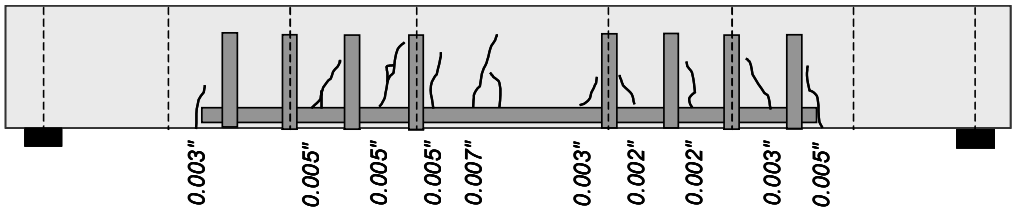

(a) After 1 Cycle

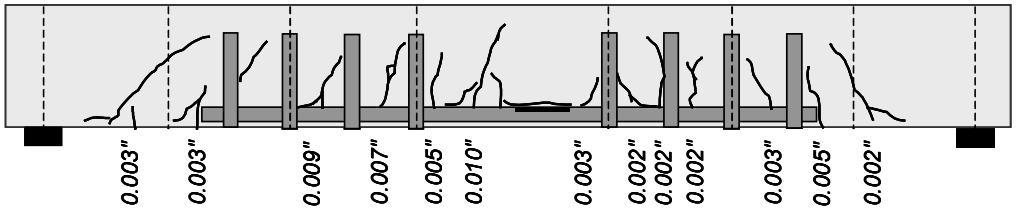

(b) After 1,000 Cycles

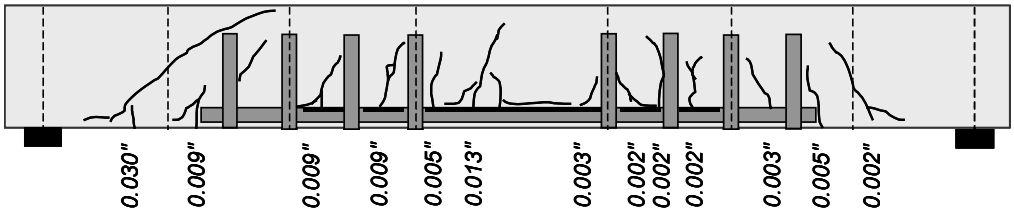

(c) After 50,000 Cycles

CFRP Debonding

Specimen D-F3

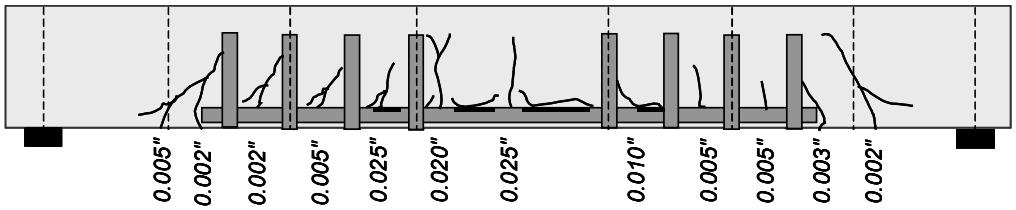

(a) After 1 Cycle

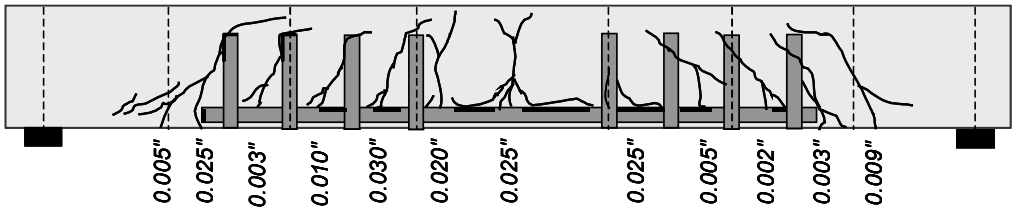

(b) After 3,000 Cycles

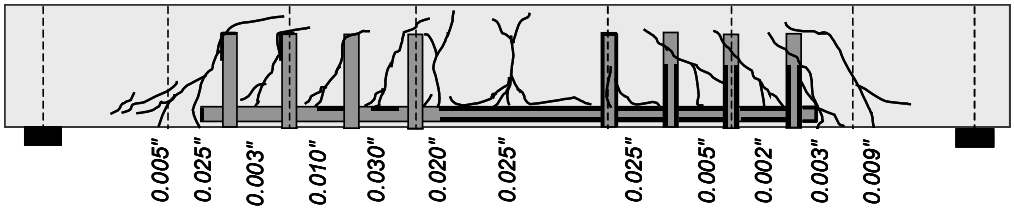

(c) After 8,990 (Failure)

CFRP Debonding

Specimen D-F4

Appendix C: Application of CFRP Composite Systems to Existing Reinforced Concrete Elements

C.1 INTRODUCTION

Four different manufacturers donated CFRP materials for use during this research project. However, the systems can be organized based on the procedures that are used to apply them into two groups: wet-layup systems and pultruded systems. These systems differ primarily in the method that is used for fabrication of the CFRP materials and also on the procedure that is used to bond the materials to the concrete surface. A description of the procedures that were used to attach these systems to the laboratory specimens is presented in this appendix. These procedures were based on the recommendations provided by the manufacturers of the composite systems.

C.2 PULTRUDED CFRP SYSTEM

C.2.1 Description of Composite System

The CFRP pultruded system used in this research project consisted of plates that were fabricated using the putrusion process. In this process, continuous carbon fiber roving is impregnated in a resin bath and pulled through a forming die at an elevated temperature. The carbon fibers were oriented along the longitudinal axis of the plate (unidirectional carbon fibers). The resin bath is usually mixed with a curing agent so that curing initiates simultaneously as the fibers are pulled through the die. The temperature, pulling speed, and length of the die are controlled to ensure that the resin fully cures before the fiber-reinforced element exits the die [Mallick, 1993]. The member is cooled with air or water after exiting the forming die. The elements are then cut to the required length using a diamond saw at the end of the pultrusion line (Figure C.1).

A limitation of this fabrication process is that only elements that have a constant cross section can be manufactured economically. An advantage of using this procedure is that the elements are fabricated in a controlled environment and excellent quality control is achieved. Also, large volume contents of fibers can be used in the composites fabricated using this procedure.

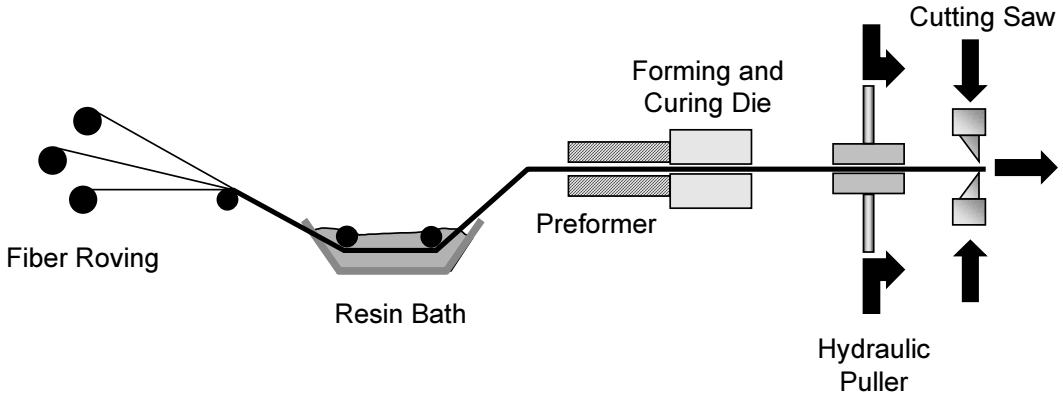

Figure C.1 Schematic Representation of the Fabrication of a Fiber Reinforced Polymer Plate using the Pultrusion Process [Mallick, 1993]

C.2.2 Application to Reinforced Concrete Element

The application of the pultruded CFRP system that was used to strengthen the reinforced concrete laboratory specimens can be summarized in the following steps and is illustrated in Figure C.2:

a) Preparation of concrete surface and CFRP plate

- Prepare concrete surface by grinding or light sandblasting to expose aggregates.
- Remove loose concrete particles generated during surface preparation using pressurized air.
- Clean concrete surface and CFRP pultruded plates with acetone until a white cloth remains white after wiping.

b) CFRP system application

- Mix epoxy paste and hardener for three minutes at approximately 400 to 600 RPM. The mixing proportions should follow the values recommended by the manufacturer.
- Apply a thin layer (approximately 1/16-in.) of mixed epoxy paste to the concrete surface, covering the area where the pultruded plates will be installed.
- Apply a layer of epoxy paste to the clean CFRP plate. The epoxy paste should have a triangular section after application on the plate
- Place CFRP plate on concrete surface and apply hand pressure to force epoxy paste out from beneath the plate.
- Clean excess epoxy from sides of plates.

A woven carbon fiber sheet was used to fabricate straps to wrap the CFRP pultruded plates at discrete locations and avoid premature debonding of the pultruded plates. These straps were applied using the procedures described for the CFRP wet-layup system in Section C.3. The procedure is illustrated in Figure C.3.

The thickness of the pultruded plates system was approximately 1/8 in. after placement on the concrete surface. Therefore, to place the woven fabric straps and avoid having a sharp bend at the plate boundary, epoxy paste was built up to form a ramp. The woven fabric straps were placed on the reinforced concrete element after the epoxy paste that formed the ramps had hardened.

a) Surface grinding

b) CFRP plate cleaning

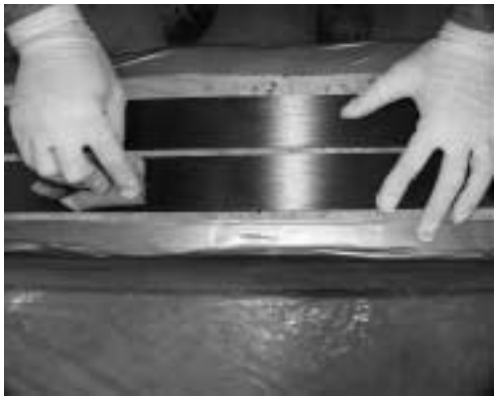

c) Mixing epoxy paste

d) Applying epoxy to surface

e) Positioning CFRP plate on beam

f) Strengthened beam

Figure C.2 Application of CFRP Pultruded Plates to Reinforced Concrete Beam

a) Cutting woven CFRP mat

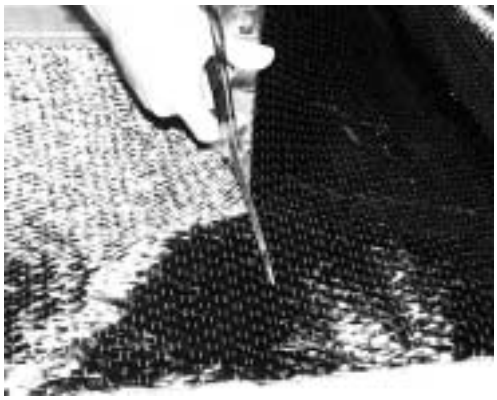

c) Placing woven straps around beam

b) Applying epoxy on concrete surface

d) Final configuration of beam

e) Final configuration of full-scale joist after strengthening

Figure C.3 Application of Woven Straps Around CFRP Pultruded Plates

C.3 WET-LAYUP CFRP SYSTEMS

C.3.1 Description of Composite Systems

The CFRP composite systems that were used in this research project consisted of dry unidirectional carbon fiber sheets that were impregnated with an epoxy resin to form the composite in the laboratory. The fabrication process is termed "wet-layup process" because the carbon fiber sheets are impregnated sequentially as they are positioned on the concrete element.

The main disadvantage of this composite system is caused by the large variability introduced by the manufacturing process. Because the epoxy resin that forms the matrix of the composite is applied manually, significant variations in the composite thickness can result. For the composites that were used in this study, the actual composite thickness ranged from 0.04 to 0.06-in. per carbon fiber ply. Recognizing this inherent variability, the manufacturer of this system suggests using the carbon fiber thickness for design calculations because the uniaxial tensile stress behavior is controlled by the carbon fibers.

C.3.2 Application to Reinforced Concrete Element

The procedure that was used in this research project to apply this CFRP composite system is summarized below. These steps were followed according to recommendations from the manufacturer of the system (Figure C.4):

a) Preparation of concrete surface

- Remove loose concrete particles from surface using a grinding tool. Remove dust generated during grinding using compressed air.
- Fill concrete voids with epoxy putty.

b) CFRP system application

- Apply epoxy primer to seal the concrete surface. Wait until primer reaches a tack-free condition before applying epoxy on the concrete surface.
- Mix two-component epoxy resin using the mixing ratio specified by the manufacturer. Mix using a power drill at a low speed (approximately 400 RPM) using an epoxy paddle.
- Apply a coat of mixed epoxy resin on the concrete surface. This layer will partially impregnate the carbon fibers after they are placed on the concrete element.
- Cut carbon fiber sheets to the required width and length.
- Place carbon fiber sheets on concrete surface over area that was previously coated with epoxy resin. Placement should begin on one end of the concrete element and continue toward the other end.

- Remove backing paper and use a ribbed roller to remove air bubbles that are trapped behind the carbon fiber sheet. Let carbon fibers impregnate in the epoxy resin for approximately 30 minutes.

- Apply a coat of epoxy resin on top of the carbon fibers to enhance impregnation and to form the composite matrix.

- Apply subsequent layers (plies) of carbon fiber sheets and epoxy coat, if required by design, following the procedure described above.

a) Unidirectional carbon fiber sheet

b) Cutting carbon fiber sheets

c) Applying epoxy to surface

d) Placing carbon fiber sheet on joist

e) Eliminating air bubbles from sheets

f) Coating sheets with epoxy

Figure C.4 Application of CFRP Wet-Layup System to Reinforced Concrete Element

Appendix D: Measured Strains

The measured strains from all test specimens are presented in this appendix. The strain gages were bonded to the reinforcing bars, CFRP composites and concrete surface. The concrete strain gages were placed on the sides of the beams for all the specimens except specimens A-LT1 and A-LT2. In these specimens, the concrete gages were placed on the top surface of the beams. Characteristics of the strain gages are listed in Table D.1.

Table D.1 Characteristics of Strain Gages

Material	Strain Gage Type	Nominal Resistance, Ohms	Gage Length, mm	Gage Factor
Steel	Foil	119.5±0.5	6	2.12±1%
CFRP	Foil	119.5±0.5	6	2.12±1%
Concrete	Wire	120±0.5	60	2.09±1%

The specimens had either one or two instrumented sections along the span as indicated in Table D.2. Strain gages were placed on the two bottom longitudinal reinforcing bars (#5), on the surface of the CFRP composite laminates and on the surface of the concrete at each instrumented section. One of the top #3 reinforcing bars was also instrumented for beams in groups I and II. Regardless of the strengthening scheme, each individual composite laminate was instrumented using one gage at each section. Concrete strain gages were placed on both sides of all beams approximately 1.5 in. from the top surface, except for specimens A-LT1 and A-LT2 where the concrete strain gages were positioned on the top surface of the beams. The locations of the instrumented sections for the 8-in. by 14-in. beams and the 8-in. by 16-in. beams are shown in Figures D.1 and D.2, respectively. The position of the strain gages in each of the materials at each instrumented section is indicated in the corresponding strain plots.

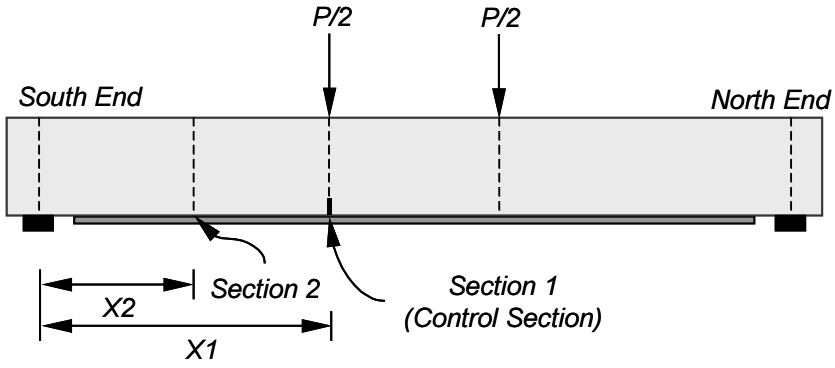

Figure D.1 Position of Instrumented Sections for 8-in. by 14-in. Beams

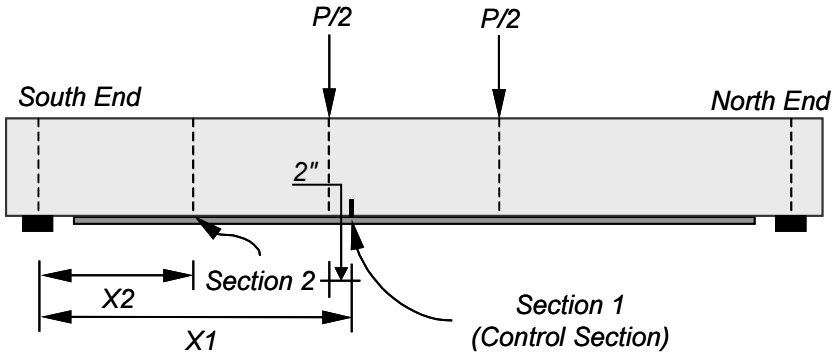

Figure D.2 Position of Instrumented Sections for 8-in. by 16-in . Beams

Table D.2 Position of Instrumented Sections for Rectangular Beam Specimens

Specimen	X1, in.	X2, in.	CFRP Bonded Length, in.
Specimens Subjected to Static Loads			
Control A and B	42	Not Instrumented	-
A1			10
A2			14
A3			30
A4			15
B1			35
B2			35
B3			35
B4		26	35
B5		30	24
Control C and D	50	Not Instrumented	-
C1			45
C2			45
C3			45
C4			45
D1			45
D2			45
D3			45
D4		26	45
D5		38	30
Specimens Exposed to Moisture			
A-LT1	42	30	35
A-LT2			35
Specimens Subjected to Fatigue Loads			
A-F1	42	26	35
A-F2			35
A-F3			35
A-F4			35
D-F1	50	38	30
D-F2			30
D-F3			30
D-F4			30

The individual strain gage readings and the average readings are presented in this appendix. The average strain gage readings were used in all calculations. Only the outputs from the instruments as were recorded during the tests without any modification are presented in this appendix. In some cases, instruments either malfunctioned or debonded during the tests. Instrument malfunction is indicated in the individual strain plots.

The strains measured in the specimens that were tested monotonically to failure are presented in Figures D.3 to D.30. Figures D.3 to D.14 show load vs. strain plots for the instrumented sections in specimen groups A and B. Figures D.15 to D.26 show load vs. strain plots of the instrumented sections in beam groups C and D. Figures D.27 to D.30 show load vs. strain plots for the beams exposed to moisture cycles (specimens A-LT1 and A-LT2).

The strains measured in the specimens subjected to fatigue loads are presented in Figures D.31 to D.46. The load vs. strain plots for specimens A-F1 to A-F4 are presented in Figures D.31 to D.38. Finally, load vs. strain plots for specimens D-F1 to D-F4 are presented in Figures D.39 to D.46.

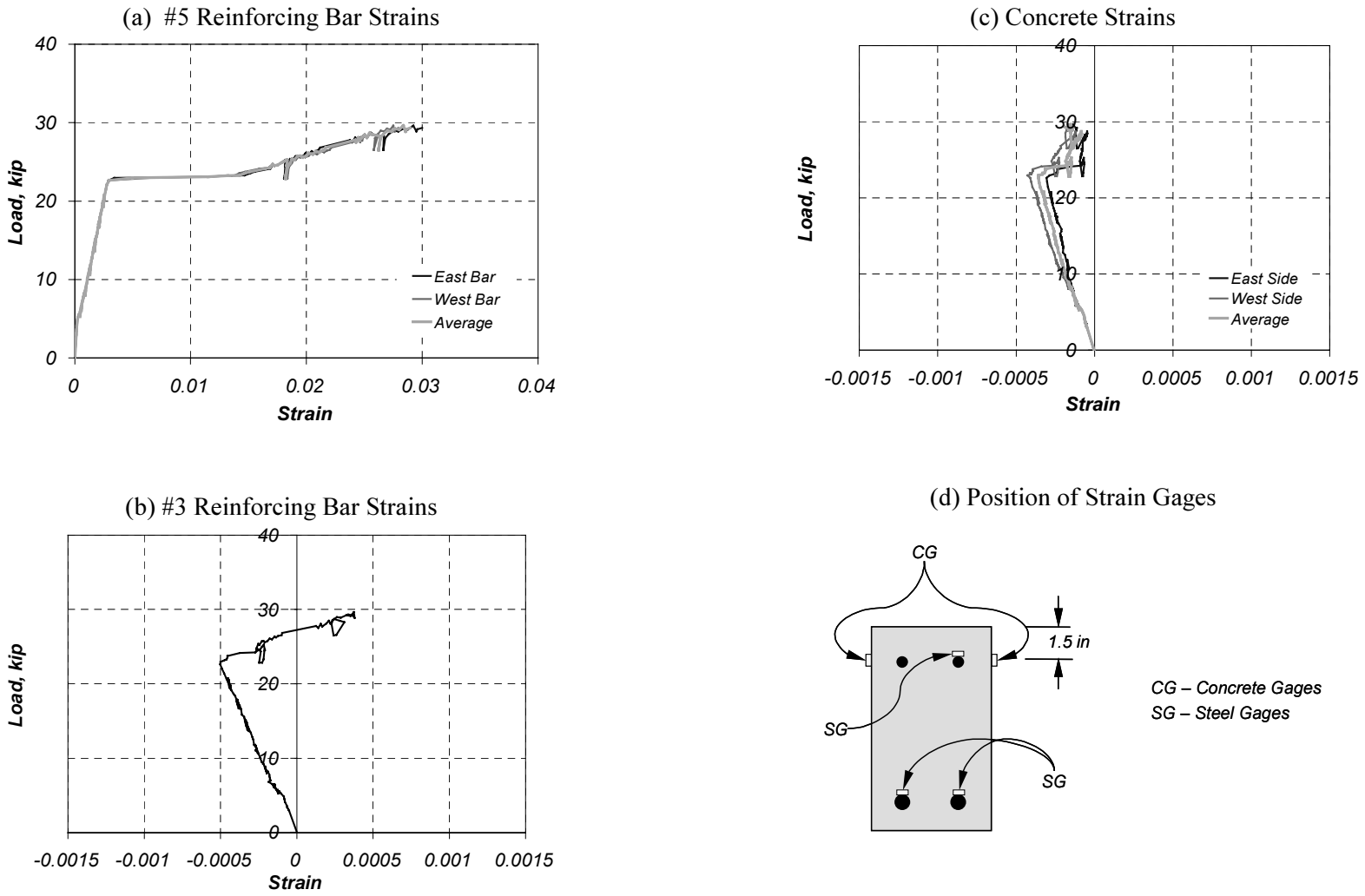

Figure D.3 Measured Strains in Control Specimen A & B (Section 1)

(a) #5 Reinforcing Bar Strains

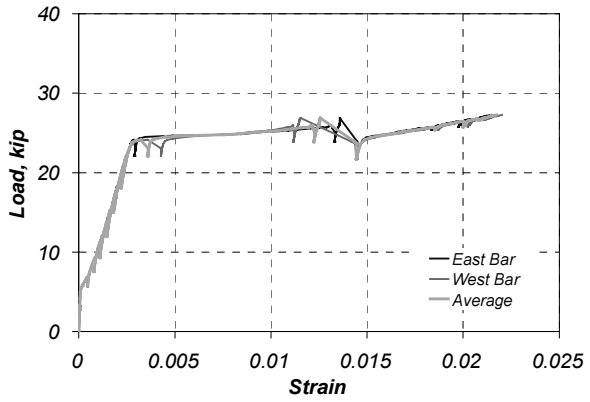

(c) CFRP Strains

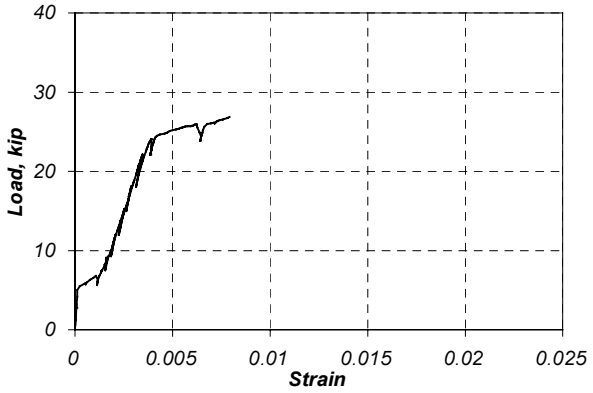

(b) #3 Reinforcing Bar Strains

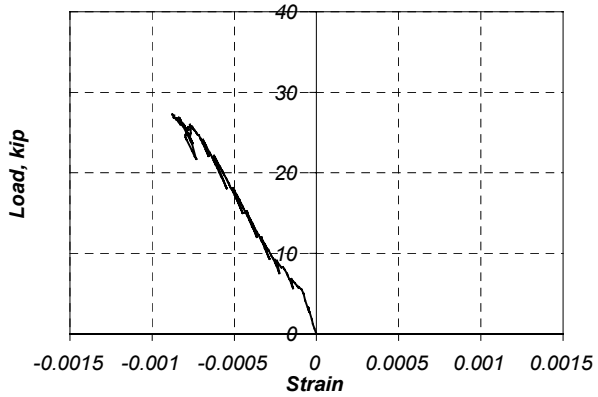

(d) Concrete Strains

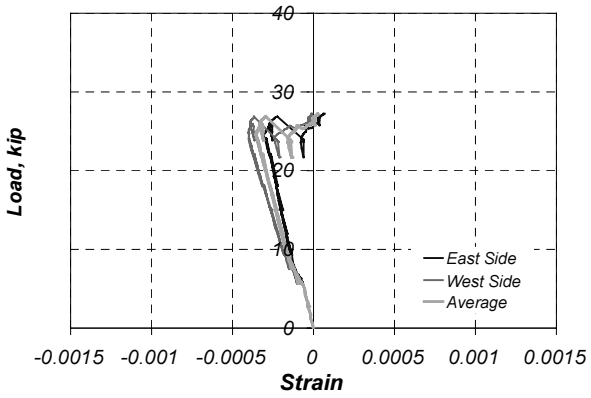

(e) Position of Strain Gages

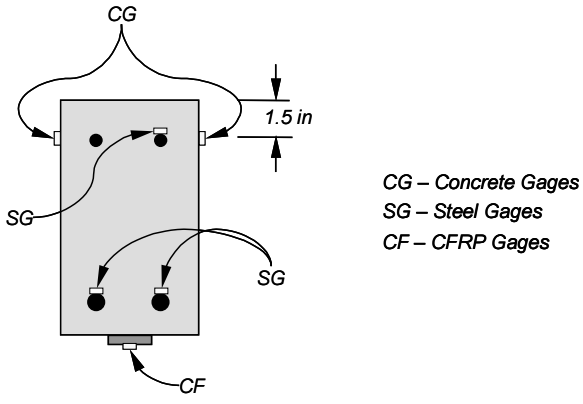

Figure D.4 Measured Strains in Specimen A-1 (Section 1)

(a) #5 Reinforcing Bar Strains

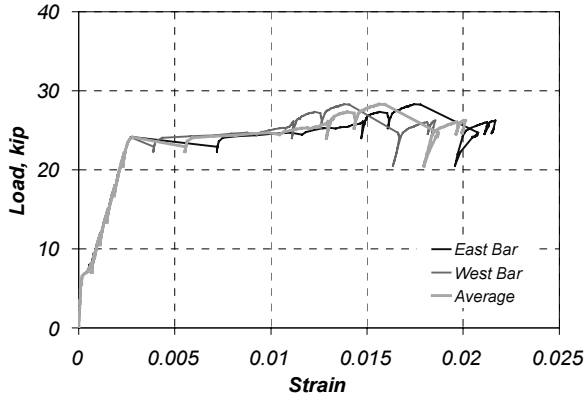

(c) CFRP Strains

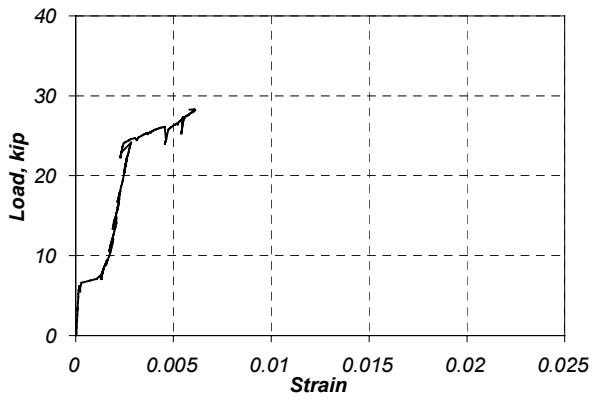

(b) #3 Reinforcing Bar Strains

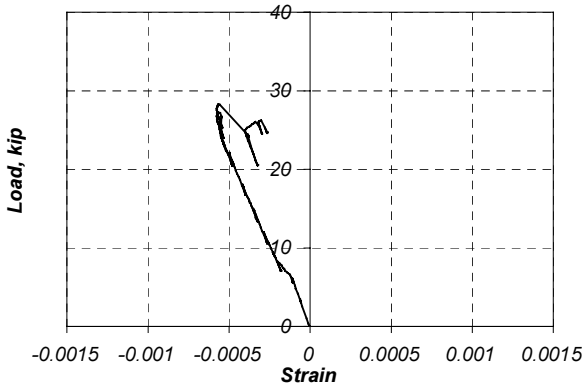

(d) Concrete Strains

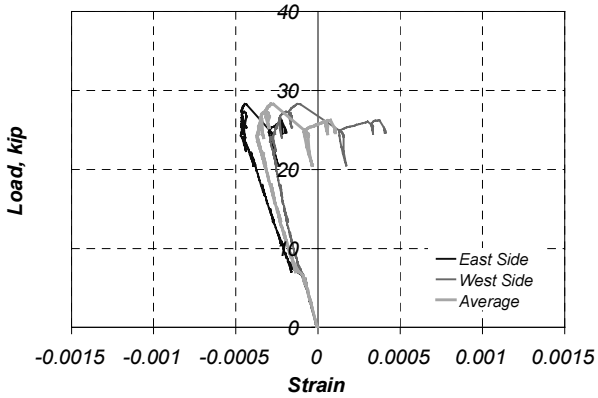

(e) Position of Strain Gages

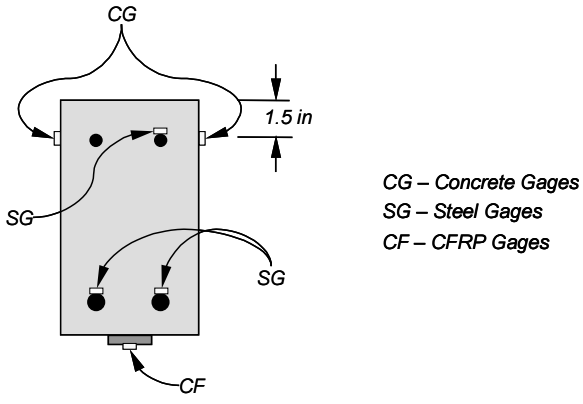

Figure D.5 Measured Strains in Specimen A-2 (Section 1)

(a) #5 Reinforcing Bar Strains

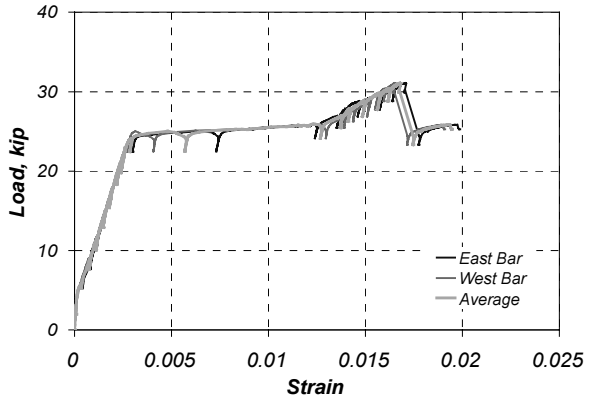

(b) #3 Reinforcing Bar Strains

Gage Malfunction

(c) CFRP Strains

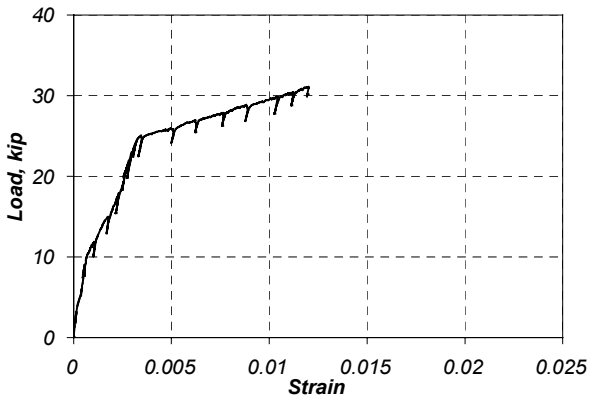

(d) Concrete Strains

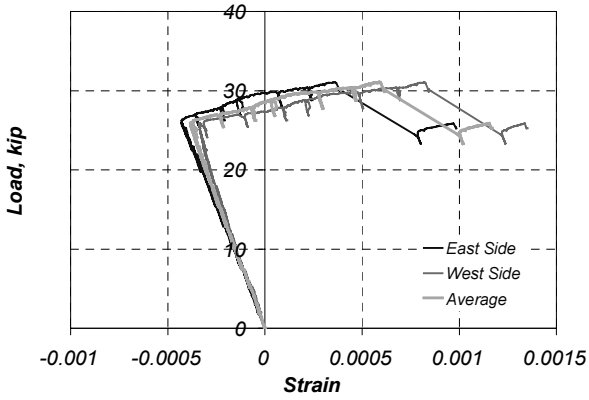

(e) Position of Strain Gages

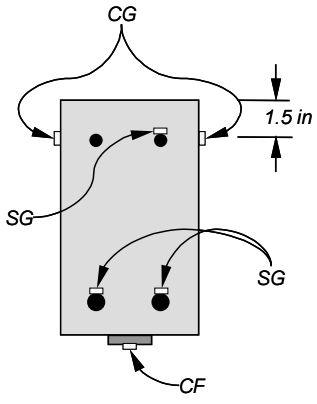

CG – Concrete Gages
SG – Steel Gages
CF – CFRP Gages

Figure D.6 Measured Strains in Specimen A-3 (Section 1)

(a) #5 Reinforcing Bar Strains

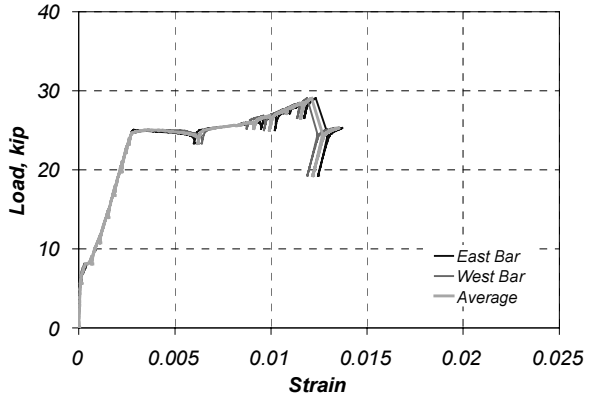

(c) CFRP Strains

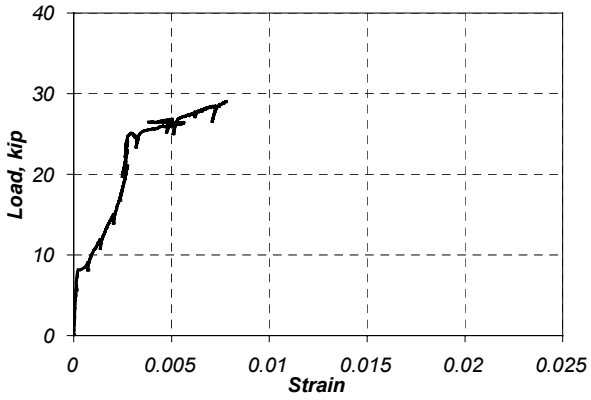

(b) #3 Reinforcing Bar Strains

Gage Malfunction

(d) Concrete Strains

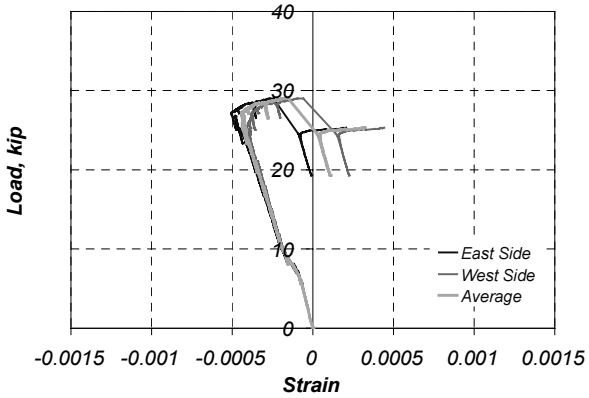

(e) Position of Strain Gages

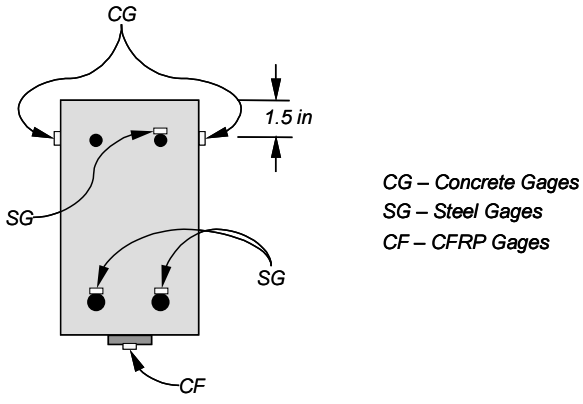

Figure D.7 Measured Strains in Specimen A-4 (Section 1)

(a) #5 Reinforcing Bar Strains

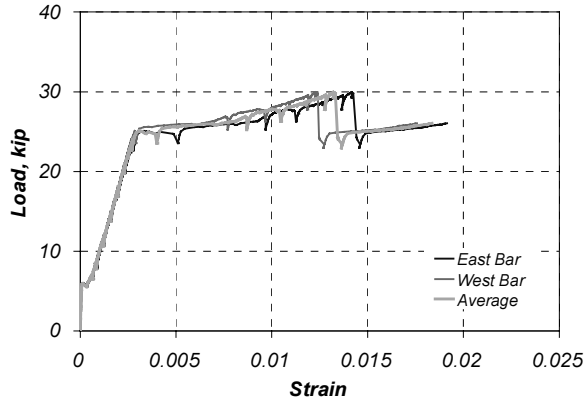

(c) CFRP Strains

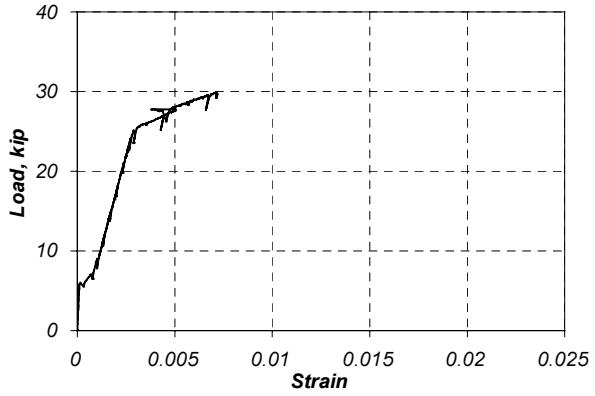

(b) #3 Reinforcing Bar Strains

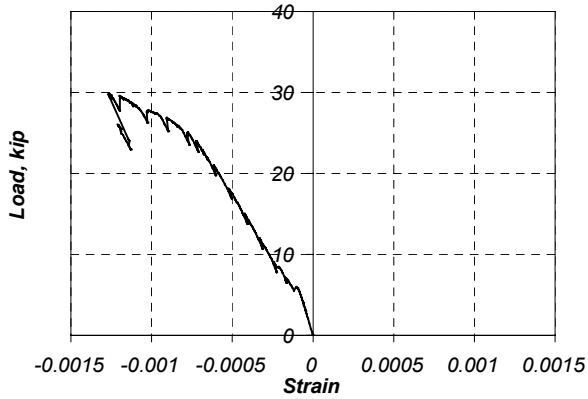

(d) Concrete Strains

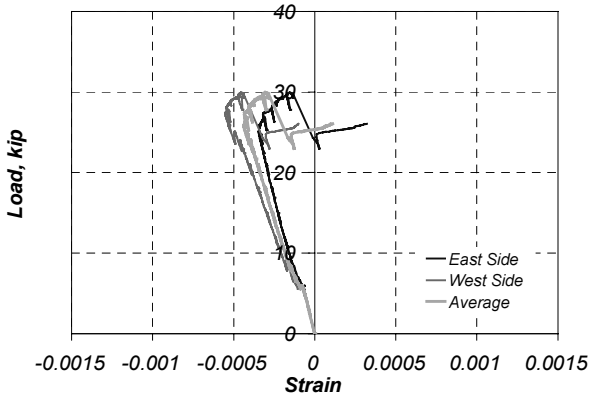

(e) Position of Strain Gages

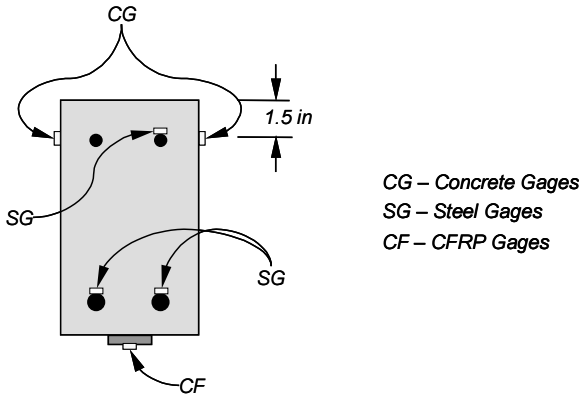

Figure D.8 Measured Strains in Specimen B-1 (Section 1)

(a) #5 Reinforcing Bar Strains

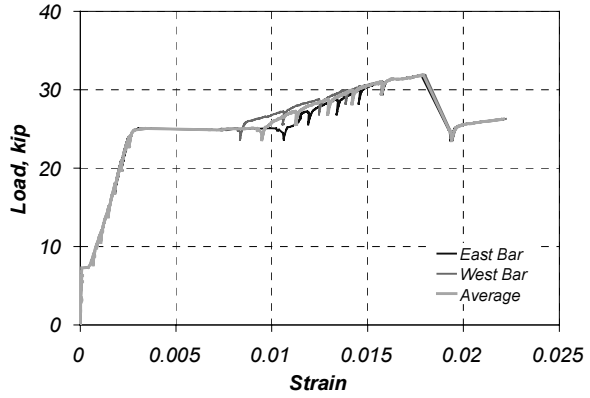

(c) CFRP Strains

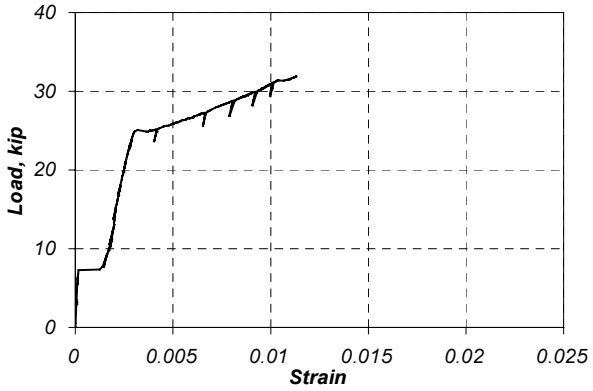

(b) #3 Reinforcing Bar Strains

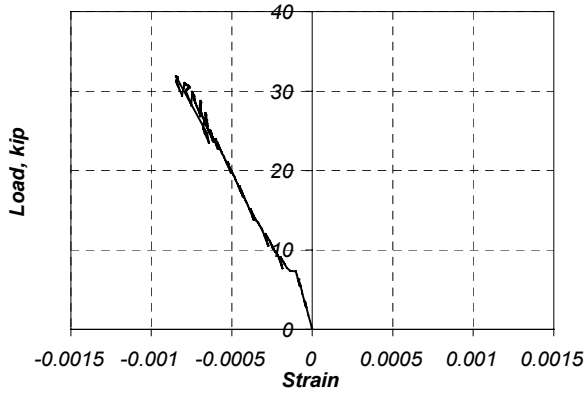

(d) Concrete Strains

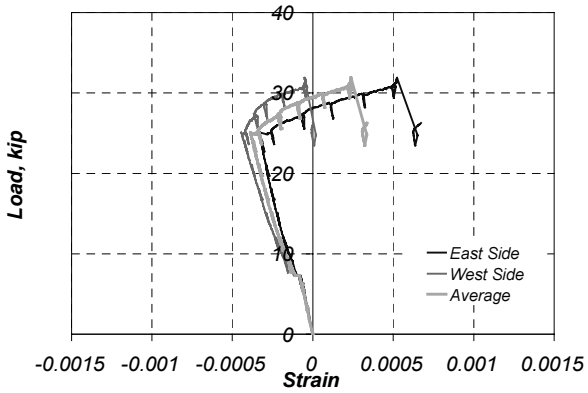

(e) Position of Strain Gages

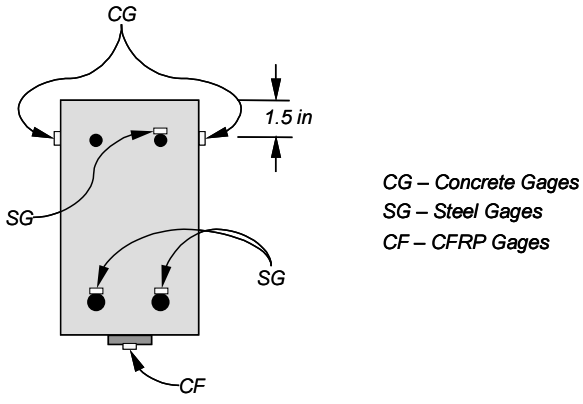

Figure D.9 Measured Strains in Specimen B-2 (Section 1)

(a) #5 Reinforcing Bar Strains

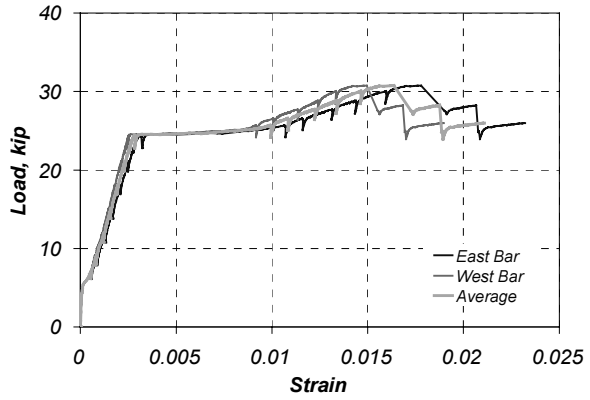

(c) CFRP Strains

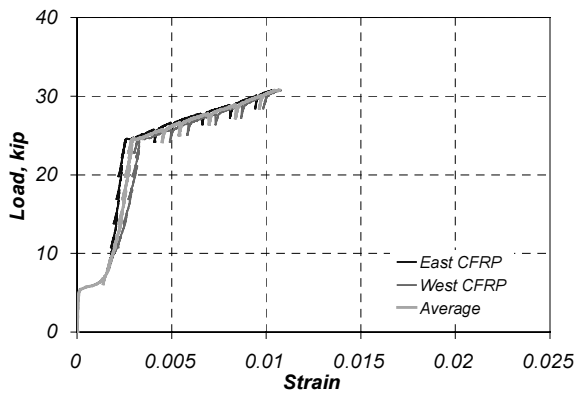

(b) #3 Reinforcing Bar Strains

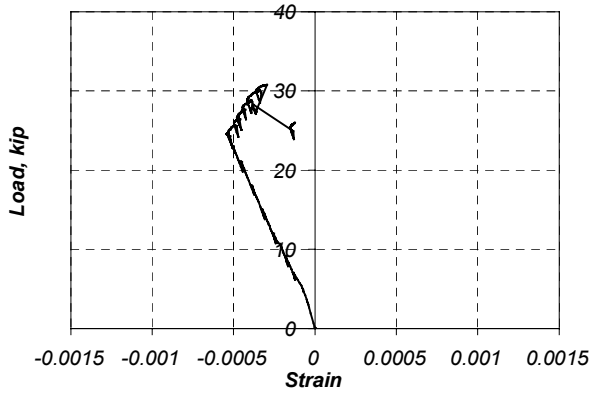

(d) Concrete Strains

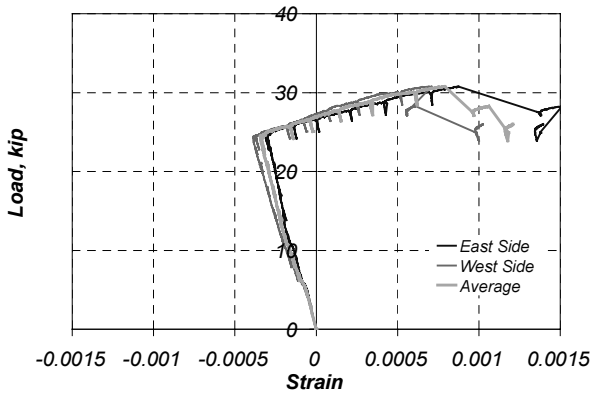

(e) Position of Strain Gages

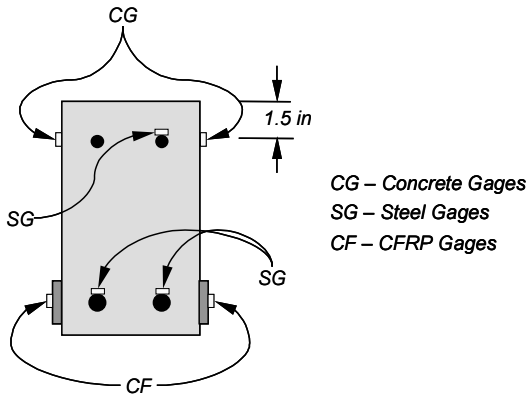

Figure D.10 Measured Strains in Specimen B-3 (Section 1)

(a) #5 Reinforcing Bar Strains

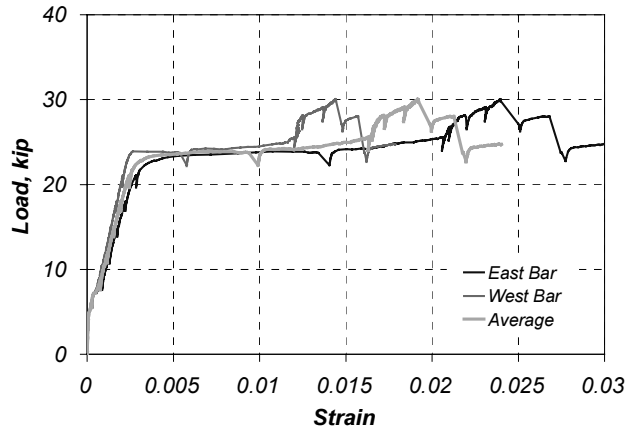

(c) Concrete Strains

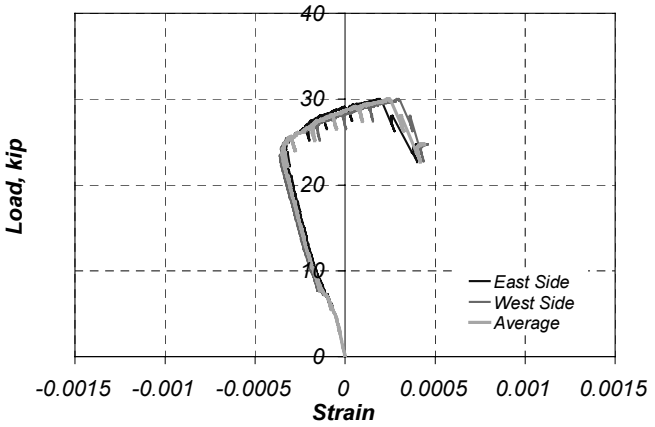

(b) CFRP Strains

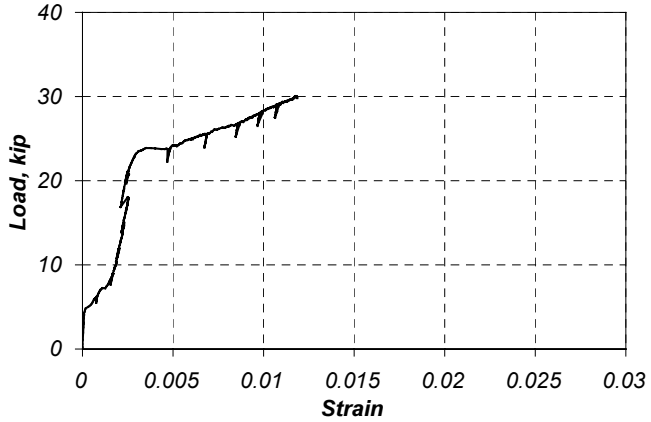

(d) Position of Strain Gages

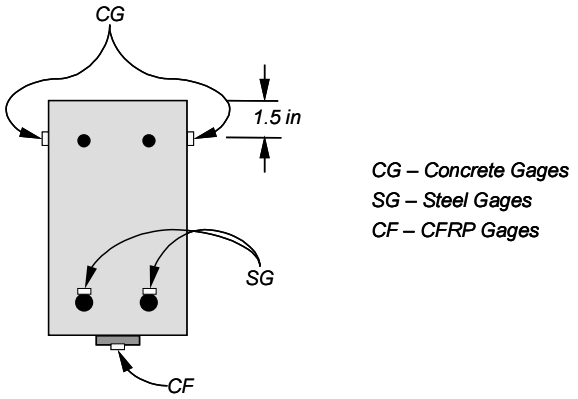

Figure D.11 Measured Strains in Specimen B-4 (Section 1)

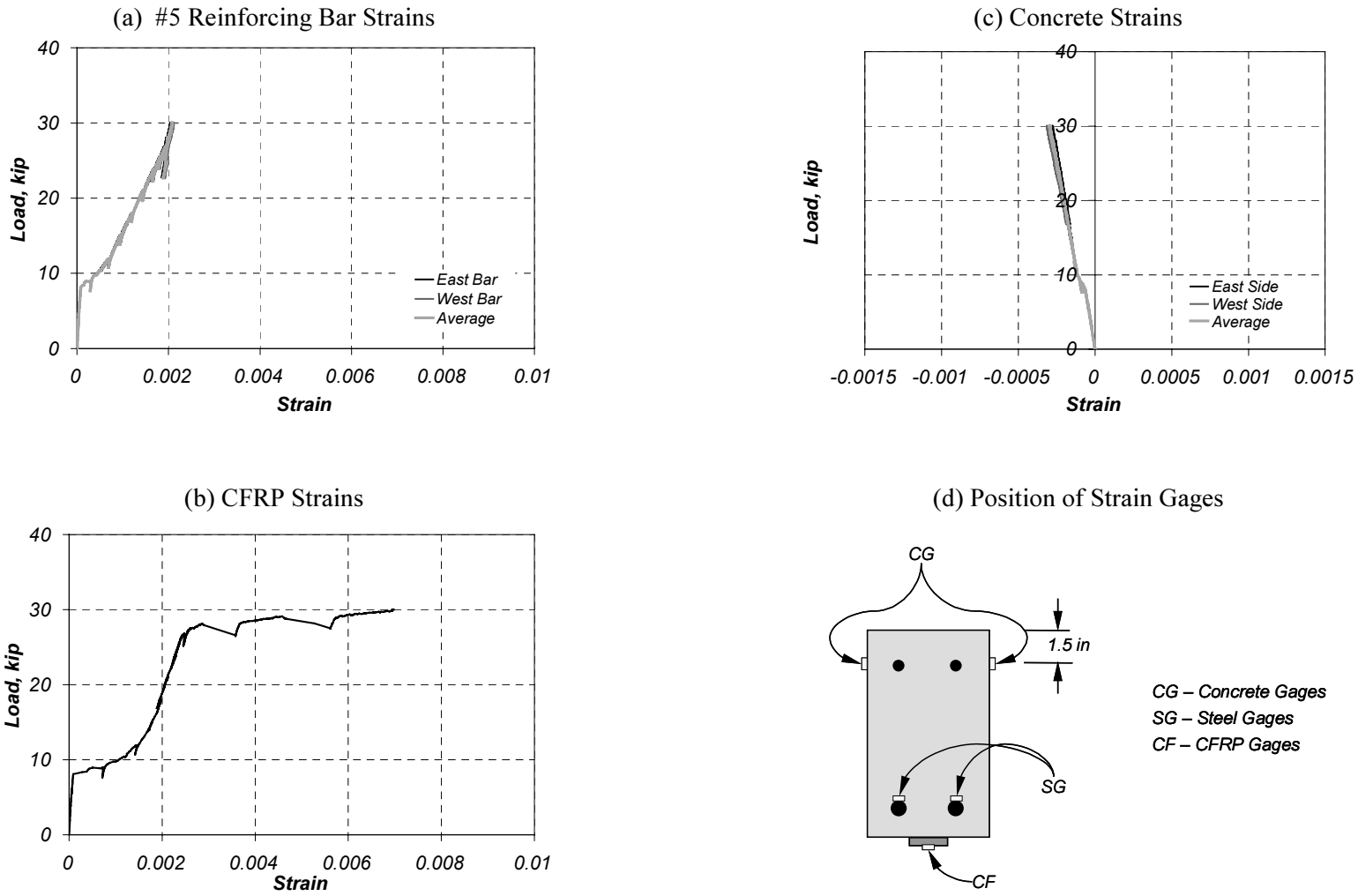

Figure D.12 Measured Strains in Specimen B-4 (Section 2)

(a) #5 Reinforcing Bar Strains

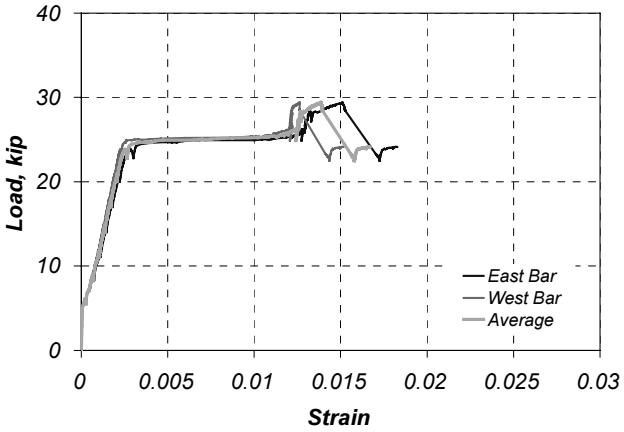

(c) Concrete Strains

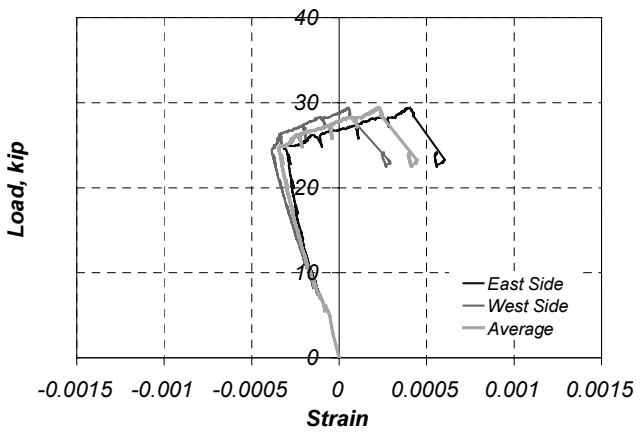

(b) CFRP Strains

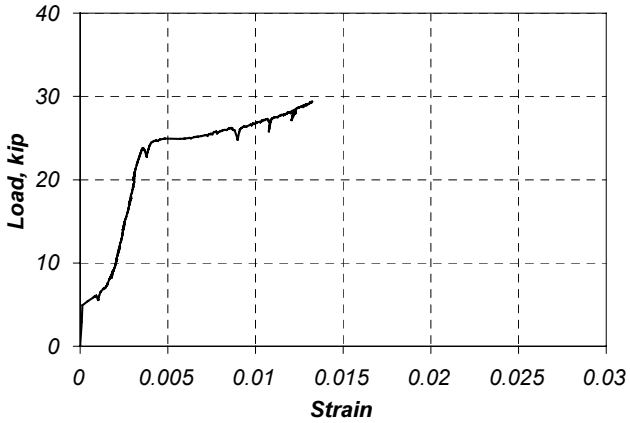

(d) Position of Strain Gages

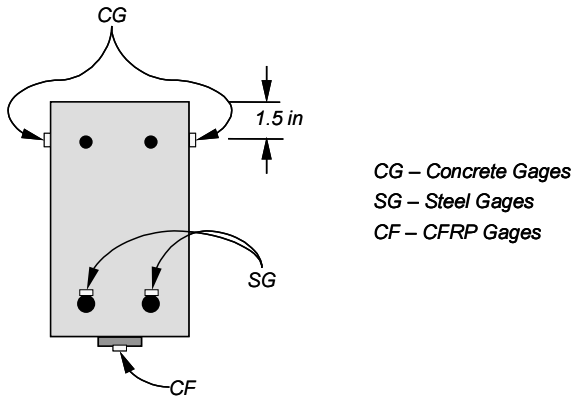

Figure D.13 Measured Strains in Specimen B-5 (Section 1)

(a) #5 Reinforcing Bar Strains

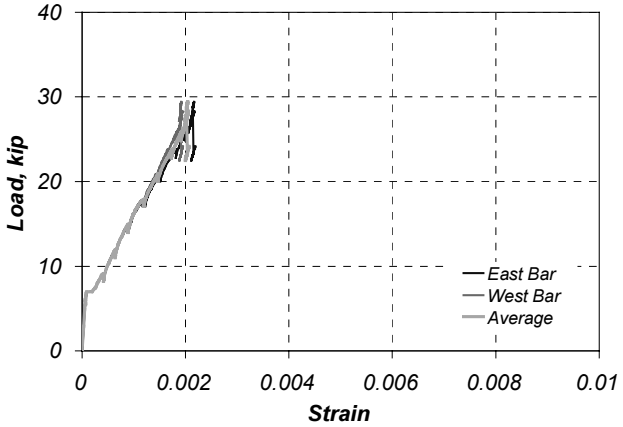

(c) Concrete Strains

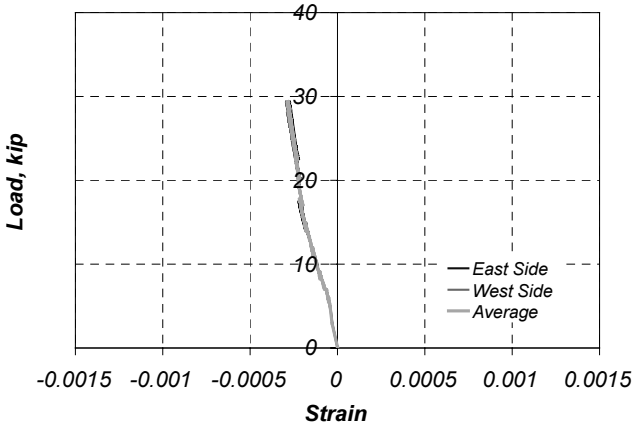

(b) CFRP Strains

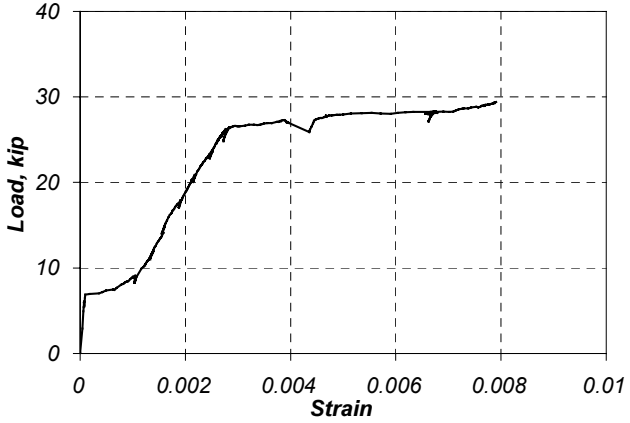

(d) Position of Strain Gages

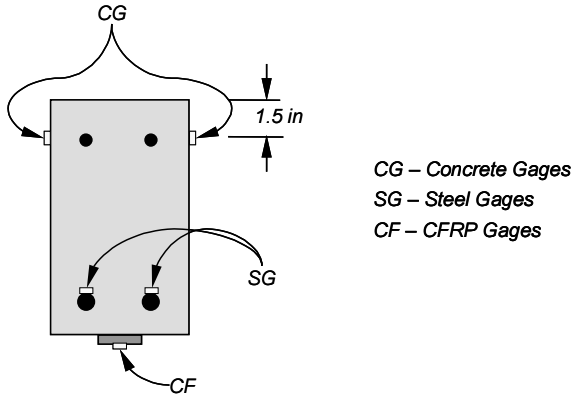

Figure D.14 Measured Strains in Specimen B-5 (Section 2)

(a) #5 Reinforcing Bar Strains

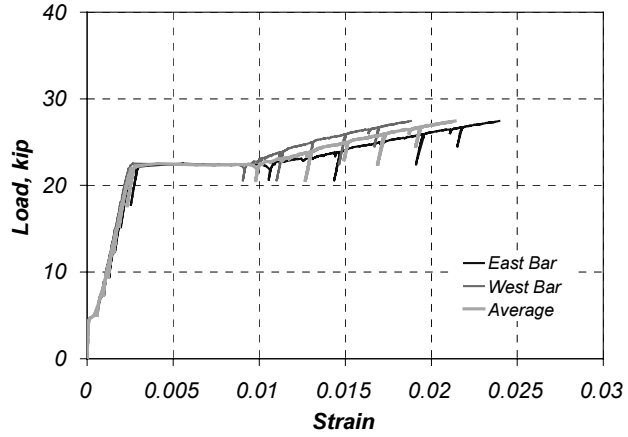

(c) Concrete Strains

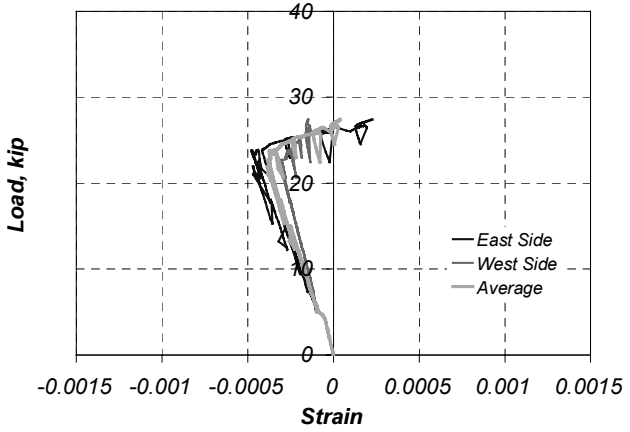

(b) #3 Reinforcing Bar Strains

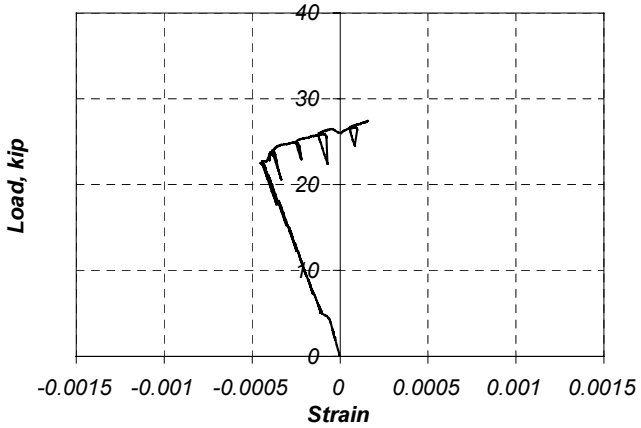

(d) Position of Strain Gages

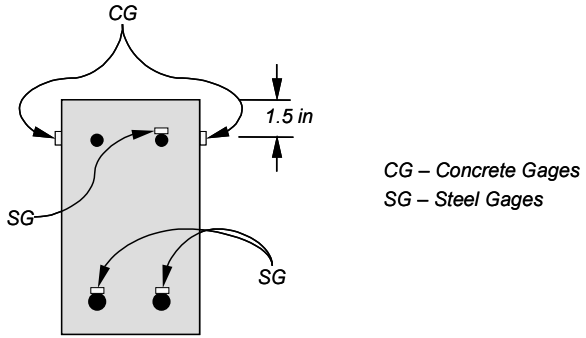

Figure D.15 Measured Strains in Control Specimen C & D (Section 1)

(a) #5 Reinforcing Bar Strains

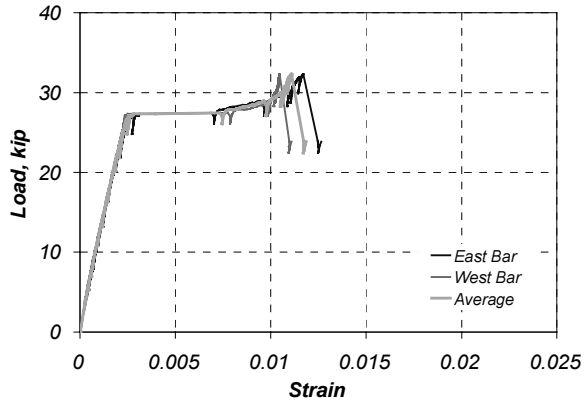

(c) CFRP Strains

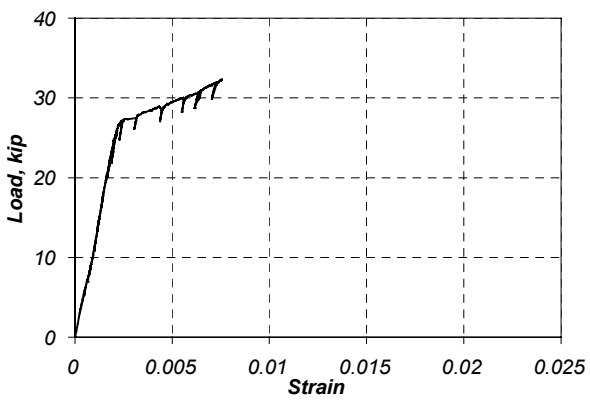

(b) #3 Reinforcing Bar Strains

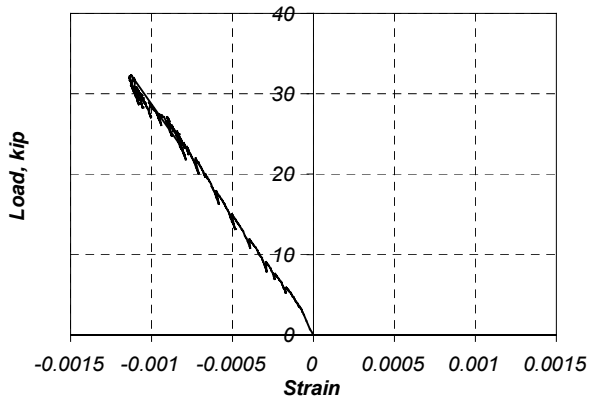

(d) Concrete Strains

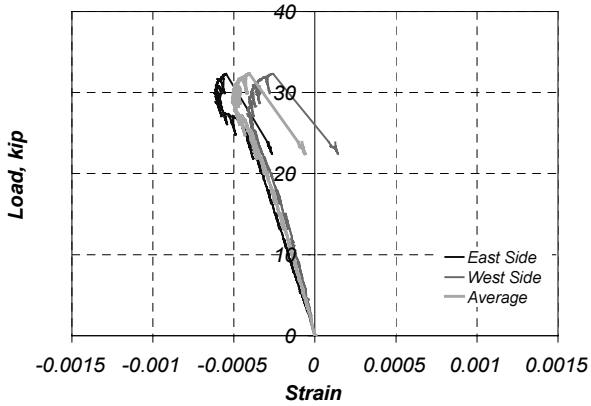

(e) Position of Strain Gages

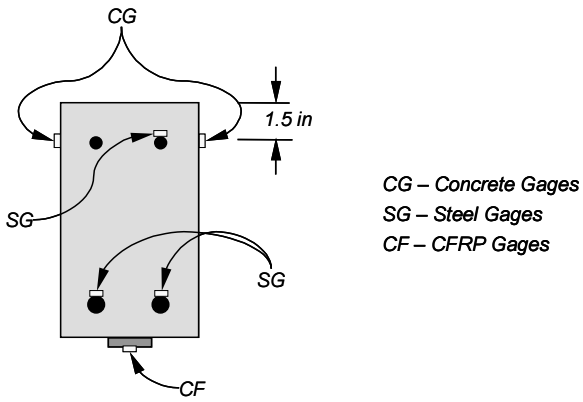

Figure D.16 Measured Strains in Specimen C-1 (Section 1)

(a) #5 Reinforcing Bar Strains

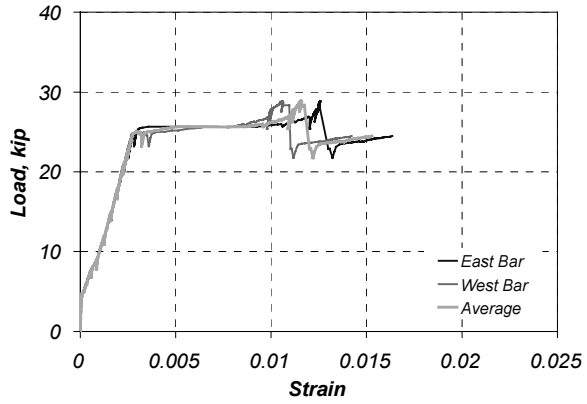

(c) CFRP Strains

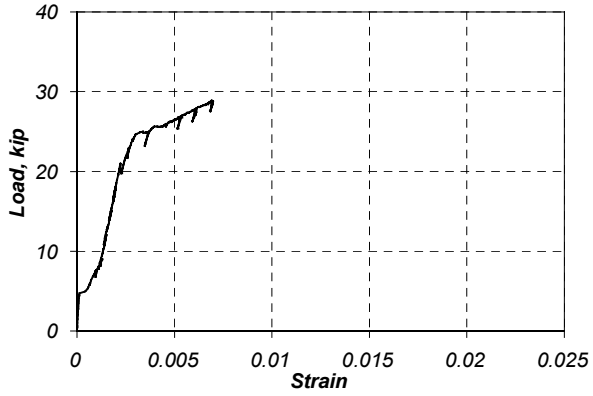

(b) #3 Reinforcing Bar Strains

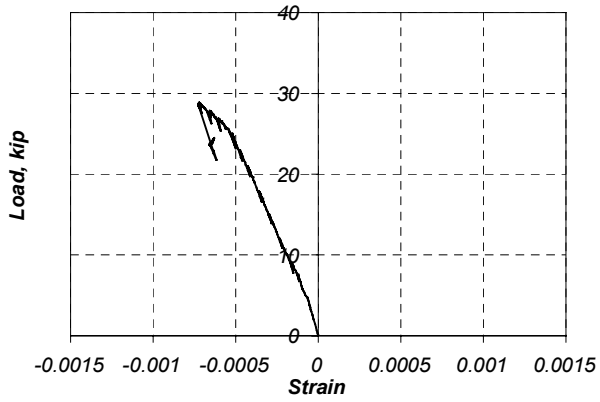

(d) Concrete Strains

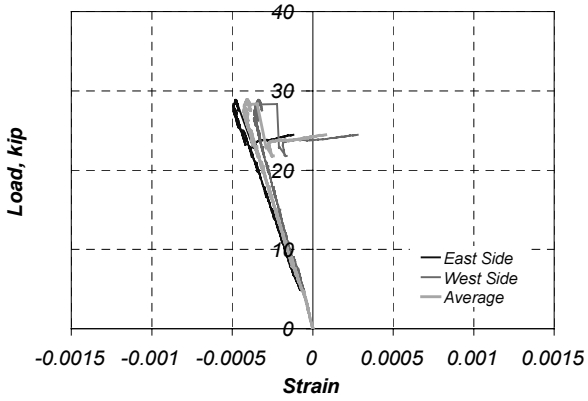

(e) Position of Strain Gages

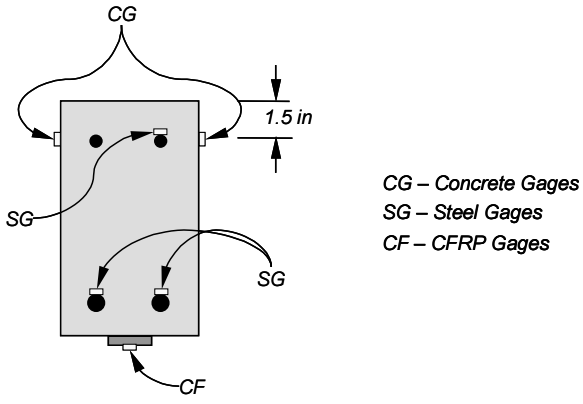

Figure D.17 Measured Strains in Specimen C-2 (Section 1)

(a) #5 Reinforcing Bar Strains

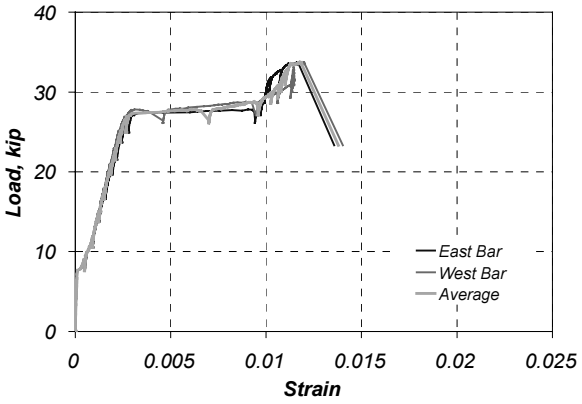

(c) CFRP Strains

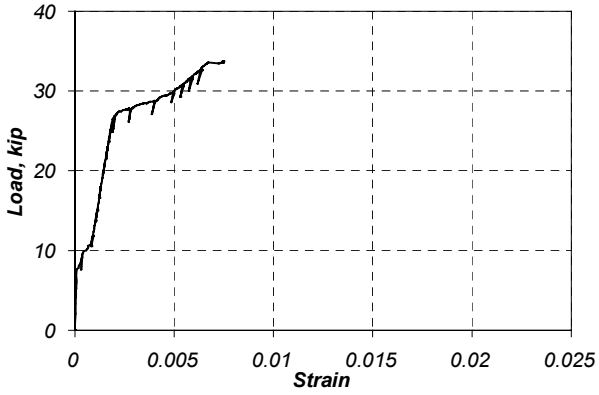

(b) #3 Reinforcing Bar Strains

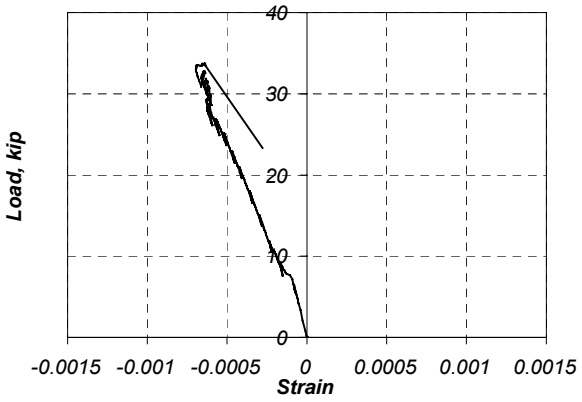

(d) Concrete Strains

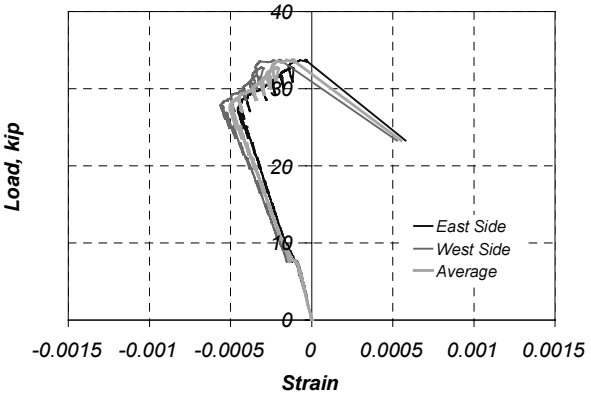

(e) Position of Strain Gages

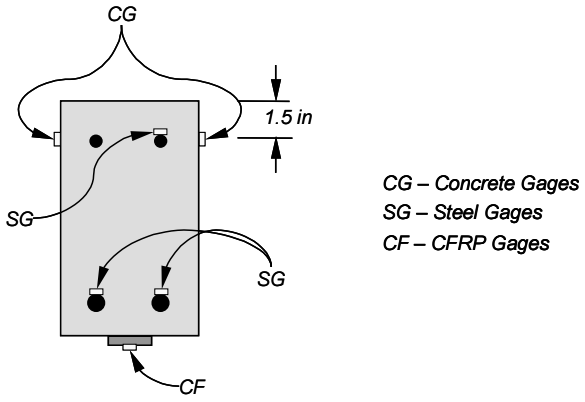

Figure D.18 Measured Strains in Specimen C-3 (Section 1)

(a) #5 Reinforcing Bar Strains

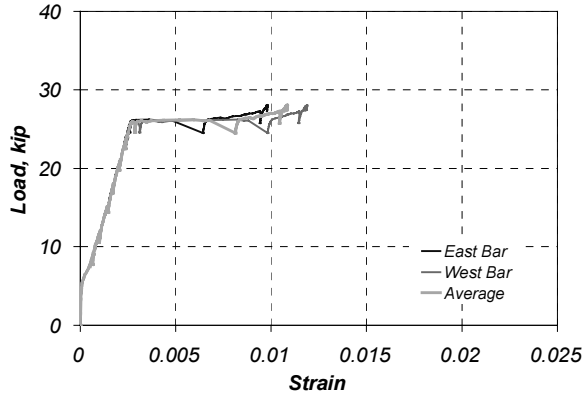

(c) CFRP Strains

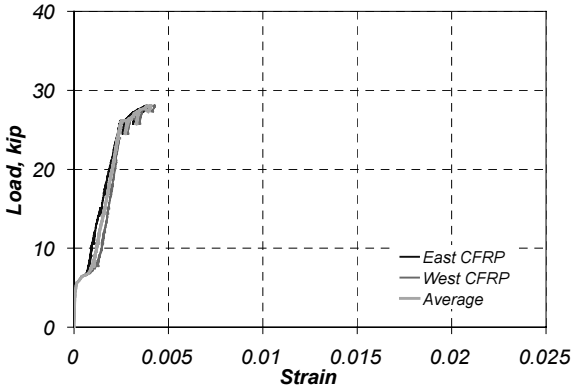

(b) #3 Reinforcing Bar Strains

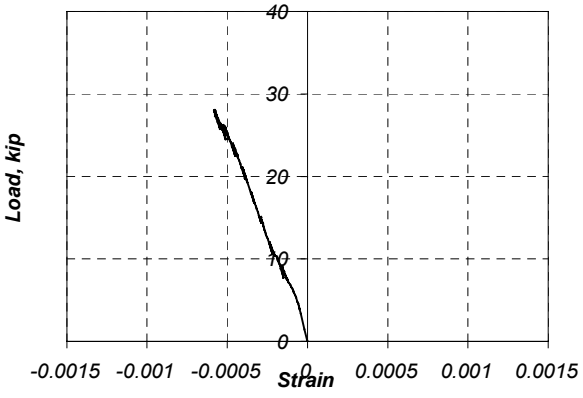

(d) Concrete Strains

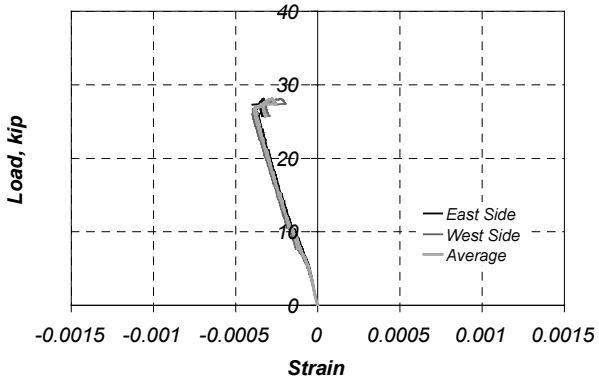

(e) Position of Strain Gages

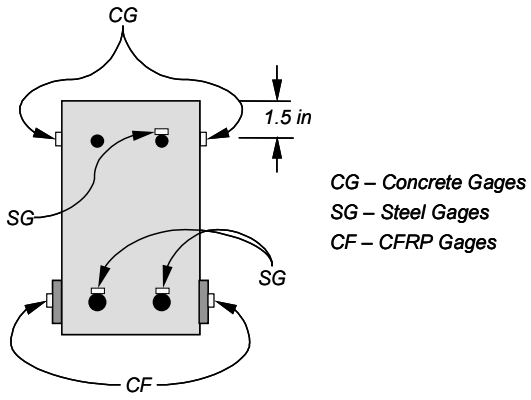

Figure D.19 Measured Strains in Specimen C-4 (Section 1)

(a) #5 Reinforcing Bar Strains

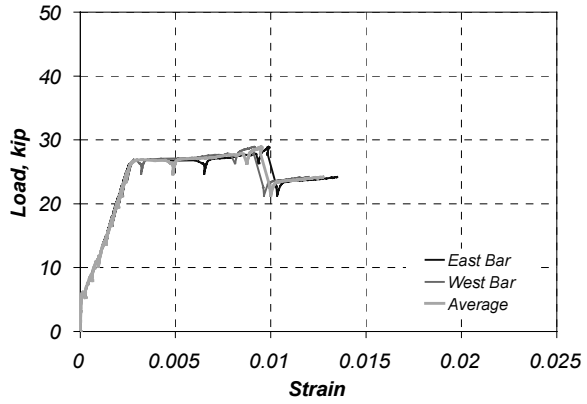

(c) CFRP Strains

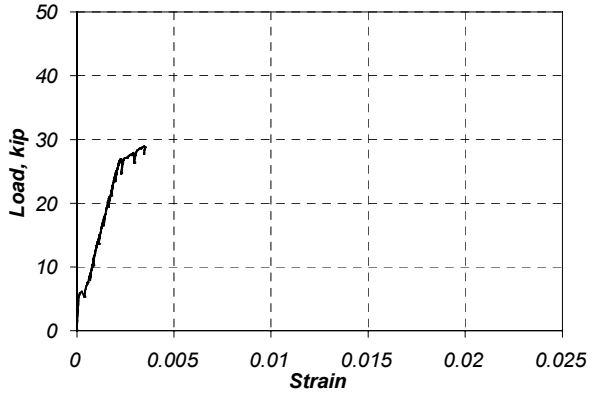

(b) #3 Reinforcing Bar Strains

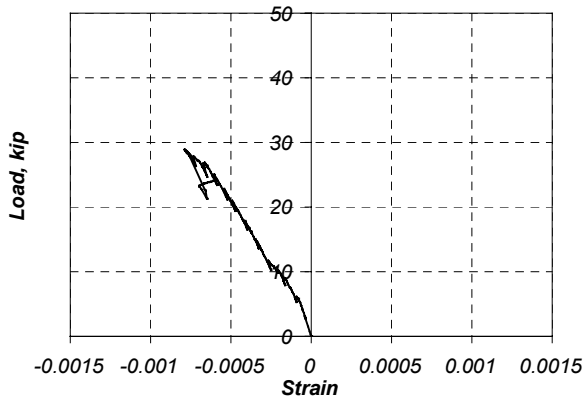

(d) Concrete Strains

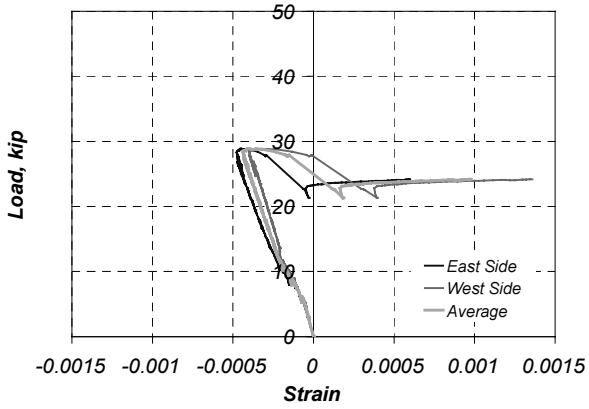

(e) Position of Strain Gages

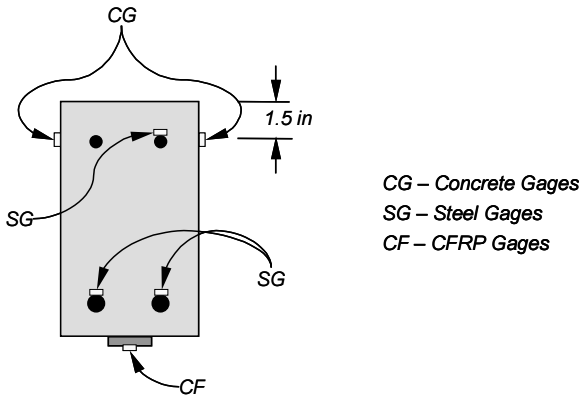

Figure D.20 Measured Strains in Specimen D-1 (Section 1)

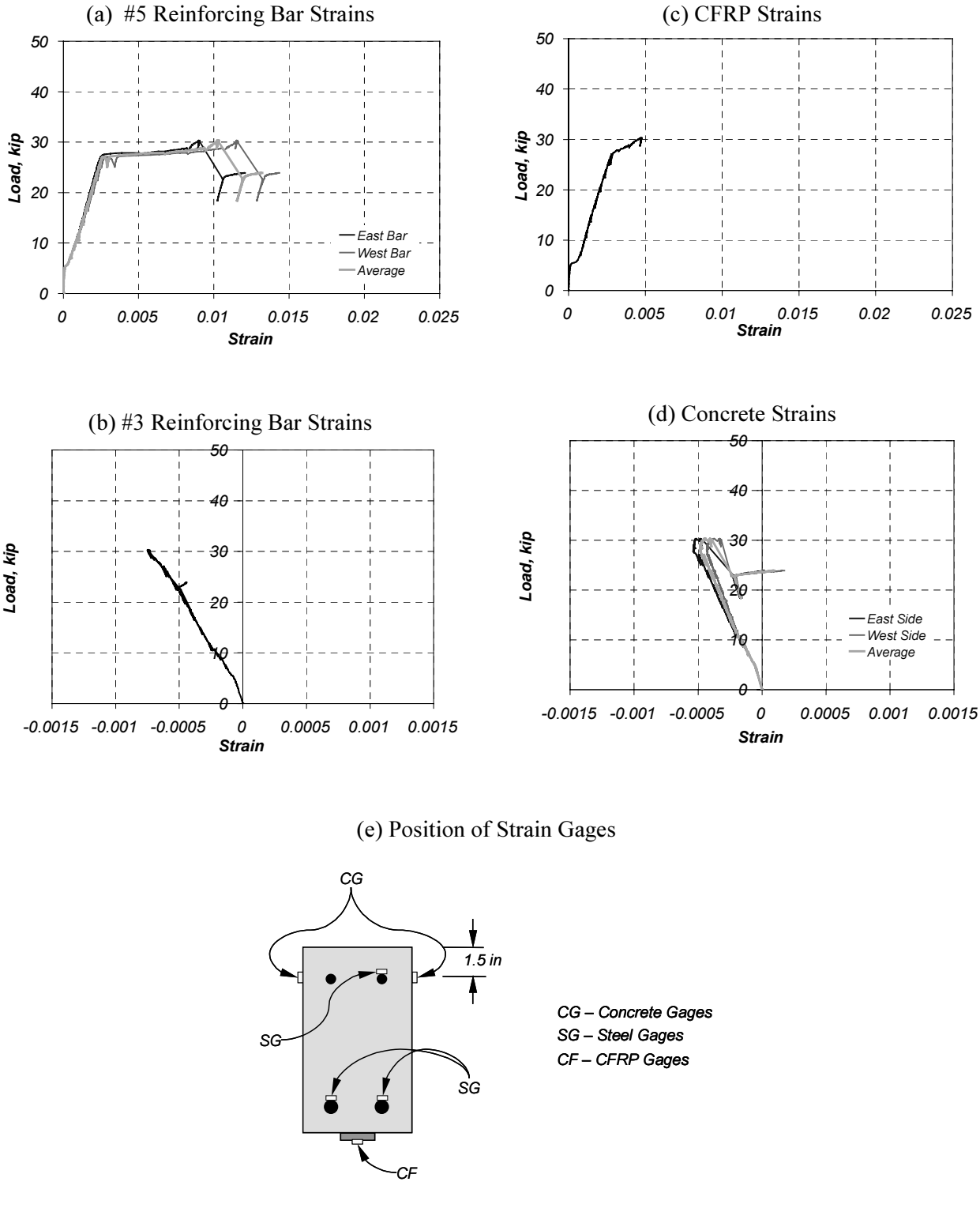

Figure D.21 Measured Strains in Specimen D-2 (Section 1)

(a) #5 Reinforcing Bar Strains

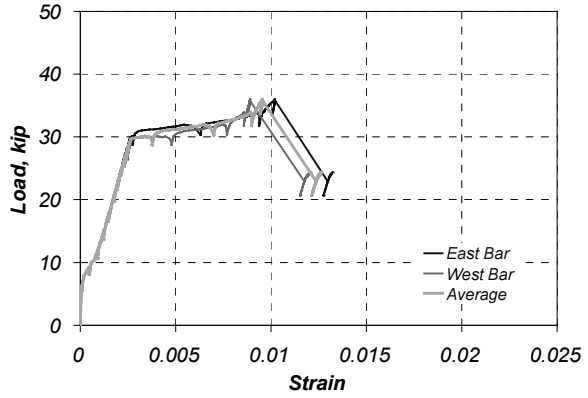

(c) CFRP Strains

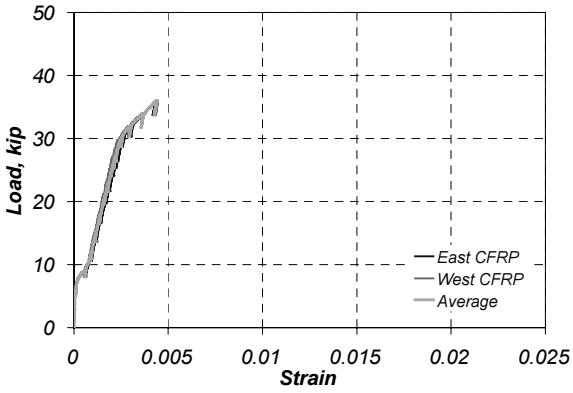

(b) #3 Reinforcing Bar Strains

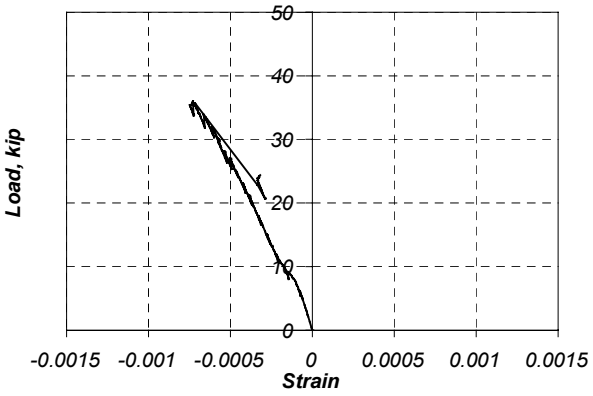

(d) Concrete Strains

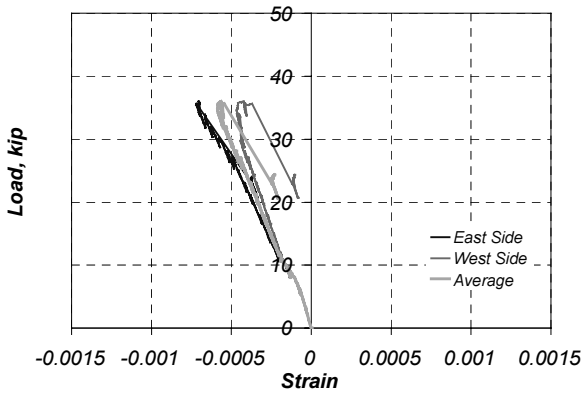

(e) Position of Strain Gages

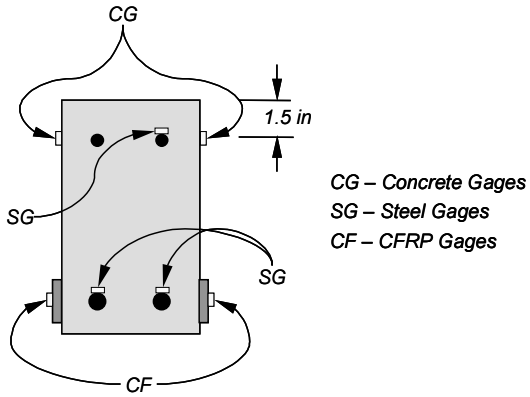

Figure D.22 Measured Strains in Specimen D-3 (Section 1)

(a) #5 Reinforcing Bar Strains

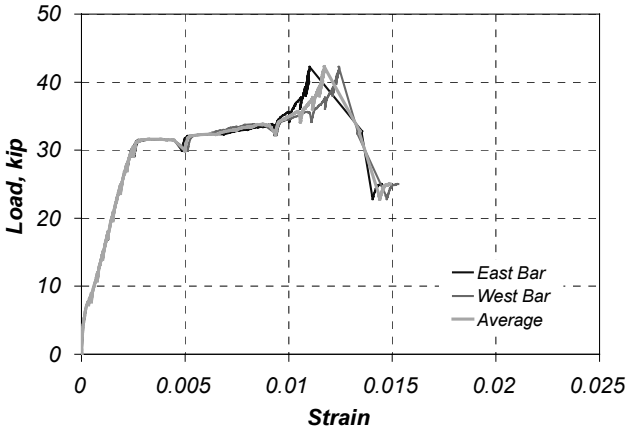

(c) Concrete Strains

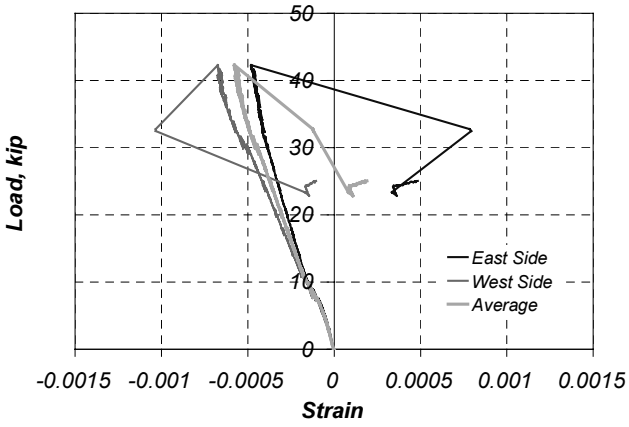

(b) CFRP Strains

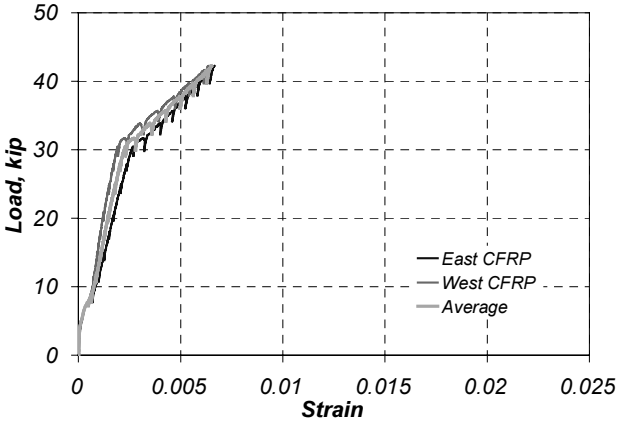

(d) Position of Strain Gages

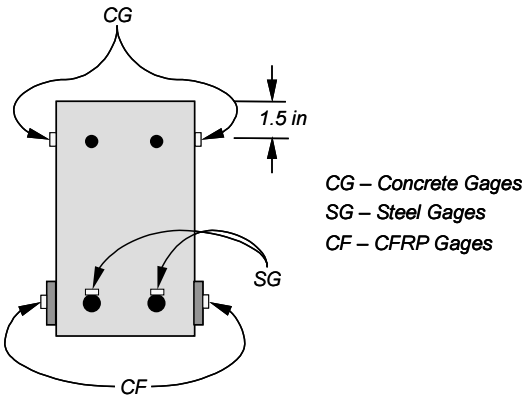

Figure D.23 Measured Strains in Specimen D-4 (Section 1)

(a) #5 Reinforcing Bar Strains

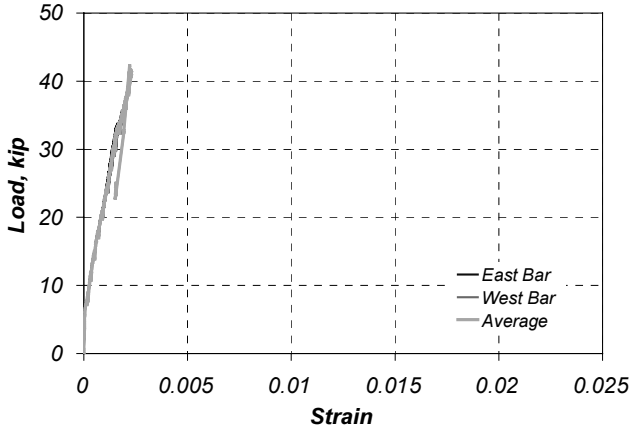

(c) Concrete Strains

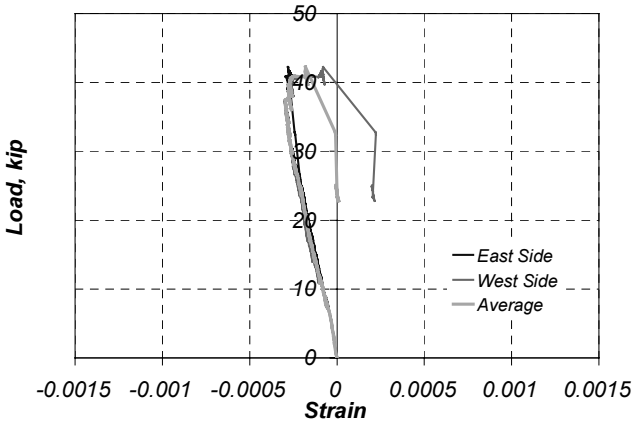

(b) CFRP Strains

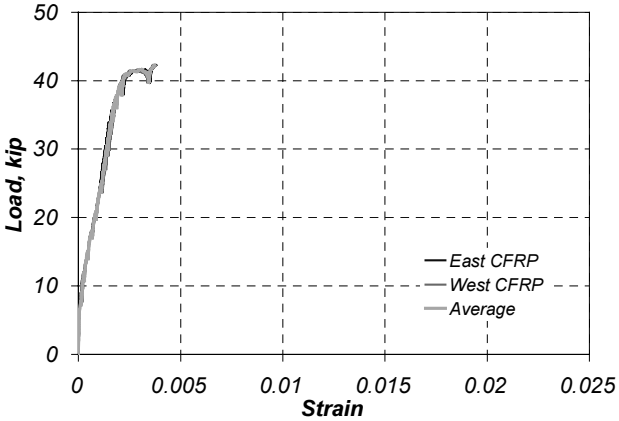

(d) Position of Strain Gages

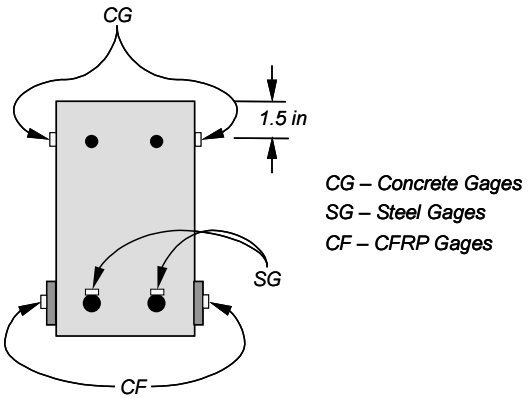

Figure D.24 Measured Strains in Specimen D-4 (Section 2)

(a) #5 Reinforcing Bar Strains

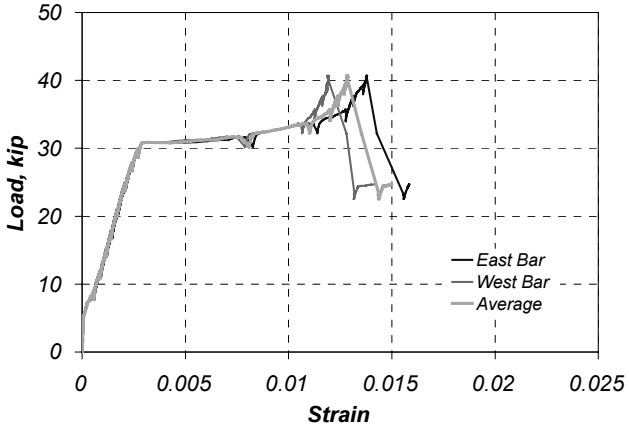

(c) Concrete Strains

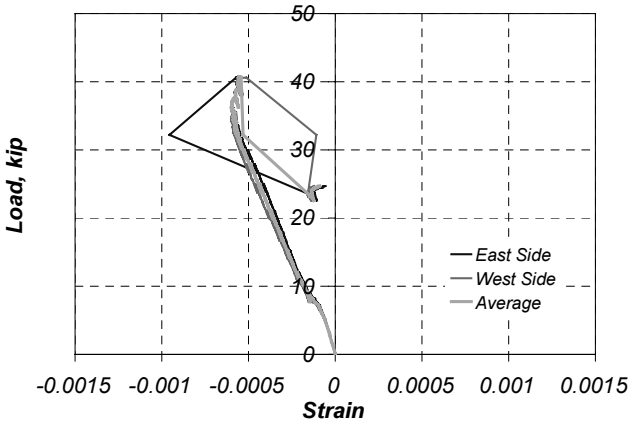

(b) CFRP Strains

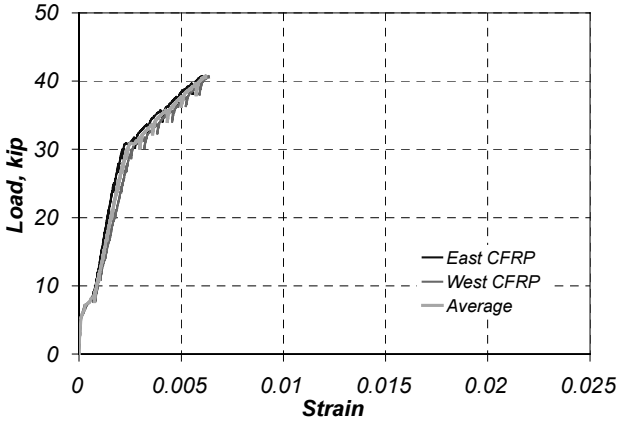

(d) Position of Strain Gages

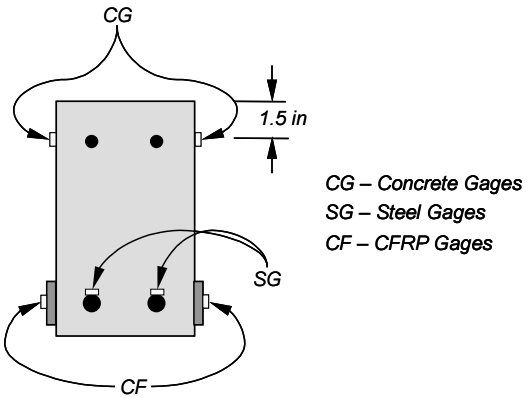

Figure D.25 Measured Strains in Specimen D-5 (Section 1)

(a) #5 Reinforcing Bar Strains

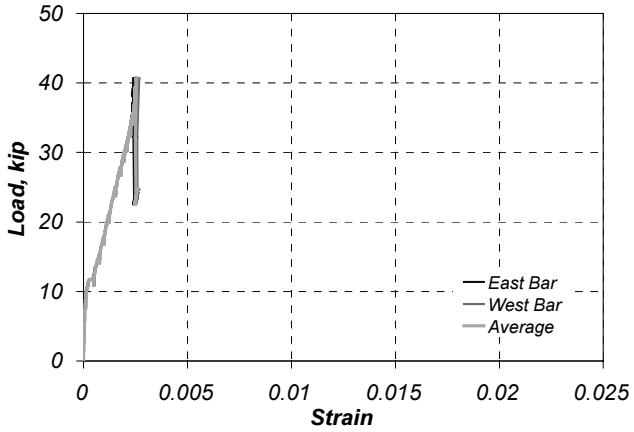

(c) Concrete Strains

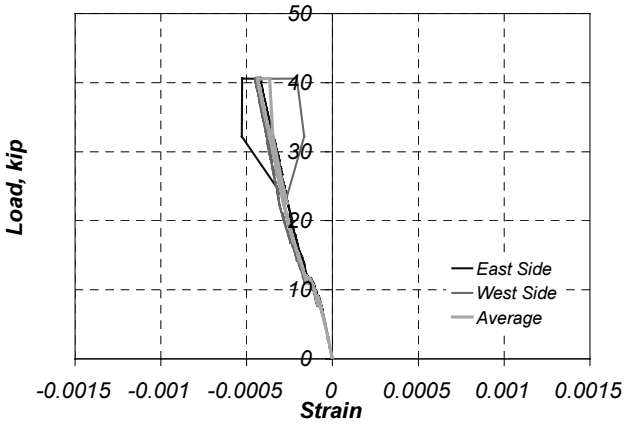

(b) CFRP Strains

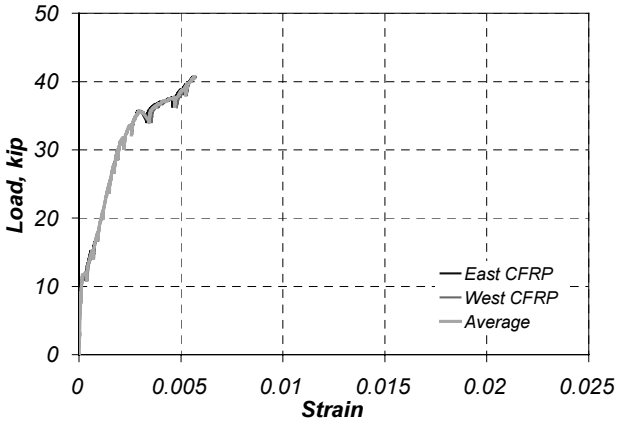

(d) Position of Strain Gages

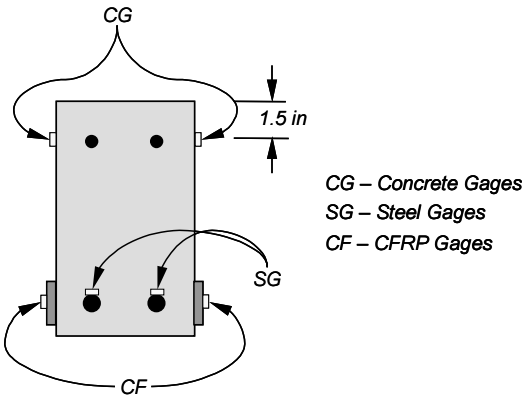

Figure D.26 Measured Strains in Specimen D-5 (Section 2)

(a) #5 Reinforcing Bar Strains

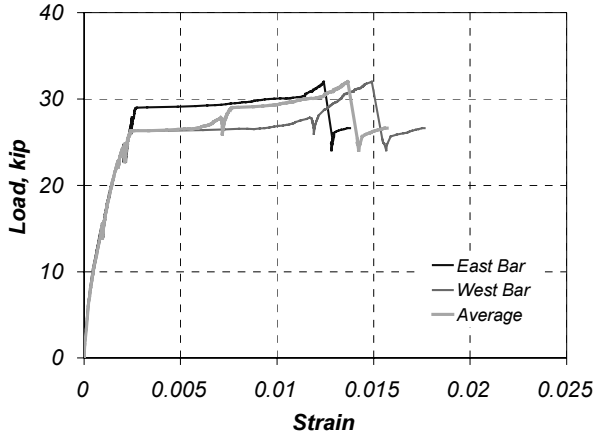

(c) Concrete Strains

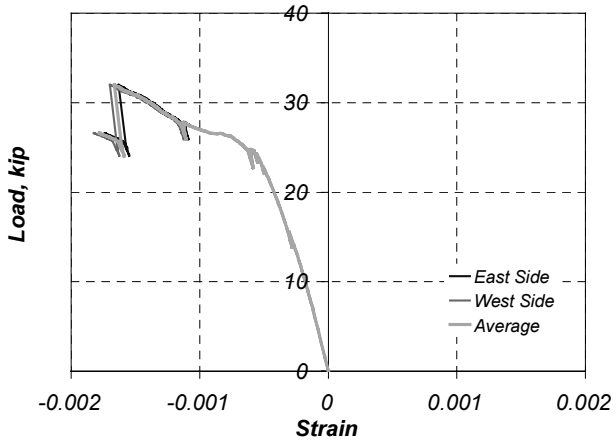

(b) CFRP Strains

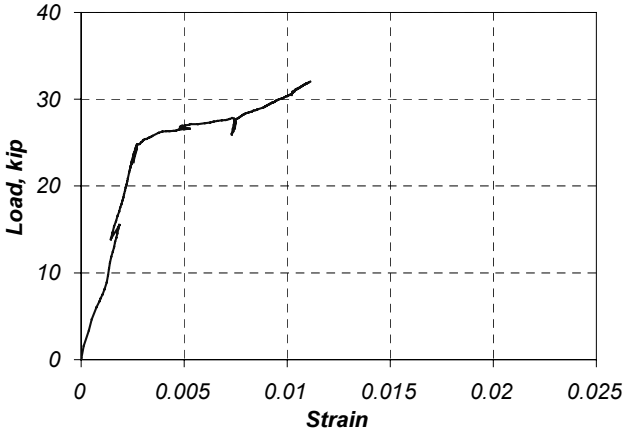

(d) Position of Strain Gages

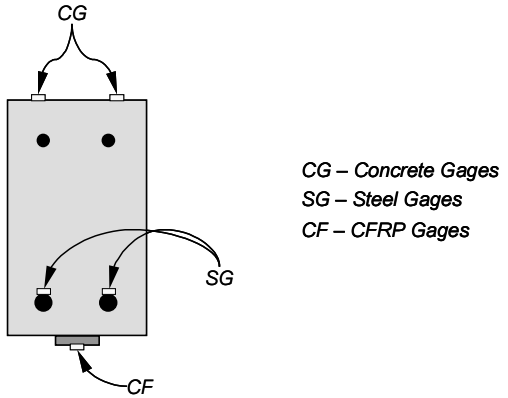

Figure D.27 Measured Strains in Specimen A-LT1 (Section 1)

(a) #5 Reinforcing Bar Strains

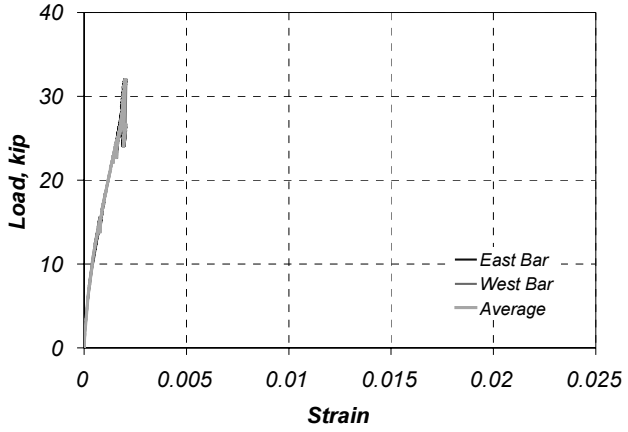

(c) Concrete Strains

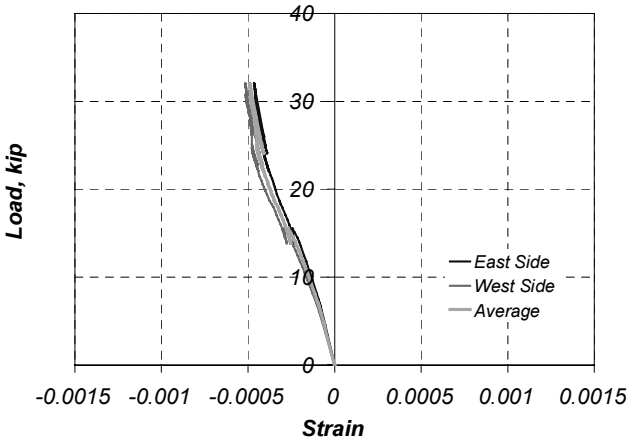

(b) CFRP Strains

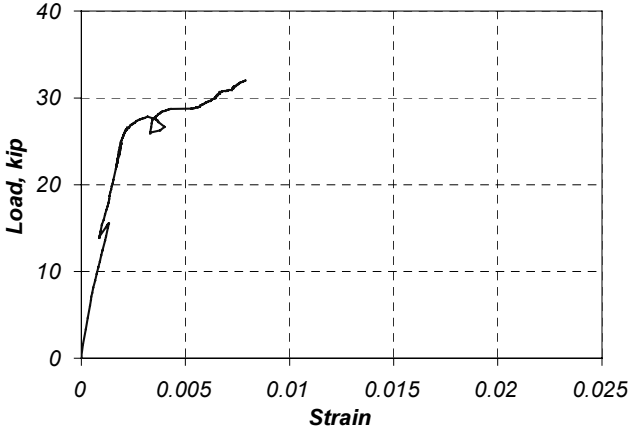

(d) Position of Strain Gages

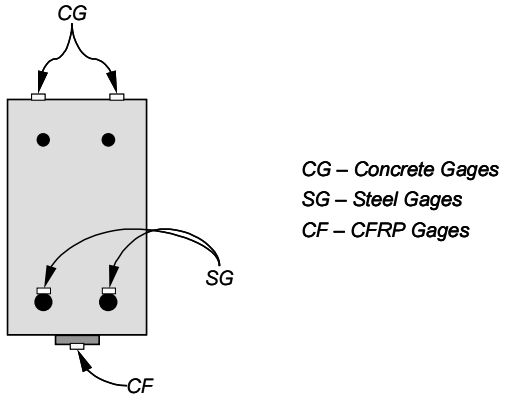

Figure D.28 Measured Strains in Specimen A-LT1 (Section 2)

(a) #5 Reinforcing Bar Strains

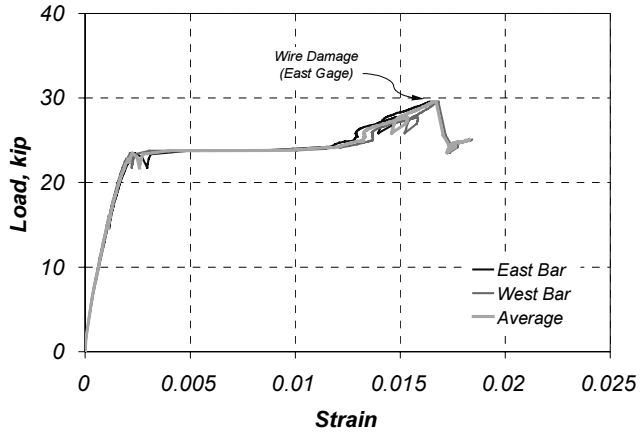

(c) Concrete Strains

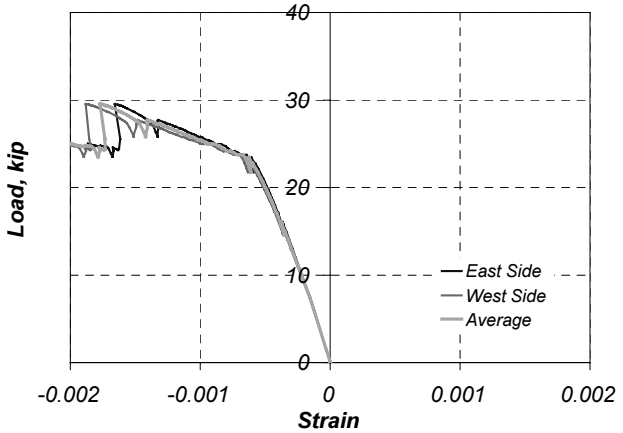

(b) CFRP Strains

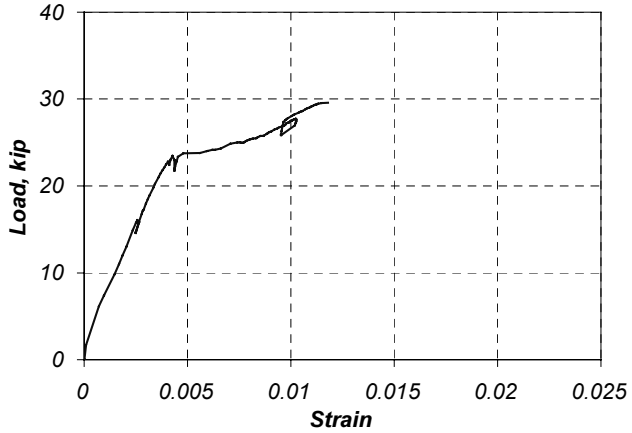

(d) Position of Strain Gages

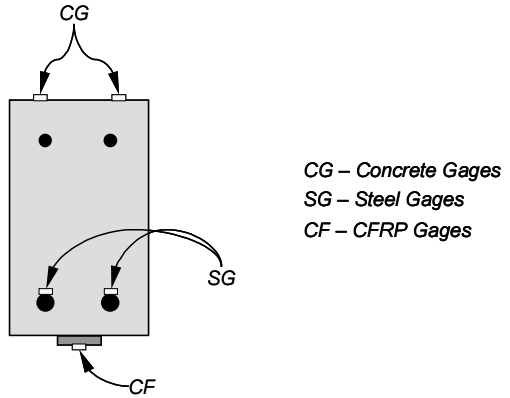

Figure D.29 Measured Strains in Specimen A-LT2 (Section 1)

(a) #5 Reinforcing Bar Strains

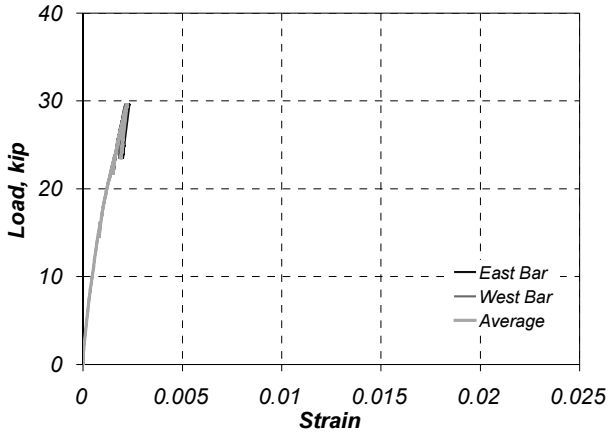

(c) Concrete Strains

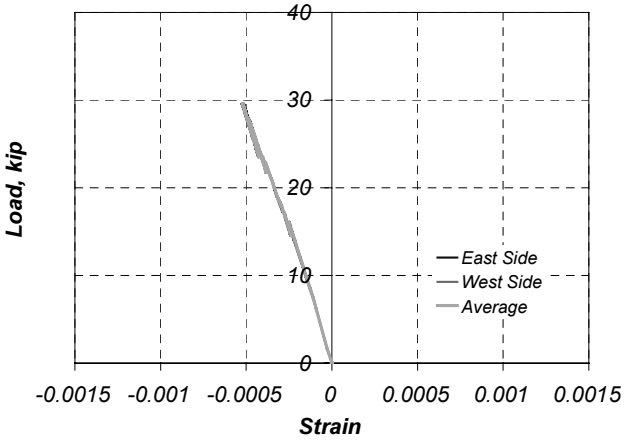

(b) CFRP Strains

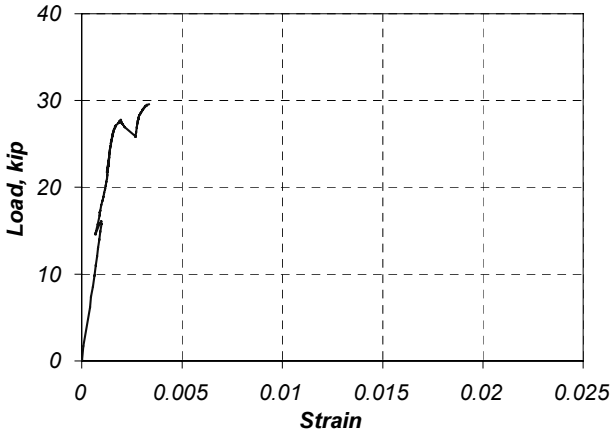

(d) Position of Strain Gages

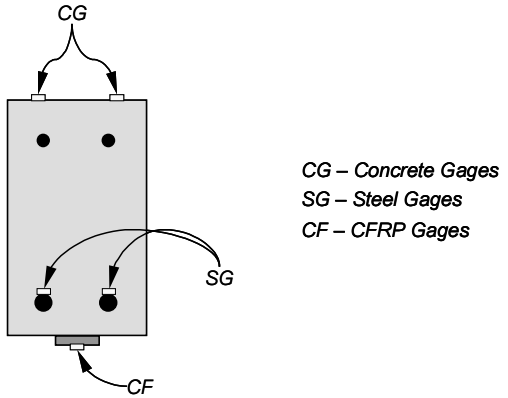

Figure D.30 Measured Strains in Specimen A-LT2 (Section 2)

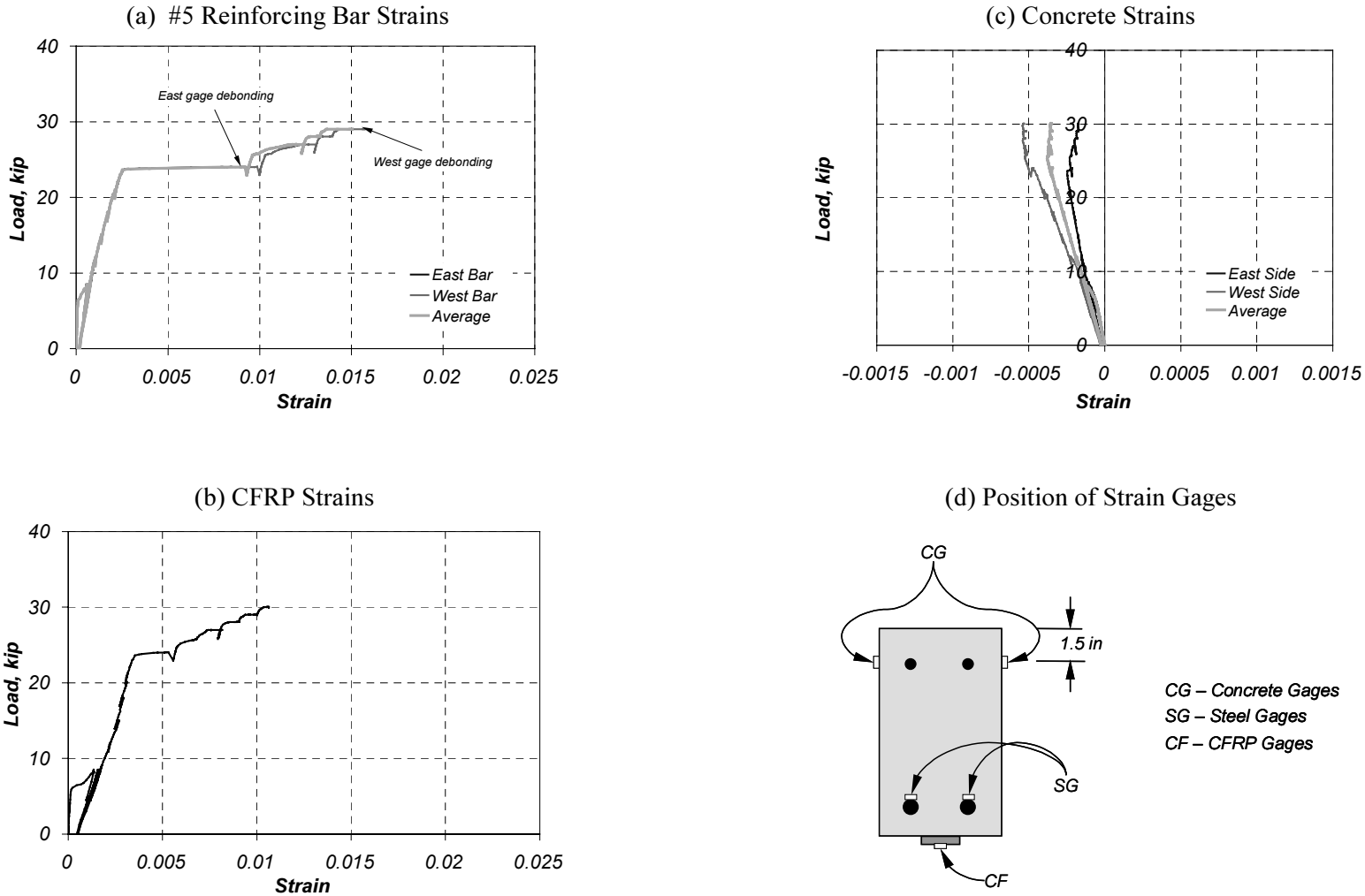

Figure D.31 Measured Strains in Specimen A-F1 (Section 1)

(a) #5 Reinforcing Bar Strains

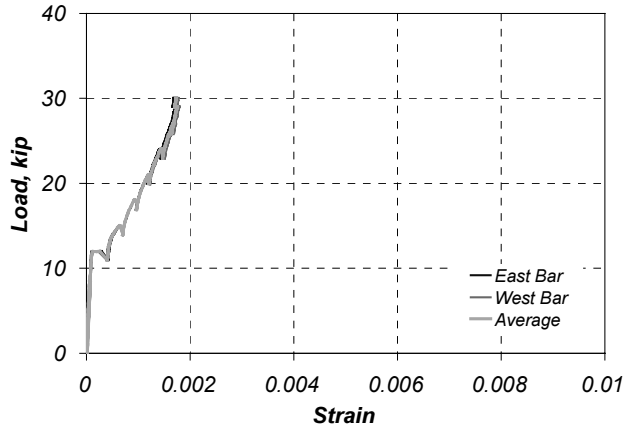

(c) Concrete Strains

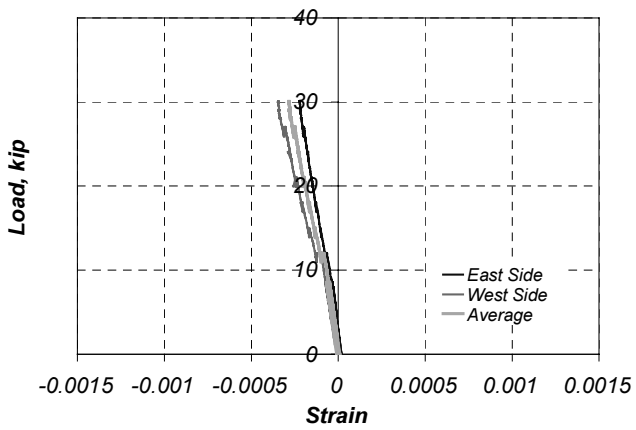

(b) CFRP Strains

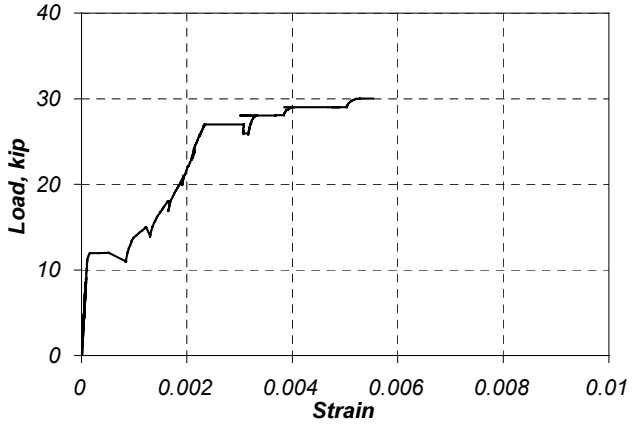

(d) Position of Strain Gages

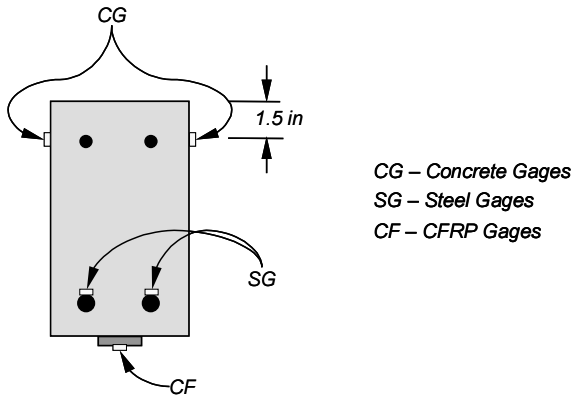

Figure D.32 Measured Strains in Specimen A-F1 (Section 2)

(a) #5 Reinforcing Bar Strains

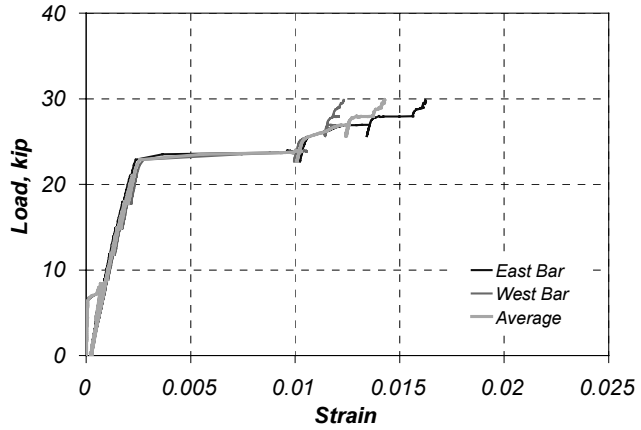

(c) Concrete Strains

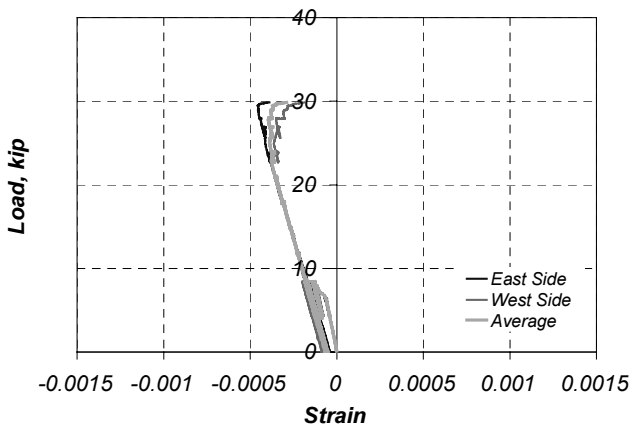

(b) CFRP Strains

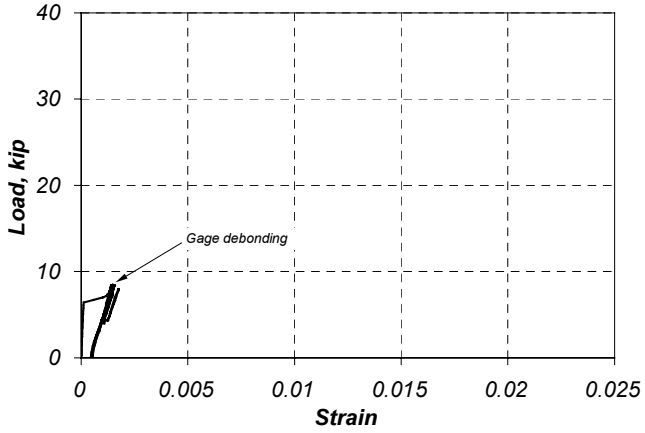

(d) Position of Strain Gages

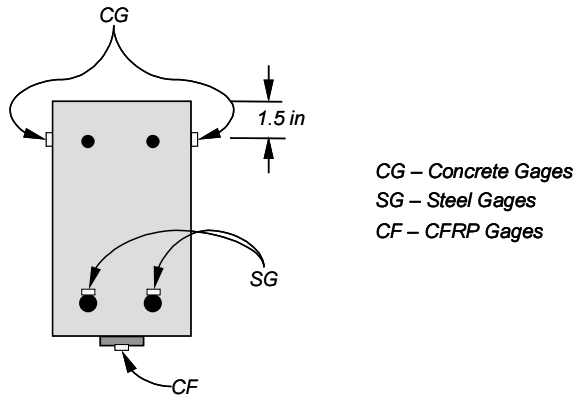

Figure D.33 Measured Strains in Specimen A-F2 (Section 1)

(a) #5 Reinforcing Bar Strains

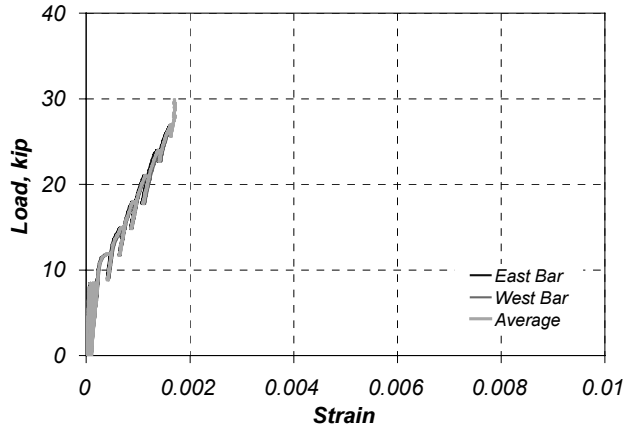

(c) Concrete Strains

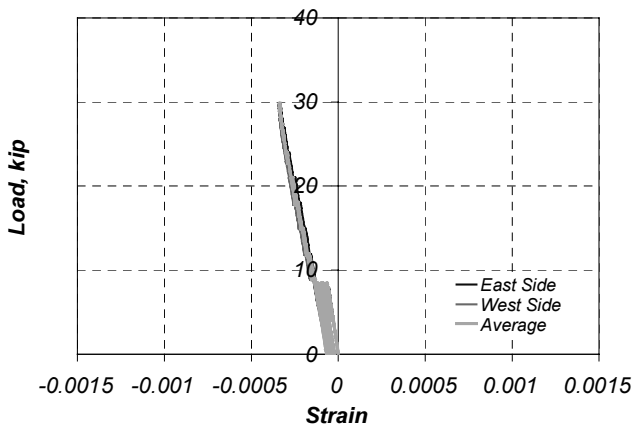

(b) CFRP Strains

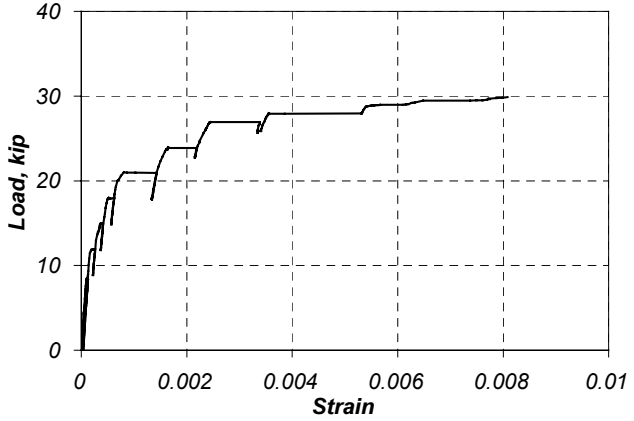

(d) Position of Strain Gages

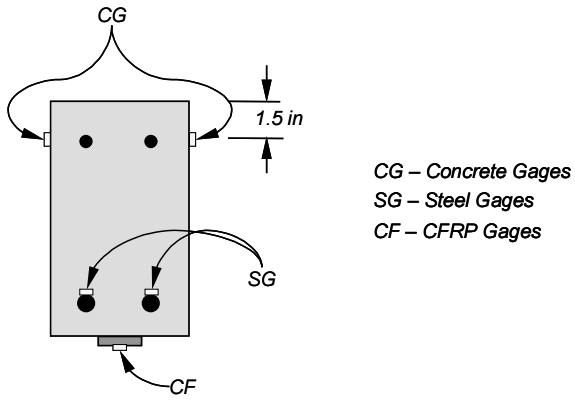

Figure D.34 Measured Strains in Specimen A-F2 (Section 2)

(a) #5 Reinforcing Bar Strains

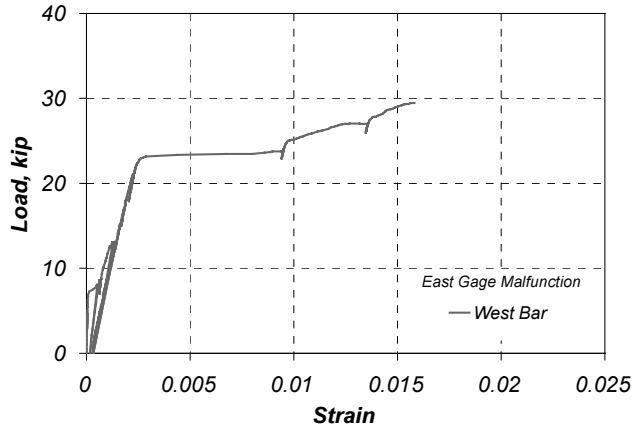

(c) Concrete Strains

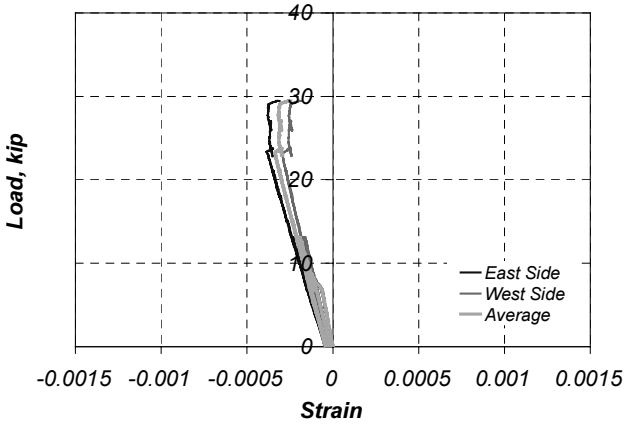

(b) CFRP Strains

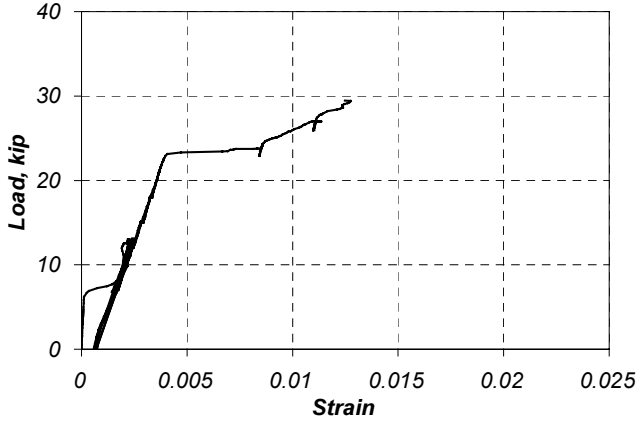

(d) Position of Strain Gages

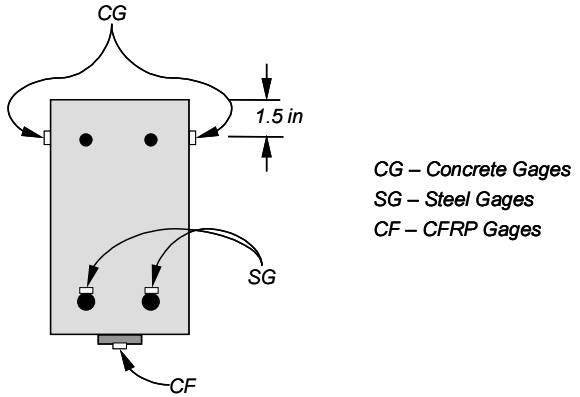

Figure D.35 Measured Strains in Specimen A-F3 (Section 1)

(a) #5 Reinforcing Bar Strains

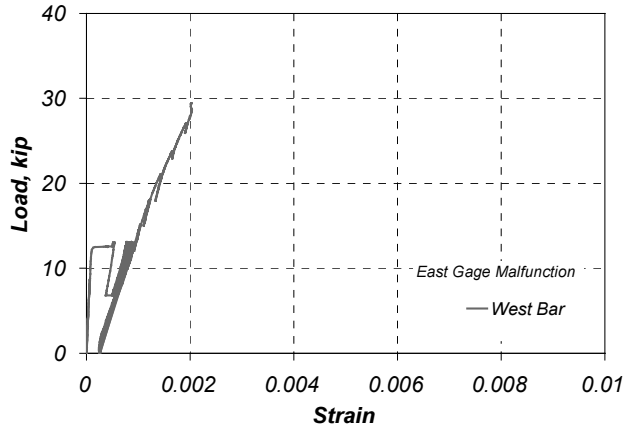

(c) Concrete Strains

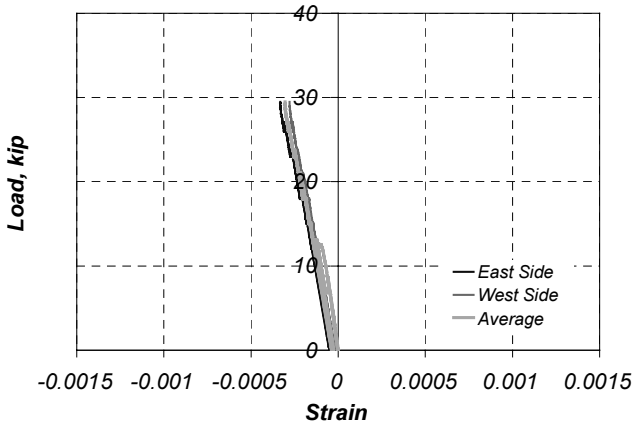

(b) CFRP Strains

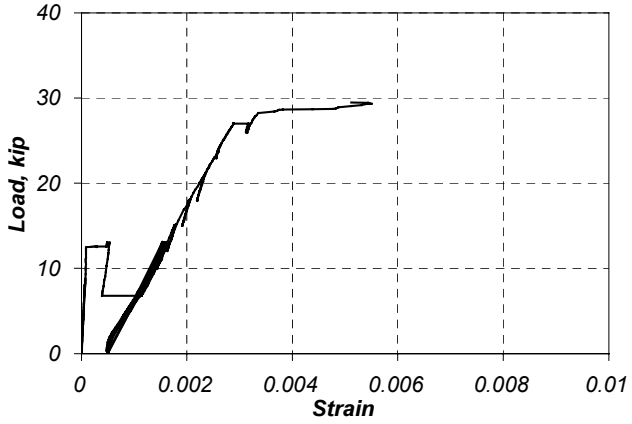

(d) Position of Strain Gages

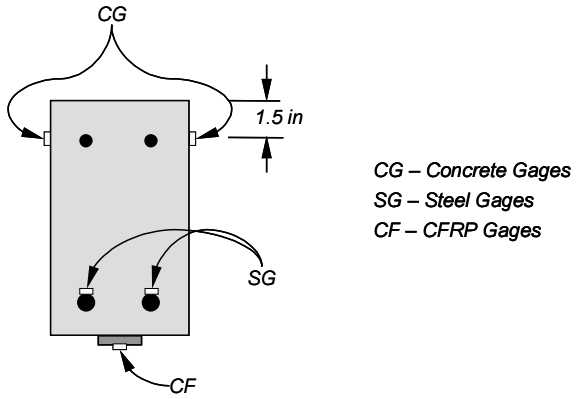

Figure D.36 Measured Strains in Specimen A-F3 (Section 2)

(a) #5 Reinforcing Bar Strains

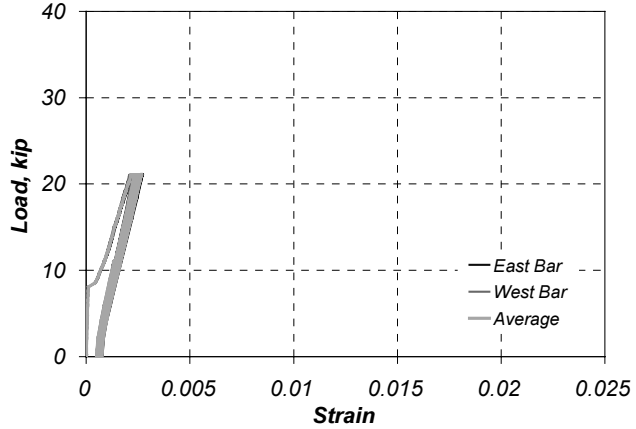

(c) Concrete Strains

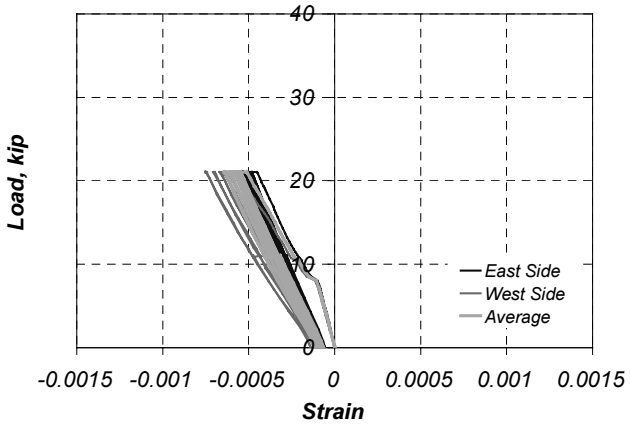

(b) CFRP Strains

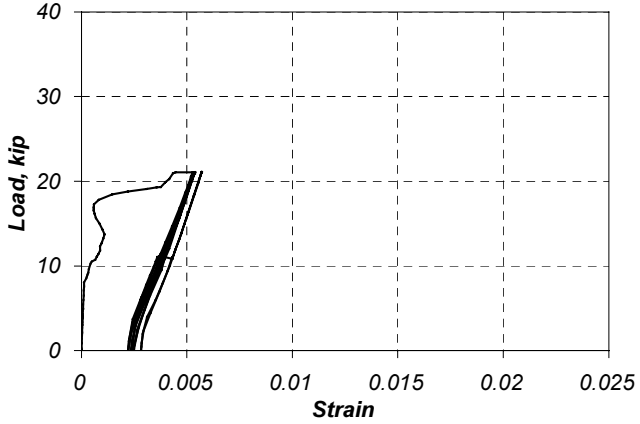

(d) Position of Strain Gages

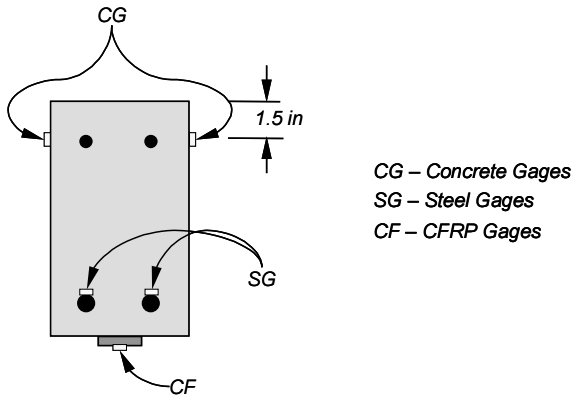

Figure D.37 Measured Strains in Specimen A-F4 (Section 1)

(a) #5 Reinforcing Bar Strains

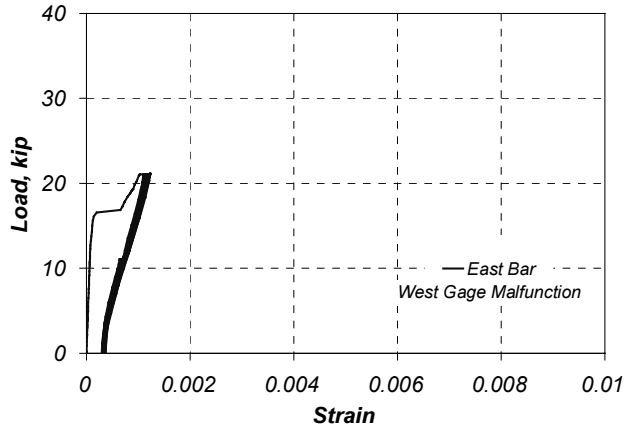

(c) Concrete Strains

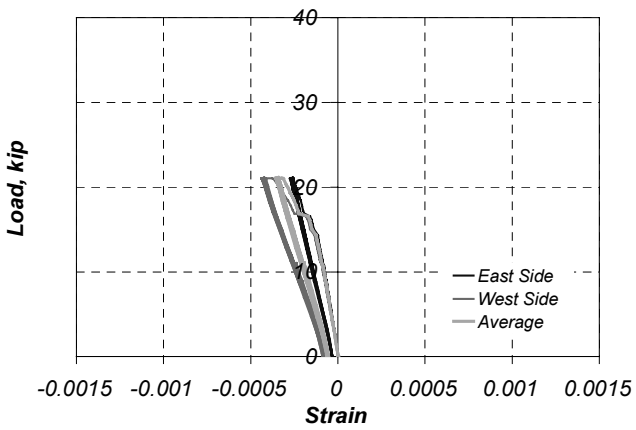

(b) CFRP Strains

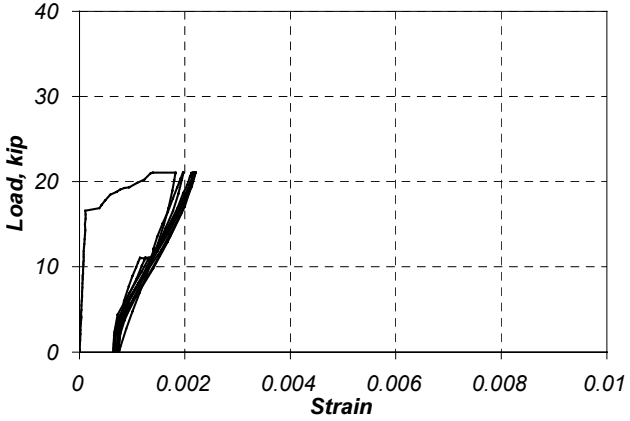

(d) Position of Strain Gages

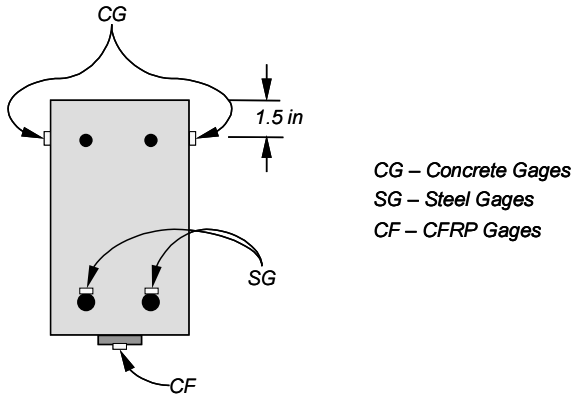

Figure D.38 Measured Strains in Specimen A-F4 (Section 2)

(a) #5 Reinforcing Bar Strains

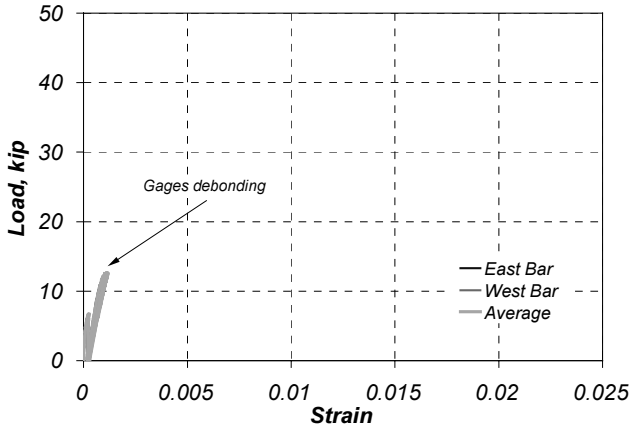

(c) Concrete Strains

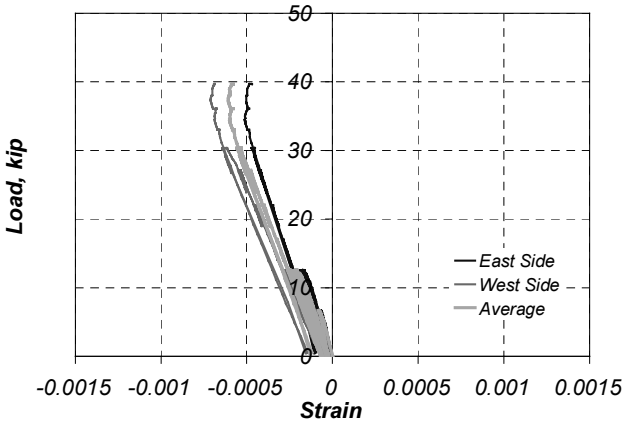

(b) CFRP Strains

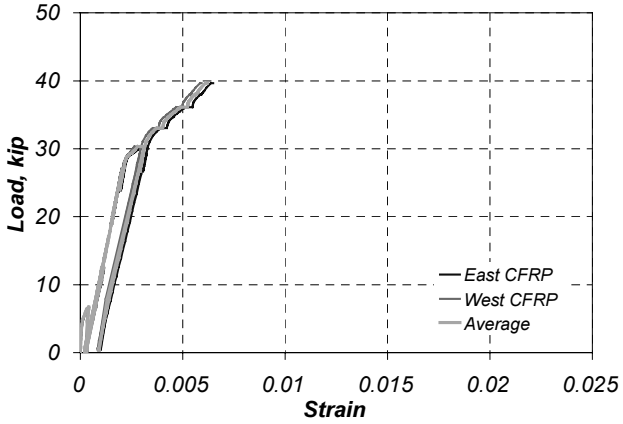

(d) Position of Strain Gages

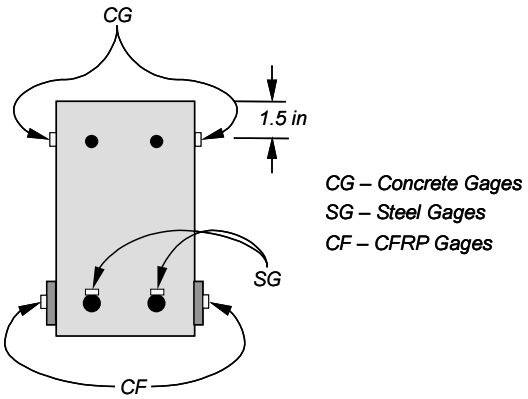

Figure D.39 Measured Strains in Specimen D-F1 (Section 1)

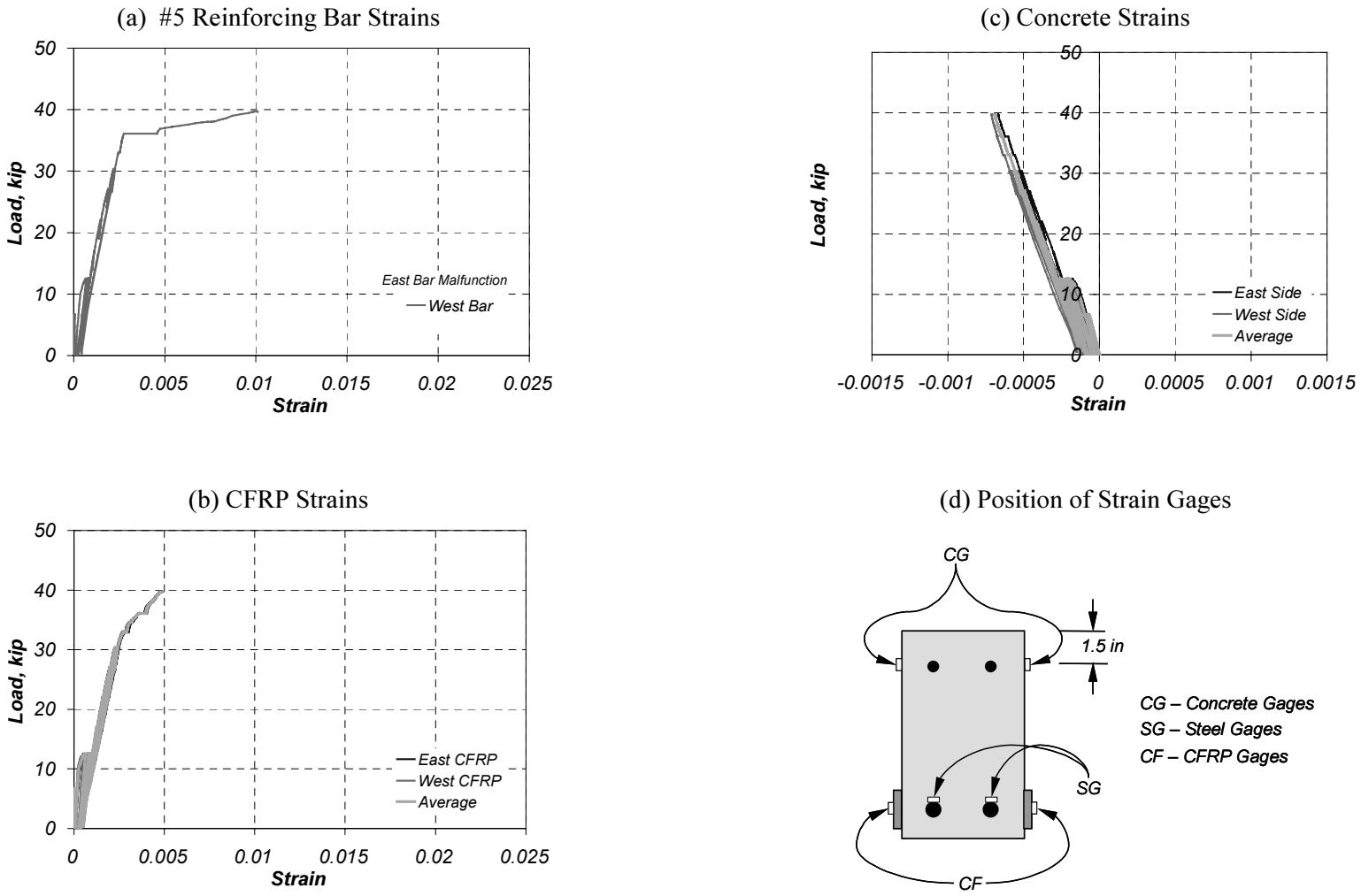

Figure D.40 Measured Strains in Specimen D-F1 (Section 2)

(a) #5 Reinforcing Bar Strains

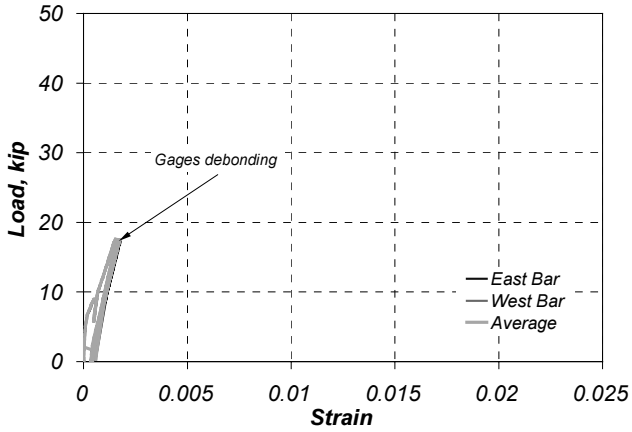

(c) Concrete Strains

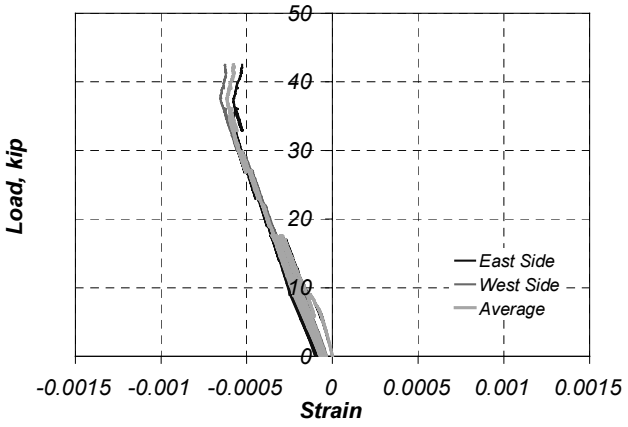

(b) CFRP Strains

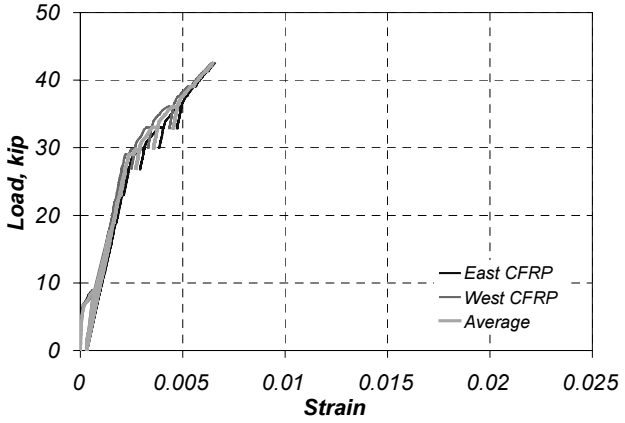

(d) Position of Strain Gages

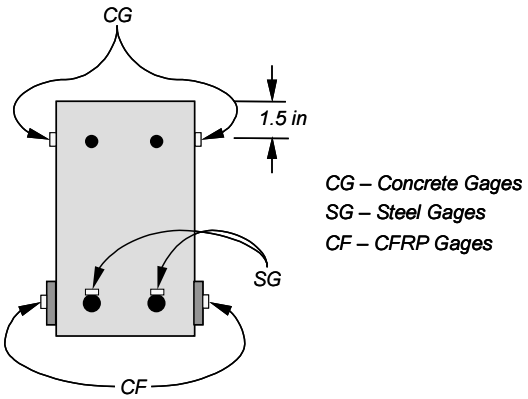

Figure D.41 Measured Strains in Specimen D-F2 (Section 1)

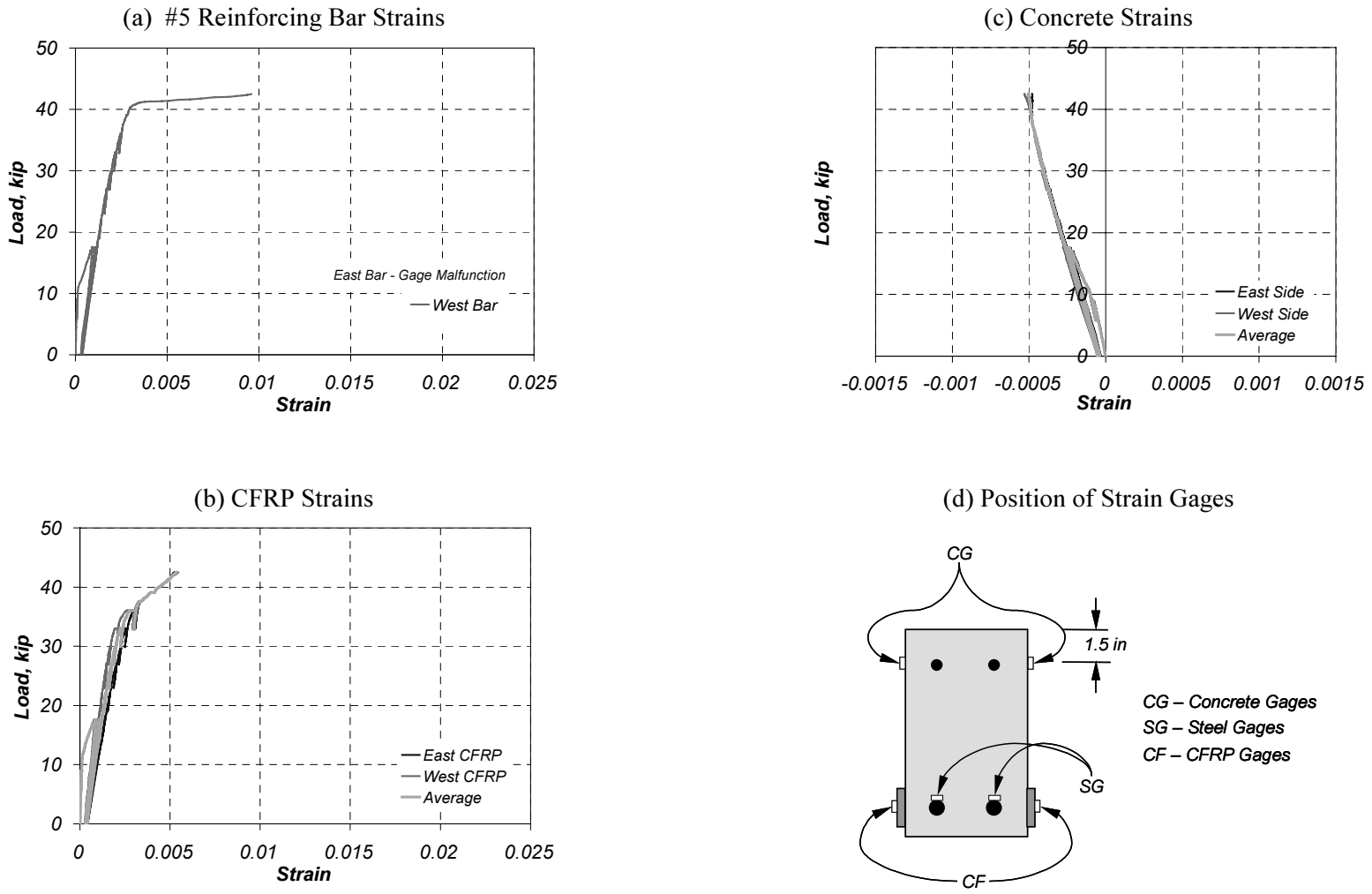

Figure D.42 Measured Strains in Specimen D-F2 (Section 2)

(a) #5 Reinforcing Bar Strains

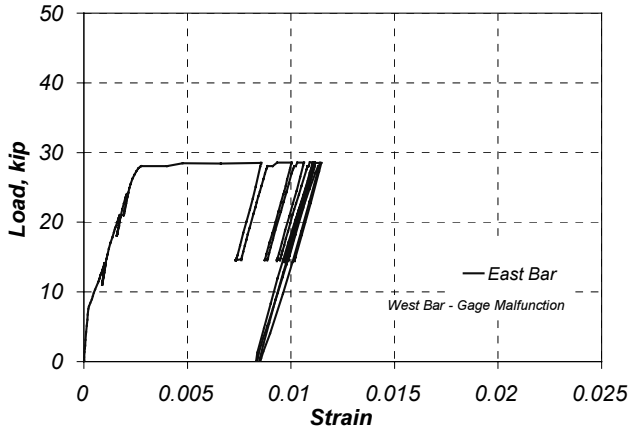

(c) Concrete Strains

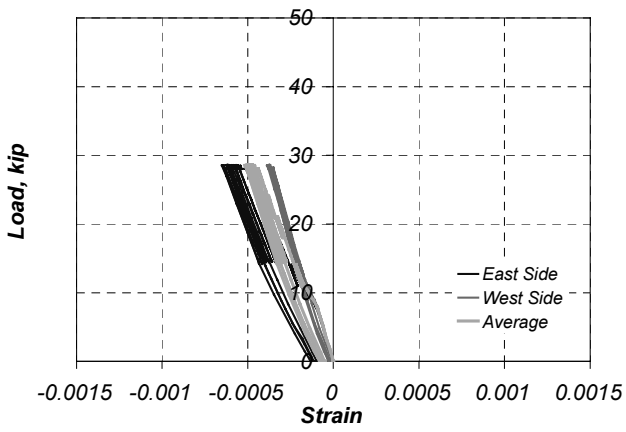

(b) CFRP Strains

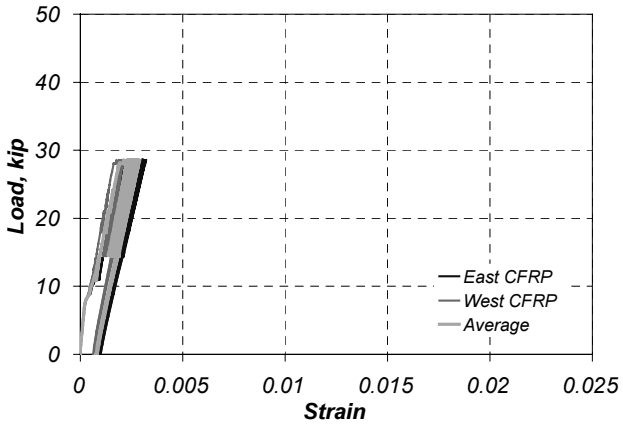

(d) Position of Strain Gages

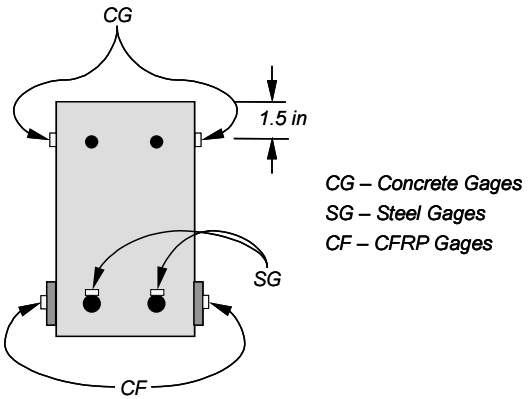

Figure D.43 Measured Strains in Specimen D-F3 (Section 1)

(a) #5 Reinforcing Bar Strains

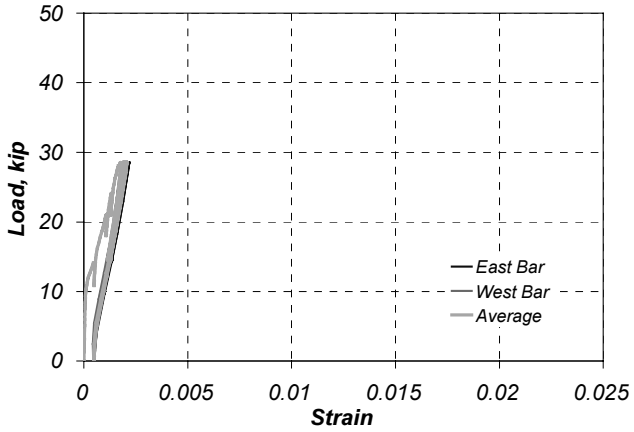

(c) Concrete Strains

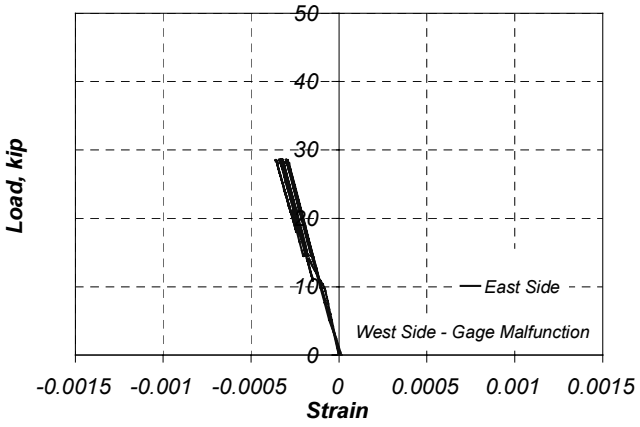

(b) CFRP Strains

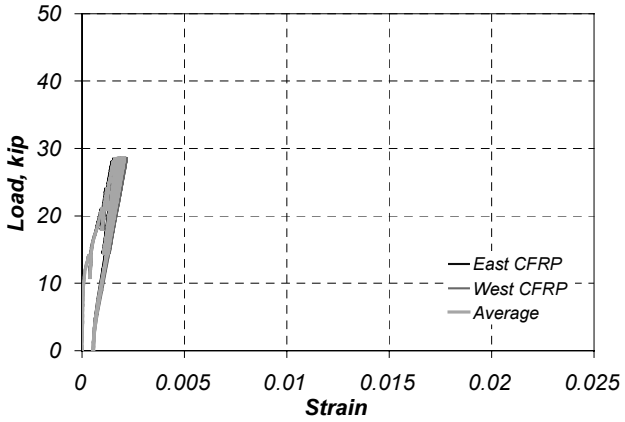

(d) Position of Strain Gages

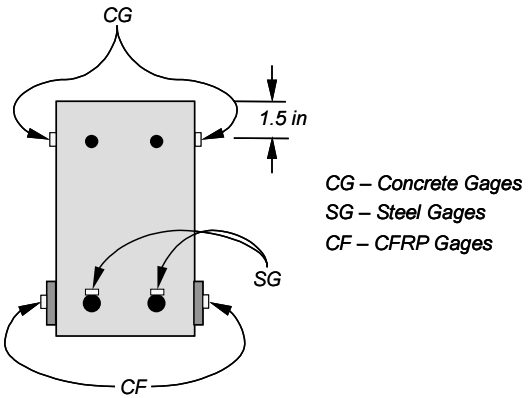

Figure D.44 Measured Strains in Specimen D-F3 (Section 2)

(a) #5 Reinforcing Bar Strains

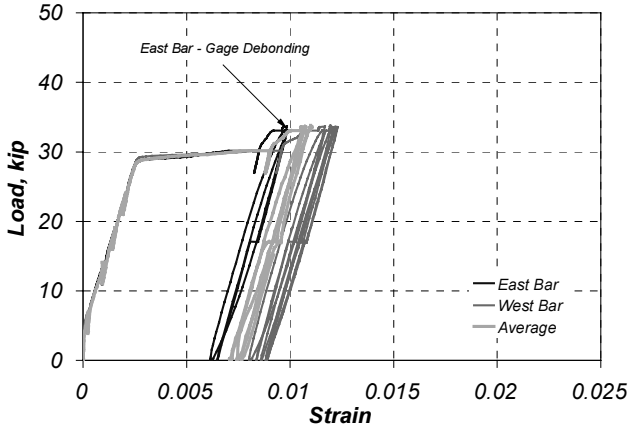

(c) Concrete Strains

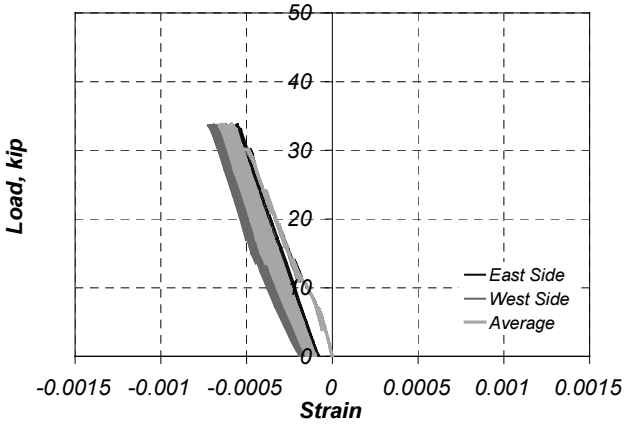

(b) CFRP Strains

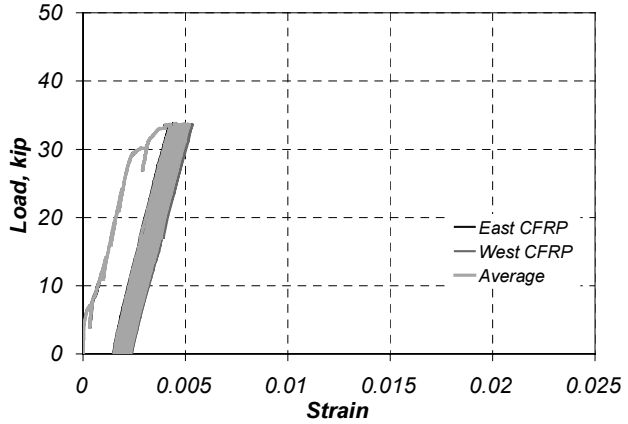

(d) Position of Strain Gages

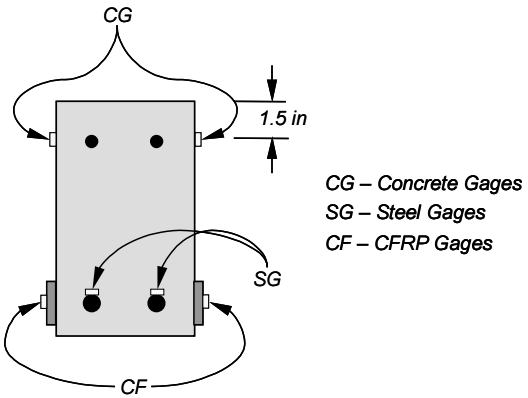

Figure D.45 Measured Strains in Specimen D-F4 (Section 1)

(a) #5 Reinforcing Bar Strains

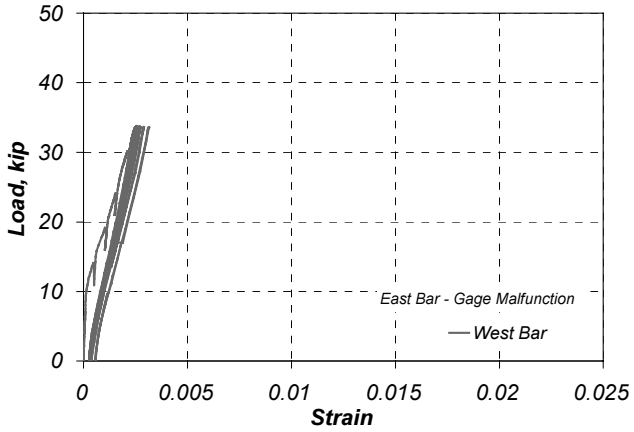

(c) Concrete Strains

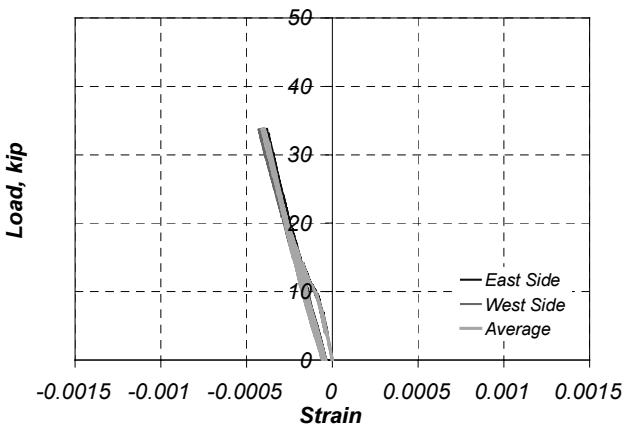

(b) CFRP Strains

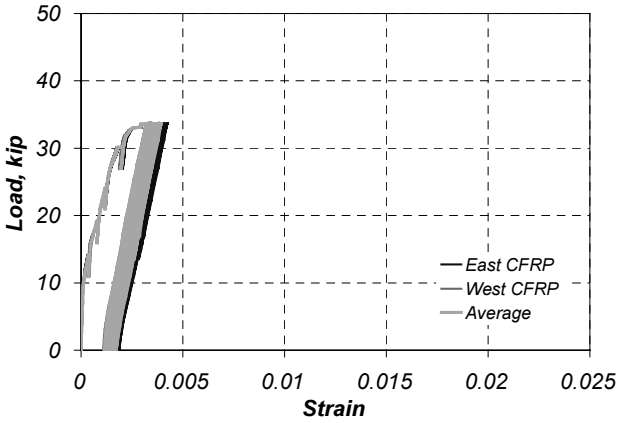

(d) Position of Strain Gages

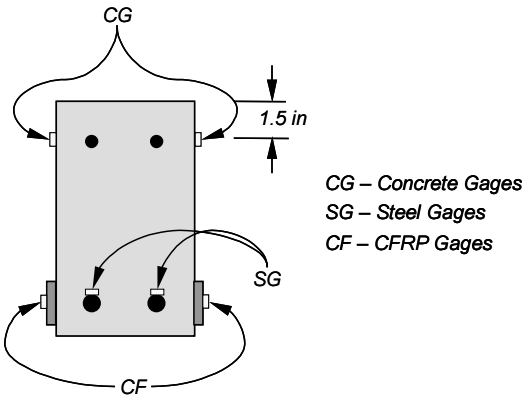

Figure D.46 Measured Strains in Specimen D-F4 (Section 2)